SOME EFFECTS OF LANGMUIR CIRCULATION ON SUSPENDED PARTICLES IN LAKES AND RESERVOIRS

BY

T. BURANATHANITT

THE THESIS SUBMITTED TO

THE UNIVERSITY OF LEICESTER

FOR THE DEGREE OF

DOCTOR OF PHILOSOPHY

AUGUST, 1979

SOME EFFECTS OF LANGMUIR CIRCULATION ON SUSPENDED PARTICLES IN LAKES AND RESERVOIRS

By T. BURANATHANITT

ABSTRACT

The quantitative extent to which the large-scale organised water motion in the surface waters of lakes and reservoirs, known as Langmuir circulation, affects the distribution and settling of suspended particles, especially the algae, is not known and has been ignored in the conventional modelling of water quality. Since the settling of these particles is an important process in determining water quality, the present study investigates the Langmuir circulation effect by means of a mathematical model, based on the two-dimensional advection-diffusion mass transport equation describing the temporal and spatial distribution of suspended particles in a typical Langmuir cell. The Langmuir circulation flow field and turbulent diffusion coefficients are empirically modelled by relating these variables to the environmental parameters.

It has been shown that Langmuir circulation does affect particle distribution and settling. For particles with small sinking speeds, the circulation causes intense mixing, resulting in essentially uniform distribution of particles over the Langmuir cell. For particles with high sinking velocities, aggregation of particles can occur, giving rise to considerable reduction in sinking losses.

Two preliminary laboratory experiments have been performed. The wind-wave tank experiment suggests that the Langmuir circulation scale of motion is dependent on the significant height of the surface waves, thus providing an empirical means of determining the size of Langmuir cells from environmental variables. The particle-settling tank experiment holds promise as a means of studying the effect of circulating flows on the distribution and settling of particles.

ACKNOWLEDGEMENT

The author would like to express his gratitude to his supervisor, Dr. D.J. Cockrell, for the guidance, valuable suggestions and criticism, and concern throughout the course of this research.

The author thanks staff from the Water Research Centre, in particular Chris Rutherfod and John Davis , for considerable help and useful suggestions given to the author. The author would also extend his thanks to the technical staff of Leicester University Engineering Department for their helpful suggestions and assistance in the design and construction of the wind-wave tank and the particle-settling tank, particularly to Stewart Brown, and also David Granby and Geof O'Connor. Assistance obtained from Ken Brodlie and Malcolm Bain of the Computer Laboratory is greatly appreciated.

Finally, the author is grateful to Professor G.D.S. MacLellan, the Head of Engneering Department, for allowing the author to use facilities in the Department for this research.

NOMENCLATURE

AA_i, AA_j	Coefficients of linear simultaneous equations; elements of tridiagonal matrix
BB_i, BB_j	" "
CC_i, CC_j	" "
C	Concentration (e.g. mass per unit volume) of material
C^*	Dimensionless concentration = C/C_o
C_E	Average concentration at time t_E
C_{ij}	Concentration at centre of grid volume ij
C_o	Reference concentration; initial concentration
CE, CW	Concentrations on the right and left faces of grid volume, respectively
CN, CS	Concentrations of the upper and lower faces of grid volume, respectively
c	specific heat of water
D	Depth of Langmuir cell; depth of water; depth of the mixed layer; depth to the thermocline
DD_i, DD_j	Terms in the linear simultaneous equations
d	Particle diameter
f	A function of
F	Time-rate of change due to net growth; fetch length
F_o	Dimensionless fetch length = gF/W_{10}^2
g	Acceleration due to gravity
H	Wave height
$H_{1/3}$	Significant wave height

i	Index for mesh point in y-direction, $y = (i-1).\Delta y$
j	Index for mesh point in z-direction, $z = (j-1).\Delta z$
k	Net growth coefficient or net production rate; thermal conductivity of water
L	Characteristic length
l	Length scale of eddies
N_c	Number of Langmuir cells in wind-wave tank
n	Index for time plane, $t = (n-1).\Delta t$, used as a subscript
n_c	Number of clear lanes in wind-wave tank
n_b	Number of dye bands in wind-wave tank
SE, SW	Coefficients for interpolation
SN, SS	"
SNZ	"
T	Time interval over which Langmuir circulation phenomena vary significantly; total time of simulation
T^*	Dimensionless time of simulation = TW_n/D
T_w	Local temperature of water
t	Time
t^*	Dimensionless time = $t\ W_n/D$
Δt	Time step length
t_E	Time at which relative concentration distribution in Langmuir cell reaches equilibrium
U, U_s	x-components of velocity for fluid and solid particles, respectively
U_o	Characteristic velocity
u', u'_s	Fluctuating velocities in x-direction for fluid and solid particles, respectively
V, V_s	y-components of velocity for fluid and solid particles, respectively
V^*	Dimensionless lateral velocity = V/W_n

V_f	Characteristic velocity of fluid
v', v'_s	Fluctuating velocities in y-direction for fluid and solid, respectively
VE, VW	Average horizontal components of velocity on the right and left faces of grid volume, respectively
W, W_s	z-componets of velocity for fluid and solid particle, respectively
W^*	Dimensionless velocity = W/W_n
W_a	Local velocity of water
w_d, W_d	Maximum downwelling velocity in Langmuir cell
W_{eff}	Effective sinking speed
W_{eff1}, W_{eff2}	Effective sinking speeds at $t=t_E$ and $t > t_E$, respectively
W_n	Wind speed
W_T	Terminal fall velocity of particle
W_T^*	Dimensionless sinking velocity of particle
W_u	Maximum upwelling speed in Langmuir cell
W_y	Wind speed at anemometer height y
W_{10}	Wind speed at height 10 m above the ground
WN, WS	Average vertical velocities on the upper and lower faces of grid volume, respectively
w', w'_s	Fluctuating velocities in z-direction for fluid and solid particle, respectively
x	(Longitudinal) cartesian coordinate
x^*	Dimensionless coordinates = x/D
y	(Lateral) cartesian coordinate
y^*	Dimensionless coordinate = y/D
Δy	Grid size in y-direction
z	(Vertical) cartesian coordinate
z^*	Dimensionless coordinate = z/D
Δz	Grid size in z-direction

β	Coefficient of proportionality
ε	Rate of turbulent energy tranfer
ε_H	Horizontal eddy diffusion coefficient
ε_m	Coefficient of diffusion for momentum
ε_M	Eddy viscosity
ε_s	Coefficient of diffusion for solid particles
$\varepsilon_x, \varepsilon_y, \varepsilon_z$	Coefficients of eddy diffusion for fluid in x-,y-, and z-directions, respectively
$\varepsilon_{sx}, \varepsilon_{sy}, \varepsilon_{sz}$	Coefficients of eddy diffusion for solid particles in x-, y-, and z-directions, respectively
$\varepsilon_{yE}, \varepsilon_{yW}$	Horizontal coefficients of diffusion on the right and left faces of grid volume, respectively
$\varepsilon_{zN}, \varepsilon_{zS}$	Vertical coefficients of diffusion on the upper and lower faces of grid volume, respectively
ϕ	A function of
λ	Characterislic length of Langmuir cell
λ_c	Convergence line spacing; cell spacing; row spacing; twice Langmuir circulation cell width
λ_w	Dominant wave length of surface wind waves
μ , ρ	Water viscosity ; $\nu = \mu / \rho$
μ_a	Air viscosity
ρ	Water density
$\Delta\rho_a$	Local air density variation
ρ_s	(Grain) density of solid particle
σ	Surface tension force

Principal Superscripts

—	the average or mean quantity
*	non-dimensional quantity

SOME EFFECTS OF LANGMUIR CIRCULATION ON

SUSPENDED PARTICLES IN LAKES AND RESERVOIRS

CONTENTS

		Pages
ACKNOWLEDGEMENT		i
NOMENCLATURE		ii
CONTENTS		vi
LIST OF TABLES		x
LIST OF FIGURES		xi
CHAPTER 1	INTRODUCTION	1 - 7
1.1	Langmuir Circulation - an organised large-scale flow structure	2
1.2	Significance of Langmuir Circulation to Water Resources Field	4
CHAPTER 2	EFFECTS OF LANGMUIR CIRCULATION ON PARTICLE SUSPENSION - A review of existing models and an outline of the present study	8 - 16
2.1	A Brief Review of Previous Field Investigations	9
2.2	Review of Existing Models	9
	2.2.1 The Model of Stommel	10
	2.2.2 The Model Of Titman and Kilham	11
2.3	The Present Study	13
CHAPTER 3	THE MATHEMATICAL MODEL	17 - 26
3.1	Basic Principles	18
3.2	Simplifications to the Basic Equation	20
3.3	The Simplified Governing Equation and General Method of Solution	23
3.4	Non-dimensionalisation of the Governing Equation	24

CHAPTER 4	LANGMUIR CIRCULATION OBSERVATIONS AND PARAMETER CORRELATION	27 - 58
4.1	Introduction	28
4.2	General Features of the Circulation	29
4.3	Response to the Wind	30
4.4	Scale of Motion	31
4.5	Some Empirical Correlation Between the Langmuir Circulation Scale of Motion and Wind/Wave Parameters	35
	4.5.1 Basic Rationale	36
	4.5.2 Correlation of Oceanic Data	39
	4.5.3 Correlation with Wind/Wave Parameters	40
4.6	Velocity Observations and Correlations	44
CHAPTER 5	A MODEL OF LANGMUIR CIRCULATION AND THE TURBULENT COEFFICIENT RELATIONSHIP	59 - 67
5.1	The Langmuir Circulation Model	60
5.2	Estimation of the Turbulent Eddy Coefficients (ε_z and ε_y)	64
CHAPTER 6	THE FINITE DIFFERENCE APPROXIMATION	68 - 90
6.1	Summary of Equations	69
6.2	Finite Difference Representation	70
6.3	Initial and Boundary Conditions	76
6.4	Values of Input Variables	77
6.5	Some Practical Tests on Stability and Accuracy of the Finite Difference Scheme	79
CHAPTER 7	NUMERICAL RESULTS AND THEIR ANALYSIS	91 - 143
7.1	Basic Information	92
7.2	Particle Distribution Patterns	
	7.2.1 Non-buoyant Particles	93
	7.2.2 Buoyant Particles	95

7.3 Effects of Cell Width-to-depth Ratio on the Retention of Non-buoyant Particles 96
7.4 The Extent of Langmuir Circulation Effects in the Modelling of Particle Distribution and Sinking Losses 97
7.5 Effective Sinking Speeds 99
7.5.1 The Well-mixed Compartment Model (zero-dimensional model) 99
7.5.2 The One-dimensional Model 101
7.6 Comparison of the Effective Sinking Loss Rates with Titman and Kilham's Results 104
CHAPTER 8 PRELIMINARY LABORATORY EXPERIMENTS ON LANGMUIR CIRCULATIONS 144 - 187
8.1 A Wind-wave Tank Experiment 145
8.1.1 Experimental Apparatus and Procedure 145
8.1.2 Determination of Average Cell Spacing 147
8.1.3 Determination of Wave Height, $H_{1/3}$ 148
8.1.4 Results 148
8.2 A Particle Settling Experiment 149
8.2.1 Experimental System 149
8.2.2 Flow Measurements 150
8.2.3 Velocity Measurements 150
8.2.4 Particle Sinking Loss Measurements 151
8.2.5 Results 152
8.3 Significance of Experiments
8.3.1 The Wind-wave Tank Experiment 155
8.3.2 The Particle Settling Experiment 160

8.3.2.1 The Circulating Flow 160

8.3.2.2 Particle motion 162

8.3.3 General Conclusions 164

CHAPTER 9 RELEVANCE OF LANGMUIR CIRCULATION TO WATER QUALITY PROBLEMS 186-196

9.1 Water Quality Models 187

9.2 Significance of Langmuir Circulation to the Settling of Algal and Other Particles

9.2.1 Summary of Relevant Results 188

9.2.2 Langmuir Circulation Effect on Algal Particles 190

9.2.3 Effect on Other Particulate Matter 191

9.3 Model Limitations 192

9.4 Suggestions for Further Work 193

CONCLUSIONS 197-199

APPENDIX I LISTING OF COMPUTER PROGRAM 200

REFERENCES 213

ADDITIONAL REFERENCES 220

LIST OF TABLES

		Pages
Table 4.1	Summary of Langmuir Circulation Theories	47
Table 4.2	Some Observations of Langmuir Circulation	48 - 50
Table 8.1	Summary of Results of the Wind-wave Tank Experiment	170
Table 8.2	Summary of results of the Particle Settling Experiment	180

LIST OF FIGURES

Figure Number		Pages
1.1	Schematic diagram of Langmuir convection cell pattern	6
1.2	Temperature and light distribution in stratified lakes	7
2.1	Streamlines of idealised section across a pair of convection cells	15
2.2	Trajectories of phytoplankton cells settling through a Langmuir cell under various conditions	15
2.3	Trajectories of fluid and solid particles in Langmuir cells in Titman and Kilham's model (1976)	16
2.4	Loss rates of particles of various sinking rates predicted by Titman and Kilham's model	16
4.1	Schematic diagram of Langmuir circulation	51
4.2	Downwelling under streaks breaking through stable stratification, from Scott et al.(1969)	52
4.3	Correlation between wind speed and wave height (from Wiegel, 1966)	53
4.4	Correlation between row spacings and wind speeds and depths of the mixed layer (oceanic data)	54
4.5	A schematic diagram showing convergence of dye at the bottom of wind-wave tank due to action of Langmuir circulation (after Faller and Caponi,1977)	55
4.6	Correlation between row spacings and dominant wave lengths	56
4.7	Correlation between row spacings and significant wave heights	57
4.8	The relationship between downwelling speed and wind speed	58

5.1 A schematic diagram of Langmuir circulation, showing streamlines and typical velocity profile used in the present model 67

6.1 A finite difference grid structure 82

6.2 Variable definitions and locations 83

6.3 to 6.9 Comparison between the numerical and exact solutions of the one-dimensional advection-diffusion equation at time 0.5/U for various values of ΔX and Δt, using the ADI-CDS method 84-90

7.1 Particle distribution at various times for $W_T^* = 1\times10^{-3}$ and $\lambda_c^* = 2.0$. 105-109

7.2 Particle distribution at various times for $W_T^* = 1\times10^{-5}$ and $\lambda_c^* = 2.0$ 110-114

7.3 Particle distribution at various times for $W_T^* = 1\times10^{-3}$ and $\lambda_c^* = 0.5$ 115-118

7.4 Particle distribution at various times for $W_T^* = 1\times10^{-5}$ and $\lambda_c^* = 0.5$ 119-123

7.5 Particle distribution at various times for $W_T^* = -1\times10^{-3}$ and $\lambda_c^* = 2.0$ 124-128

7.6 Particle distribution at various times for $W_T^* = -1\times10^{-5}$ and $\lambda_c^* = 2.0$ 129-132

7.7 Effects of cell width-to-depth ratio on the retention of particles (for $W_T^* = 1\times10^{-3}$) 133

7.8 Variations of mean concentration C^* with time t^* for $\lambda_c^* = 2.0$, and W_T^* between 1×10^{-3} and 1×10^{-5} 134

7.9 Variations of mean concentration C^* with time t^* for $\lambda_c^* = 0.5$, and W_T^* between 1×10^{-3} and 1×10^{-5} 135

7.10 Variations of effective sinking speed W^*_{eff1} for various values of sinking speed W^*_T and row spacing-to-depth ratio λ^*_c 136

7.11 Variations of effective sinking speed W^*_{eff2} for various values of sinking speed W^*_T and row spacing-to-depth ratio λ^*_c 137

7.12 Ratio of effective sinking speed to particle fall speed (W^*_{eff2}/W^*_T) as a function of λ^*_c and W^*_T 138

7.12a Variations of the ratio W^*_{eff}/W^*_T with Δt^* (< 6000) and W^*_T for a fixed value of $\lambda^*_c = 2.5$ 139

7.13 Finite difference grid structure and variable locations for a 1-dimensional model 140

7.14 Effective sinking speeds W^*_{eff} as a function of time t^* and depth z^* in 1-dimensional model, for $\lambda^*_c = 2.0$ and $W^*_T = 1\mathrm{x}10^{-3}$ 141

7.15 Effective sinking speed W^*_{eff} as a function of time t^* and depth z^* in 1-dimensional model, for $\lambda^*_c = 2.0$ and $W^*_T = 1\mathrm{x}10^{-5}$ 142

7.16 A comparison between loss rates, for various particle sinking speeds, predicted by the algebraic relationship (zero-dimensional model), Titman and Kilham's model, and the present model 143

8.1 A schematic diagram of the wind wave tank used in the present experiment 166

8.2 Illustrations of the conductivity probe for measuring wave height 167

8.3 A schematic diagram showing the position of dye bands on the channel bed in relation to Langmuir cells 168

8.4 Photographs showing dye bands in the wind-wave tank for various conditions as viewed from above the test section 169

8.5 Cell spacing λ_c/D as a function of dominant wave length λ_w/D (after Faller and Caponi, 1977 ,1978) 171

8.6 Cell spacing λ_c /D as a function of significant wave height $H_{1/3}/D$ 172

8.7 An illustration of the basic apparatus used in the particle settling experiment 173-174

8.8 Examples of photographs of the flow patterns obtained by stroboscopic photography 175

8.9 to 8.12 Circulation flow patterns revealed by photographs and the deduced velocity vectors, in the four experimental conditions 176-179

8.13 Distribution of sinking losses across the tank at end of an elapsed time of 9.5 minutes for the four experimental conditions 181

8.14 An example of particle relative distribution deduced from photographs, for experimental condition no. 3 and at time 3.0 minutes. Units on contours are arbitrary 182-183

8.15 Correlation between Langmuir cell sizes and significant wave heights 184

8.16 A diagrammatical sketch of a recommended experimental arrangement for investigating the effects of erodible lower boundary on Langmuir cell geometry 185

9.1 Average effective sinking speeds, at every 1/10 th of the mixed layer depth in 1-dimensional model, as functions of sinking speeds W_T^* and for fixed cell size $\lambda_c^* = 2.0$ 196

SOME EFFECTS OF LANGMUIR CIRCULATION ON SUSPENDED PARTICLES IN LAKES AND RESERVOIRS

CHAPTER 1 INTRODUCTION

The large-scale organised flow structure in the surface waters of lakes and reservoirs, known as Langmuir circulation, is described. Attention is then drawn to the need for understanding the probable rôle and extent of this circulation on the suspension and settling of phytoplankton and sediment particles, particularly in relation to modelling of water quality in lakes and reservoirs.

CHAPTER 1 INTRODUCTION

1.1 Langmuir Circulation - an organised large scale flow structure.

In open waters such as lakes and oceans, when the wind speed is in excess of a critical value (about 3 m/s)*, a banded structure appears on the water surface, with the bands or stripes lying more or less in the direction of the wind. The stripes may be composed of algae or organic foam, or accumulation of surface debris, all of which are indicative of the convergence of the surface waters. In the absence of natural surface tracers such as these, scattering cards, pieces of paper or dye onto the water surface, has also shown that convergence stripes exist (Assaf et al., 1971; Harris and Lott, 1973). Surface water in the stripes seems to move downwind faster than water in between the stripes. Measurements of vertical velocities beneath the surface indicate downwellings beneath the stripes (or convergence lines) and upwellings between them. A picture emerges of an organised circulation, composed of pairs of counter-rotating longitudinal helical roll vortices, axes parallel to the wind direction (see Fig.1.1). This wind-induced circulation in lakes and oceans was first recognised by Langmuir (1938), and has subsequently become known as Langmuir circulation.

Published literature indicates that the most variable feature of Langmuir circulation is the convergence line spacing (row spacing), ranging from 2 to 25 m in lakes and from 2 to 300 m in the ocean (Pollard, 1977). At any one time circulation cells of different sizes may co-exist together, smaller and less well-defined stripes occuring between the larger, well-defined and more persistent ones (Scott et al., 1969; Walther, 1967; Assaf et al., 1971). However, many investigators, noting only the well-defined stripes, have reported a somewhat regular spacing of the stripes (Langmuir, 1938; Myer, 1968; George and Edwards, 1973).

* (Scott et al., 1969)

Precise circulation depth is difficult to measure, but, in stratified water bodies, the vertical dimension of the largest circulation cells is generally believed to correspond to the surface mixed layer depth in lakes (the epilimnion) and oceans. Alternatively, the cell depth may extend to the bed in shallow waters. The circulating motion in Langmuir cells is relatively strong and appears to be related to the wind speed. The maximum downwelling speed is approximately 1% of the wind speed and nearly one quarter of the surface wind drift (Scott et al., 1969). The maximum upwelling speed is about one-third or so of the maximum downwelling (Langmuir, 1938).

Mechanisms proposed for the generation of Langmuir circulation prior to 1971 were reviewed by Faller (1971). Six mechanisms were discussed, namely, shearing instability of the Ekman Layer; coupling of atmospheric vortices to water; thermal convection process; cross-wind stress variation caused by a surface film; transfer of energy of surface ripples to the Langmuir cells by action of the surface films; and interaction of surface wave trains. Most of these have been discounted either because they do not agree with field observation or they fail to provide enough energy to create circulation of observed strengths. Wind and surface wave interaction has received most attention. More recently, sophisticated theoretical models have been developed based on the physics of either wind and waves, or waves alone (Leibovich and Ulrich, 1972; Craik and Leibovich, 1976; Leibovich, 1977a; Leibovich and Radhakrishnan, 1977; Garrett, 1976; Gamelsrød, 1975; Leibovich, 1977b; Craik, 1977; Mobley and Faller, 1977). Because of the complexity of the phenomena and the extreme difficulty of performing tests, all the plausible theories suffer from lack of verification data, while some models have been discarded because of their unjustified assumptions or because their predictions contradict available observations. At the present time there is no universally accepted rational theory of Langmuir circulation and much work remains to be done in the theoretical development. This should proceed hand in hand with verification processes.

Despite these difficulties and lack of precise knowledge concerning physics of the circulation, limited information on the general features of the circulation, in combination with empirical correlations of some of the observed variables, will be shown to provide useful data for study of some Langmuir-circulation related problems. The Langmuir circulation concept is developed in greater detail in Chapters 4 and 5.

1.2 Significance of Langmuir Circulation to the Water Resources Field.

One of the most important parameters in determining water quality and ecological state of water resources systems such as lakes and reservoirs, is the production and distribution of microscopic plant life (i.e. phytoplankton). Since phytoplankton is the dominant producer of organic materials in water impoundments, significant changes in population because of the changes in the aquatic environment can affect many water quality parameters and lake ecology. Accurate understanding of the processes which influence the changes in phytoplankton population is vitally important in water quality management.

In stratified lakes, active production is usually confined to the epilimnion or the mixed layer. The net production of phytoplankton depends on, among other factors, their vertical distribution in relation to the photic depth, that is the depth of light penetration where photosynthesis can take place (Fig.1.2). The distribution of phytoplankton population remaining in suspension and its motion in and out of the photic zone may be expected to affect the phytoplankton production in the mixed layer. The above motion may be induced by a large-scale advection in the mixed layer such as Langmuir circulation.

Another important factor which depends on and, in turn, affects the total amount of phytoplankton in the mixed layer, is the sinking loss, i.e. the quantity of phytoplankton that sinks out of this layer. Determination of this is important since it is a major process by which particulate matters and raw organic materials are removed from the epilimnion to supplement the nutrient pool and sedimentation in the impoundment. If recycled back into the epilimnion, these nutrients can enhance further phytoplankton growth.

Distribution and sinking of other suspended particles, such as sediment particles obtained from catchment runoff, may also be similarly affected by Langmuir circulation. Suspended sediments are important to lake water quality because they are the principal cause of water turbidity which can alter the photic depth and hence affects phytoplankton production in the mixed layer. Furthermore, some types of sediments are capable of forming floc blankets in the presence of weak agitating water currents. These can sink at a higher velocity than individual particles and can take some algae down with them. This gives rise to further sinking loss of phytoplankton (Smith, 1975).

In view of the critical importance to water quality of phytoplankton and sediment distributions in the mixed layer, any investigation to determine the nature and extent of the effects of Langmuir circulation on these particles would be a valuable step to a better understanding and hence more accurate modelling of primary productivity in lakes and reservoirs.

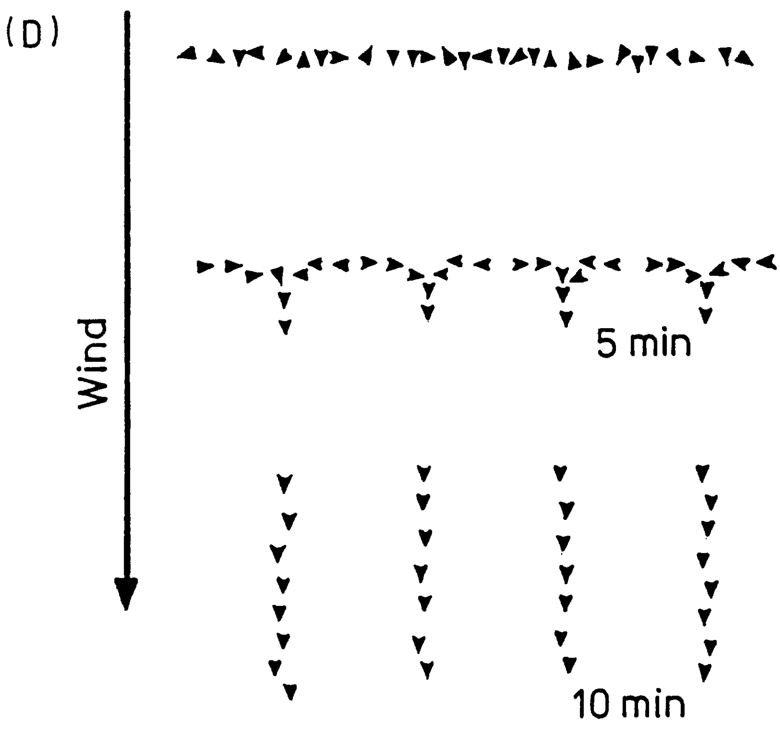

Fig.1·1 Langmuir convection cell patterns. A, Surface pattern illustrating wind-row or streak formation(strippled area) at sites of convergence, vectors representing surface water movement. B, Vertical profile of convection cell pattern. C, The relationship between downwelling speed at convergences and wind intensity; regression line drawn by eye. D, Diagrammatic representation of the behaviour of cards on lake surface in the presence of Langmuir cells as viewed from above. (A,B and C taken from Smayda, 1970. D from Harris and Lott, 1973)

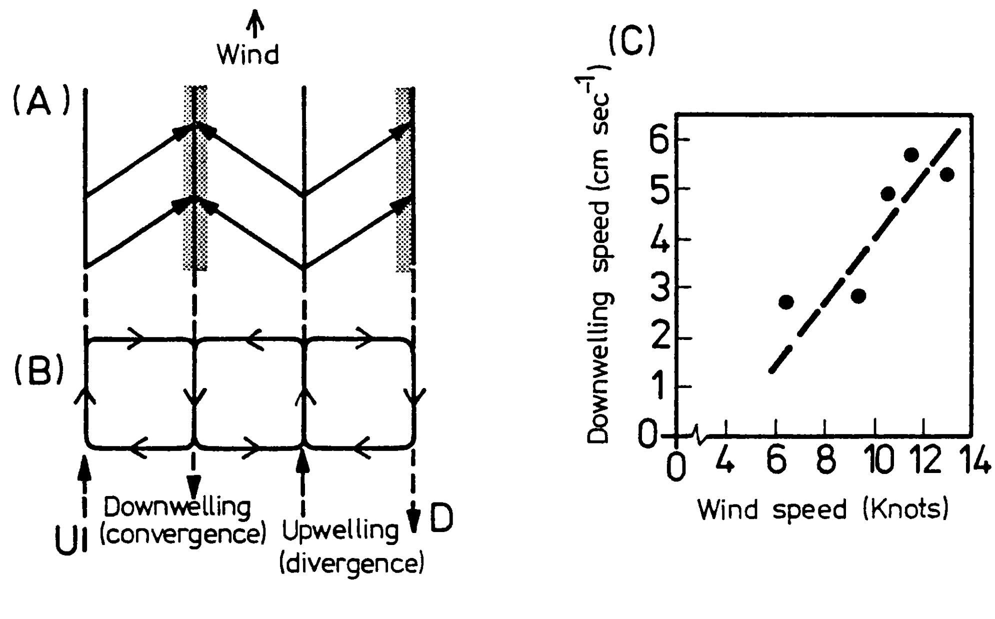

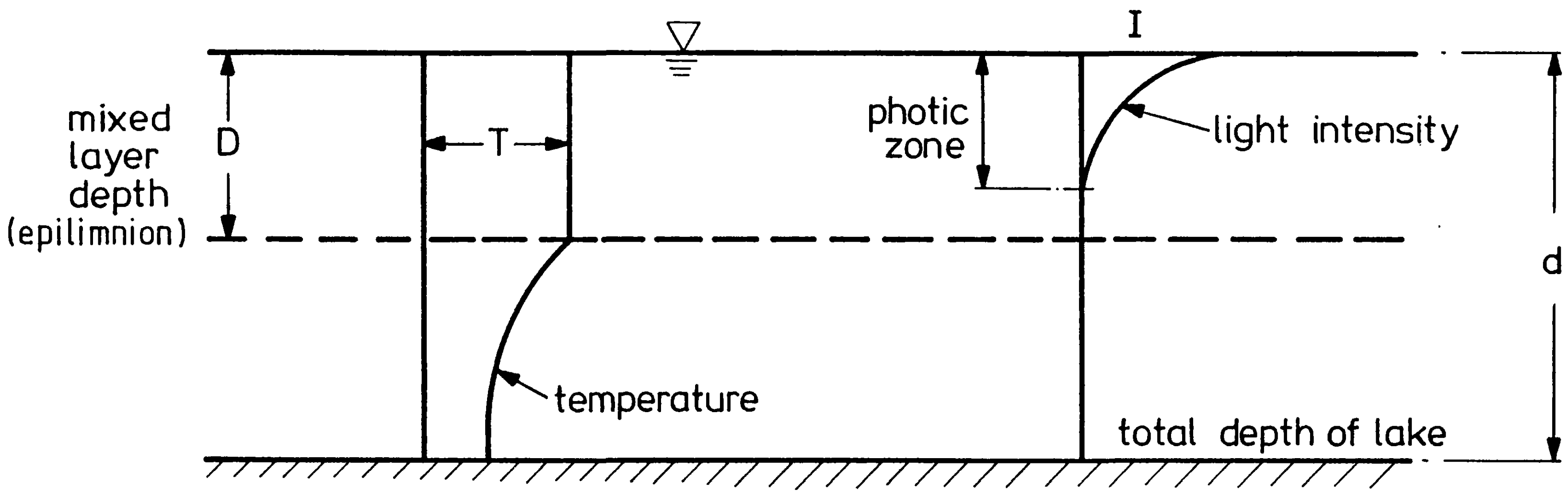

Fig. 1·2 Temperature and light distribution in stratified lakes.

SOME EFFECTS OF LANGMUIR CIRCULATION ON
SUSPENDED PARTICLES IN LAKES AND RESERVOIRS

CHAPTER 2 EFFECTS OF LANGMUIR CIRCULATION ON PARTICLE SUSPENSION - A review of existing models and an outline of the present study.

A review is made of previous investigations concerning the effects of Langmuir circulation on the distribution of particulate matters in the mixed layer of large water bodies and the associated sinking loss from this layer. The present study is then introduced. This offers an alternative approach, by accounting explicitly for the advection and turbulent transfer of particles within a Langmuir cell, to determine the relative significance of the circulation phenomena in modelling the distribution of suspended particles (e.g. phytoplankton).

CHAPTER 2 EFFECTS OF LANGMUIR CIRCULATION ON PARTICLE SUSPENSION - A review of existing models and an outline of the present study.

2.1 A Brief Review of Previous Field Investigations.

Few field observations concerning the distribution of particles in Langmuir cells have been published. Those reported are qualitative in nature and inadequate to illustrate how particles are aggregated in the cells. For instance, Stommel (1949) reported an observation in a lake that Langmuir circulations concentrate phytoplankton into linear arrays in the direction of the wind. Similar phenomena have also been observed in a shallow reservoir by George and Edwards (1973). Because the observed plankton include phytoplankton as well as zooplankton, the motility of the latter makes it impossible to separate how phytoplankton alone are affected by the circulation. Observations by Sutcliffe et al. (1971) that surface film and organic phosphate were concentrated in the convergences may perhaps indicate the ability of the circulation to aggregate buoyant particles, but its effects on the non-buoyant particles are not known. Therefore the rôle of Langmuir circulation in forming concentrations of particles and dictating both their distribution and sinking loss rates is not adequately described by the existing field observations.

2.2 Review of Existing Models.

Analytical models also have subsequently been used to give a more complete picture of how particles might be affected by

Langmuir circulation. Complex phenomena are being described, consequently few models exist which are worthy of close study. Two of these are reviewed below.

2.2.1 The Model of Stommel.

Following Langmuir's early observations and his speculation as to the existence of wind-driven circulation (Langmuir, 1938), the first analytical model designed to investigate the suspension and settling of solid particles in a series of steady helical cells (analogous to those proposed by Langmuir) was made by Stommel (1949). His study was initiated by an observation in a lake that a greater variability in plankton counts was obtained when net tows were taken up or down wind compared with those made across wind. Stommel considered whether Langmuir circulation was responsible for concentrating plankton in lines. Evaluating the trajectories of small particles sinking passively through steady regular convection cells of the Langmuir form (Fig. 2.1), his model showed that different types of trajectories were obtained depending on the ratio of the particle sinking velocity to the maximum upward velocity. Fig. 2.2 illustrates the trajectories of solid particles settling through a Langmuir cell under various conditions.

The case most relevant to the phytoplankton suspension problem is when particles fall (or ascend) at a lesser speed than the maximum vertical speed in the cells (Fig. 2.2B). His model showed that closed trajectories in the form of oval shaped "retention region" are developed in the upward currents, in which particles, once trapped, are retained, whilst particles outside the retention region sink out of the cells. The size of this retention region decreases with increasing particle sinking speed.

Although with laminar flow a "retention region" (i.e. a region that particles neither leave nor enter) exists, with turbulent flow a loss of particles occurs. The simplicity of Stommel's model is such that it is impossible to assess the likely distribution of particles in the circulation zone and the particle sinking loss from it. Nevertheless the idea of a retention region trapping some particles to re-circulate within the cell, leads to the general belief that the circulation is retaining particles which might otherwise sink out of the mixed layer.

Hutchinson (1967) extended Stommel's concepts to consider the means by which phototaxic organisms maintained a given depth despite moderate vertical movement (Fig. 2.2D). Later Smayda (1970) used these concepts to show that for marine diatoms with a relatively high sinking speed of 500 m/day in a weak circulation field, the ratio of the sinking speed to the maximum upwelling speed was within the range in which the circulation can be expected to influence the phytoplankton suspension. For typical sinking rates of most diatoms (typical sinking speeds ranging from 0.003 to 0.03 cm/s), his model showed that water current velocities of only 0.01 to 0.001 of those observed in the circulation cells would keep the bulk of phytoplankton species in suspension in the euphotic zone.

2.2.2 The Model of Titman and Kilham.

Since Stommel's work appeared in 1949, little further development occurred until 1976, when Titman and Kilham attempted to estimate the effect of Langmuir circulation pattern on the sinking loss rates of phytoplankton from the mixed layer. They modified Stommel's model of circulation to include the observation that the maximum upwelling speed is generally half of that of the maximum downwelling speed (Fig. 2.3A). A typical calculation assumed Langmuir circulation of 10 m depth, a particle sinking speed of 85 m/day, and a maximum rate of downwelling of 1 cm/s. This model used Stommel's particle trajectory method to separate Langmuir circulation into a retention region and an outside region from which particles could migrate from the cells (Fig. 2.3B).

Although Titman and Kilham's results indicate that particles may be kept in prolonged suspension within Langmuir circulation with a large reduction in sinking loss, certain aspects of their model are questionable, and this casts doubt on the results obtained. For example, their model is unclear in considering the partitioning of particles between the retention region and that outside. Similarly, the mechanism for transferring particles from the retention region and the subsequent sinking of these particles from the mixed layer lack credibility. The assumption of a constant exchange rate of 2.0 /day appears unrealistic and has no physical foundation. Such a turbulent transfer process should be dependent upon the turbulent intensity in the mixed layer, which may somehow be related, among other parameters, to wind speed and water stability. Their method of estimating particle loss rates is unsubstantiated and their approximation of the circulation shape to a square form is an oversimplification. It is evident that the physical representations of the circulation, its turbulent transfer processes, and the method of calculating loss rates from it, as used in Titman and Kilham's model,are unsatisfactory, and these will not be considered further.

2.3 The Present Study.

The ability of Langmuir circulation in keeping a significant volume of suspended particles to continually re-circulate within the mixed layer appears to be demonstrated. But the relationship between this re-circulation of particles to the particle aggregation and sinking loss cannot be adequately described by the available models and field investigations to date.

The problem could be investigated by making direct measurements of the variables concerned in a lake or reservior. For example, Rutherford (1976) suggested field measurements on certain labelled particles or organisms. Such measurements must be made across the circulation cells and over a wide range of prevailing winds, thermal conditions and turbulence structures. For complete understanding, the prevailing temperature profiles, turbulence distribution, velocity field, and particle concentrations, must be measured simultaneously. Such an experimental undertaking is, however, beyond the limit of the present technical capability (Fasham, 1978). In view of this limitation, a mathematical model study is a necessary step to justify the large-scale costly experimental project, and, in addition, provides a theoretical framework for such a field sampling programme.

The present study, with the following main objectives, is proposed:

1. To develop a mathematical model based on an advection-diffusion mass transport equation, in which particle transfers by water motion and turbulence are explicitly described, for investigating the influence of Langmuir circulation on particle distribution and sinking loss (Chapter 3);
2. To determine the significance of Langmuir circulation effects in the modelling of particle distribution and sinking loss in the

mixed layer, by comparing the results of the present two-dimensional model with those predicted by the conventional zero - (i.e. one-layer mixed compartment) and the one-dimensional models (Chapter 7);

3. To enhance understanding of the circulation phenomena by carrying out preliminary laboratory experiments, obtaining experimental evidence, and thereby exploring the possibility of physical modelling, within the laboratory, of the circulation phenomena (Chapter 8).

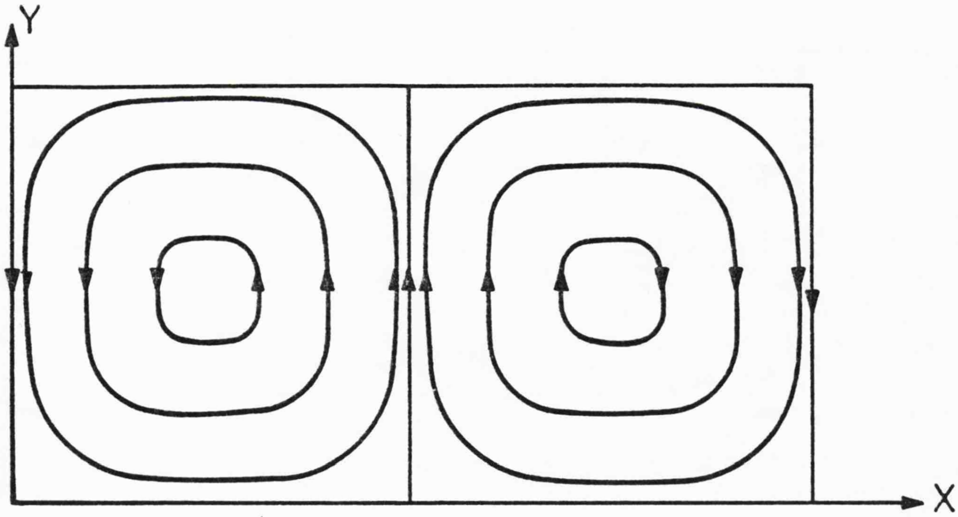

Fig. 2·1 The streamlines of an idealised vertical section across a pair of convection cells. The arrows show the direction of water flow.

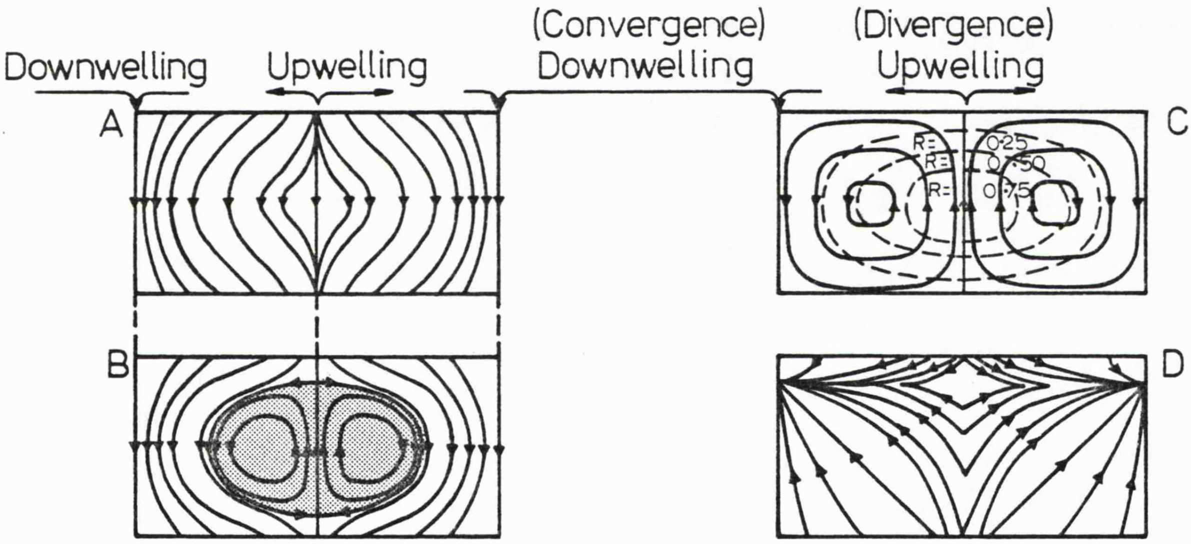

Fig. 2·2 The trajectories of phytoplankton cells settling through a Langmuir convection cell under various conditions. The streamlines represent direction of movement of phytoplankton with depth. To right of upwelling(convergence) area,convection cell rotates clockwise, and counter-clockwise to left. A, Trajectories of phytoplankton particles whose sinking speed is just sufficient to settle out of the convection cell (R = 1). B, Trajectories of phytoplankton particles whose sinking speed is one half (R = 0.5) of those in panel A. The shaded area represents a zone of closed trajectories, or the region of retention where phytoplankton cells swirl around; outside of this region they sink through the convection cell. C, Solid lines represent the streamlines of Langmuir convective motion. Dashed lines are the boundaries of the "regions of retention" for phytoplankton particles sinking at various speeds relative to that of current velocity (R values). D, Trajectories of mobile organisms seeking to maintain themselves below and near surface in convection cells leading to their accumulation in the convergences located approximately at the areas in D where the trajectories collect at the extreme left and right. A,B,C modified from Stommel(1949); D from Hutchinson(1967).

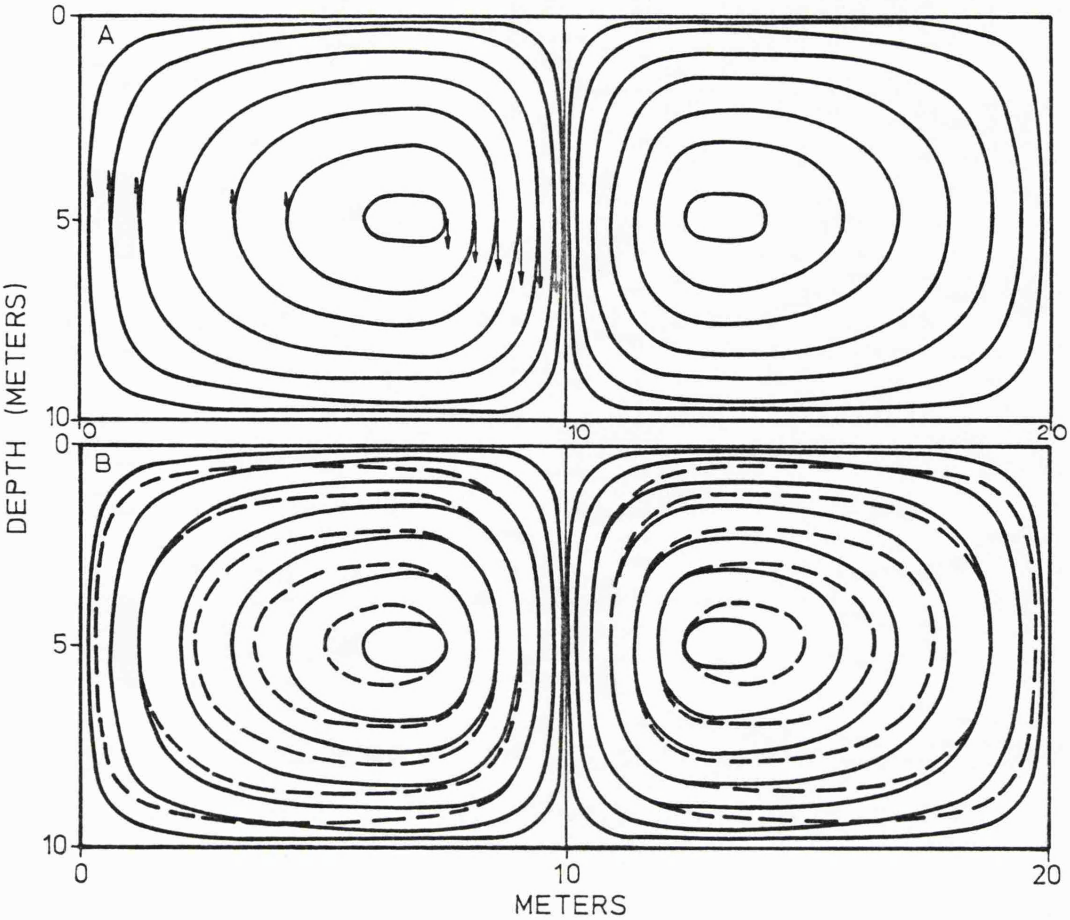

Fig 2·3 A, Vertical cross-section view of Langmuir circulation as produced by a model modified from Stommel (1949). Tangential vectors are velocity vectors. The solid closed curves are streamlines, paths followed by small parcels of water. The vertical scale is depth below the surface; horizontal scale is horizontal distance.
B, Streamlines of grapgh A on which are superimposed the trajectories followed by particles with a sinking rate of 85 m/day (broken line curves). The region within the outermost trajectory is the region of retention for particles of this sinking rate. (After Titman and Kilham (1976).

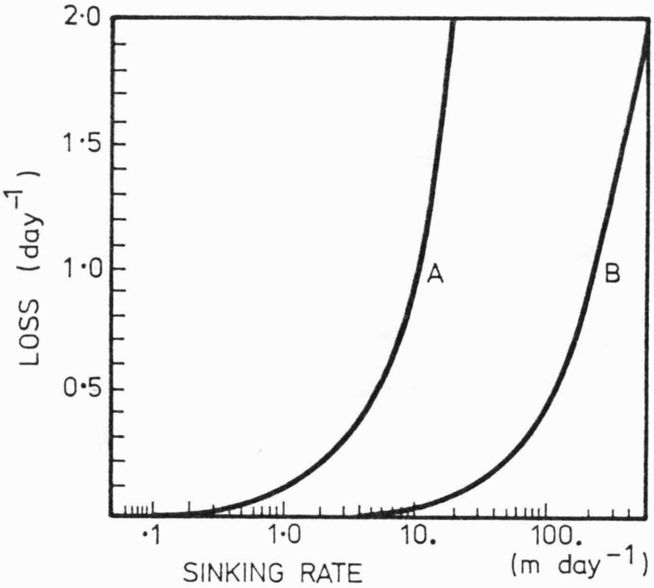

Fig 2·4 Loss rates for particles of various sinking rates as predicted by the algebraic relationship (loss = S.R./depth; curve A) and for the particles in the circulation system of Fig.2.3 (curve B). (After Titman and Kilham, 1976)

SOME EFFECTS OF LANGMUIR CIRCULATION ON
SUSPENDED PARTICLES IN LAKES AND RESERVOIRS

CHAPTER 3 THE MATHEMATICAL MODEL

The development of a model describing the distribution of suspended matter in a typical Langmuir cell is outlined, based on the simplified two-dimensional time dependent advection-diffusion mass transport equation for particles in turbulent flow. A general method of solution is briefly described.

CHAPTER 3 THE MATHEMATICAL MODEL

3.1 Basic Principles.

The dispersion of particles, such as phytoplankton and sediments, within the main body of turbulent flow may be represented by an advection-diffusion process. In this process, particle distribution results from combined action by local time-mean velocities and diffusion caused by both molecular and turbulent transfer. Such a representation has been found to explain adequately many particle-suspension problems, notably those associated with sediment transport and sedimentation.

The differential equation describing the time-distribution of conservative suspended material in a turbulent flow field is derived from the statement of the material mass conservation principle (Sayre, 1968), to give

$$\frac{\partial C}{\partial t} + U\frac{\partial C}{\partial x} + V\frac{\partial C}{\partial y} + W\frac{\partial C}{\partial z} = \frac{\partial}{\partial x}\left\{\varepsilon_x \frac{\partial C}{\partial x}\right\} + \frac{\partial}{\partial y}\left\{\varepsilon_y \frac{\partial C}{\partial y}\right\} + \frac{\partial}{\partial z}\left\{\varepsilon_z \frac{\partial C}{\partial z}\right\} \qquad (3.1)$$

in which

t = time;

x, y, z = cartesian coordinates;

C = turbulent-average concentration of material, expressed in mass per unit volume of suspension;

U, V, W = x, y, z components of water velocity, respectively;

$\varepsilon_x, \varepsilon_y, \varepsilon_z$ = corresponding turbulent diffusion coefficients which include molecular diffusivity.

For non-conservative materials such as phytoplankton, additional terms representing the rate of change of concentration caused by sources and sinks of the material, such as those produced by biological and chemical reactions, need to be added to the right-hand side of equation (3.1).

Considering equation (3.1), the first term on the left-hand side denotes the local change of concentration of material with time. The 2nd, 3rd and 4th terms are the advective fluxes of material. The terms on the right-hand side represent the diffusive fluxes of the material. Sayre (1968) discusses in detail the assumptions implicit in the derivation and application of this equation and notes that it describes the diffusion process satisfactorily if the substance is in solution form or if the solid particles to which it is applied are of low concentration, so that the volume occupied by the solids is negligible.

For small volume concentrations, equation (3.1) applied to the diffusion of suspended particles becomes

$$\frac{\partial C}{\partial t} + U_s \frac{\partial C}{\partial x} + V_s \frac{\partial C}{\partial y} + W_s \frac{\partial C}{\partial t} = \frac{\partial}{\partial x}\left\{\varepsilon_{sx} \frac{\partial C}{\partial x}\right\} + \frac{\partial}{\partial y}\left\{\varepsilon_{sy} \frac{\partial C}{\partial y}\right\} + \frac{\partial}{\partial z}\left\{\varepsilon_{sz} \frac{\partial C}{\partial z}\right\} \tag{3.2}$$

in which U_s, V_s and W_s are the velocity components of the suspended particles rather than the water velocity, and ε_{sx}, ε_{sy} and ε_{sz} denote the coefficients of diffusion for the suspended particles in the x, y, z directions, respectively. The solution of equation (3.2) yields the concentration distribution of particles, provided that the velocities and diffusion coefficients for the particles are known at all points and times throughout the flow system, together with the specifications of appropriate boundary conditions. Such provisions cannot be realised in practice and hence to achieve practical solutions various simplifications must be made to the equation.

3.2 Simplifications to the Basic Equation.

If the particles are smaller than the size of the smallest scale of turbulent eddies, they will tend to follow the turbulent components of the fluid. This situation is closely approximated by most suspended particles in lakes (e.g. for phytoplankton, the typical size range is about 5 μm to 1500 μm; its density is roughly 1.01 to 1.03 times that of water; and the smallest scale of turbulence in lakes is in the order of 1 cm or so). Such particles may be regarded as being passively carried by the water motion, and at the same time, sink slowly at their sinking speeds with respect to the surrounding water. Hence

$$\begin{aligned} u' &= u'_s , \\ v' &= v'_s , \\ w' &= w'_s , \\ U_s &= U , \\ V_s &= V , \\ W_s &= W + W_T \end{aligned} \tag{3.3}$$

are assumed to hold, in which U, V and W are the fluid velocity components and U_s, V_s and W_s are the solid particle velocities; W_T is the fall velocity or sinking speed in turbulent water; z - direction is taken to be positively downward; and the primed quantities are the velocity fluctuations. After combining the above equation with equation (3.2), the governing equation becomes

$$\frac{\partial C}{\partial t} + U\frac{\partial C}{\partial x} + V\frac{\partial C}{\partial y} + (W + W_T)\frac{\partial C}{\partial z} = \frac{\partial}{\partial x}\left(\varepsilon_{sx}\frac{\partial C}{\partial x}\right) + \frac{\partial}{\partial y}\left(\varepsilon_{sy}\frac{\partial C}{\partial y}\right) + \frac{\partial}{\partial z}\left(\varepsilon_{sz}\frac{\partial C}{\partial z}\right) . \tag{3.4}$$

Experiments have shown that for small particles within the Stokes' range, a condition satisfied by most phytoplankton and sediment particles in a lake, the mean fall velocity is approximately that in still water (Rouse, 1938; Brush et al., 1962; Murray, 1970). With this assumption the sinking speed can be measured directly or estimated analytically.

It is assumed that the mechanisms that control the mass and momentum transfer of fluid are identical (Reynolds' anology), i.e.

$$\varepsilon_M = \varepsilon_m \tag{3.5}$$

where ε_M is the eddy viscosity or coefficient of diffusion for momentum, and ε_m is that for fluid mass. The validity of the Reynolds analogy may be criticized since it can be argued, for instance, that the pressure fluctuations in turbulent fluid can transport momentum but not mass. However, Jobson and Sayre (1970) were among others who found experimentally that the turbulent diffusion coefficient for fluid mass, ε_m, is, at least as a first approximation, equal to the turbulent diffusion coefficient for momentum, ε_M. Now, if the solid particles follow the motion of the fluid, as explicitly assumed in equation (3.3), then an equality such as $\varepsilon_{si} = \varepsilon_i$, $i = x, y, z$ exists. Experimental evidence by Brush et al. (1962) shows that this assumption is valid for small particles within the Stokes' range. Therefore, in the present model it will be assumed that

$$\varepsilon_s = \varepsilon_M = \varepsilon_m \, . \tag{3.6}$$

For a more rigorous approach, a general relationship

$$\varepsilon_s = \beta \, \varepsilon_m \, , \tag{3.7}$$

could be used, in which β is a proportionality coefficient, which decreases from unity with increasing particle size, implying that large suspended particles have higher inertia and so do not respond to all the velocity fluctuations within flow.

With the above simplifications, equation (3.4) can now be written

$$\frac{\partial C}{\partial t} + U \frac{\partial C}{\partial x} + V \frac{\partial C}{\partial y} + (W + W_T) \frac{\partial C}{\partial z} = \frac{\partial}{\partial x} \left(\varepsilon_x \frac{\partial C}{\partial x} \right) + \frac{\partial}{\partial y} \left(\varepsilon_y \frac{\partial C}{\partial y} \right) + \frac{\partial}{\partial z} \left(\varepsilon_z \frac{\partial C}{\partial z} \right), \tag{3.8}$$

that is, the flow and diffusion parameters of the suspended particles, such as phytoplankton, in turbulent flow can be approximated by those of the flow, as well as by the particle sinking speed in still water.

So far the governing equation applies to the conservative or inert particles and may not be strictly satisfied by phytoplankton cells which are characterised by growth. In these circumstances an additional term representing the time-rate of change of concentration due to net growth, F (that is, the net balance between production by photosynthesis and loss rate by respiration, mortality, grazing, etc.), must be added to the mass balance equation. In its simplest form, this term can be expressed as

$$F = kC , \tag{3.9}$$

in which k is the net growth coefficient or net production rate, and C is the concentration of phytoplankton. Since the phytoplankton growth rate depends on several factors, such as nutrient conditions, light intensity, temperature, respiration rate of the cells, grazing rate, etc. (Rutherford, 1976), it cannot be reliably determined without complete knowledge of the influencing variables. For simplicity and to enable the phytoplankton suspension in Langmuir cells to be studied in isolation from other phenomena, growth rates are ignored, i.e. phytoplankton cells are assumed to behave similarly to inert particles.

3.3 The Simplified Governing Equation and General Method of Solution.

If the Langmuir circulation is essentially steady for a given environmental condition, and the time taken for it to become fully established is short compared with the time of interest, it can be considered that a fully-developed steady circulation flow field occurs simultaneously at the onset of the appropriate wind. Langmuir circulation is assumed to be orientated with its longitudinal axis parallel to the wind direction and extending across the lake and a typical Langmuir cell can be used to study effects on particle suspension. Since steady uniform motion of the water in the direction of the wind has no effect, other than to move particles uniformly in the direction of the wind, the problem may be considered to be two-dimensional and equation (3.8) reduced to

$$\frac{\partial C}{\partial t} + V \frac{\partial C}{\partial y} + (W + W_T) \frac{\partial C}{\partial z} = \frac{\partial}{\partial y} \left(\varepsilon_y \frac{\partial C}{\partial y} \right) + \frac{\partial}{\partial z} \left(\varepsilon_z \frac{\partial C}{\partial z} \right) . \qquad (3.10)$$

The x-axis is directed downwind, the z-axis positively downward from the origin at the lake surface, and the y-axis transversely along the water surface.

Equation (3.10) can be solved numerically, by integrating its finite difference approximation, for the spatial and temporal distribution of particle concentration within the Langmuir cell. To obtain the solution the following quantities must be specified:

(i) the extent of flow field, i.e. the width and depth of a Langmuir circulation;

(ii) the flow field and diffusion field, i.e. V, W, ε_y and ε_z of Langmuir circulation at all points and time;

(iii) the sinking speed of particles, W_T;

and (iv) appropriate initial and boundary conditions.

Since for a given condition, similar Langmuir cells are assumed to be formed, each being a mirror image of its adjacent cells, then a typical cell may be studied in isolation. The boundary conditions appropriate to this situation are:

(i) There will be no particles leaving the cell through the top and side boundaries;

(ii) Turbulent exchange of particles across the bottom boundary of the cell is neglected because of the suppression of turbulence there by very stable layers of underlying water. Only advective flux of material occurs across this boundary.

With such boundary conditions, a solution of the finite difference equation is marched forwards in time to give particle distribution in the cell at future successive time intervals. Other quantities, such as sinking loss through the bottom boundary of the circulation cell at various times are thereby estimated.

3.4 Non-dimensionalisation of the Governing Equation.

To obtain generalised data, equation (3.10) is non-dimensionalised using the following variables:-

$$
\begin{aligned}
C^* &= C/C_o ;\\
y^* &= y/L_o ;\\
z^* &= z/L_o ;\\
V^* &= V/U_o ;\\
W^* &= W/U_o ;\\
W_T^* &= W_T/U_o ;\\
\varepsilon^* &= \varepsilon/(L_o U_o) ;\\
\text{and} \quad t^* &= t/(L_o/U_o) ;
\end{aligned}
\tag{3.11}
$$

in which L_o is the characteristic length, U_o the characteristic velocity and C_o the characteristic reference concentration. The non-dimensional equation written in conservation form is then

$$
\frac{\partial C^*}{\partial t^*} + \frac{\partial}{\partial y^*} (V^* C^*) + \frac{\partial}{\partial z^*} \left[(W^* + W_T^*) C^* \right] = \frac{\partial}{\partial y^*} \left(\varepsilon_y^* \frac{\partial C^*}{\partial y} \right) + \frac{\partial}{\partial z^*} \left(\varepsilon_z^* \frac{C^*}{\partial z^*} \right)
\tag{3.12}
$$

The limits of integration become

y^* from 0 to $\lambda_c/(2\ L_o)$;

z^* from 0 to D/L_o ;

and t^* from 0 to $T^*(= T/(L_o/U_o))$;

in which λ_c is the convergence line spacing (twice the Langmuir circulation cell width) and T is the total time of simulation corresponding to a time interval over which the Langmuir circulation characteristics vary significantly.

The specification of Langmuir circulation variables, i.e. the cell geometry, velocity and turbulent diffusion fields will be discussed in Chapters 4 and 5. Finite differencing solution techniques, the handling of the boundary conditions, and values of the variables of the problem are deferred until Chapter 6. Further analyses of the basic numerical results, including the comparison of these with those from some typical zero- and one-dimensional models usually employed in water quality studies, follows in Chapter 7.

SOME EFFECTS OF LANGMUIR CIRCULATION ON
SUSPENDED PARTICLES IN LAKES AND RESERVOIRS

CHAPTER 4 LANGMUIR CIRCULATION OBSERVATIONS AND PARAMETER CORRELATION

Because of the present lack of a satisfactory Langmuir circulation theoretical model, published data on basic structures of the circulation, e.g. the shape, scale of motion, and associated velocities, are examined in some detail. The purpose of this is to obtain relevant information to aid the construction of an empirical model of the circulation for the present study, to be developed in Chapter 5, and to establish typical ranges of the circulation variables in lake and reservoir environment. Correlation relationships, which attempt to relate the circulation variables to the environmental parameters, such as wind/wave parameters, and the mixed layer depth, are also discussed.

CHAPTER 4 LANGMUIR CIRCULATION OBSERVATIONS AND PARAMETER CORRELATION

4.1 Introduction

Since Langmuir (1938) first produced evidence of the existence of roll vortices in the surface layers of lakes and oceans, which are now named after him, a number of theoretical explanations have been advanced for their generating mechanisms. As yet, no theory has received unanimous acceptance. Many have been shown to be inadequate (Scott et al., 1969; Faller, 1971; Pollard, 1977). The more recent and plausible ones tend to employ complex parameterisation and are often based on questionable assumptions that need justification. Because of the complexities, these models are not thoroughly tested. The theories of Langmuir circulation up to 1971 have been reviewed by Scott et al. (1969), Craik (1970) and Faller (1971). A review of the more recent developments is made by Pollard (1977). Although important, the theoretical explanation of the cause of Langmuir circulation is not directly relevant to the present study, which is concerned with the consequences of the circulation on suspended matter. However, a brief summary of these theories with references is tabulated in Table 4.1.

Despite the lack of an established and well-proven theory, the circulation's pattern and magnitude of flow, the scale of motion (e.g. the width and depth of the circulation), and the variations of these features with the changes in the prevailing conditions, may be established from field and laboratory observations. The empirical model derived by this prodedure can be useful, at least as a first approximation, in studying the consequences of the circulation on some processes in lakes. Because the literature often contains conflicting observations on Langmuir circulation variables, it is therefore necessary to examine observations in some detail.

4.2 General Features of the Circulation.

Observations made by Langmuir (1938) and by numerous other investigators (see Table 4.2) show clearly that when a sufficiently strong wind (above 3 m/s on the average) blows over lakes and oceans, a parallel system of organised roll-type vortices is rapidly formed below the water surface (Fig. 4.1), which may extend down to the bottom of the mixed layer. Velocity measurements indicate that the shape of the circulation takes the form of alternate left- and right-hand vortices, aligned more or less along wind, with the speed of downwelling water greater than that of the upwelling flow. The surface velocities are found to be strongest in the convergence zones (regions of downwelling), varying approximately sinusoidally across the cell width (Gordon, 1970; Langmuir, 1938). The difference between the downwelling and upwelling velocities (Langmuir, 1938; Myer, 1971; Maratos, 1971; Harris and Lott, 1973) suggests that the circulation cell is asymmetric, with the downwelling flow concentrated in a zone under the convergence line occupying a third or less of the cell width. Myer (1971) found that the onset of the circulation was characterised by downwelling under a newly formed streak, in a jet up to 1 m wide, which could penetrate through stable stratification (Fig. 4.2), and the width of the jet tended to increase with water stability. The observation by Welander (1963) also confirmed that the downwelling is in a form of concentrated jet.

4.3 Response to the Wind.

Langmuir circulation does not normally exist when the wind speed is less than about 3 m/s (Faller and Woodcock, 1964; Harris and Lott, 1973; Ichiye, 1967; Langmuir, 1938; Myer, 1971; Scott et al., 1969; Welander, 1963), though Katz et al. (1965) plotted the rib spacings in dye patches down to zero wind speed, and Ichiye remarked that striations in dye patches could exist even in calm seas if there was a pronounced swell. When the wind speed was less than 3 m/s, Myer observed the circulation to form in Lake George, New York, but this almost always occurred under surface cooling (unstable) conditions.

The response of the circulation to the wind appears to be relatively rapid. After the onset of winds larger than 3 m/s, Langmuir circulation develops within a few tens of minutes. Katz et al. recorded that, when the 5 m/s wind shifted through 70 degrees, the initial rib patterns consisting of three large ribs were broken up in 30 minutes, and a number of small ribs developed, aligning with the new wind direction. Langmuir noted lines of seaweed realigning themselves within 20 minutes when the wind direction shifted by 90 degrees. Scott et al. observed that streaks formed almost instantaneously in a lake when wind rose rapidly to speeds greater than 3 m/s. On the other hand, Maratos (1971) estimated that streak orientation responded within minutes to major wind shifts. Welander, however, suggested that the reorientation was initially confined to a relatively thin surface layer. He found that 10 minutes after a shift in 9 m/s wind, surface streaks had arranged themselves in the new wind direction and surface floats converged into these streaks, but the floats at 1 and 2 m depths continued to move in the original direction. The length of the response time was not measured by Welander.

It appears therefore that when the depth of the circulation is relatively shallow, such as in a lake situation, the response time is more rapid than with the much deeper circulation cells in the ocean. The response may begin at the surface, as described by Welander, and works its way down but, in all cases, the total response time is within a few tens of minutes or less.

4.4 Scale of Motion

The spacing between streaks or convergence lines is considered to be an indication of the lateral sizes of the Langmuir cells. Most investigators have reported that streak spacing is somewhat regular, implying that the cells are relatively uniform in size for a given set of meteorological conditions (Scott et al., 1969). Table 4.2 shows that the most frequently observed feature of Langmuir circulation is the row spacing, ranging from 2 to 25 m in lakes and from 2 to 300 m in the ocean. In many cases, cells of several different scales are reported to exist together at any one time. Langmuir (1938) reported 100 to 200 m streak spacing on the sea surface with smaller streaks in between, and in Lake George, New York, he noted that between well-defined, persistent streaks there were numerous smaller and less well-defined ones. When the mixed layer is very deep, Assaf et al. (1971) reported a hierarchy of two or three cell sizes coexisting in the ocean off Bermuda, and Harris and Lott (1973) stated that, in Lake Ontario, the distance between streaks (3-4 m) increased with time, new streaks forming between streaks already observed. Scott et al. (1969) said that one to three poorly-defined streaks frequently appeared between long, well-defined ones, and that the poorly-defined streaks disappeared quickly when the wind died. Faller and Woodcock (1964) may have observed the same phenomenon, though they assumed that the larger spacings they saw were actually two or three cell widths apart.

The reason for the occurrence of these poorly defined transient streaks is not clear. The streaks might be caused by the natural variability of the wind/wave field which tends to produce circulation cells of various sizes apart from the dominant ones, or it might be related to the dynamic features of Langmuir circulation during a transient period. Harris and Lott (1973) offered one explanation based on their observation of row spacings in Lake Ontario. They usually observed oil, fat, and other pollutants collecting in streaks, which made them visible. When such oil and fat streaks were carried down into the water column (as were leaves and flotsam in Langmuir's observation), their appearance between the existing streaks in the upwellings could account for the generation of new streaks between the existing ones, and this would explain the disappearance of the existing streaks. Harris and Lott often observed that every second streak is heavily marked by its surface film. Another explanation of the existence of small vortices (small scale streaks on the water surface) was given by Faller (1978). He had observed in a laboratory test that a light wind blowing over a regular pattern of relatively small amplitude waves could produce vigorous circulation. This, he believed, is the primary generating mechanism of Langmuir circulation. With irregular wind-generated waves the primary mechanism will generate transient circulation cells of many scales. Larger, secondary scales of circulation may form by non-linear interactions of the primary circulation cells, which may grow to dominate the entire pattern of flow throughout the fluid layer. However, it is often noted that the occurrences of many scales of circulation are more frequent under certain circumstances. In lakes, Myer (1971) reported that secondary streaks were often observed in cases of surface cooling (unstable). In larger bodies of water, such as the ocean or the Great Lakes, Assaf et al. (1971) had observed two coexistent sets of streaks under moderate winds (5 to 15 m/s wind speeds), with the spacing of the larger streaks equal to the depth of the mixed layer.

Observations that record all streak spacings, regardless of their appearance, may not be a good measure of the dominant scales deeper in the water. Katz et al.'s results supported this viewpoint, showing that, for the same wind, smaller convergence line spacings were measured at the surface than below. Myer's observations, based on the shapes of the isotherms and the motion of drouges, indicate the shallow existence of the small scale circulation and the increase of the circulation scale with depth (Myer, 1971).

The only explicit observations of the depth of Langmuir circulation (of the dominant scale), and hence the cell width to depth ratio, were made by Myer (1971). Taking the depth of the circulation to be the depth at which isotherm displacement was no longer observable, he found the penetration depths of 2 to 7 m in Lake George, New York, under stable (surface heating) conditions for 2 to 6 m/s winds. Following the interpretation made by Pollard (1976), Fig. 16 in Myer (1971) seems to indicate that the ratio of streak spacing to the penetration depth is about 1 to 3 under stable conditions and 0.2 to 0.3 for unstable conditions. Elsewhere in Myer (1968), typical values of this ratio for Lake George were also given, being about 1.4 for stable conditions and 0.3 if unstable. In the absence of any more relevant information, it is considered that these values be used, as a first approximation, to estimate the relative size of Langmuir circulation cells in inland lakes of moderate sizes.

The factors which control the circulation scales have not been unambiguously determined. Langmuir (1938) found, in Lake George, larger streak spacings (15 to 25 m) in October and November than in May and June (5 to 10 m), suggesting a correlation with depths of the seasonal thermocline. Scott et al. (1969) supported this observation, finding significant correlation between the streak separation and the depth to the first stable layer. Apparently in this case, Langmuir circulation in Lake George did not usually mix the diurnal heat input right down to the seasonal thermocline (at about 10 m depth) but formed a secondary thermocline a few metres above it. Other authors, for example Faller and Woodcock (1964), did not find this correlation with the depth of the thermocline, in the oceanic situations, to be significant. On the other hand, Faller and Woodcock (1964) and Maratos (1971) obtained significant correlation between wind speed and streak spacing, an observation not supported by Scott et al. (1969). However, with data obtained from Lake George, Myer (1971) noted a small increase in the mean streak spacing with increasing wind speed.

For oceanic cases, several correlated relationships have been reported for Langmuir circulation scale of motion (see Table 4.2). No unified relationship is evident. The general difficulty arises from lack of adequately comprehensive field data on Langmuir circulation (e.g. streak spacing, depth of the circulation or the depth of the induced mixed layer, upwelling and downwelling speeds), and those of prevailing environmental conditions (e.g. wind speed, and parameters associated with the state of surface waves, such as wavelength, wave height, fetch, wind duration, etc.). However, in lake and reservoir situations, there appears to be no relationship for the scale of Langmuir circulation in the literature. Although the data obtained in Lake George studies (e.g. Scott et al. (1969), and Myer (1971)) seem to be the most comprehensive to date, their nature prevents comparison with those from oceanic observations. For example, Scott et al. (1969)

measured all streaks regardless of their appearance, while Faller and Woodcock (1964) and Maratos (1971) apparently measured only the large-scale well-defined streaks. Faller (1971) attributed this observational difference to the effects of different heights of the observer's viewing, for the scale of the observed spacings often appears to be related to the size of the boat being used. Maratos (1971), on the other hand, measured row spacings from aerial photographs taken from a helicopter at some height (about 366 to 91 m) above the ocean.

4.5 Some Empirical Correlations between the Langmuir Circulation Scale of Motion and Wind/Wave Parameters.

The correlated relationships, referred to in the preceding section and summarised in Table 4.2, are based on statistical analyses of the observed data in order to relate the circulation scale of motion (the convergence line spacing and/or the circulation depth) to the wind speed (Faller and Woodcock, 1964; Katz et al., 1965; Maratos, 1971) or to the depth of the mixed layer (Faller and Woodcock, 1964; Maratos, 1971). Such simple relationships cannot be expected to portray adequately the response of the circulation scale of motion to the complex changes in the environmental state of the water body. However, in such a complex phenomenon involving several variables, the method of dimensional analysis may be applied to group the significant variables affecting the quantities under consideration. The resulting relationship can then be used to determine whether or not there is some form of generalised relationship between the non-dimensional variables.

4.5.1 Basic Rationale

To identify the significant variables affecting the circulation scale of motion, the following view of the phenomena is adopted.

Langmuir circulation is considered to be fundamentally generated by wind/wave interactions, and the resulting downwelling motion brings warm water downwards against density stratification to a depth where stability is strong enough to resist further penetration. This depth, where the balance between Langmuir circulation mixing and the stability of the water column occurs, corresponds to the depth of the mixed layer. Being inhibited at this depth, the downwelling water accumulates and spreads laterally forming some natural equilibrium scale of circulation appropriate to this depth and to the strength of the supplied downward energy. If this depth of penetration is shallow and the wind is strong, more water will be accumulated and consequently the width of the circulation cells increases. If the erosion of the stable interface is slow, then a quasi-equilibrium may be assumed to exist between the cell spacing, the depth of the cell, and the wind/wave actions which provide the energy to carry water downwards. Therefore, the row spacing (an indication of the lateral dimensions of Langmuir cells) is expected to be dependent, at least, upon the depth of the circulation (the mixed layer depth) and the parameters expressing the wind/wave action, i.e.

$$\lambda_c = \phi \text{ (D, wind/wave parameters)}, \tag{4.1}$$

in which λ_c is the cell spacing, and D is the cell depth.

Generally, the most basic parameters which govern the wind/wave actions are wind speed, fetch length and wind duration. However, if the combined effects of wind speed, fetch length and wind duration can be approximately described by a single characteristic parameter of the surface waves, such as the significant wave height ($H_{\frac{1}{3}}$), or the dominant wave length (λ_w), equation (4.1) may then be written in a non-dimensional form as

$$\frac{\lambda_c}{D} = f\left(\frac{H_{\frac{1}{3}}}{D} \quad \text{or} \quad \frac{\lambda_w}{D}\right) . \tag{4.2}$$

The functional relationship given by equation (4.2) forms a basis to test an approximate generalised relationship for Langmuir circulation scales. The choice of $H_{\frac{1}{3}}$ is deliberate so that the number of wind/wave variables can be reduced to a single parameter for easy comparison between data obtained from different places with varying wind speed, fetch length, and wind duration. When $H_{\frac{1}{3}}$ is not directly measured, some empirical relationships are available to relate it to wind speed, fetch length, and wind duration. For example, Wu (1973) proposed an empirical formula to predict wave growth with fetch under a steady wind, based on extensive correlated data of Wiegel (1964) from both natural situations and wind-wave tanks,

$$\frac{g\,H_{\frac{1}{3}}}{W_y^{\,2}} = 0.0031\left(\frac{gF}{W_y^{\,2}}\right)^{0.466} , \tag{4.3}$$

applicable for $gF/W_y^{\,2}$ less than 10^5, in which $H_{\frac{1}{3}}$ is the significant wave height (defined as the average height of the largest one-third waves); W_y is the wind speed at the anemometer height y (usually taken to be 10 m); g is the gravitational acceleration; and F is the fetch length.

Similarly, Bretschneider (1966) gave two empirical formulae, in which, for intermediate fetches, i.e. F_o ($= gF/W_{10}^2$) $<$ 1.4×10^4,

$$H_{\frac{1}{3}} = 2.4 \times 10^{-3} F_o^{\frac{1}{2}} \left(\frac{W_{10}^2}{g} \right) , \tag{4.4}$$

and, for fully-developed seas, i.e. $F_o \geq 1.4 \times 10^4$,

$$H_{\frac{1}{3}} = 0.28 \left(\frac{W_{10}^2}{g} \right) . \tag{4.5}$$

Equations (4.3), (4.4) and (4.5) are superimposed in the diagram taken from Wiegel (1964) (see Fig.4.3).

Unfortunately, since most published data on Langmuir circulations do not contain sufficient information to determine $H_{\frac{1}{3}}$, the more general correlations such as equation (4.2) cannot be tested. However, by the following reasoning, an approximate correlation test of oceanic data may be made.

Usually wave fields in open seas are not fetch-limited, and wave heights depend on wind speed and, to some extent, on the wind duration. For low wind speed blowing for some time, the wave field is very close to being fully developed (Bretschneider, 1966). In such a case, the significant wave height ($H_{\frac{1}{3}}$) depends on the wind speed alone (see equation 4.5). Hence

$$\lambda_c = \phi \, (D, W_n) , \tag{4.6}$$

in a non-dimensional form,

$$\frac{\lambda_c}{D} = f \left(\frac{W_n^2}{gD} \right) , \tag{4.7}$$

which may then be used to correlate the observed oceanic data.

4.5.2 Correlation of Oceanic Data

Available oceanic data of Maratos (1971) (W_n = 3 to 8 m/s; D = 9 to 11 m) and those of Faller and Woodcock (1964) (W_n = 4 to 11 m/s; D = 17 to 62 m), which cover a wide range of conditions, have been plotted in Fig. 4.4. The plotted results clearly suggest some form of correlation according to equation (4.7). There is one data point of Faller and Woodcock that deviates from this trend. This deviation may be caused by the uncertainty of row spacing measurements in the open sea. Because of lack of surface tracer, convergence zones can exist without being visible, so it is quite possible that this reading was taken for two, rather than one spacing. If this row spacing were reduced by half, then the plotted point would fall on the correlated trend. A curve has been drawn tentatively through the plotted points to indicate this trend. Bearing in mind the assumption made of a fully-developed sea, which may not be strictly valid, and the unsteady features of the row spacing, Fig. 4.4 is encouraging. Without any better correlations, it is suggested that it may be used to estimate the scale of Langmuir circulation at sea.

However, the results reported by Assaf et al. (1971) do not support this correlation. Assaf et al.'s results (W_n = 10 to 15 m, and D = 30 to 87 m) give the ratio of cell spacing to the mixed layer depth (λ_c/D) consistently about 1.0. No explanation can be given though it is possible that the reported cell spacings and wind speeds could have been subjected to some kind of averaging, thus affecting the results. Faller and Woodcock's results give the cell spacing to the mixed layer depth ratio of approximately 1.1 on the average, and so do those of Maratos. Thus it seems that, as a good first approximation, either the cell spacing of the Langmuir circulation that extend down to the mixed layer depth could be assumed to be equal to the mixed layer depth, or better still Fig. 4.4 could be used.

As far as lakes and reservoirs are concerned, there is no generalised relationship published for the scale of Langmuir circulation. Lake George data are perhaps the most comprehensive to date, but the reported data cannot be used to substantiate a relationship such as equation (4.2). To do this, characteristic variables pertinent to surface wind waves, in addition to those of Langmuir circulation, must be known. If the wave heights are not measured directly, at least fetch lengths with the corresponding wind speeds must be recorded, so that information concerning surface waves may be predicted by some empirical formulae such as equations (4.3) to (4.6).

4.5.3 Correlation with Wind/Wave Parameters

In the absence of better data, attention has reverted to laboratory tests on Langmuir circulation in order to obtain additional data to correlate the parameters.

Recent laboratory experiments on Langmuir circulations by Faller and Caponi (1978) show that the scale of Langmuir circulation may be related to the characteristic scale of the wind-generated surface waves. In these experiments, Langmuir circulation was generated by blowing air over the water surface. By introducing dye ($KMnO_4$) on to the bottom of the tank, the spacing of the cells which extended down the water depth was observed from the regular spacing of the longitudinal dye bands formed across the tank (Fig. 4.5). Faller and Caponi found that these row spacings were related to the scale of surface waves, represented by the average dominant wave length in their experiments. The results for various combinations of water depths (from 2 to 15 cm), fetch lengths (1.27 to 4.77 m), and winds (which produced wave lengths between 6 to 13 cm) were plotted in the non-dimensional form according to the relationship

$$\frac{\lambda_c}{D} = \phi\left(\frac{\lambda_w}{D}\right) \tag{4.8}$$

in Fig. 4.6, in which D is the water depth, taken to be the mixed layer depth in natural situations. It should be noted that equation (4.8) is basically the same as equation (4.2) discussed earlier. The use of a non-dimensional representation makes possible direct comparison with field observational data. Several field observations including those of Faller and Woodcock (1964) had also been plotted in Fig. 4.6, but these consistently fell at the lower end of the points plotted from laboratory data.

In the absence of specific records about surface waves, these oceanic data had been assumed to represent fully-developed seas and wave lengths were computed from an empirical formula given by Neumann and Pierson (1966). In view of uncertainties in laboratory and field measurements of wavelengths and row spacings, as well as other experimental errors, it is quite plausible that a universal relationship in the form of equation (4.8) may exist. A smooth curve drawn through the cluster of experimental points, passing generally to the left of the oecanic data to account for the possibility that the sea might not be fully-developed, demonstrates the relationship

$$\frac{\lambda_c}{D} = 4.8 \left[1 - \exp\left(- 0.5 \frac{\lambda_w}{D}\right)\right] \quad , \tag{4.9}$$

in which D is the water depth in the wind-wave tank or the mixed layer depth for natural cases; λ_w is the dominant wave length of the surface waves. The scattering of the oceanic data was attributed to the influences of such factors as the surface heat flux, internal waves, the strength of the thermocline, etc., which may not be significant in the laboratory tank. Faller and Caponi (1978) also discussed in detail some other lines of reasoning that equation (4.9) might not be applicable as a universal relationship.

In order to corroborate Faller and Caponi's results, an essentially similar experiment was conducted by the author (Chapter 8). Results obtained, also plotted in Fig. 4.6, follow those of Faller and Caponi. In this experiment the significant wave height ($H_{\frac{1}{3}}$) was also measured and used as the principal variable rather than the wave length. Results according to equation (4.2), i.e. $\lambda_c/D = \phi(H_{\frac{1}{3}}/D)$, are given in Fig. 4.7. The figure shows that the scale of Langmuir circulation can also be correlated by equation (4.2), and a smooth curve has tentatively been fitted through the plotted points. It should be noted that these results are no more accurate than those used to establish equation (4.9).

To test the prediction of Langmuir cell scale of motion for fetch-limited situations such as those in lakes and reservoirs, a typical state of water surface leading to streaking in Lake George as given in Liebovich and Ulrich (1972) may be used: values for wavelengths varying from 2 to 4 m, the average amplitude of the order of 4 cm when the wind speed is 4 to 5 m/s. For this wind speed, the typical depth of Langmuir circulation (or mixed layer) estimated from Myer's (1971) data is about 3 m. Taking $H_{\frac{1}{3}}$ to be 1.61 times the average wave height, as suggested by Wiegel (1964), $H_{\frac{1}{3}}$ is estimated to be 12.3 cm, which leads to $H_{\frac{1}{3}}/D = 0.0234$ and $\lambda_w/D = 0.545$. Curves in Fig. 4.6 and 4.7 predict the ratio of row spacing to cell depth of 1.3, which lies in the range of value 1 to 3 reported in Myer (1968, 1971). Myer also quotes a typical value as 1.4. Another condition given by George and Edwards (1973, 1976) for a shallow reservoir has been considered. In Eglwys Nynydd in Wales, Langmuir circulations with row spacings of 4 to 6 m were observed to extend to the bottom of the reservoir, whose depth is 3.5 m on the average. Taking a typical wind speed to be 4 to 6 m/s and the fetch length of 800 m for the mid-lake conditions, $H_{\frac{1}{3}}/D$ is estimated to be 0.029 and this, by Fig. 4.7, gives a predicted value of $\lambda_c/D = 1.5$. Comparing this predicted value with the observed cell spacing to depth ratios of 1.14 to 1.70, with an average of 1.43, the prediction by Fig. 4.7 is considered satisfactory.

Since no better methods exist for the prediction of Langmuir circulation scale, the correlation given by Fig. 4.7 in terms of the significant wave height is used to give an estimate of the relative size of Langmuir circulation cells in lakes.

More accurate and extensive observations in laboratories and natural situations and a significant overlap of the data are desirable in order to substantiate equations (4.2) and (4.9). In laboratory experiments conducted so far, the relative scale of wave height to the depth of mixed layer is large and probably not realised in the natural situation. In real situations, however, the scale of the waves is relatively small especially in the fetch-limited situations. Therefore most prototype data fall on the lower end of the scale. But while one can rationalise the difference between the two types of observations so that a single curve appears to fit all data, it may be argued that the two classes of data arise from different physical situations and thus may not fall on the same curve.

4.6 Velocity Observations and Correlations

There is unanimous agreement that the surface velocity in the direction of the wind is larger in convergence or streak zones than out of them. Langmuir laid a cord on the surface perpendicular to the streak lines and noted that it developed well-defined waves, forwards (in the direction of the wind) in the streaks and backwards out of them (see Fig. 4.1). Gordon (1970), Harris and Lott (1973), Ichiye (1967), and Katz et al. (1965) using computer cards and dye have all noted the same effects and have variously estimated the shear velocity between the flow in the convergence and divergence zones as 1 to 3, 5 to 10, 6 and 17 cm/s.

There have been several attempts to measure the downwelling velocity in the convergence zone, and the corresponding upwelling between them. Langmuir, Scott et al., Sutcliffe et al. (1963) and Harris and Lott used drag plate current meters. Langmuir also watched the downward motion of dye in a convergence zone, while Gordon estimated the upwelling velocity from the rate of divergence of coloured dye. Myer (1971), in addition to dye studies, estimated vertical velocities from the displacement of isotherms (Fig. 4.2). He found the downward motion to be concentrated in the form of narrow jets under streaks (i.e. 0.2 to 1 m; c/f the observed row spacings of 2 to 10 m) with the downwelling velocity increased from the surface and maximum at about half the depth of the circulation (the depth at which isotherm displacement was no longer observable). Myer observed that the downwelling speed appeared to decrease below this maximum to zero at some lower depth. From repeated crossing of the same streak, maximum downwelling speeds in the jet were estimated to be 2 to3 cm/s in stable conditions, and 5 cm/s or more in unstable conditions. Woodcock (1950) measured the vertical velocity necessary to submerge the pelagic Sargassum that accumulate in the streaks. Maratos (1971) compared the sinking rate of fine sand in and between the streak zones with the sinking rates in still water to estimate the vertical velocities in Langmuir circulation.

Faller (1971) reviewed data on downwelling (prior to 1971) and correlated the vertical downward velocity (w_d) with the wind speed (W_n) by

$$w_d = 0.85 \times 10^{-2} W_n, \text{ for } W_n > 3 \text{ m/s}, \tag{4.10}$$

which gives the downwelling speed roughly 1 cm/s per 1 m/s wind. The plot of w_d v.s. W_n as published by Scott et al. (1969), which includes data of Sutcliffe et al. (1963), Woodcock (1944), as well as data collected from Lake George, is shown in Fig. 4.8, on which equation (4.10) is represented. Harris and Lott's (1973) data from Lake Ontario have also been plotted and these can be fitted approximately on the same straight line, though some scatter of points about the line is observed. The scatter of Lake Ontario data may probably indicate that w_d is not dependent solely on W_n. Recalling the previous discussion that Langmuir circulation may be related to wind/wave action, a speculated correlation therefore is,

$$\frac{w_d^{\,2}}{gD} = \phi\left(\frac{H_{\frac{1}{3}}}{D}\right) . \tag{4.11}$$

For oceanic situation, where $H_{\frac{1}{3}}$ can be described by wind speed, this relation becomes

$$\frac{w_d^{\,2}}{gD} = \phi\left(\frac{W_n^2}{gD}\right) . \qquad (4.12)$$

Whether or not these correlations are valid cannot easily be tested from the existing published data, because not all relevant parameters required in equations (4.11) and (4.12) were measured in the field test programmes. For the present, therefore, equation (4.10) will be used to compute the maximum downwelling velocity.

So far as is known, complete measurements of the velocity fields associated with Langmuir circulation have never been attempted, for example, very few observers have measured upwelling velocities. Langmuir (1938) estimated the upwelling rate between dye streaks as 1 to1.5 cm/s, about one-half of the downwelling velocity, which he observed. Gordon's (1970) estimate, made from dye observations, was similar.

A few references to horizontal velocity measurement perpendicular to the wind can be found (Langmuir, 1938 ; Woodcock, 1944 ; Harris and Lott, 1973). Although these velocities can be inferred from the convergence of floating materials into streaks, only Langmuir has estimated their magnitude. By tracking surface debris he estimated a transverse velocity to be 2 to 3 cm/s.

TABLE 4.1

Theories of Langmuir Circulation (mainly after Pollard (1976))

Theory	Origin	Present status
Convective instability, rolls aligned by wind.	Analogy with atmospheric boundary layer, see review by Kuettner (1971).	Not a primary mechanism, as cells often observed to grow in stable conditions and break down stable stratification.
Coupling with atmospheric rolls.	Unknown, mentioned by Stommel (1951).	Discontinued, atmospheric vortices move too fast over ocean surface.
Modification of wind over surface slicks.	Welander (1963).	Discontinued, atmospheric vortices move too fast over ocean surface; energy supply 100 times too small (Myer, 1971).
Instability of Ekman spiral.	Faller (1964).	Not a primary mechanism, cannot account for the observed growth rates.
Damping of capillary waves in slicks provides radiational stress to drive rolls.	Kraus (1967); a forerunner of Garret's (1976) theory below.	Discontinued, as cells may exist in the absence of surface contaminants. Also energy supplied too small to explain the observed rates.
Interaction of two linear wave-trains.	Stewart and Schmitt (1968)	Discontinued, cannot provide vorticity.
"Eddy pressure" of surface waves.	Faller (1969).	Discontinued, cannot provide vorticity.
Interaction of pairs of inviscid wave trains in in a shear flow.	Craik (1970).	Discontinued by Leibovich and Ulrich (1972), inviscid theory creates vorticity of wrong sign.
Instability of shear flow in a rotating system.	Gammelsrød (1975).	Appears unlikely, basic state doubtful, predict cell structure in conflict with observations (Pollard, 1976); cells cannot grow to detectable level (Leibovich and Radhakrisnan, 1977).
Interaction of pairs of viscous wave trains in a shear flow.	Craik and Leibovich (1976).	Appears unlikely, predicts maximum wave amplitudes in divergence zones in conflict with observations.
Interaction of waves and surface current, with wave dissipation (a "feed-back loop"	Garrett (1976)	Qualitatively, can explain all observed features of circulations; requires quantitative testing (Pollard, 1976); model deviates from the understood usage of wave-mean-flow interaction analysis, several assumptions need justification (Leibovich and Radhakrisnan, 1977; Mobley and Faller, 1977).
Interaction of wave trains with shear flow.	Leibovich (1977), Leibovich and Radhakrisman (1977).	Time-independent version of basically the same model of Craik and Leibovich (1976); under conditions appropriate for the action of the model mechanism, numerical solution of primitive Navier-Stokes equations shows no Langmuir circulations (Mobley and Faller, 1977); wave height highest in upwelling regions in conflict with observations, but authors raise doubt about field observations; untested.
Interaction of wind and pairs of wave trains, an integration of Navier-Stokes equations.	Mobley and Faller (1977)	Early yet in development, still some doubt as the rate of growth of vortices heavily depends on the grid size used in numerical integration; untested.
Instability of random wave field with an average uniform Stokes' drift, likened to thermal convective instability.	Craik (1977), Leibovich (1977b).	General physical processes similar to Craik and Leibovich (1976) and Leibovich (1977a), probably would fail (Mobley and Faller, 1977); untested.

TABLE 4.2

Some Observations of Langmuir Circulation

(mainly after Pollard (1976))

NOTE: Depths of mixed layer are invariably assumed to be equivalent to depth scale of circulations

Author	Ocean or Lake	Row spacing		Depth of mixed layer (m)	Vertical velocity		Forward velocity in convergence zone (cm/s)	Reorientation time (min.)	Minimum wind speed (m/s)	Other comments
		(m)	comments		(cm/s)	Down or up				
Langmuir (1938)	Lake George	5–10 15–25	May–June Oct.–Nov. wind $\sim$ 4–8 m/s	10–15 m	1–2 2–3 1–1.5 for wind $\sim$ 6 m/s	down (avg. 0–6 m) down (at 2 m) and up	> 0	20	4	
	Ocean	100–200						20		
Woodcock (1950)	Ocean				> 3	down			4	
Stommel (1951)	Pond on Cape Cod			Less than 30 cm deep				1–2		
Sutcliffe et al. (1963)	Ocean				3–6	down			$\sim$ 3	Downwelling speed (W_d) appears directly proportional to wind speed (W_n). $\underset{(cm/s)}{W_d} = 0.82 \times 10^2 \underset{(m/s)}{W_n}$
Welander (1963)	Baltic Sea	8	wind 8–9 m/s					10	5	
Faller and Woodcock (1964)	Ocean	20–50	wind 4–11 m/s	17–62					3	Wind W_n and row spacing R correlated, $\underset{(m)}{\overline{R}} = 4.8 \times \underset{(m/s)}{\overline{W_n}}$ Depth D and wind W_n correlated, $\underset{(m)}{\overline{D}} = 4.0 \times \underset{(m/s)}{\overline{W_n}}$ $\overline{R}/\overline{D}$ = 1.1 on average

TABLE 4.2 (continued (2))

Author	Ocean or Lake	Row spacing (m)	Row spacing comments	Depth of mixed layer (m)	Vertical velocity (cm/s)	Vertical velocity Down or up	Forward velocity in convergence zone (cm/s)	Reorientation time (min.)	Minimum wind speed (m/s)	Other comments
Katz et al. (1965)	Ocean	2–10 10–45	surface 0–7m(deep)				> 0	30		Wind W_n and row spacing R correlated $\underset{(m)}{R} = 4.0 \times \underset{(m/s)}{W_n}$
Owen (1966)	Ocean	1.5		thermocline depth 40 m	0.2	down				Calm, thermally driven (not Langmuir circulations), only 61 cm deep
Ichiye (1967)	Ocean	20–200	Actually quotes "tens to hundreds metres"				17			
Scott et al. (1969)	Lake George		"All streaks measured regardless of appearances"	1.5–8.5 (depth of first stable layer)	4–7 (vary with wind speed)	down (collected results prior to 1969)		"almost instantaneous"	3 for persistent streaks	Row spacing R and depth to first stable layer correlated; Wind W_n and depth to stable layer correlated (a plot given); Confirms asymmetrical shape of circulations; $w_d(m/s) = 0.85 \times 10^{-2}\ W_n(m/s)$ from plot
Gordon (1970)	Ocean	5			1.5	up for wind 4.6 m/s	1–3 (3.5 cm/s for 4.6 m/s wind, varies sinusoidally across circulation width)			
Assaf et al. (1971)	Ocean	3–6 5–12 30–50 90–300	calm Hierarchy in 5–15 m/s wind	7–300			5–10			Medium row spacings same order of magnitude as the mixed layer depth, and $R/D \approx 1$ for this group
Maratos (1971)	Ocean	6–16	for wind $\sim$ 3–8 m/s	9–11	2.2 0.8	down up for wind 6 m/s		2–4		R = 0.5 to 1.5 times thermocline depth D; $\overline{\frac{R}{D}}$ on average = 1.1; R and W_n correlated, $R(m) = 0.1 + 2.8 \times W_n(m/s)$;

TABLE 4.2 (continued (3))

Author	Ocean or Lake	Row spacing (m)	Row spacing comments	Depth of mixed layer (m)	Vertical velocity (cm/s)	Vertical velocity Down or up	Forward velocity in convergence zone (cm/s)	Reorientation time (min.)	Minimum wind speed (m/s)	Other comments
George and Edwards (1973)	shallow reservoir	4–6		circulations extended down to bottom, average depth 3.5 m				4		R/D = 2 to 2.83
Myer (1971)	Lake George	1–5 2–11	wind 4 m/s wind 8 m/s	2–7 (depth to first stable layer, for stable conditions)	2–3 5	down (stable) down (unstable)				"All spacings measured regardless of appearance"; Width of warm jet ~ 0.1–0.7 m (stable); Max. downwelling occurs ~ at mid depth under streak.
Myer (1968)	Lake George	——— Basically the same as Myer (1971) ———								R/D = 1.4 (typical) for stable conditions; = 0.3 (typical) for unstable. (Stable and unstable refer to surface heating and cooling, respectively.)
Harris and Lott (1973)	Lake Ontario	3–4			2–9 for various winds	down	< 6		2 (unstable) 3 (stable)	Downwelling speed and wind speed correlated (plot given); Downwelling speed correlated with stability parameter (Monin – Obukov length)(plot given).
Faller (1969)	Wind-wave tank experiment		observed from dye bands on the tank bottom	taken to be depth of water				too short to measure; but almost instantaneous as soon as gravity waves appear		R/D = 2.5 to 3.0
Faller (1971) (a review)	"		"	"						Confirms R/D = 2.5 to 3.0 ; quoted observation by van Straatan in shallow water of depth 9 cm, and R/D = 4.4 .
Faller and Caponi (1977, 1978)	"		" and floats spacings on surface	" water depth 2–15 cm				"		$\frac{R}{D}$ and $\frac{\lambda_W}{D}$ correlated by, $\frac{R}{D} = 4.8\,(1 - \exp(-0.5\frac{\lambda_W}{D}))$, where λ_W = "dominant" wave length of surface waves.

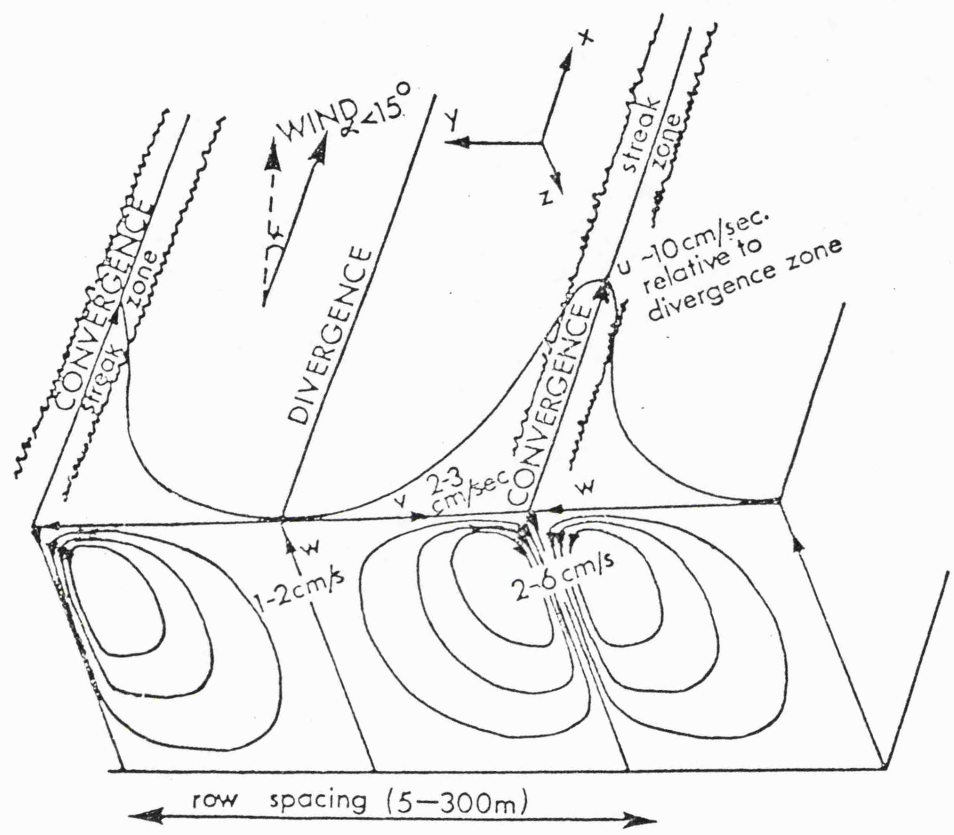

Fig. 4.1 Schematic diagram of Langmuir circulations (After Pollard, 1976)

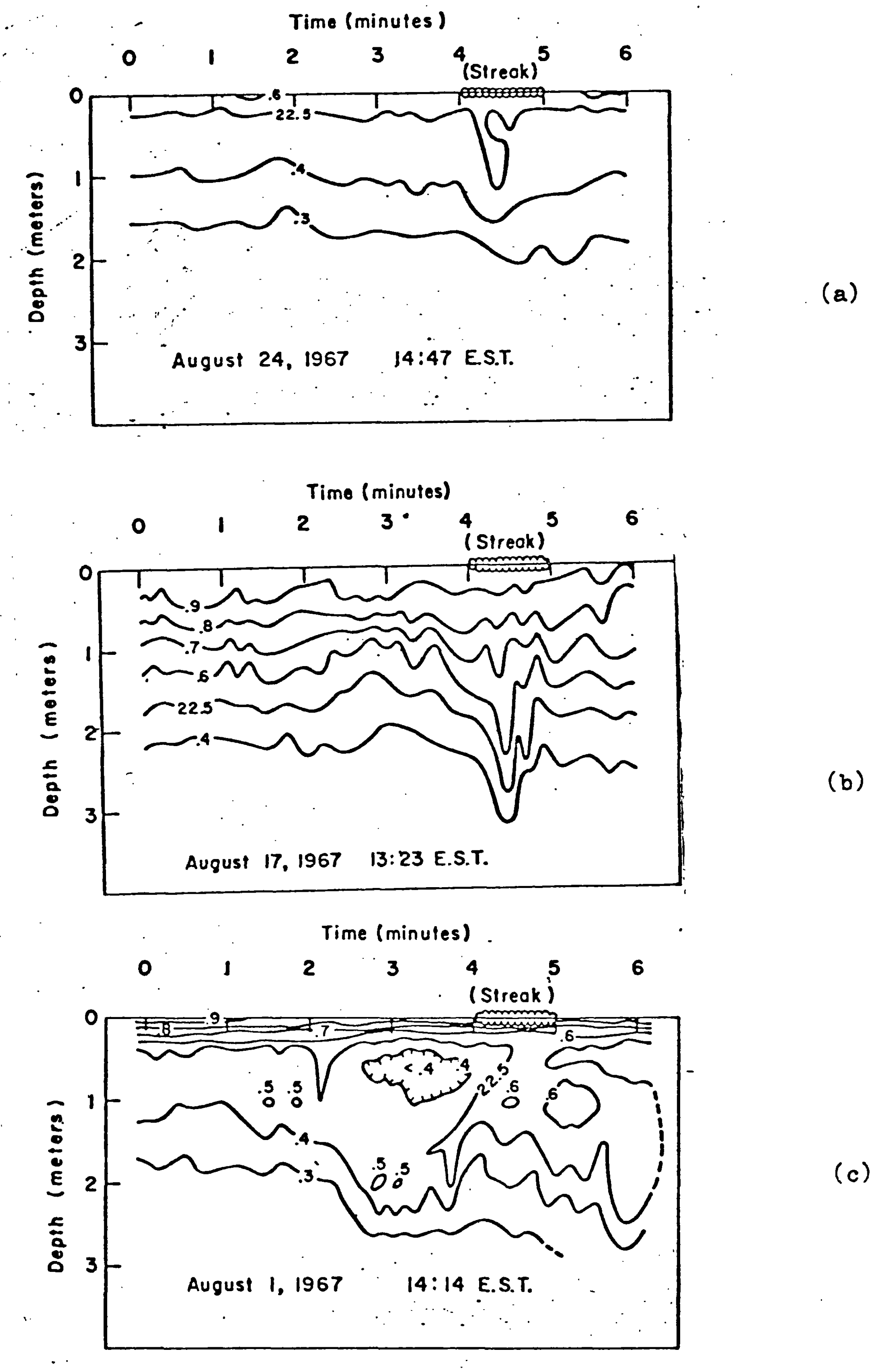

Fig. 4.2 Downwelling velocities under streaks breaking through stable stratification (from Scott,et al.,1969)
(a) Thermal structure near the surface layer for a case in which streaking was just beginning. First streaks were observed at 3 minutes after time zero. (b) Streaking had been observed at 1 minute past time zero. (c) Streaking had been observed for more than 10 minutes. (After Myer, 1968)

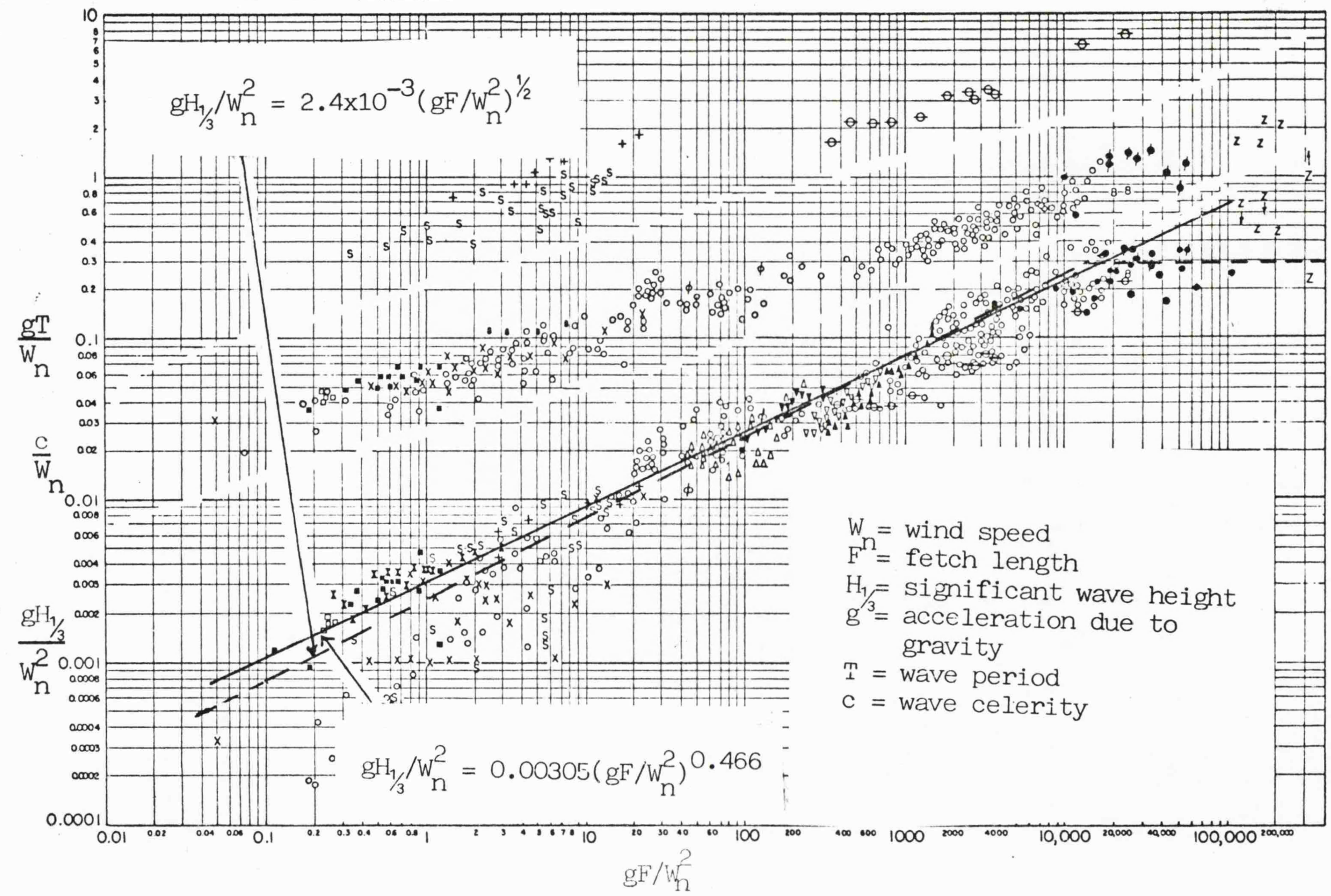

Fig. 4.3 Correlation between wind speeds and wave heights.
(after Wiegel, 1966)

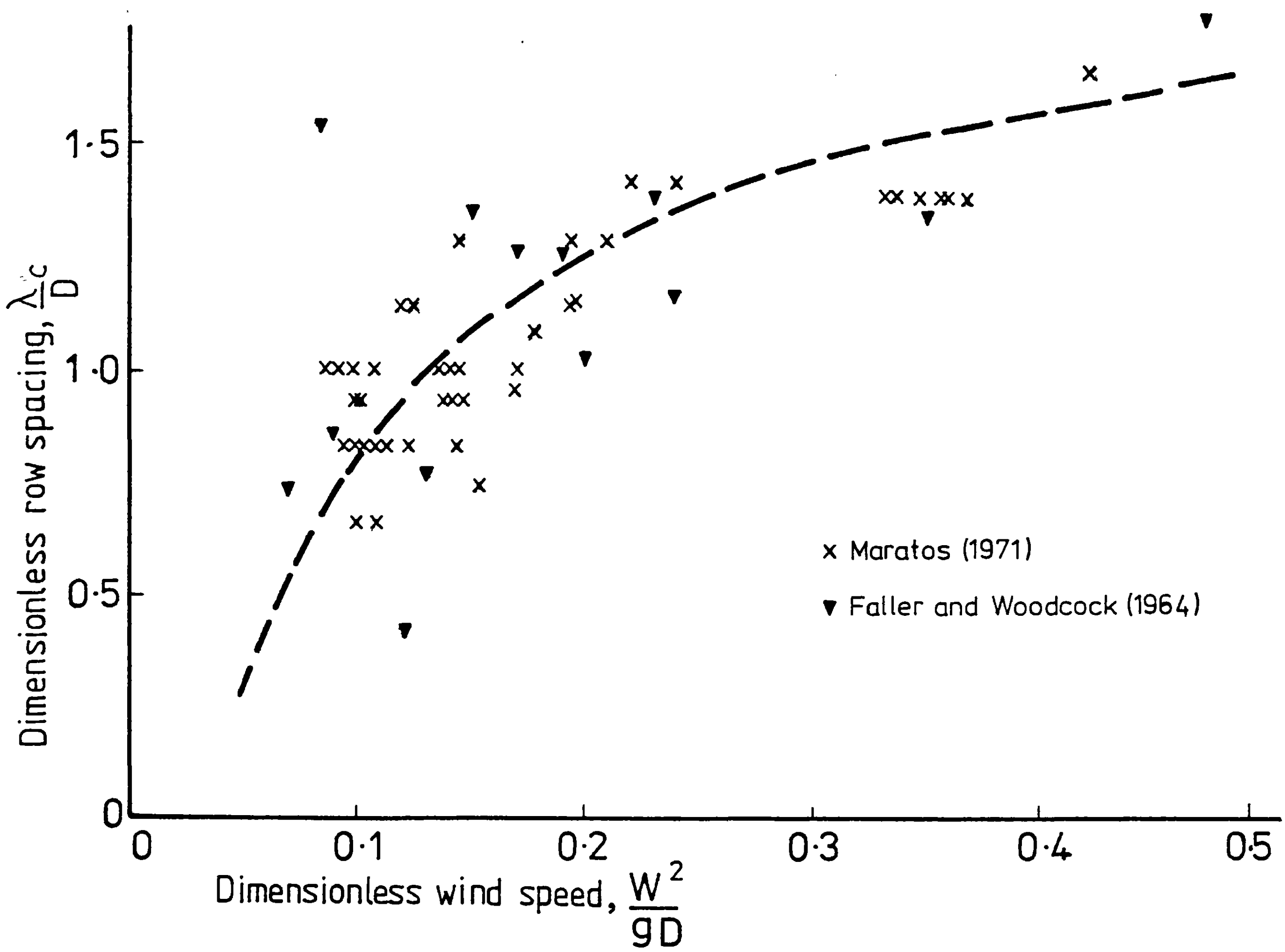

Fig.4·4 Correlation between the row spacings with wind speed and depth of the mixed layer (oceanic data).

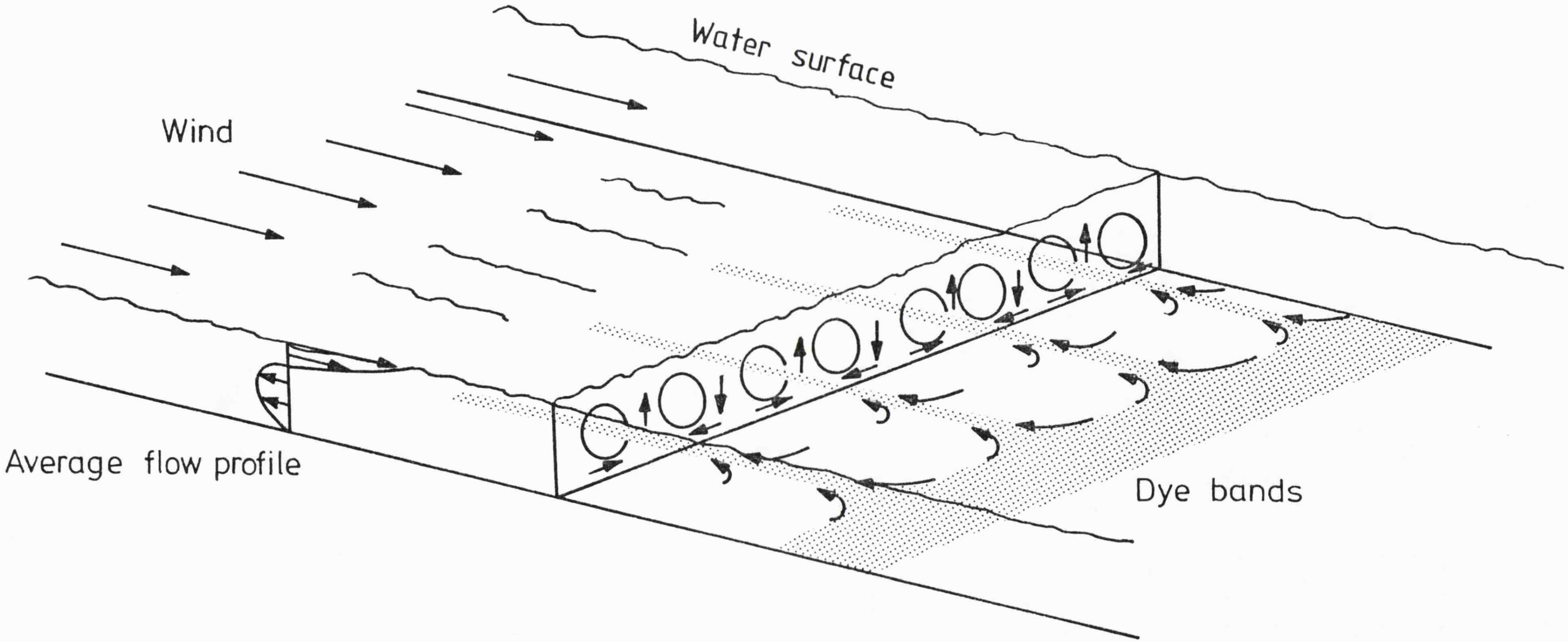

Fig. 4·5 A schematic diagram showing the convergence of dye at the bottom of the wind-wave tank due to the action of Langmuir circulations.
(After Faller and Caponi, 1977)

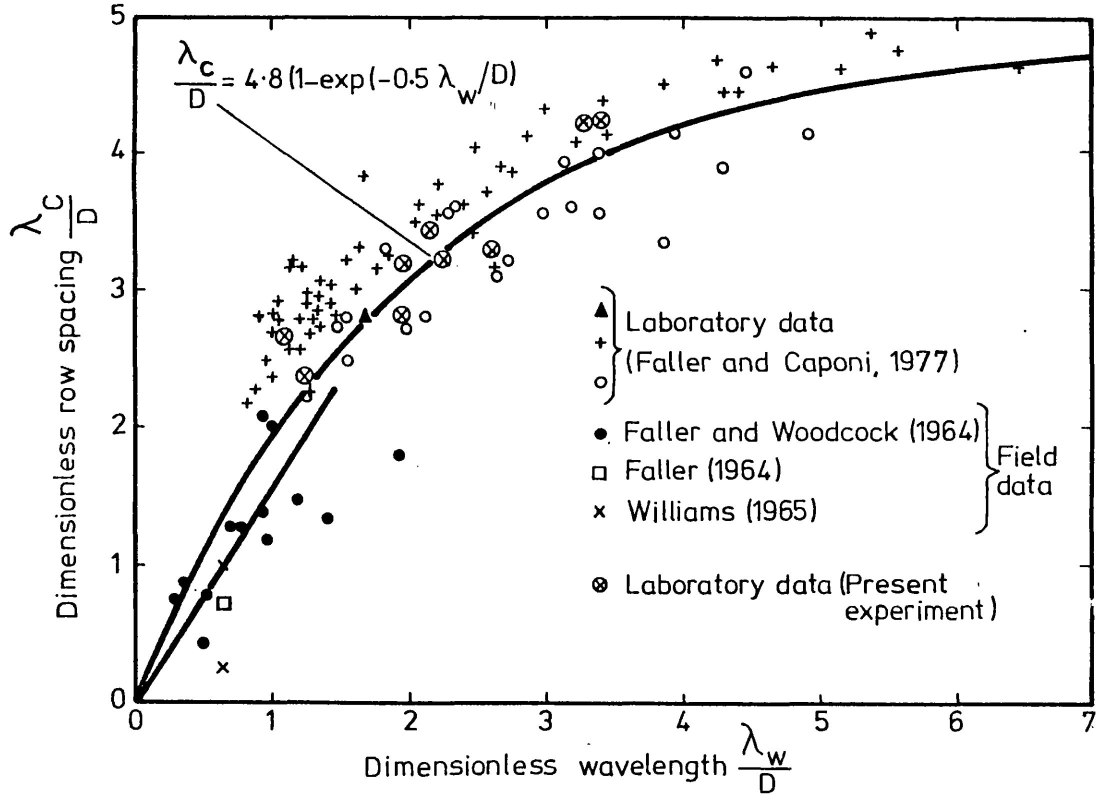

Fig. 4·6 Correlation between row spacings and dominant wave Lengths.

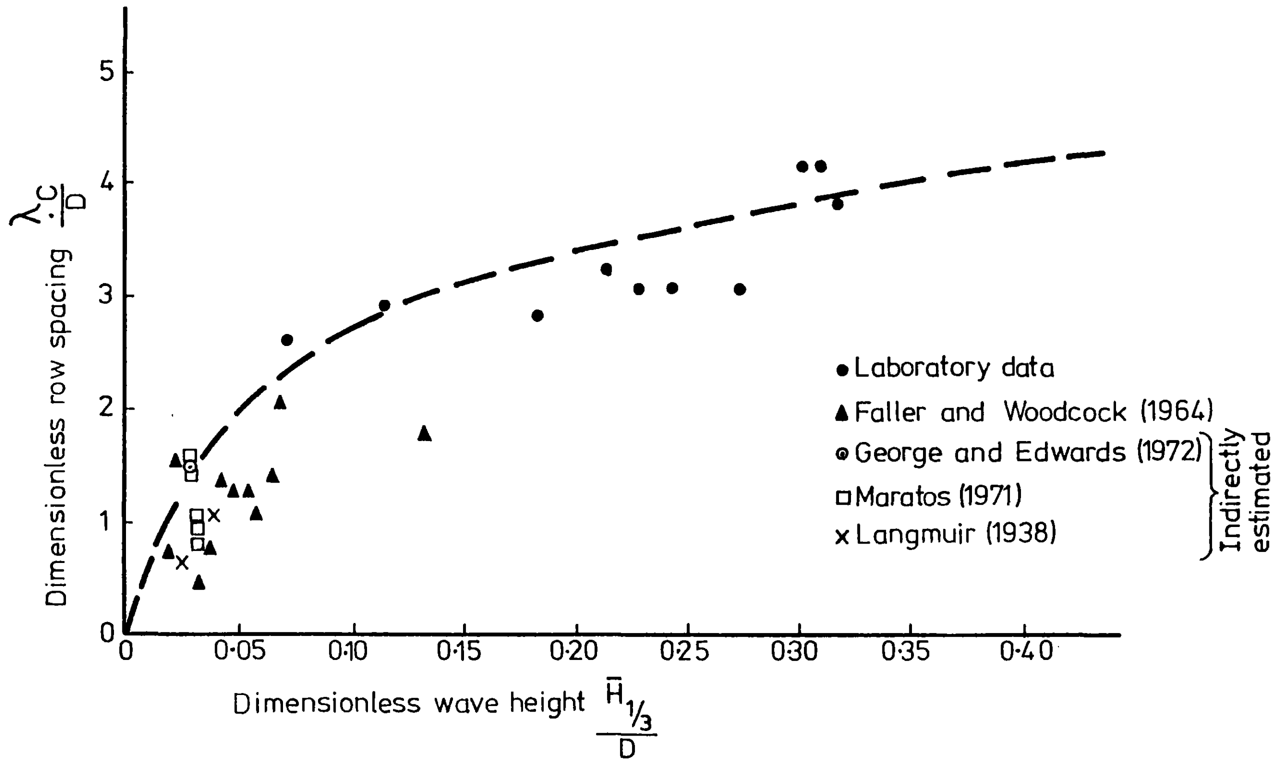

Fig 4·7 Correlations between row spacing and significant wave heights.

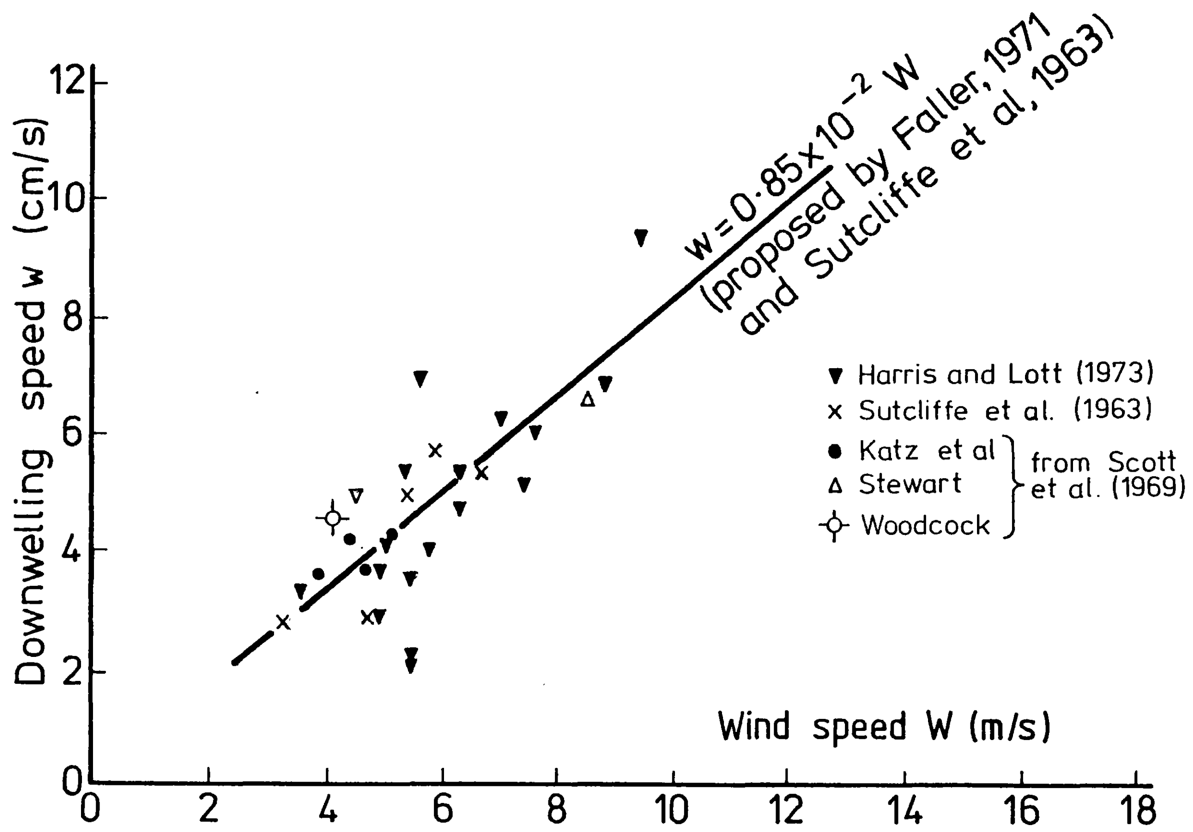

Fig. 4·8 The relationship between downwelling speed and wind speed.

SOME EFFECTS OF LANGMUIR CIRCULATION ON
SUSPENDED PARTICLES IN LAKES AND RESERVOIRS

CHAPTER 5 A MODEL OF LANGMUIR CIRCULATION AND THE TURBULENT DIFFUSION COEFFICIENT RELATIONSHIP

A model of flow pattern and the eddy diffusion coefficients within a Langmuir cell are described. These relationships are empirical, with the flow model containing several of the observed features discussed in the preceding chapter and the turbulent diffusion coefficient being connected to the wind speed. In combination, these provide an adequate representation, for the present study, of the turbulent flow in a typical Langmuir cell in the mixed layer.

CHAPTER 5 A MODEL OF LANGMUIR CIRCULATION AND THE TURBULENT DIFFUSION COEFFICIENT RELATIONSHIP

5.1 The Langmuir Circulation Model

An empirical model of the circulation within Langmuir vortices will be developed for the present study, using the information on the observed characteristic features of the circulation and how these features vary with the environmental conditions, which were established in Chapter 4. Since it is based on few observed parameters and on limited knowledge of the magnitude of the downwelling and upwelling velocities, it is not possible for the model to be sophisticated. However, it contains several essential characteristic features which are observed in the real situation. The following assumptions are made:-

The two-dimensional circulation cells should have an asymmetrical shape because of the difference in the downwelling and upwelling velocities. The water motion is intensified in the form of a jet under the convergence zone, with the width of the downwelling jet assumed to be 0.1 of the convergence line spacing (row spacing), approximately corresponding to the observation reported by Myer (1971) . The depth of the circulation is taken to be the mixed layer depth. Small-scale or transient circulations, when existing, will extend only a short distance down from the water surface in comparison with the circulation scale of interest (the mixed layer depth) and, hence, will be ignored. Wave motions will not be considered, the lake surface being assumed to be a rigid lid. Myer (1971) observed that the downwelling velocity appears to increase from the water surface to a maximum value somewhere around the mid-depth and decreases again to zero at the bottom of the cell. Therefore, at depth $z = 0.5\,D$, where D is the total depth of the cell, as shown in Fig. 5.1, the flow is assumed to be non-divergent and the vertical velocities approach their maximum values. At this depth the downwelling and upwelling are assumed to vary sinusoidally in the y-direction across the cell width, in which for $0 \leq y \leq 0.4\,\lambda_c$,

$$\begin{cases} W(y,z = 0.5D) = -W_u \cos\left(\dfrac{5\pi y}{4\lambda_c}\right) \quad ; \\ V(y,z = 0.5D) = 0 \quad ; \end{cases}$$

and for $0.4\lambda_c \leq y \leq 0.5\lambda_c$,

$$\begin{cases} W(y,z = 0.5D) = W_d \cos\left(\dfrac{5\pi}{2} - \dfrac{5\pi y}{\lambda_c}\right) \quad ; \\ V(y,z = 0.5D) = 0, \end{cases}$$

where $W(y,z)$ and $V(y,z)$ are mean vertical and horizontal velocities at point (y,z), respectively; W_u is the maximum upwelling mean velocity; W_d is the maximum downwelling mean velocity; and λ_c is the row spacing. The coordinate system is shown in Fig. 5.1. The variations of the vertical velocities are also assumed to vary sinusoidally with depth z. The appropriate expression for the vertical velocity components are given by

$$W(y,z) = \begin{cases} -W_u \cos\left(\dfrac{5\pi y}{4\lambda_c}\right) \sin\left(\dfrac{\pi z}{D}\right), \quad \text{for } 0 \leq y \leq 0.4\lambda_c\ ; & (5.1a) \\ W_d \cos\left(\dfrac{5\pi}{2} - \dfrac{5\pi y}{\lambda_c}\right) \sin\left(\dfrac{\pi z}{D}\right), \quad \text{for } 0.4\lambda_c \leq y \leq 0.5\lambda_c . & (5.1b) \end{cases}$$

From continuity, $\frac{\partial W}{\partial z} + \frac{\partial V}{\partial y} = 0$, from which

$$V = \int - \frac{\partial W}{\partial z} \, \partial y .$$

Hence the corresponding horizontal velocity components are given by

$$V(y,z) = \begin{cases} \frac{4}{5} W_u \frac{\lambda_c}{D} \sin\left(\frac{5\pi y}{4\lambda_c}\right) \cos\left(\frac{\pi z}{D}\right), \text{ for } 0 \leqslant y \leqslant 0.4\lambda_c ; & (5.2a) \\ \\ \frac{1}{5} W_d \frac{\lambda_c}{D} \sin\left(\frac{5\pi}{2} - \frac{5\pi y}{\lambda_c}\right) \cos\left(\frac{\pi z}{D}\right), \text{ for } 0.4\lambda_c \leqslant y \leqslant 0.5\lambda_c & (5.2b) \end{cases}$$

Also from the flow continuity consideration,

$$W_u = \frac{1}{4} W_d . \tag{5.3}$$

The mean flow pattern may be obtained from these velocities by defining $V = \frac{\partial \psi}{\partial z}$ and $W = - \frac{\partial \psi}{\partial y}$, in which ψ is the stream function:

$$\psi = \frac{4}{5} W_u \frac{\lambda_c}{\pi} \sin\left(\frac{5\pi y}{4\lambda_c}\right) \sin\left(\frac{\pi z}{D}\right), \text{ for } 0 \leqslant y \leqslant 0.4\lambda_c ; \tag{5.4a}$$

and,

$$\psi = \frac{1}{5} W_d \frac{\lambda_c}{\pi} \sin\left(\frac{5\pi}{2} - \frac{5\pi y}{\lambda_c}\right) \sin\left(\frac{\pi z}{D}\right), \text{ for } 0.4\lambda_c \leqslant y \leqslant 0.5\lambda_c . \tag{5.4b}$$

The flow pattern according to the above equations is plotted in Fig. 5.1.

Equations (5.1a) and (5.1b) result in an upwelling velocity smaller than that deduced from Langmuir's observation (1938), the latter being about $\frac{1}{2}$ to $\frac{1}{3}$ of the downwelling. With the assumption of sinusoidal variations, larger value of W_u could be obtained by increasing the width of the downwelling jet, for example, if the jet width were $0.167\lambda_c$, W_u equals $\frac{1}{2} W_d$. However, such a large size of downwelling jet is in conflict with Myer's observation. In view of the uncertainties in the field measurements of the upwelling and downwelling velocities, it will be assumed that the model equations (5.1), (5.2) and (5.3) are representative. This is a crucial assumption since the particle distribution in a Langmuir cell may be expected to depend on W_u as well as on the general flow pattern. It is noted that Assaf et al. (1971) have also used $W_u = \frac{1}{4} W_d$ in their analysis.

To relate the circulation flow field to the environmental parameters, the downwelling velocity W_d is expressed in terms of the wind speed W_n by the empirical equation described in Chapter 4,

$$W_d = 0.85 \times 10^{-2} W_n . \tag{4.10}$$

Expressing the velocity components in non-dimensional form, using the non-dimensional variables described in Chapter 3, the equations become

$$W^*(y^*,z^*) = \begin{cases} -\frac{W_d^*}{4} \cos\left(\frac{5\pi y^*}{4\lambda_c^*}\right) \sin(\pi z^*), \text{ for } 0 \leq y^* \leq 0.4\lambda_c^*; & (5.1a') \\ \\ W_d^* \cos\left(\frac{5\pi}{2} - \frac{5\pi y^*}{\lambda_c^*}\right) \sin(\pi z^*), \text{ for } 0.4\lambda c^* \leq y^* \leq 0.5\lambda_c^*; & (5.1b') \end{cases}$$

and,

$$V^*(y^*,z^*) = \begin{cases} \frac{W_d^*}{5} \lambda_c^* \sin\left(\frac{5\pi y^*}{4\lambda_c^*}\right) \cos(\pi z^*), \text{ for } 0 \leq y^* \leq 0.4\lambda_c^*; & (5.2a') \\ \\ \frac{W_d^*}{5} \lambda_c^* \sin\left(\frac{5\pi}{2} - \frac{5\pi y^*}{\lambda_c^*}\right) \cos(\pi z^*), \text{ for } 0.4\lambda_c^* \leq y^* \leq 0.5\lambda_c^*; & (5.2b') \end{cases}$$

and,

$$W_d^* = 0.85 \times 10^{-2} , \qquad (4.10')$$

in which,

$$W^* = W/W_n \quad ; \quad V^* = V/W_n \quad ; \quad W_d^* = W_d/W_n \quad ;$$

$$y^* = y/D \quad ; \quad z^* = z/D \quad ; \quad \lambda_c^* = \lambda_c/D \quad .$$

Since W_d^* is a constant, the only variable required to specify the non-dimensional mean velocity field is λ_c^* (= λ_c/D).

5.2 Estimation of the Turbulent Eddy Coefficients (ε_z and ε_y)

In the present mathematical model, the mass transfer coefficients for suspended matter in the lake environment have been assumed to be equal to the turbulent coefficients for momentum transfer (eddy viscosity) which are related to the Reynolds stresses, generated by the wind. These eddy coefficients are not only a function of spatial location but also depend on wind speed, current structures, and the thermal stability of the water. The latter factor is known to suppress turbulence and hence to reduce vertical turbulent mixing. In the mixed layer, however, the temperature distribution is essentially uniform and the effects of density stratification may be ignored. Hence the eddy coefficients may be assumed to be described by their neutral values.

Little is known about the form of these eddy coefficients. Direct determinations from the statistical properties of turbulence fluctuations, or from the concept of turbulent energy cascade processes through eddies of various sizes, are not sufficiently well-developed for practical applications. In practice therefore, eddy coefficients are specified by some form of empirical or semi-empirical relationships with little support from fundamental studies. Sometimes, indeed, they are regarded as being constant. Despite this difficulty, an empirical model of vertical eddy coefficient is adopted for this study. This model is proposed by Bengston (1973), in which the eddy viscosity in the vertical (ε_z) is related to wind speed and the depth of the thermocline (the size of the largest eddy scale) by

$$\varepsilon_z = 2.0 \times 10^{-5} W_n D \tag{5.5}$$

and is taken to be constant through the depth of the mixed layer. This model is simple and satisfactorily predicts a greater rate of turbulent mixing with wind speed and with increasing thermocline depth. The latter implies enhanced mixing due to turbulence and hence a greater diffusion coefficient. However, the model is based on field data derived from small to moderate-sized lakes, where the thermocline depth was not greater than 15 m.

Defining $\varepsilon_z^* = \varepsilon_z/(W_n D)$, equation (5.5) is rewritten

$$\varepsilon_z^* = \frac{\varepsilon_z}{W_n D} = 2.0 \times 10^{-5} . \tag{5.5'}$$

Field measurements show that the horizontal coefficients of diffusion are larger than those in the vertical direction by about one to two orders of magnitude. This difference arises from the different scales of horizontal and vertical turbulence. The horizontal diffusion coefficients are found to be strongly dependent on the spatial scale and follow the 4/3-power law (Murthy, 1972), in which $\varepsilon_H \propto \text{const.}\ \varepsilon^{\frac{1}{3}} \ell^{\frac{4}{3}}$, where ε_H is the horizontal eddy coefficient of diffusion; ε is the rate of turbulent energy dissipation; and ℓ is the length scale. Density stratification in the water column affects the vertical diffusion and this reinforces the difference between the two diffusivities. Hence, when dealing with the local scales of the order of few metres or less (as is the approximate size of the computational grid used in the present numerical study) one cannot be certain of their relative magnitudes. However, it is generally admitted (e.g. Bowden, 1970) that, for a scale of the order of metres or less, Kolmogorov's laws of locally isotropic turbulence apply fairly well in all three-dimensions. Therefore it could by assumed that, if the computational grids are small enough and density stratification is negligible, then the eddy coefficients of diffusivity may be regarded as isotropic. i.e.

$$\varepsilon_y = \varepsilon_z \quad . \tag{5.6}$$

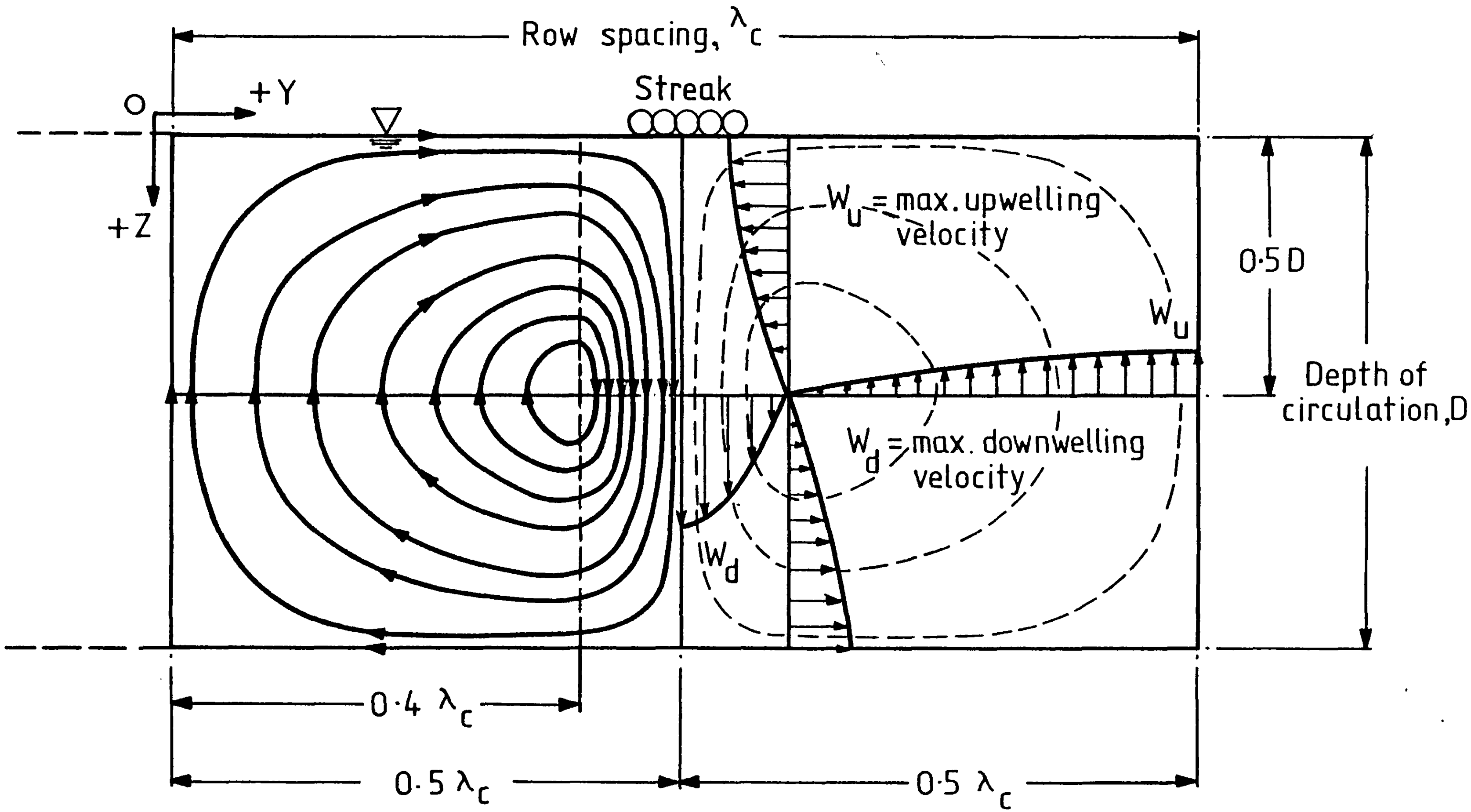

Fig 5·1 A schematic diagram of Langmuir circulations, showing streamlines and typical velocity profiles.

SOME EFFECTS OF LANGMUIR CIRCULATION ON
SUSPENDED PARTICLES IN LAKES AND RESERVOIRS

CHAPTER 6 THE FINITE DIFFERENCE APPROXIMATION

A finite difference numerical method is used to approximate the partial differential equation governing the advection and diffusion transport of suspended particles. This chapter gives the summary of the governing equations established in the preceding chapters, followed by a description of the finite difference representation, the treatment of initial and boundary conditions, the input variables, and some practical tests on stability and accuracy of the finite difference scheme.

The computer program listing and corresponding flow chart are given in Appendix I.

CHAPTER 6 THE FINITE DIFFERENCE APPROXIMATION

6.1 Summary of Equations

The basic equation is the dimensionless mass balance equation for the suspended particles in two-dimensional flow, written in conservation form:

$$\frac{\partial C^*}{\partial t^*} + \frac{\partial}{\partial y^*}(V^*C^*) + \frac{\partial}{\partial z^*}[(W^* + W_T^*)C^*] = \frac{\partial}{\partial y^*}\left(\varepsilon_y^* \frac{\partial C^*}{\partial y^*}\right) + \frac{\partial}{\partial z^*}\left(\varepsilon_z^* \frac{\partial C^*}{\partial z^*}\right), \tag{3.12}$$

in which the starred quantities are the non-dimensional variables given in equation (3.11). C^* denotes the mean concentration of particles; t^* is time; y^* and z^* are the cartesian coordinate system; V^* and W^* are the mean horizontal and vertical velocity components of the flow; W_T^* is the sinking speed of the particles; and ε_y^* and ε_z^* are the eddy diffusion coefficients. In non-dimensionalising these variables, the characteristic length (L_o) is the depth of Langmuir cell D, the characteristic velocity (U_o) is the wind speed W_n, and the reference concentration (C_o) is the initial concentration.

The velocity distribution in a Langmuir cell is given by the non-dimensionalised velocity profiles:

$$W^*(y^*,z^*) = \begin{cases} -\dfrac{W_d^*}{4}\cos\left(\dfrac{5\pi y^*}{4\lambda_c^*}\right)\sin(\pi z^*), \text{ for } 0 \leq y^* \leq 0.4\lambda_c^*, & (5.1a') \\[2ex] W_d^* \cos\left(\dfrac{5\pi}{2} - \dfrac{5\pi y^*}{\lambda_c^*}\right)\sin(\pi z^*), \text{ for } 0.4\lambda_c^* \leq y^* \leq 0.5\lambda_c^*, & (5.1b') \end{cases}$$

and,

$$V^*(y^*,z^*) = \begin{cases} \dfrac{W_d^*}{5}\,\lambda_c^*\,\sin\left(\dfrac{5\pi y^*}{4\lambda_c^*}\right)\,\cos(\pi z^*), \text{ for } 0 \leqslant y^* \leqslant 0.4\lambda_c^*, & (5.2a') \\ \\ \dfrac{W_d^*}{5}\,\lambda_c^*\,\sin\left(\dfrac{5\pi}{2} - \dfrac{5\pi y^*}{\lambda_c^*}\right)\cos(\pi z^*), \text{ for } 0.4\lambda_c^* \leqslant y^* \leqslant 0.5\lambda_c^*; & (5.2b') \end{cases}$$

in which the maximum downwelling velocity W_d^* $(= W_d/W_n)$ is given by the empirical equation,

$$W_d^* = 0.85 \times 10^{-2} \; . \qquad (4.10')$$

The eddy diffusion coefficients are assumed to be constant over the Langmuir cell region and given by the empirical relationship,

$$\varepsilon_y^* \left(= \frac{\varepsilon_y}{W_n D}\right) = \varepsilon_z^* \left(= \frac{\varepsilon_z}{W_n D}\right) = 2 \times 10^{-5} \; . \qquad (5.5')$$

In the subsequent discussion, for convenience, the superscript (*) will be dropped from the non-dimensional variables.

Basically, for a given spatial distribution of velocities and diffusion coefficients and specified initial and boundary conditions, equation (3.12) can be solved by integrating the finite difference equation which approximates to it. The solution is advanced in time to yield distribution of particles in a Langmuir cell at various time intervals.

6.2. Finite Difference Representation

The flow region corresponding to a single Langmuir cell is divided into a finite number of grid volumes by a rectangular mesh as shown in Fig.6.1. The variables are defined at the intermediate locations given in Fig.6.2, in which the concentration is specified at the centre of the grid volume, and the velocity components and diffusion coefficients are located at the interfaces of the grid volume. This grid structure allows the finite difference approximations to equation (3.12) to be derived directly from the integral form of the mass conservation law for each volume element. The procedure has several advantages over other grid arrangements, including better physical interpretation of each term in the finite difference equation and ease of handling of the boundary conditions, and the resulting finite difference schemes conserve mass of particles over the flow region.

Because the explicit finite difference schemes have been shown to impose severe restrictions on the integration time step to be prohibitively small for stable solutions of equation (3.12), an implicit method of solution is adopted. The alternating-direction implicit (ADI) method proposed by Peaceman and Rachford (1955) has been used. This method makes use of a splitting of the time step for multi-dimensional problems to obtain an implicit formulation, which requires only the inversion of a tridiagonal matrix in the solution. It possesses several good properties, first, for linearised problems, its accuracy is to the second order in time and space. Then, when used with centred-space derivatives, the scheme is free of numerical diffusion (Roache, 1972; Peaceman , 1977), a desirable property in the present context. Further, the anticipated unconditional stability of the method allows larger time steps than could be obtained by explicit methods. The scheme is efficient and well suited to problems with rectangular boundaries.

Applied to the particle mass transport equation (3.12), the Peaceman-Rachford alternating-direction implicit (ADI) method advances the solution from time level n to n + 1 in the following two steps:-

Step 1: (Row sweeping, i.e. explicit in z- , implicit in y-)

$$\frac{C_{ij}^{**} - C_{ij}^{n}}{\Delta t/2} = -\frac{\delta}{\delta y}(VC)^{**} - \frac{\delta}{\delta z}(W_s C)^n + \frac{\delta}{\delta y}\left(\varepsilon_y \frac{\delta C}{\delta y}\right)^{**} + \frac{\delta}{\delta z}\left(\varepsilon_z \frac{\delta C}{\delta z}\right)^{n} . \quad (6.1)$$

Step 2: (Column sweeping, i.e. explicit in y- , implicit in z-)

$$\frac{C_{ij}^{n+1} - C_{ij}^{**}}{\Delta t/2} = -\frac{\delta}{\delta y}(VC)^{**} - \frac{\delta}{\delta z}(W_s C)^{n+1} + \frac{\delta}{\delta y}\left(\varepsilon_y \frac{\delta C}{\delta y}\right)^{**} + \frac{\delta}{\delta z}\left(\varepsilon_z \frac{\delta C}{\delta z}\right)^{n+1} , \quad (6.2)$$

in which, C_{ij} are the concentrations at the centres of grid volumes; $\frac{\delta}{\delta y}$, etc. are the finite difference analogues of the space derivatives. The intermediate values C_{ij}^{**} have no physical meaning. W_s stands for the vertical component of velocity for solid particles, and is equal to $W + W_T$. Δt is the time interval between time levels n + 1 and n .

Centred differencing is used for space derivatives. Referring to the grid structure and variable locations in Fig.6.1 and 6.2, the space derivatives are approximated by

$$\frac{\partial (VC)}{\partial y} \approx \frac{\delta (VC)}{\delta y} = \frac{VE.CE - VW.CW}{\Delta y_{ij}} \quad (6.3)$$

$$\left\{ = \frac{\text{Advection across the right face} - \text{Advection across the left face}}{\Delta y_{ij}} \right\} \quad ;$$

$$\frac{\partial(W_s C)}{\partial z} \approx \frac{\delta(W_s C)}{\delta z} = \frac{WS.CS - WN.CN}{\Delta z_{ij}} , \tag{6.4}$$

$$\left\{ = \frac{\text{Advection across the bottom face} - \text{Advection across the top face}}{\Delta z_{ij}} \right\}$$

where VE, VW, WS, WN and CE, CW, CS, CN are the velocities and concentrations at the right, left, bottom and top of the grid volume, respectively. The concentrations at the interfaces are interpolated from the values at the centres of the two bordering volumes. That is,

$$\left.\begin{aligned} CE &= (1 - SE).C_{ij} + SE.C_{i+1,j} \\ CW &= (1 - SW).C_{i-1,j} + SW.C_{ij} \end{aligned}\right\} \tag{6.3'}$$

where $SE = (y_{i+1} - y_i)/(y_{i+2} - y_i)$,

and $SW = (y_i - y_{i-1})/(y_{i+1} - y_{i-1})$.

Similarly,

$$\left.\begin{aligned} CS &= (1 - SS).C_{ij} + SS.C_{i,j+1}, \\ CN &= (1 - SN).C_{i,j-1} + SN.C_{ij}. \end{aligned}\right\} \tag{6.4'}$$

where $SS = (z_{j+1} - z_j)/(z_{j+2} - z_j)$,

$SN = (Z_j - z_{j-1})/(z_{j+1} - z_{j-1})$.

For uniform grid spacings, SW, SE, SS and SN are all equal to 0.5.

The diffusion terms are differenced as follows:-

$$\frac{\partial}{\partial z}\left(\varepsilon_y \frac{\partial C}{\partial y}\right) = \frac{\left(\varepsilon_y \frac{\partial C}{\partial y}\right)_E - \left(\varepsilon_y \frac{\partial C}{\partial y}\right)_W}{\Delta y_{ij}}$$

$$= \underbrace{\frac{\varepsilon_{yE}}{\Delta y_{ij} . \Delta y_E}\left(C_{i+1,j} - C_{ij}\right)}_{\text{Diffusion through the right face}} - \underbrace{\frac{\varepsilon_{yW}}{\Delta y_{ij} . \Delta y_W}\left(C_{ij} - C_{i-1,j}\right)}_{\text{Diffusion through the left face.}} , \quad (6.5)$$

and,

$$\frac{\partial}{\partial z}\left(\varepsilon_z \frac{\partial C}{\partial z}\right) = \underbrace{\frac{\varepsilon_{zs}}{\Delta z_{ij} . \Delta z_s}\left(C_{i,j+1} - C_{ij}\right)}_{\text{Diffusion through the bottom face}} - \underbrace{\frac{\varepsilon_{zN}}{\Delta z_{ij} . \Delta z_N}\left(C_{ij} - C_{i,j-1}\right)}_{\text{Diffusion through the top face.}} \quad (6.6)$$

It can be shown that the above finite differencing is capable of physical interpretation and obeys the integral conservations of mass over the grid volume (ij).

Substituting equations (6.3), (6.4), (6.5), (6.6) into equations (6.1) and (6.2) and re-arranging terms, the following equations are obtained:

For the first one-half time step (y-sweep),

$$AA_i\, C^{**}_{i-1,j} + BB_i . C^{**}_{ij} + CC_i . C^{**}_{i+1,j} = DD_i\ , \tag{6.7}$$

in which the coefficients are given by

$$AA_i = \left[- \frac{VW.(1 - SW).\Delta t}{2\Delta y_{ij}} - \frac{\Delta t.\varepsilon_{yW}}{2\Delta y_{ij}.\Delta y_W} \right] ,$$

$$BB_i = \left[1 + \frac{\Delta t.VE.(1 - SE)}{2\Delta y_{ij}} - \frac{\Delta t.VW.SW}{2\Delta y_{ij}} + \frac{\Delta t.\varepsilon_{yE}}{2\Delta y_{ij}.\Delta y_E} + \frac{\Delta t.\varepsilon_{yE}}{2\Delta y_{ij}.\Delta y_W} \right]$$

$$CC_i = \left[\frac{\Delta t.VE.SE}{2\Delta y_{ij}} - \frac{\Delta t.\varepsilon_{yE}}{2\Delta y_{ij}.\Delta y_E} \right] ,$$

$$DD_i = \left[\frac{\Delta t.WN.(1 - SN)}{2\Delta z_{ij}} + \frac{\Delta t.\varepsilon_{zN}}{2\Delta z_{ij}.\Delta z_N} \right] . C^n_{i,j-1}$$

$$+ \left[1. - \frac{\Delta t.WS.(1 - SS)}{2\Delta z_{ij}} + \frac{\Delta t.WN.SN}{2\Delta z_{ij}} - \frac{\Delta t.\varepsilon_{zs}}{2\Delta z_{ij}.\Delta z_s} - \frac{\Delta t.\varepsilon_{zN}}{2\Delta z_{ij}.\Delta z_N} \right] . C^n_{ij}$$

$$+ \left[- \frac{\Delta t.WS.SS}{2\Delta z_{ij}} + \frac{\Delta t.\varepsilon_{zs}}{2\Delta z_{ij}.\Delta z_s} \right] . C^n_{i,j+1}\ .$$

For the second one-half time step (z-sweep),

$$AA_j . C^{n+1}_{i,j-1} + BB_j . C^{n+1}_{ij} + CC_j . C^{n+1}_{i,j+1} = DD_j\ , \tag{6.8}$$

in which

$$AA_j = \left[- \frac{\Delta t.WN.(1 - SN)}{2\Delta z_{ij}} - \frac{\Delta t.\varepsilon_{zN}}{2\Delta z_{ij}.\Delta z_N} \right] ,$$

$$BB_j = \left[1. + \frac{\Delta t.WS.(1 - SS)}{2\Delta z_{ij}} - \frac{\Delta t.WN.SN}{2\Delta z_{ij}} + \frac{\Delta t.\varepsilon_{zs}}{2\Delta z_{ij}.\Delta z_s} + \frac{\Delta t.\varepsilon_{zN}}{2\Delta z_{ij}.\Delta z_N} \right] ,$$

$$CC_j = \left[\frac{\Delta t.WS.SS}{2\Delta z_{ij}} - \frac{\Delta t.\varepsilon_{zs}}{2\Delta z_{ij}.\Delta z_s} \right] ,$$

$$DD_j = \left[\frac{\Delta t.VW.(1 - SW)}{2\,\Delta y_{ij}} + \frac{\Delta t.\varepsilon_{yW}}{2\,\Delta y_{ij}.\Delta y_W}\right] . C^{**}_{i-1,j}$$

$$+ \left[1. - \frac{\Delta t.VE.(1 - SE)}{2\,\Delta y_{ij}} + \frac{\Delta t.VW.SW}{2\,\Delta y_{ij}} - \frac{\Delta t.\varepsilon_{yE}}{2\,\Delta y_{ij}.\Delta y_E} - \frac{\Delta t.\varepsilon_{yW}}{2\,\Delta y_{ij}.\Delta y_W}\right] . C^{**}_{i,j}$$

$$+ \left[- \frac{\Delta t.VE.SE}{2\,\Delta y_{ij}} + \frac{\Delta t.\varepsilon_{yE}}{2\,\Delta y_{ij}.\Delta y_E}\right] . C^{**}_{i+1,j} \quad .$$

Equations (6.7), (6.8) result in a tridiagonal system of linear simultaneous equations which can be efficiently solved by the Thomas algorithm (von Rosenberg, 1969) which is a modified Gaussian elimination procedure. However, in order to keep the round-off error from building up, the tridiagonal matrix is required to be diagonally dominant, i.e.

$$|BB| \geq |AA| + |CC| \tag{6.9}$$

for every row of the matrix. Diagonal dominance results if the cell Reynolds numbers $\left(\frac{V\Delta y}{\varepsilon_y} \text{ and } \frac{W_s \Delta z}{\varepsilon_z}\right) \leq 2$. In the case of the cell Reynolds number ≥ 2, limitations on the size of the time step Δt has to be made to satisfy the conditions in equation (6.9). A criterion is used, in which the time step

$$\Delta t \leq \min.\left\{ \min. \frac{2\,\Delta y}{(|VE| + |VW|)},\ \min. \frac{2\,\Delta z}{(|WS| + |WN|)}\right\} . \tag{6.10}$$

6.3. Initial and Boundary Conditions

The initial and boundary conditions applicable to the problem are as follows:-

(1) Initial condition

The initial distribution of particles in a Langmuir cell is assumed to be uniform.

(2) Top and side impermeable boundaries (boundaries B_1, B_2 and B_3 in Fig.6.1)

The physical condition at these boundaries requires that there will be no advective and diffusive fluxes of materials across the boundaries. Using the grid structure shown in Fig.6.1, this requirement is handled by setting to zero the advective and diffusive flux terms on the faces of the grid volumes that coincide with the boundaries.

(3) Bottom permeable boundary (boundary B4)

There is no diffusive flux across this boundary surface. Only an advective flux can take place. These conditions are satisfied by putting the diffusive flux terms for the faces of the grid volumes lying along this boundary to zero. The non-zero advective flux which gives rise to the sinking loss of material from the Langmuir cell, is computed from the values of the concentrations and velocities at the boundary. The concentration values are estimated by linear extrapolation from the values of the concentrations at the centres of two interior grid volumes nearest to the boundary, i.e., referring to Fig. 6.1 and 6.2,

$$CS_{i,NZ-1} = (1. - SNZ).C_{i,NZ-1} + SNZ.C_{i,NZ-2} , \tag{6.11}$$

in which $SNZ = -(Z_{NZ} - Z_{NZ-1})/(Z_{NZ} - Z_{NZ-2})$, and (NZ-1) is the number of grid volumes in the z-direction.

6.4. Values of the Input Variables

Values of the independent variables of the problems, representing typical conditions found in lakes and reservoirs, are listed in Table 6.1 in their dimensional magnitudes. When combined, these variables yield 4 basic non-dimensional variables which are also tabulated in

Table 6.1. Hence, given an initial concentration of particles in non-dimensional unit at time zero, the particle distribution and changes in their total mass in a Langmuir cell at various time t^* up to T^* can be determined for various combinations of cell sizes λ_c^* and sinking (rising) speed W_T^* .

Table 6.1 Values of Variables

A.	Dimensional variables	Ranges of values
	1. Depth of the mixed layer = Langmuir cell depth (D)	3 to 10 m
	2. Row spacing/cell depth (λ_c/D)	0.5 to 2.5
	3. Wind speed (W_n)	3 to 10 m/s
	4. Sinking (or rising) speed of particles (W_T)	1 to 200 m/day
	5. Time of simulation = time that Langmuir circulation phenomena vary significantly	1 hour, or more
	6. Initial concentration	any value
B.	Non-dimensional variables	
	1. Row spacing/cell depth ($\lambda_c^* = \lambda_c/D$)	0.5 to 2.5
	2. Particle sinking (or rising) speed ($W_T^* = W_T/W_n$)	10^{-7} to 10^{-3}
	3. Time of simulation ($T^* = TW_n/D$)	10^2 to 5×10^4
	4. Initial concentration (C_o^*)	100

6.5. Some Practical Tests on Stability and Accuracy of the Finite Difference Scheme

Some knowledge of the stability and accuracy of the adopted finite difference scheme may be acquired by comparing the computed numerical results with the known solutions of the equations of similar type. Comparisons of this nature aids ~~verification~~ of computer coding and provides indication of the optimum grid length and time step sizes to be used in solving the problem. Since there is no closed form solution available for the two-dimensional advection-diffusion equation, a simplified one-dimensional equation (c.f. equation 3.12) having a known analytical solution has been used, in the present study, for comparison tests. This equation is

$$\frac{\partial C}{\partial t} + \frac{\partial}{\partial x}(UC) = \varepsilon_x \frac{\partial^2 C}{\partial x^2} , \qquad (6.12)$$

in which C is the concentration; U is the constant velocity; ε_x is the constant diffusion coefficient; x and t are the distance and time, respectively. These variables are non-dimensional. Subjected to the following initial and boundary conditions:-

$$C(0,t) = 1.0 \qquad , \text{ for } t \geq 0$$

$$C(x,0) = 0 \qquad \text{" } x \geq 0$$

$$C(\infty,t) = 0 \qquad \text{" } t \geq 0 ,$$

the analytical solution is given by (Ogata and Banks, 1961) .

$$C(x,t) = \frac{1}{2} \exp\left(\frac{Ux}{\varepsilon_x}\right) \operatorname{erfc}\left[\frac{x + Ut}{2(\varepsilon_x t)^{\frac{1}{2}}}\right] + \frac{1}{2} \operatorname{erfc}\left[\frac{x - Ut}{2(\varepsilon_x t)^{\frac{1}{2}}}\right] , \qquad (6.13)$$

in which erfc [ ] denotes the complementary error function. The solution is exact for $0 \leq x \leq 1.0$, provided that the concentration front has not advanced more than $\frac{2}{3}$ from $x = 0$. In the calculations, the diffusion coefficient ε_x is set equal to 2×10^{-5} and the velocity U is varied between the values anticipated in a Langmuir cell, i.e. from 10^{-3} to 9.5×10^{-3} , and numerical solutions are obtained for several combinations of grid sizes and time steps. In all cases, uniform grids have been employed, ranging from 20 to 100 grid points. The results of some of these comparisons are shown in Fig. 6.3 to Fig.6.9.

The numerical solution has a general tendency to oscillate about $C = 1.0$ in the region behind the front. This overshoot (or wiggle) is a typical characteristic of the centred-in-distance differencing of spatial derivatives. The overshoot decreases as either the diffusion coefficient or the number of grid intervals increases. Reducing the time step Δt does not improve the situation. Roache (1972) has found that, by keeping the grid Reynolds number $\left(\frac{U\Delta x}{\varepsilon_x}\right)$ to be less than 2 , these overshoots can be eliminated. This condition places a rather severe restriction on grid size to be excessively small and, consequently, requiring very small time step length, which is impractical. However, for the present grid arrangement, the shape of the front is well represented, in general, and no large artificial (numerical) diffusion is apparent, indicating that the alternating-direction implicit method, with centred space differencing, possesses minimal artificial diffusion. For the severest case, when $U = 9.5 \times 10^{-3}$, the comparison shows that satisfactory resolution and accuracy can be obtained with a 50 uniform grid when the dimensionless time step is about 2 , with some oscillation occurring over parts of the solution. Fig.6.9 shows clearly that arbitrarily large values of Δt cannot be used in this scheme even though the von Neumann stability analysis indicates unconditional stability. Nevertheless, the alternating-direction implicit scheme has been found to permit the use of larger time step lengths than would be possible with typical explicit methods, thus saving considerable computer time in long simulation runs.

A time step length as large as 4 dimensionless units has been found to satisfy the condition for diagonal dominance of the tridiagonal matrix (equation 6.9). Trial runs have been made to solve the two-dimensional advection-diffusion equations for the Langmuir circulation problem (equation 3.12), using this time step length and a 50 x 50 uniform grid. In this case, no overshoot was observed and the solution remains stable even when the time step is increased to 10 dimensionless units. But, using this large time step,(10 units),the tridiagonal matrix is no longer diagonally dominant and hence inaccurate solution might have been obtained.

The disappearance of overshoots in the two-dimensional cases when the flow velocity is variable throughout the flow field is similarly noted by Roache (1972). He has observed that no overshoot is experienced if the Reynolds number of the grids in the vicinity of the flow boundaries are kept below 2 . In the present case, the maximum velocity at the boundary grids is 10^{-3} , and using with 50 uniform grids, i.e. $\Delta y = \Delta z = 0.02$ and with $\varepsilon_y = \varepsilon_z = 2 \times 10^{-5}$, the maximum grid Reynolds number is $\frac{1 \times 10^{-3} \times 0.02}{2 \times 10^{-5}} = 1.0$, thus confirming Roache's observation.

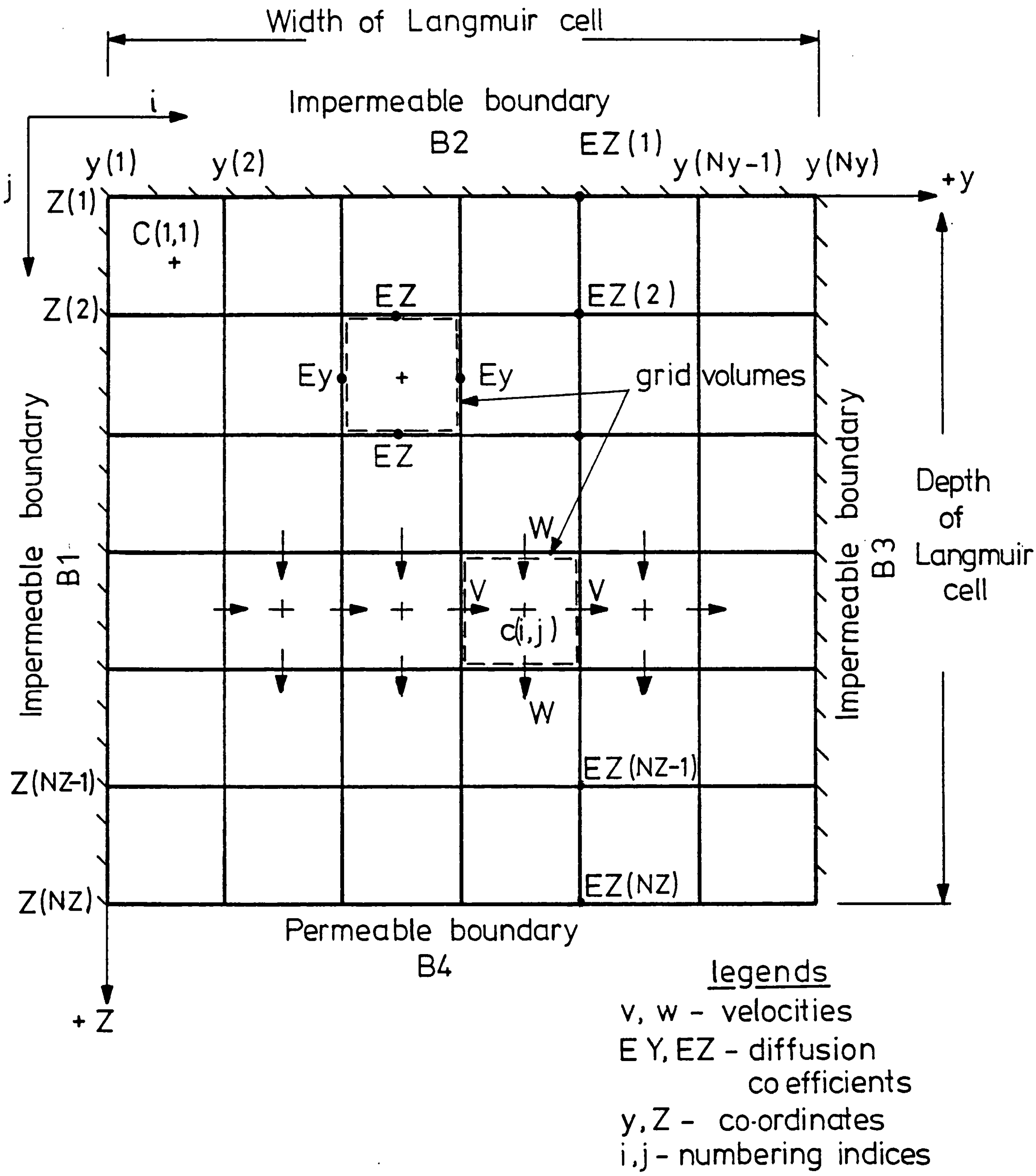

Fig. 6.1. Finite difference grid structure

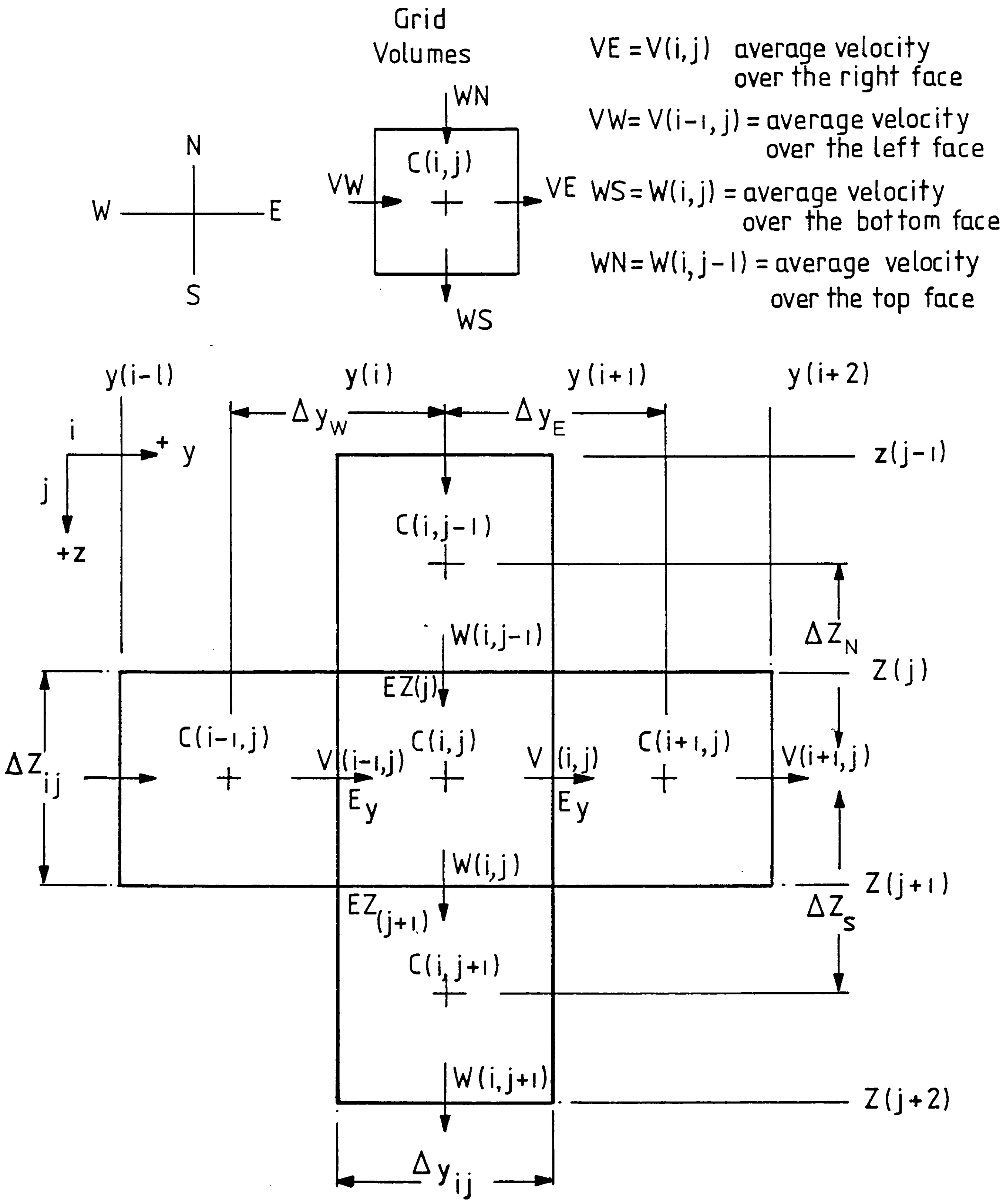

Fig. 6·2 Variable definitions and locations

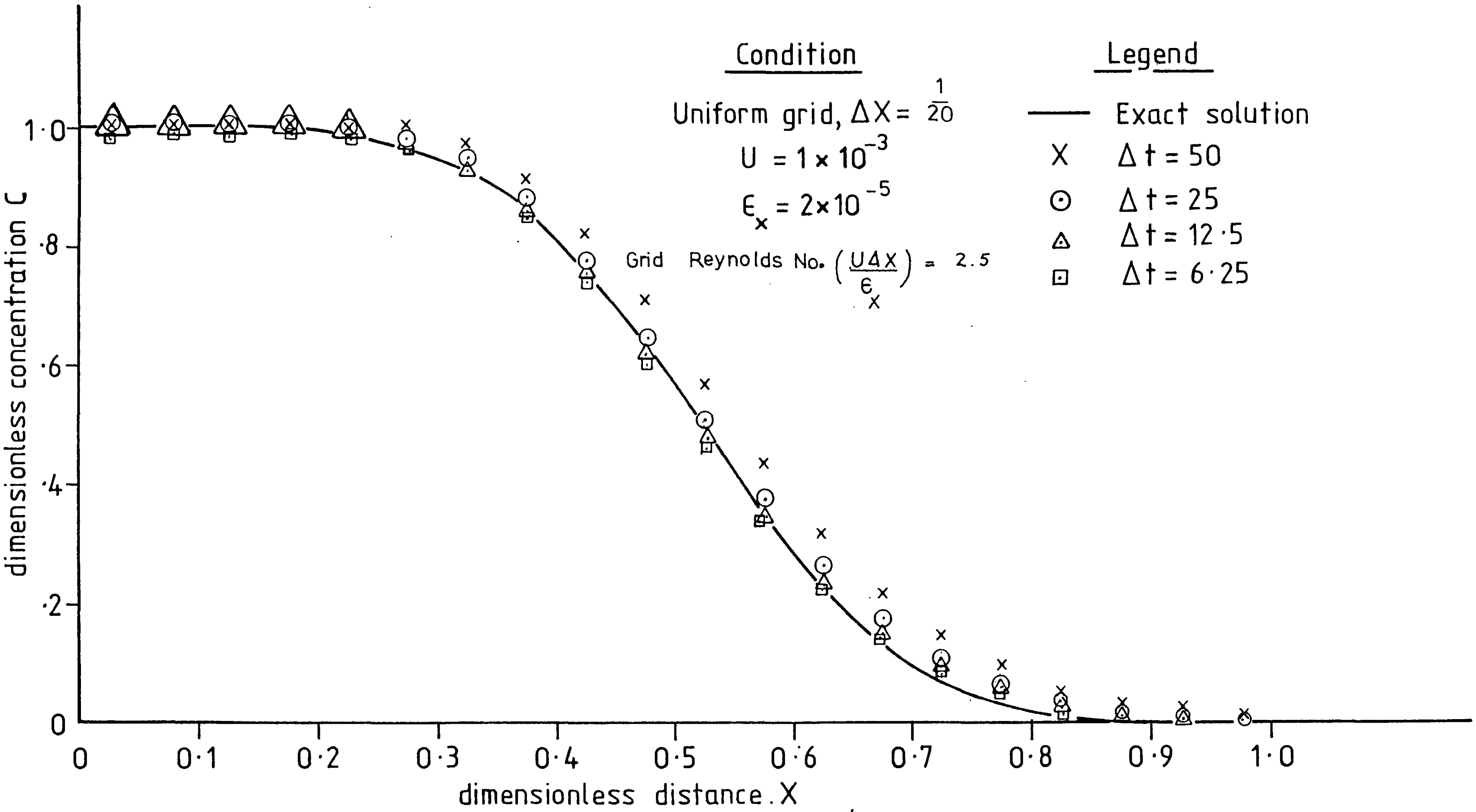

Fig. 6·3 Concentration profiles at time $t = 0 \cdot 5/U$, by the ADI–CDS method, using various time steps lengths Δt.

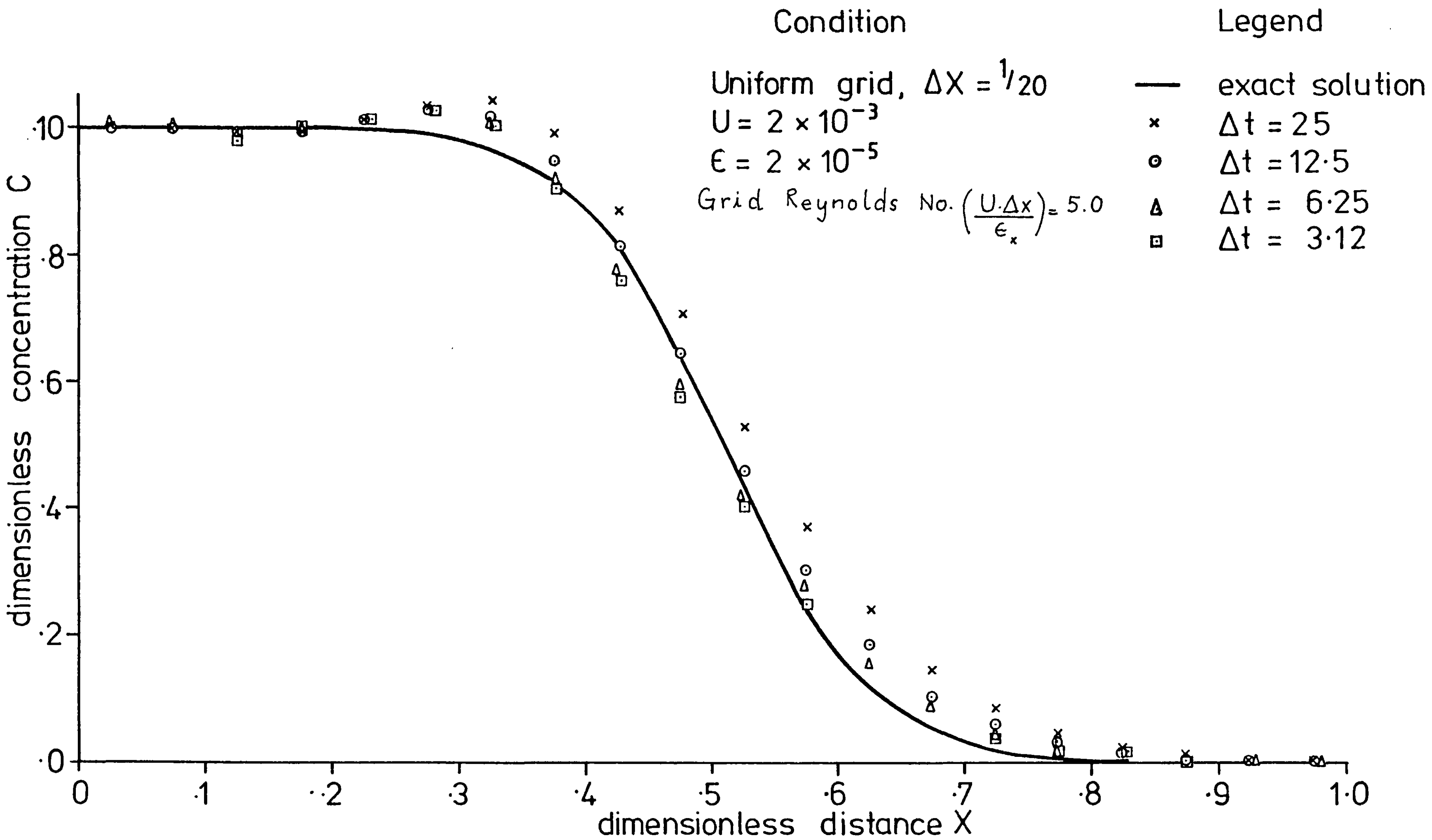

Fig. 6.4. Concentration profiles at time $t = 0{\cdot}5/U$, by the ADI - CDS method, using various time step length Δt

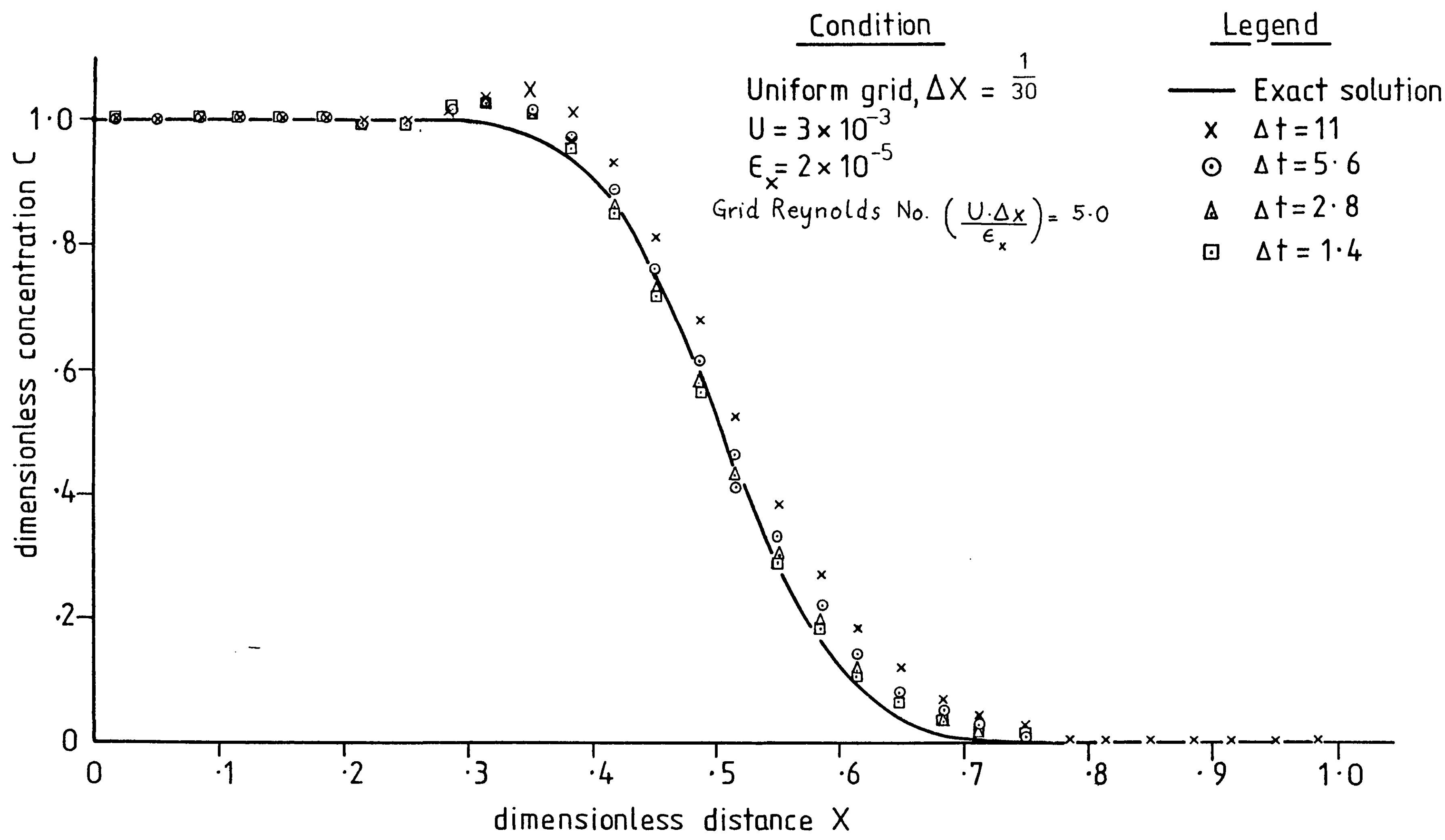

Fig. 6·5 Concentration profiles, at time $t = 0 \cdot 5/U$, by the ADI-CDS method using various time step lengths Δt

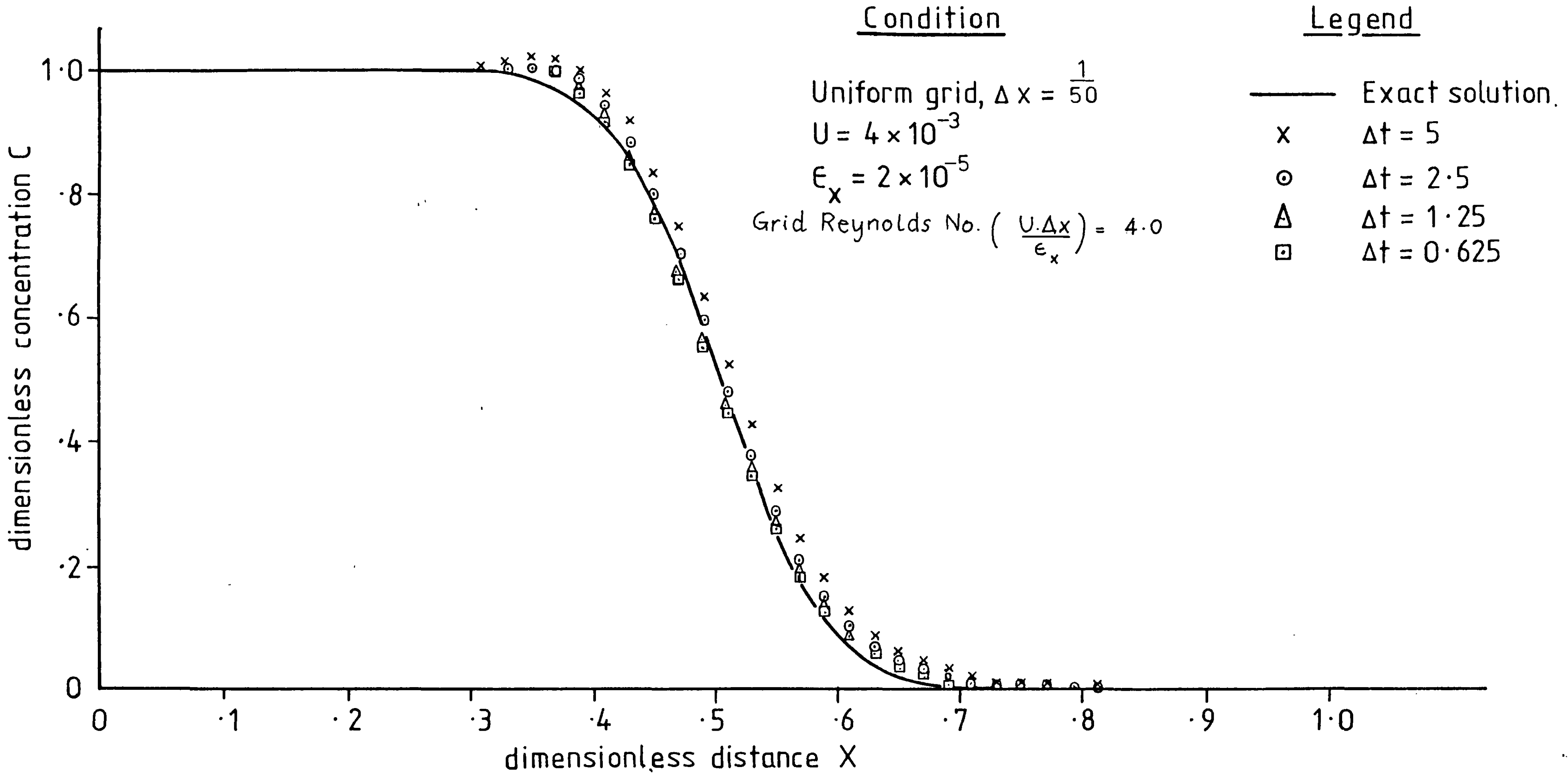

Fig. 6·6 Concentration profiles at time $t = 0{\cdot}5/U$, by the ADI-CDS method using various time step lengths Δt.

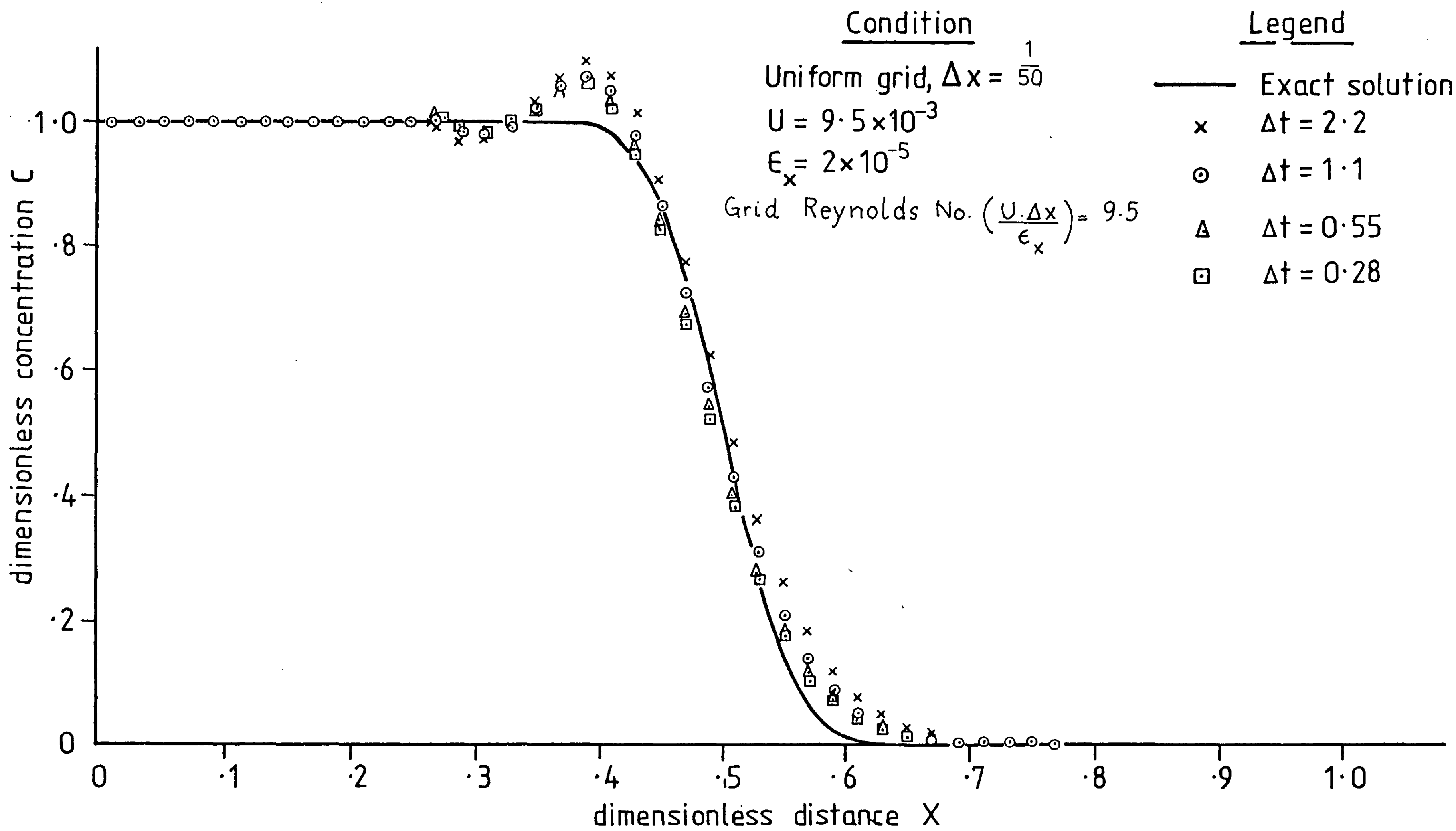

Fig. 6·7 Concentration profile at time $t = 0\cdot5/U$, by the ADI-CDS method, using various time step lengths Δt

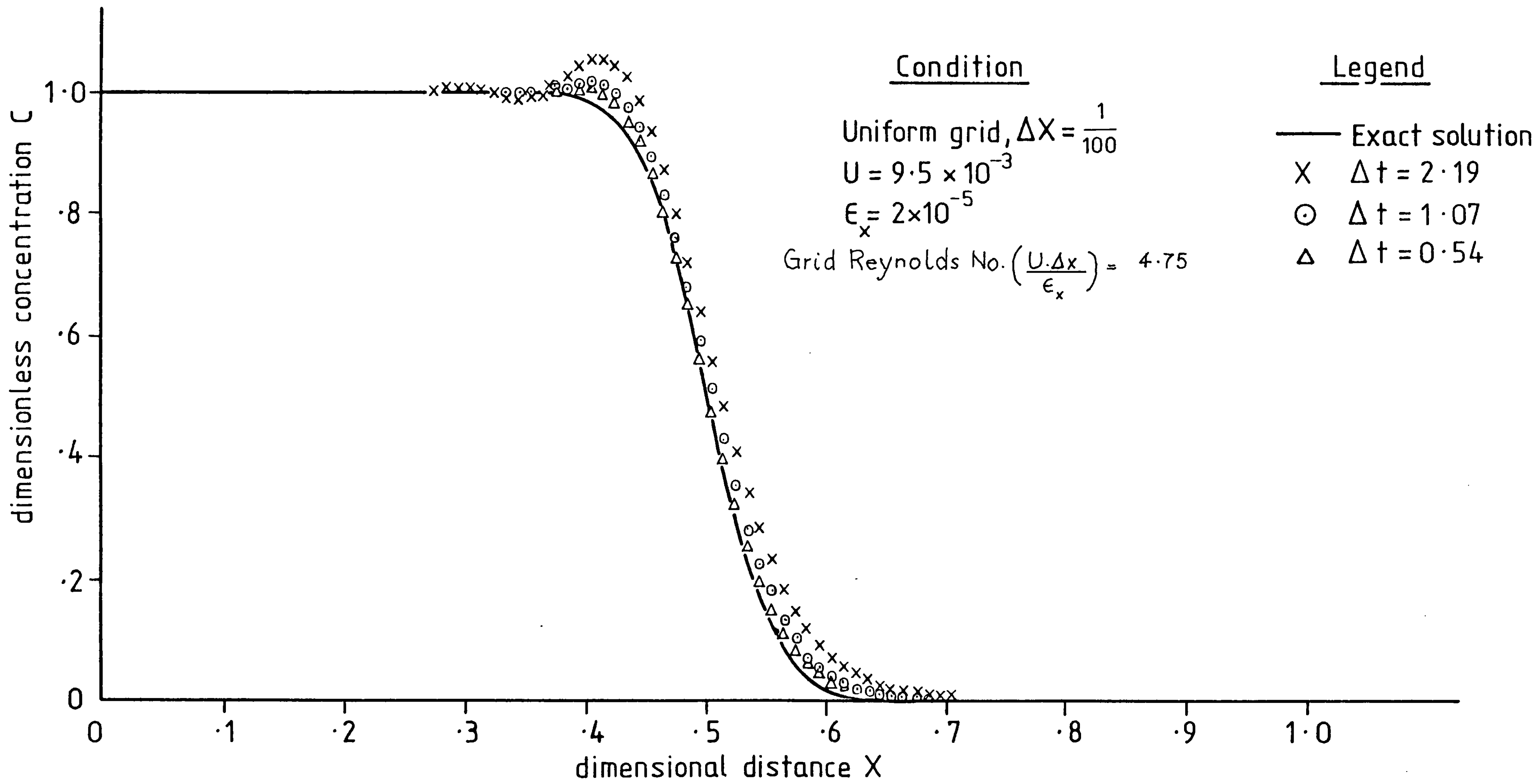

Fig. 6·8 Concentration profiles at time $t = 0\cdot5/U$, by the ADI-CDS method, using various time step length Δt.

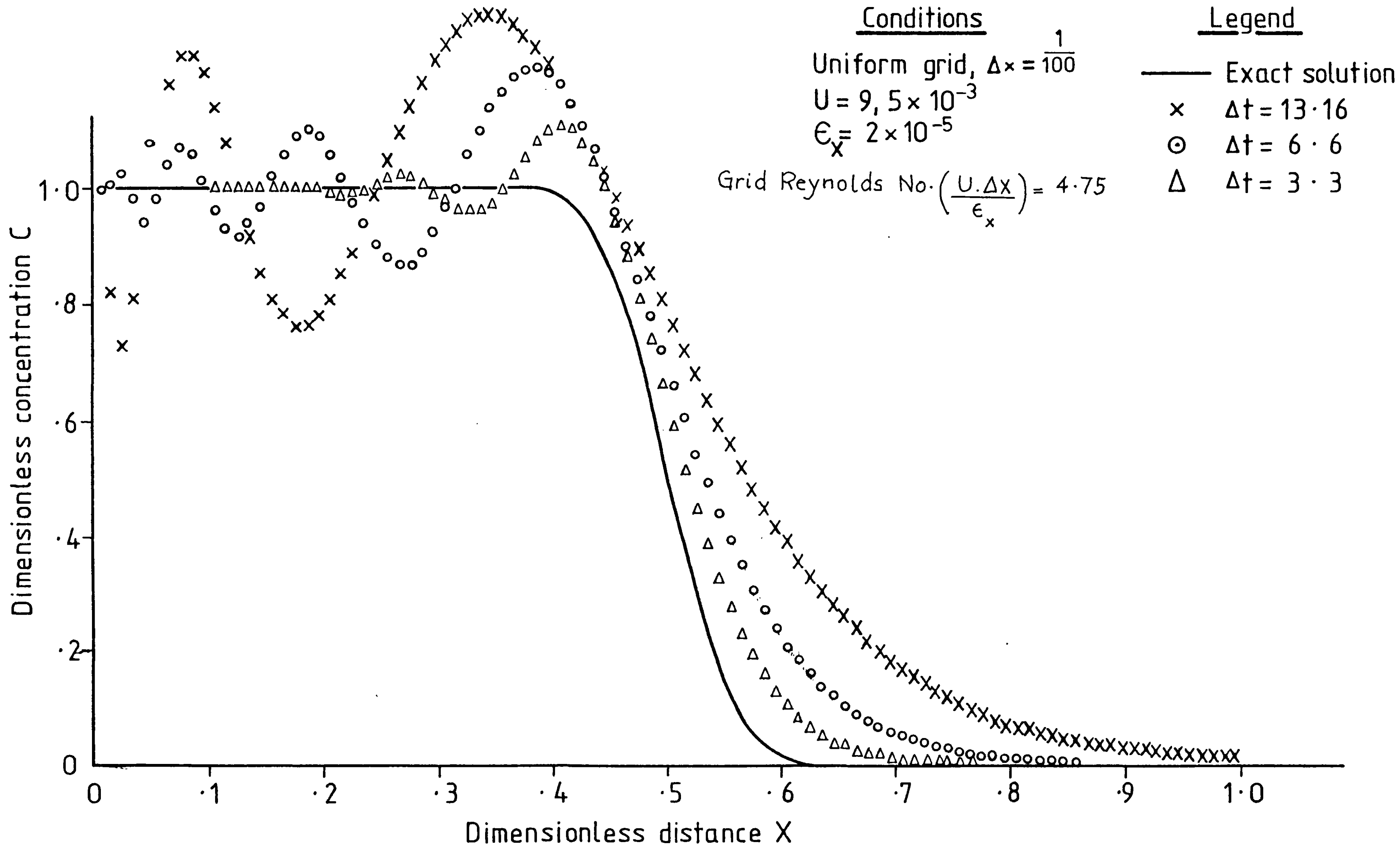

Fig. 6·9 Concentration profiles at time $t = 0 \cdot 5/U$, by the ADI-CDS method, using various time step lengths Δt.

SOME EFFECTS OF LANGMUIR CIRCULATION ON SUSPENDED PARTICLES IN LAKES AND RESERVOIRS

CHAPTER 7 NUMERICAL RESULTS AND THEIR ANALYSIS

Computed time-distributions of particle concentration in a Langmuir cell were obtained by numerical solution of the finite difference equation developed in Chapter 6, for various conditions of cell geometry and sinking (or ascending) speed, starting from an initial uniform distribution. Some examples are shown to illustrate the general distribution patterns of both buoyant and settleable particles in the cell. To assess the relative significance of Langmuir circulation effects in modelling particle distribution and sinking loss, predictions of time changes in the mass concentration within the mixed layer which have been obtained from conventional zero- (well mixed epilimnion) and one-dimensional models are compared with those computed by the present two-dimensional representation. A method by which the effects of Langmuir circulation could be included in these conventional models is outlined. Finally, a comparison is made between the Langmuir circulation's effect on loss rate, predicted by the present model, with that of Titman and Kilham (1976).

CHAPTER 7 NUMERICAL RESULTS AND THEIR ANALYSIS

7.1. Basic Information

Most computations of the computer program listed in Appendix I were made on the CDC Cyber 73 at the University of Leicester. A limited number of runs were also made on the much larger and faster CDC 7600 computer at the University of Manchester Regional Computing Centre. In all calculations, a 50 x 50 uniform grid (i.e. $\Delta y^* = \Delta z^* = 0.02$) and the time step length $\Delta t = 4.0$ were used. This combination represents a compromise between accuracy of solution and the available computing time. One typical simulation, from $t^* = 0$ to 5×10^4, takes approximately 6 hours on the Cyber 73 and about 20 minutes on the CDC 7600.

A large number of solutions were obtained by varying the row spacing to depth ratio λ_c^* between 2.5 and 0.5, and the sinking (or ascending) speed W_T^* between 1×10^{-3} to 1×10^{-6} at conveniently selected increments. Results are in the form of spatial distribution of particles over a Langmuir cell, the calculated sinking flux and total sinking loss at various selected times between $t^* = 0$ and 5×10^4. Computation terminates when either the end of simulation is reached or the mass of particles remaining in the Langmuir cell falls to a negligible amount (i.e. about 0.1% of the original mass). Only selected examples are given in this chapter, further solutions are available from the author.

7.2. Particle Distribution Patterns

7.2.1. Non-buoyant particles

Figure 7.1 illustrates the evolution with time, from an initially uniform distribution, of the particle distribution pattern, for a large row spacing-to-depth ratio $\lambda_c^* = 2.0$ and a large dimensionless particle sinking speed $W_T^* = 1 \times 10^{-3}$. Initially, transient patterns develop with the downwelling motion advecting low concentrations from the surface downwards, pushing high concentrations at the lower boundary of the cell upwards. During this time period concentration gradients are greatest. These are subsequently smoothed out by mixing which is developed in the circulation, resulting in the general aggregation of particles within the central portion and the upwelling side of the cell, while particle concentration in the surface layer and in the downwelling zone remains very low. Maximum concentration occurs at about mid-depth and at y^* about 0.55. At time t^* about 2000 to 3000, an equilibrium pattern of distribution develops, after which the relative distribution of particles in the cell is invarient, implying an equilibrium between the mixing and the sinking loss out of the cell. Concentration contours have been plotted to show the particle relative distribution pattern, contour 6 representing the mean concentration at that time. The position of contour 6 in relation to the lower boundary of the cell is significant in that it indicates whether the sinking flux of material out of the cell occurs at a concentration greater or less than the mean value. In Fig.7.1 material flux from the cell occurs at a concentration value which is much less than the mean. In this example, as t^* reaches about 2×10^4, a negligible quantity of particles is left in the cell.

In Fig.7.2, the particles in the same circulation cell ($\lambda_c^* = 2.0$) have a smaller sinking speed ($W_T^* = 1 \times 10^{-5}$) . The development of the distribution pattern is generally similar to that in the earlier example, except that concentration gradients throughout the cell are very small. Essentially uniform concentration occurs over most parts of the cell with the exception of somewhat lower values near the surface and immediately under the convergence line. The time taken to develop the equilibrium pattern of concentration distribution is longer than for the previous case, t^* being about 4000 to 5000 . If the sinking speed W_T^* were lower than 1×10^{-5} (not illustrated), the concentration distribution is essentially uniform over the cell, indicating that if particles have low sinking speeds (say, W_T^* less than 1×10^{-5}), Langmuir circulation becomes a stirring mechanism which rapidly smoothes out any concentration gradients created by the sinking loss.

Figures 7.3 and 7.4 depict the particle distribution patterns when $\lambda_c^* = 0.5$, i.e. in cells of small width-to-depth ratio. The sinking speeds, W_T^* , are 1×10^{-3} and 1×10^{-5} respectively. At the higher sinking speed, the aggregation of particles into a local maximum is still pronounced in the upwelling zone (at z^* approximately 0.3), but more lateral mixing occurs in this case. Although the general particle distribution is non-uniform, the concentration at the lower boundary of the cell is equal to the mean concentration in the cell, hence the sinking loss may be expected to be similar to that in a well-mixed situation. Equilibrium distribution develops at $t^* = 1000$ to 2000 . At the smaller sinking speed (Fig.7.4), particle distribution is essentially uniform throughout the cell except for the shallow layer immediately below the surface (to z^* some 0.5 units) and under the convergence line.

It can therefore be seen that the higher the sinking speed and the larger the cell width-to-depth ratio are,the more readily particles can be aggregated by Langmuir circulation into local regions of high concentration and low concentration. High concentrations generally extend from the central part of the cell, where the maximum occurs, to the upper part of the upwelling region. The concentrations immediately below the surface and in the convergence region represent minimum values. In the vicinity of the cell lower boundary, values are generally below the mean concentration.

With small particle sinking speeds (say W_T^* less than 1×10^{-5}), the enhanced circulation and mixing gives rise to an essentially uniform distribution of particles, where concentration differences are difficult to detect. As the cell width-to-depth ratio decreases, lateral mixing is enhanced, giving rise to lesser concentration gradients in that direction. However, with high particle sinking speed (say, when W_T^* greater than 1×10^{-5}), aggregation of particles occurs in the form of an elongated zone occupying the central part of the cell and the upper portion of the upwelling region. The maximum concentration centre moves towards the upwelling zone as the cell width decreases.

Since it is generally observed that essentially uniform concentration occurs when the particle sinking speed $W_T^* \leq 1 \times 10^{-5}$ regardless of cell width-to-depth ratio, therefore $W_T^* = 1 \times 10^{-5}$ may be regarded as the limit conditions for non-buoyant particles, below which Langmuir circulation cannot cause particle aggregation.

7.2.2. Buoyant Particles

For buoyant particles, the general patterns of concentration distribution with time are illustrated in Figs. 7.5 and 7.6 for a row spacing-to-depth ratio $\lambda_c^* = 2.0$ and ascending speeds W_T^* of -1×10^{-3} and -1×10^{-5}, respectively. The early transient evolution is basically similar to those of settleable particles inverted. Upward motion enhances the buoyant effect in rapidly bringing more particles to the surface, though some are swept back to lower depths by the downwelling. Figure 7.5 shows that very high particle concentration occurs under the convergence line. At the centre of the cell, the concentration is generally higher than those in the upwelling zone and near the cell lower boundary. In this case, equilibrium distribution is reached between time $t^* = 2000$ to 3000.

In Fig.7.6 ($\lambda_c^* = 2.0$ and $W_T^* = -1 \times 10^{-5}$), a concentration difference of about 4% is still observed between the maximum and the minimum. With buoyant particles, it has been found that uniform distribution occurs over the cell at $W_T^* \approx -1 \times 10^{-6}$, an order of magnitude smaller than the case shown in Fig.7.6. Also with buoyant particles, no local maxima in the form of central cores are established.

7.3. Effect of Cell Width-to-Depth Ratio on the Retention of Non-Buoyant Particles

The effects of Langmuir cell width on the distribution pattern of settleable particles have been illustrated in Section 7.2.1. Here, the influence of the cell width on the retention of particles within the cell and hence on the sinking loss rate is shown by plotting, for a fixed value of sinking speed, the mean concentration $\overline{C}^*$ at various times against the row spacing-to-depth ratio λ_c^*. Figure 7.7 represents the case when $W_T^* = 1 \times 10^{-3}$ and λ_c^* varies between 2.5 and 0.5. It can be seen that cells with larger width-to-depth ratios retain more particles in suspension thus reducing sinking loss. Superimposed on Fig.7.7 is a curve showing the variation in the mean concentration with time for the well-mixed Langmuir cell. The graph clearly demonstrates that as the cell width-to-depth ratio decreases the well-mixed situation is approached.

7.4. The Extent of Langmuir Circulation Effects in the Modelling of Particle Distribution and Sinking Loss

The extent of the circulation effects in the modelling of particle distribution within the mixed layer and the sinking loss from it can be investigated by comparing the particle distribution profiles and sinking loss obtained from the present two-dimensional model with those predicted by some conventional models employed in practical water quality study, which ignore Langmuir circulation effects. Typical representations of these conventional models are the zero-dimensional well-mixed compartment model and the one-dimensional model. The well-mixed compartment model assumes a uniformly mixed epilimnion at all times. Ignoring the diffusive transfer of material through the lower boundary, the change in the mean concentration $\overline{C}$ with time t for particles of sinking speed W_T in the epilimnion of depth D is given by the governing equations

$$\frac{\partial \overline{C}}{\partial t} = - \frac{W_T}{D} \overline{C} \quad , \tag{7.1}$$

whose solution is

$$\overline{C}(t) = \overline{C}_o \, e^{-\frac{W_T}{D} t} \tag{7.2}$$

where $\overline{C}_o$ is the initial concentration at $t = 0$. Written non-dimensionally, equation (7.2) becomes

$$\overline{C}^*(t^*) = e^{-W_T^* t^*} \quad . \tag{7.2'}$$

The one-dimensional model is based on the advection-diffusion formulation describing only the variation with depth of quantities of interest; lateral uniformity is assumed. The governing equation is

$$\frac{\partial C^*}{\partial t^*} + \frac{\partial}{\partial z^*} (W_T^* C^*) = \frac{\partial}{\partial z^*} \left(\varepsilon_z^* \frac{\partial C^*}{\partial z^*} \right) \quad , \tag{7.3}$$

in which W_T^* is the dimensionless sinking speed of the particle; and ε_z^* is the vertical eddy diffusion coefficient. Equation (7.3) is subjected to the same boundary conditions in the vertical direction as the present model (equation 3.12). The solution to it can be obtained from the present two-dimensional model simply by making lateral velocity component V^* zero. A review of the physical concepts of these two conventional models may be found in Rutherford (1976).

Figures 7.8 and 7.9 show variations of the mean concentration at various times from $t^* = 0$, for $\lambda_c^* = 2.0$ and 0.5 , respectively, with different values of sinking speeds from 1×10^{-3} to 1×10^{-5} . In the two-dimensional model (equation 3.12), the mean concentration is obtained by averaging over the Langmuir cell, and in the one-dimensional model, by averaging over the mixed layer depth. The figures show clearly that, at any time, the one-dimensional model predicts a smaller quantity of particles remaining in the mixed layer (and hence a larger sinking loss) than those predicted by the zero-dimensional well-mixed compartment and the two-dimensional models. For the case considered, i.e. $\lambda_c^* = 2.0$, when the particle sinking speeds are high, the two-dimensional model predicts a lower sinking loss from the mixed layer than do the two conventional models, and predictions from the former approach those from the zero-dimensional (well-mixed) model as the sinking speed decreases. When $\lambda_c^* = 0.5$ (Fig.7.9), the predictions by the two-dimensional and the well-mixed models are in closer agreement at all sinking speeds, being comparable for low sinking speeds but less comparable with somewhat higher sinking loss at high sinking speeds. These figures demonstrate the significant effect in lakes and reservoirs of Langmuir circulation in considerably reducing sinking loss, at least for particles with the dimensionless sinking speed W_T^* greater than 1×10^{-5} .

7.5. Effective Sinking Speeds

Langmuir circulation effects may be incorporated in the zero-dimensional (well-mixed) model and in the one-dimensional model by using effective sinking speeds in place of the particle terminal fall speeds. These effective sinking speeds are those speeds at which particles would have to sink, to give equivalent concentration profiles and sinking losses observed in Langmuir circulation. Because a direct determination of these effective sinking speeds is beyond present technical capability (discussed in page 13), the current numerical study can be useful in providing simulated data on concentration profiles and sinking losses, from which effective sinking speeds may be determined.

7.5.1. The Well-Mixed Compartment Model (zero-dimensional)

The effective sinking speed for this model may be determined by computing the value of W_T^* in equation (7.2') which gives the same prediction of the mean concentration $\overline{C}^*$ as that from the two-dimensional model at the corresponding time. Figures 7.7, 7.8 and 7.9 indicate that the concentration-time curve plotted semi-logarithmically consist of two portions, a non-linear portion in the early time and a straight line portion after an equilibrium particle distribution pattern has been established. If the time step Δt^* used in the zero-dimensional model were larger than the time to reach equilibrium distribution t_E^*, then the simulation for one time step can be divided into two parts, from $t^* = 0$ to t_E^* and from $t^* = t_E$ to Δt^*. Using these two sub-steps, two values of effective sinking speeds are entailed, the first to obtain, from the initial concentration, the mean concentration at t_E^*, and the second to compute the mean concentration at the end of the time step Δt^*. That is,

$$\overline{C}_{t_E} = \overline{C}_o \, . \, e^{-W_{eff1} \cdot t_E} , \tag{7.4a}$$

and

$$\overline{C}_{\Delta t} = \overline{C}_{t_E} \, . \, e^{-W_{eff2} \cdot (\Delta t - t_E)} \tag{7.4b}$$

in which the non-dimensionalised parameters are implied without specifying them by means of superscripts $*$; $\overline{C}_{t_E}$ is the mean concentration at t_E ; $C_{\Delta t}$ is the mean concentration at the end of any time step Δt ; W_{eff1} and W_{eff2} are the effective sinking speeds applicable for times between 0 and t_E and $t > t_E$, respectively.

Using results from the present two-dimensional model with Langmuir circulation, W_{eff1} and W_{eff2} can be found as follows. By inspection, in most cases, t_E is found to be $\leq$ 6000 . Taking $t_E = 6000$, $\overline{C}_o = 100$, and $\overline{C}_E$ to be $\overline{C}$ at $t = 6000$ from the two-dimensional results, then equation (7.4a) gives for W_{eff1} ,

$$W_{eff1} = \frac{\ln(\overline{C}_o/\overline{C}_E)}{t_E} \, . \tag{7.5}$$

Similarly, from (7.4b),

$$W_{eff2} = \frac{\ln(\overline{C}_{t_E} / \overline{C}_{\Delta t})}{(\Delta t - t_E)} \quad . \tag{7.6}$$

In equations (7.6), $\overline{C}_{\Delta t}$ and Δt can be any corresponding values on the linear portion of the $\overline{C}$ v.s. t curve. Figures 7.10 and 7.11 illustrate the variation of the effective sinking speeds W_{eff1} and W_{eff2}, respectively, for various values of sinking speed W_T and row spacing-to-depth ratio λ_c. Expressing these effective sinking speeds as a fraction of the terminal fall speed of the particle, the ratio of the effective sinking speed to particle fall speed as a function of W_T and λ_c can be prepared. A representative example for W_{eff2}/W_T is shown in Fig.7.12.

If the time step Δt in the zero-dimensional model is less than 6000, the effective sinking speed is a function of Δt as well as of W_T and λ_c. Figure 7.12a illustrates the variation of the ratio W_{eff}/W_T with Δt (<6000) and W_T for $\lambda_c = 2.5$. Similar curves can be prepared for other values of λ_c.

7.5.2. The One-Dimensional Model

It is proposed that the effective sinking speed for the one-dimensional model be determined as follows. Using the vertical concentration profiles at various times simulated by the two-dimensional model, the one-dimensional equation is solved, yielding appropriate values of sinking speeds at various depths and times.

In the present derivation, the following definite-difference structure has been adopted, in which, referring to the grid structure in Fig.7.13, for the grid volume j ,

$$\left.\frac{\partial C}{\partial t}\right|_j = \frac{C_j^{n+1} - C_j^n}{\Delta t} \quad , \tag{7.7}$$

$$\left.\frac{\partial (WC)}{\partial z}\right|_j^{n+\frac{1}{2}} = \frac{(WS.CS)^{n+\frac{1}{2}} - (WN.CN)^{n+\frac{1}{2}}}{\Delta z_j} \tag{7.8}$$

where

$$\left.\begin{aligned} WS &= W_j \quad , \\ WN &= W_{j-1} \quad , \\ CS &= C_{j+\frac{1}{2}} = \tfrac{1}{2}(C_{j+1}^{n+\frac{1}{2}} + C_j^{n+\frac{1}{2}}) \quad , \\ CN &= C_{j-\frac{1}{2}} = \tfrac{1}{2}(C_j^{n+\frac{1}{2}} + C_{j-1}^{n+\frac{1}{2}}) \quad , \end{aligned}\right\} \tag{7.9}$$

that is, the spatial derivatives are centred in distance and in time plane at $n + \frac{1}{2}$. All the symbols have their own usual meanings as already established in Chapter 6. The concentration at time level $n + \frac{1}{2}$ is the average of the values at times $n + 1$ and n, i.e.

$$C^{n+\frac{1}{2}} = \tfrac{1}{2}(C^{n+1} + C^n) \quad . \tag{7.10}$$

The diffusion term is approximated by

$$\frac{\partial}{\partial z}\left.\left(\varepsilon_z \frac{\partial C}{\partial z}\right)\right|_j^{n+\frac{1}{2}} = \frac{\varepsilon_z}{\Delta z_j^2}(C_{j+1}^{n+\frac{1}{2}} - C_j^{n+\frac{1}{2}}) - \frac{\varepsilon_z}{\Delta z_j^2}(C_j^{n+\frac{1}{2}} - C_{j-1}^{n+\frac{1}{2}}) \quad . \tag{7.11}$$

Substituting equations (7.7), (7.8), (7.9), (7.10) and (7.11) into equations (7.3) and rearranging, the general equations for grid volume j is

$$W_{j-1}.AA_j + W_j.BB_j = CC_j \ , \tag{7.12}$$

where $AA_j = \frac{\Delta t}{2\Delta z_j}(C_j^{n+\frac{1}{2}} + C_{j-1}^{n+\frac{1}{2}})$,

$BB_j = -\frac{\Delta t}{2\Delta z_j}(C_j^{n+\frac{1}{2}} + C_{j+1}^{n+\frac{1}{2}})$,

and $CC_j = (C_j^{n+1} - C_j^{n}) - \frac{\varepsilon_z.\Delta t}{\Delta z_j^2}(C_{j+1}^{n+\frac{1}{2}} - C_j^{n+\frac{1}{2}}) + \frac{\varepsilon_z.\Delta t}{\Delta z_j^2}(C_j^{n+\frac{1}{2}} - C_{j-1}^{n+\frac{1}{2}})$,

with $C^{n+\frac{1}{2}} = \frac{1}{2}(C^{n+1} + C^{n})$.

Equation (7.12) is subjected to the same boundary conditions at the lower permeable boundary as described for two dimensional case (See Chapter 6). This results in NZ - 1 simultaneous equations, where NZ is the number of mesh points,

$$W_1.BB_1 = CC_1 \tag{7.12a}$$

$$W_1.AA_2 + W_2.BB_2 = CC_2 \tag{7.12b}$$

$$W_2.AA_3 + W_3.BB_3 = CC_3 \tag{7.12c}$$

$$\vdots \qquad\qquad \vdots$$

$$W_{j-1}.AA_j + W_j.BB_j = CC_j \tag{7.12d}$$

$$\vdots \qquad\qquad \vdots$$

$$W_{NZ-2}.AA_{NZ-1} + W_{NZ-1}.BB_{NZ-1} = CC_{NZ-1} \ . \tag{7.12e}$$

At Δt time-increments, the coefficients AA_j, BB_j, and CC_j may be readily computed from the known values of concentration profiles. Then equation (7.12a) gives

$$W_1 = CC_1/BB_1 \quad . \tag{7.13a}$$

Substituting this in equation (7.12b), W_2 can be obtained, i.e.

$$W_2 = \frac{CC_2}{BB_2} - W_1 . \frac{AA_2}{BB_2} \quad . \tag{7.13b}$$

Thus, in general,

$$W_j = \frac{CC_j}{BB_j} - W_{j-1} \cdot \frac{AA_j}{BB_j} \quad . \tag{7.13c}$$

Hence all W_j values, from $j = 1$ to $NZ - 1$, can be determined. Figures 7.14 and 7.15 illustrate the computed effective sinking speeds for the one-dimensional model adopted in this section, with Δt given by the usual criterion $\Delta t \leq \min. (\Delta z/W_T, \Delta z^2/\varepsilon_z)$, and $\Delta z = 0.1$, for the sinking speeds of 1×10^{-3} and 1×10^{-5}, respectively, and λ_c equals 2.0 .

7.6. Comparison of the Effective Sinking Loss Rates with Titman and Kilham's Results

A comparison of the predicted effective sinking loss rates has been made in Fig.7.16, with Titman and Kilham's example (Titman and Kilham, 1976) for the case of the downwelling speed equals 1.0 cm/s and the row spacing-to-depth ratio of 2.0 . The present calculations predict effective loss rates to be generally smaller than the conventionally used loss rates in zero-dimensional well mixed models, when particle sinking speeds are high. The effective loss rates converge to the conventional values for low particle sinking speeds. In all cases, the present estimates are larger than those of Titman and Kilham.

Fig. 7.1 Particle distribution in a Langmuir cell at various times t^*, for dimensionless sinking speed $W_T^* = 1 \times 10^{-3}$ and cell spacing-to-depth ratio $\lambda_c^* = 2.0$. Values of contours are shown adjacent to the plots.

PLOT 7.1(a) LAMBDA= 2.00 T^*= 0.20000E03
WT= 0.100E-02

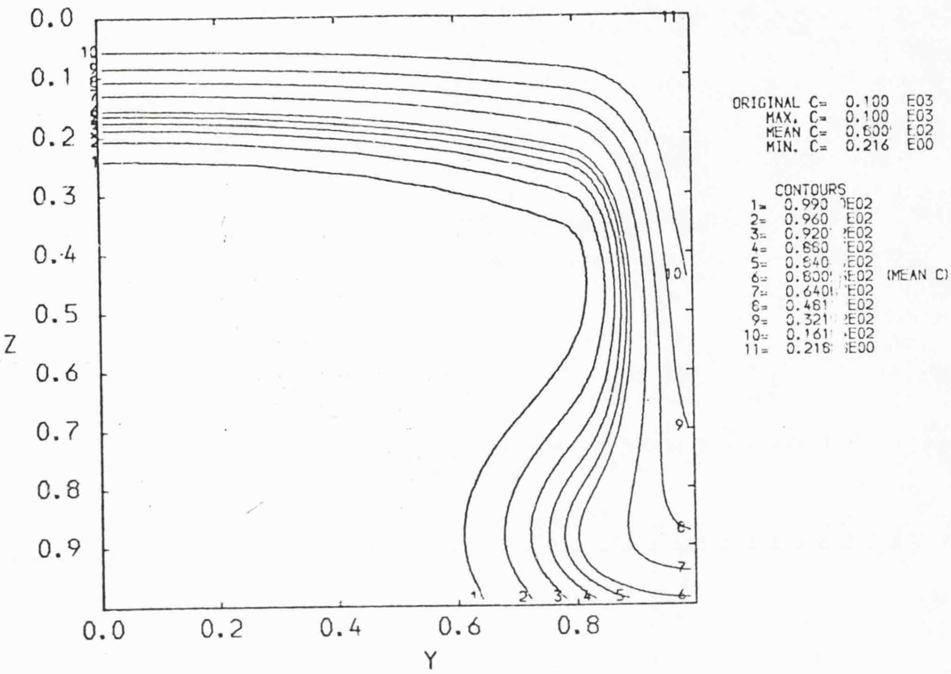

PLOT 7.1(b) LAMBDA= 2.00 T^*= 0.40000E03
WT= 0.100E-02

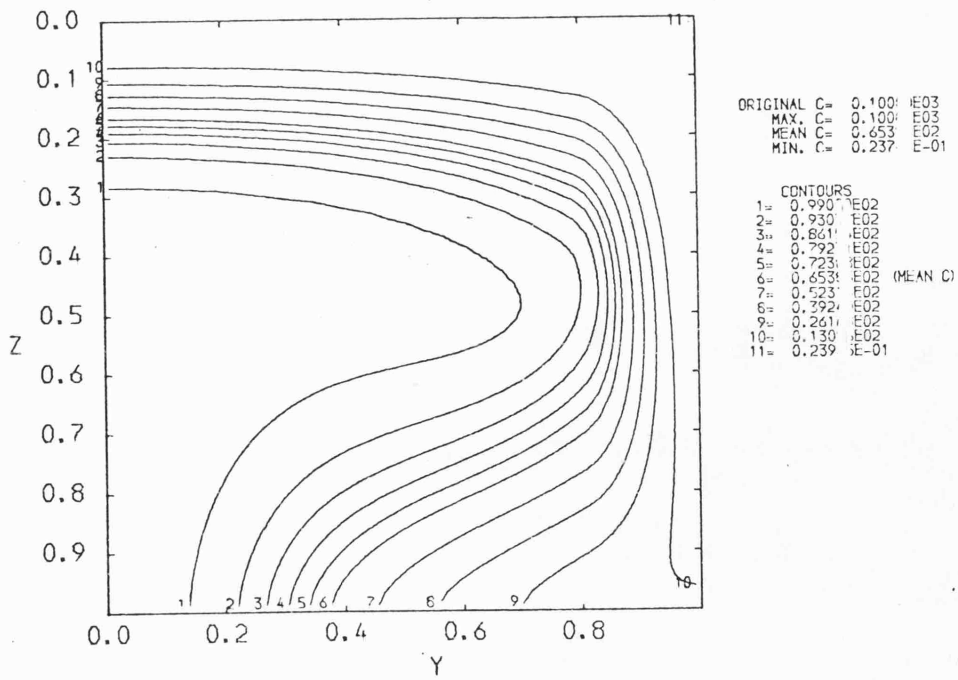

PLOT 7.1(c) LAMBDA= 2.00 T$\overset{*}{=}$ 0.60000E03
WT= 0.100E-02

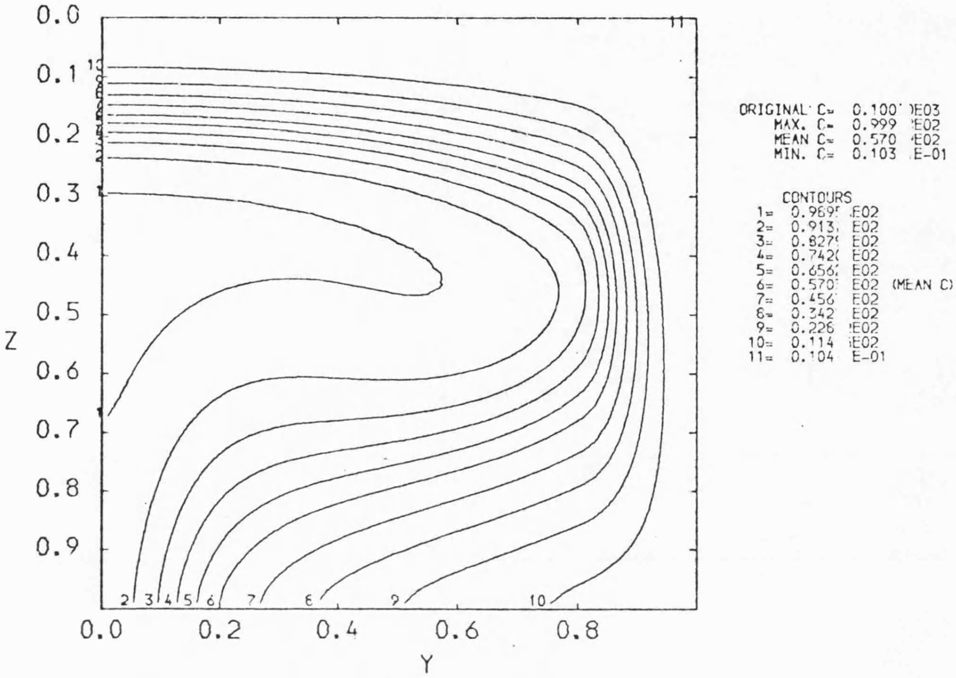

PLOT 7.1(d) LAMBDA= 2.00 T$\overset{*}{=}$ 0.80000E03
WT= 0.100E-02

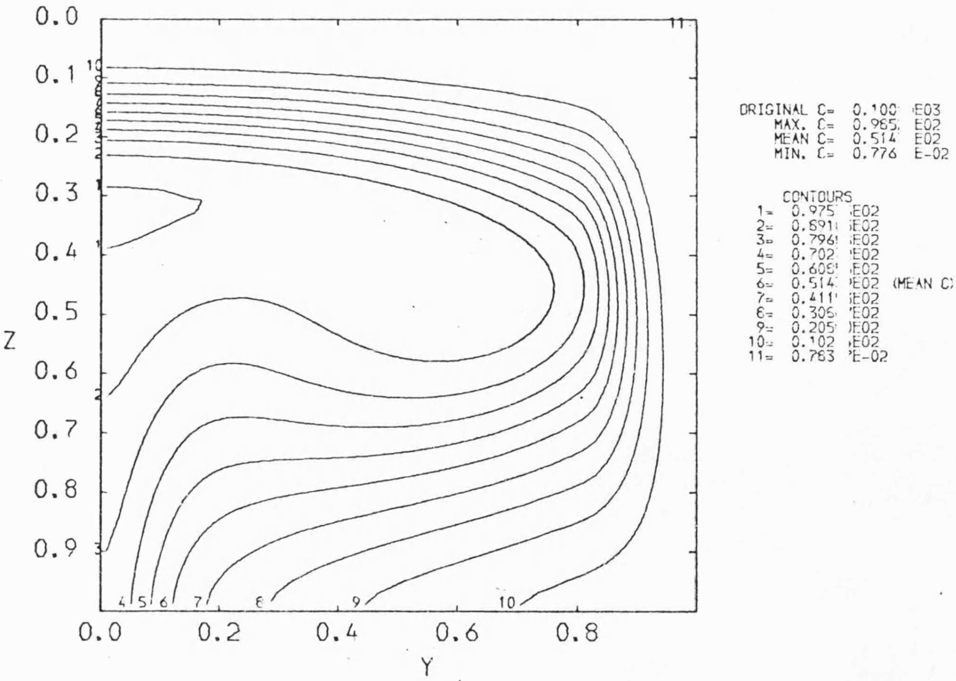

PLOT 7.1(e) LAMBDA= 2.00 T*= 0.40000E04
WT= 0.100E-02

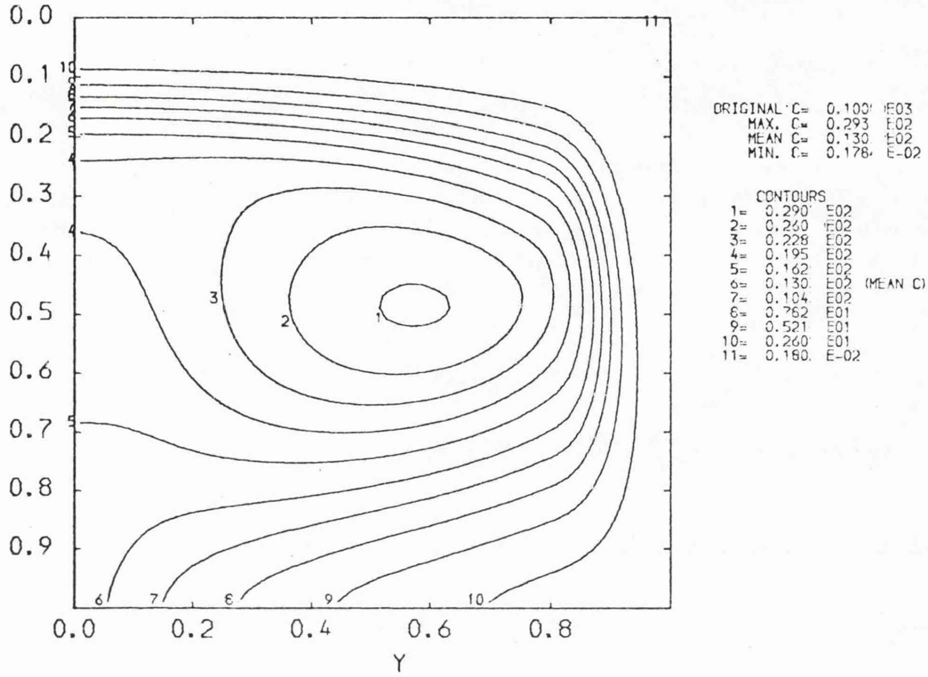

PLOT 7.1(f) LAMBDA= 2.00 T*= 0.60000E04
WT= 0.100E-02

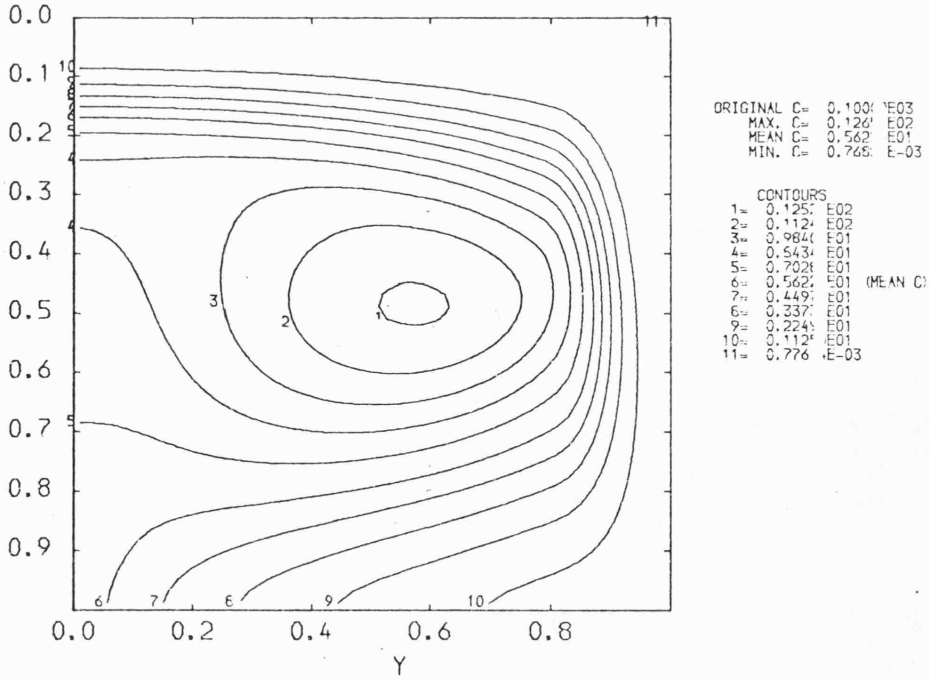

PLOT 7.1(g) LAMBDA= 2.00 T^*= 0.20000E05
WT= 0.100E-02

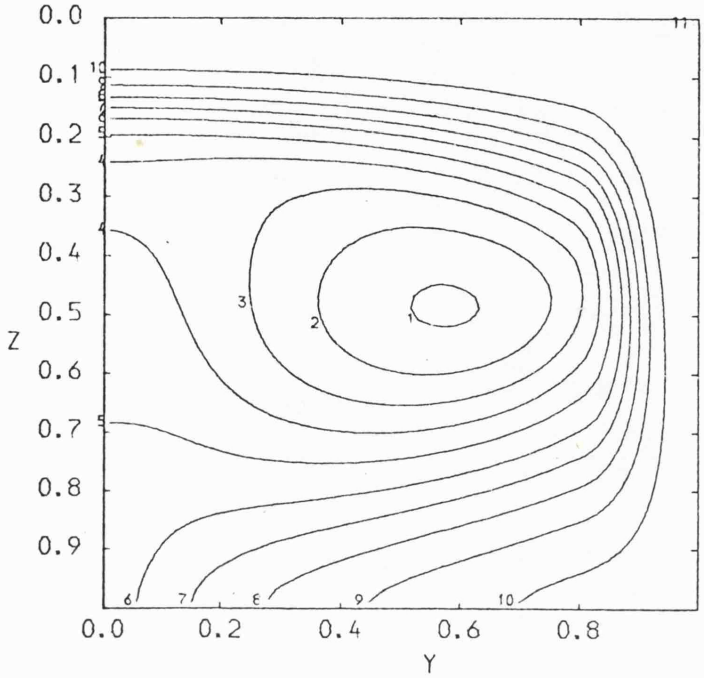

ORIGINAL C= 0.100 E03
MAX. C= 0.351 E-01
MEAN C= 0.156 E-01
MIN. C= 0.213 E-05

CONTOURS
1= 0.347 E-01
2= 0.312 E-01
3= 0.273 E-01
4= 0.234 E-01
5= 0.195 E-01
6= 0.156 E-01 (MEAN C)
7= 0.124 E-01
8= 0.936 E-02
9= 0.624 E-02
10= 0.312 E-02
11= 0.215 E-05

PLOT 7.1(h) LAMBDA= 2.00 T^*= 0.22000E05
WT= 0.100E-02

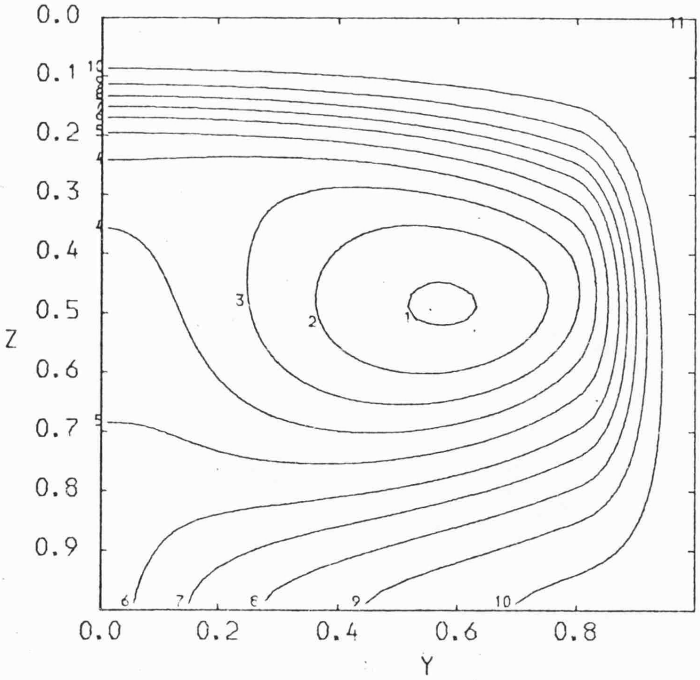

ORIGINAL C= 0.100 E03
MAX. C= 0.151 E-01
MEAN C= 0.672 E-02
MIN. C= 0.920 E-06

CONTOURS
1= 0.149 E-01
2= 0.134 E-01
3= 0.117 E-01
4= 0.100 E-01
5= 0.841 E-02
6= 0.672 E-02 (MEAN C)
7= 0.538 E-02
8= 0.403 E-02
9= 0.269 E-02
10= 0.134 E-02
11= 0.929 E-06

Fig. 7.2 Particle distribution in a Langmuir cell at various times t^*, for dimensionless sinking speed W_T^* = 1×10^{-5} and cell spacing-to-depth ratioo $\lambda_c^* = 2.0$.

PLOT 7.2(a) LAMBDA= 2.00 T^*= 0.20000E03
WT= 0.100E-04

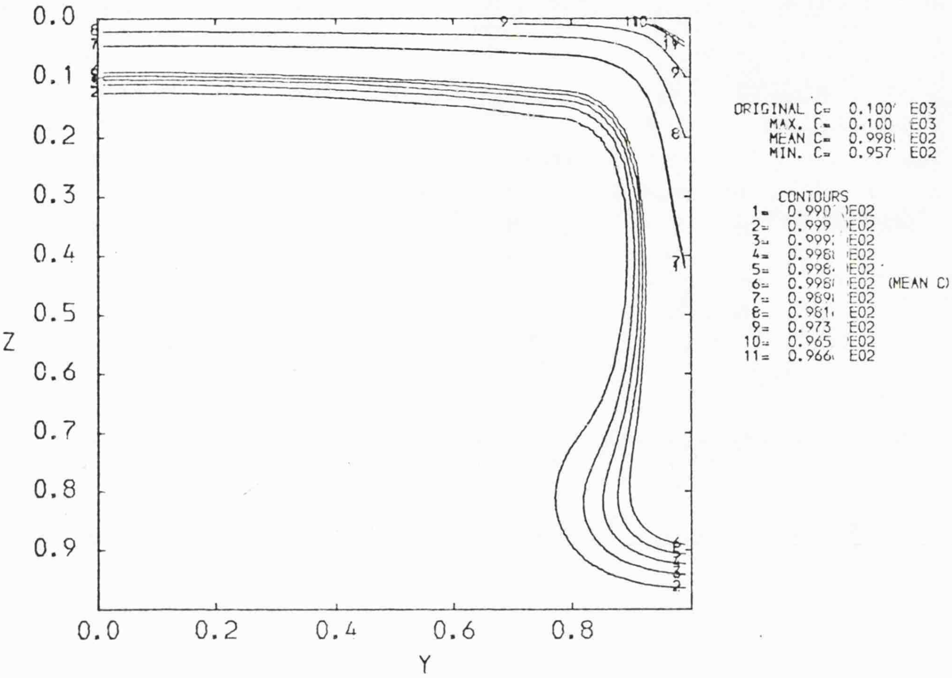

PLOT 7.2(b) LAMBDA= 2.00 T^*= 0.40000E03
WT= 0.100E-04

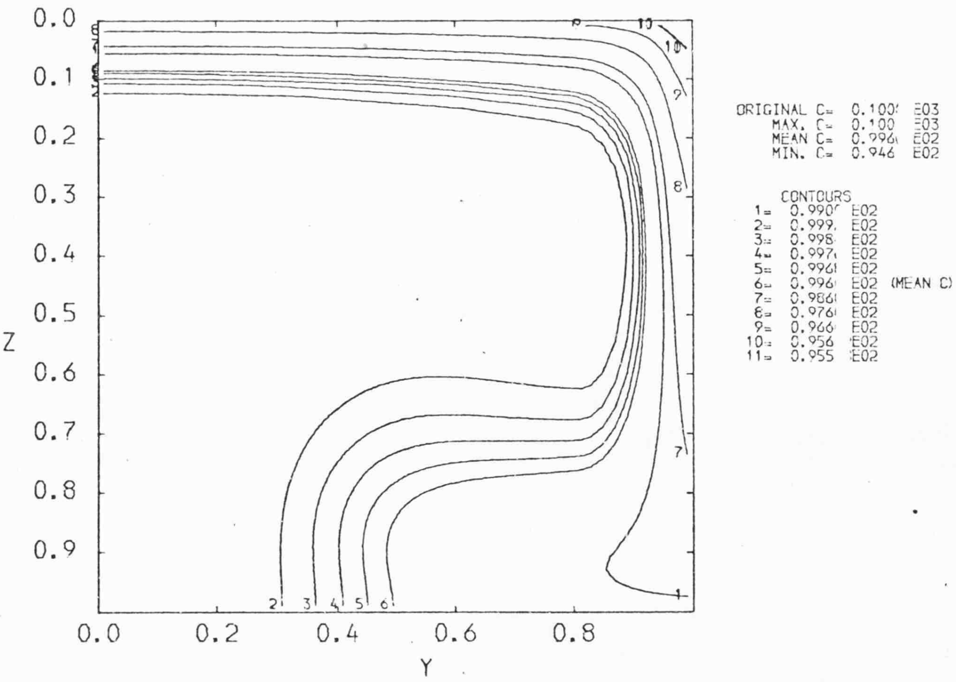

PLOT 7.2(c) LAMBDA= 2.00 T^{*}= 0.60000E03
WT= 0.100E-04

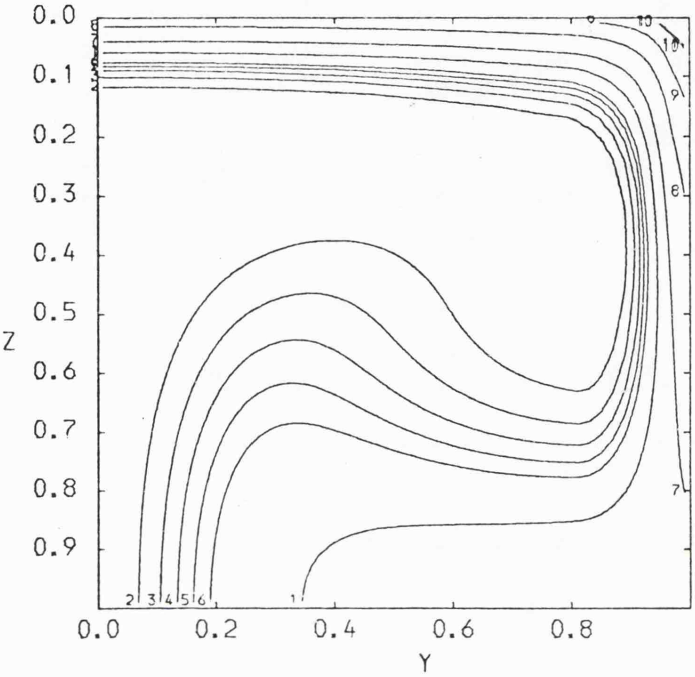

ORIGINAL C= 0.100 E03
MAX. C= 0.100 E03
MEAN C= 0.994 E02
MIN. C= 0.943 E02

CONTOURS
1= 0.990 E02
2= 0.996 E02
3= 0.997 E02
4= 0.996 E02
5= 0.995 E02
6= 0.994 E02 (MEAN C)
7= 0.963 E02
8= 0.973 E02
9= 0.963 E02
10= 0.953 E02
11= 0.952 E02

PLOT 7.2(d) LAMBDA= 2.00 T^{*}= 0.80000E03
WT= 0.100E-04

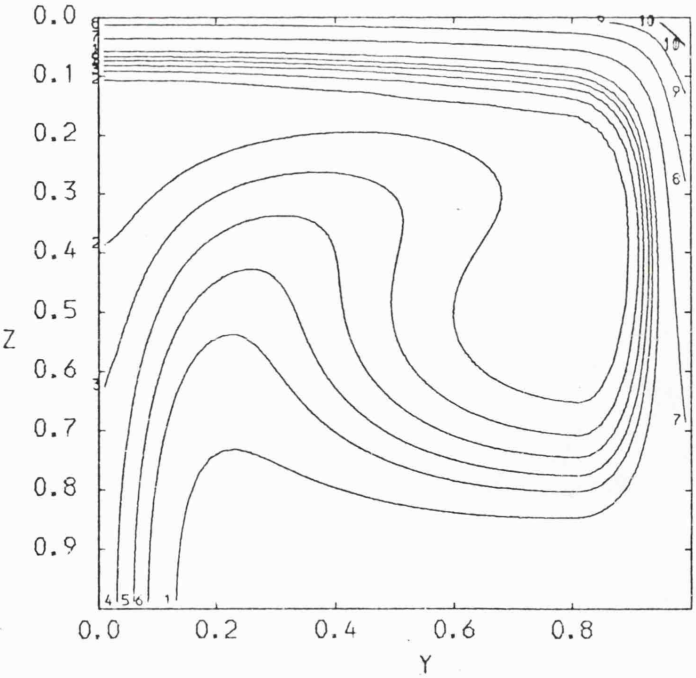

ORIGINAL C= 0.100 E03
MAX. C= 0.999 E02
MEAN C= 0.992 E02
MIN. C= 0.942 E02

CONTOURS
1= 0.989 E02
2= 0.998 E02
3= 0.996 E02
4= 0.995 E02
5= 0.993 E02
6= 0.992 E02 (MEAN C)
7= 0.982 E02
8= 0.972 E02
9= 0.962 E02
10= 0.952 E02
11= 0.951 E02

PLOT 7.2(e) LAMBDA= 2.00 T^{*}= 0.40000E04
WT= 0.100E-04

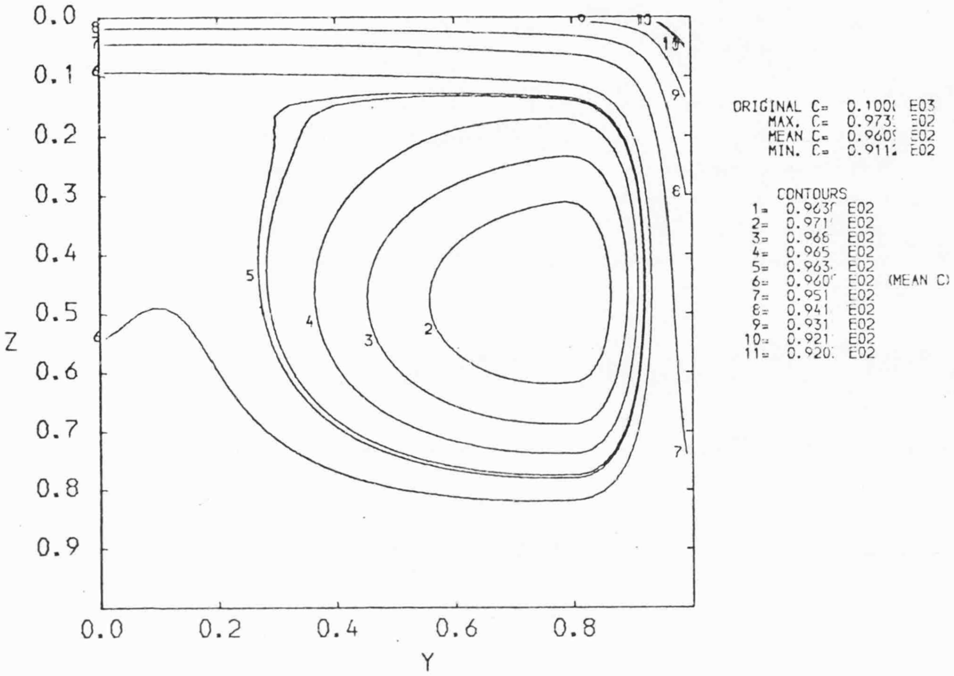

PLOT 7.2(f) LAMBDA= 2.00 T^{*}= 0.60000E04
WT= 0.100E-04

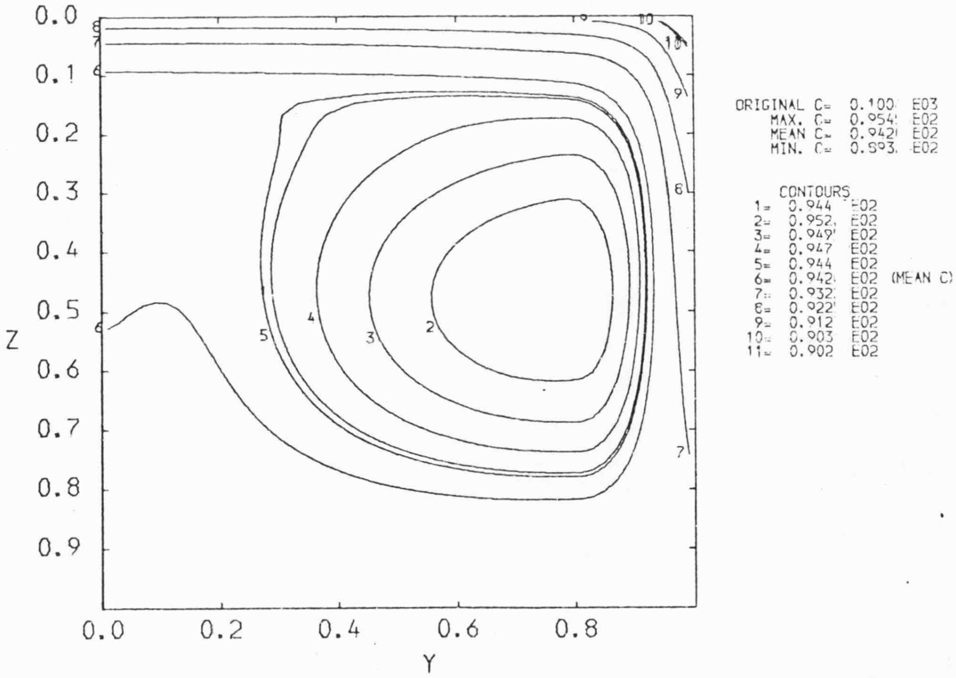

PLOT 7.2(g) LAMBDA= 2.00 T^{*}= 0.20000E05
WT= 0.100E-04

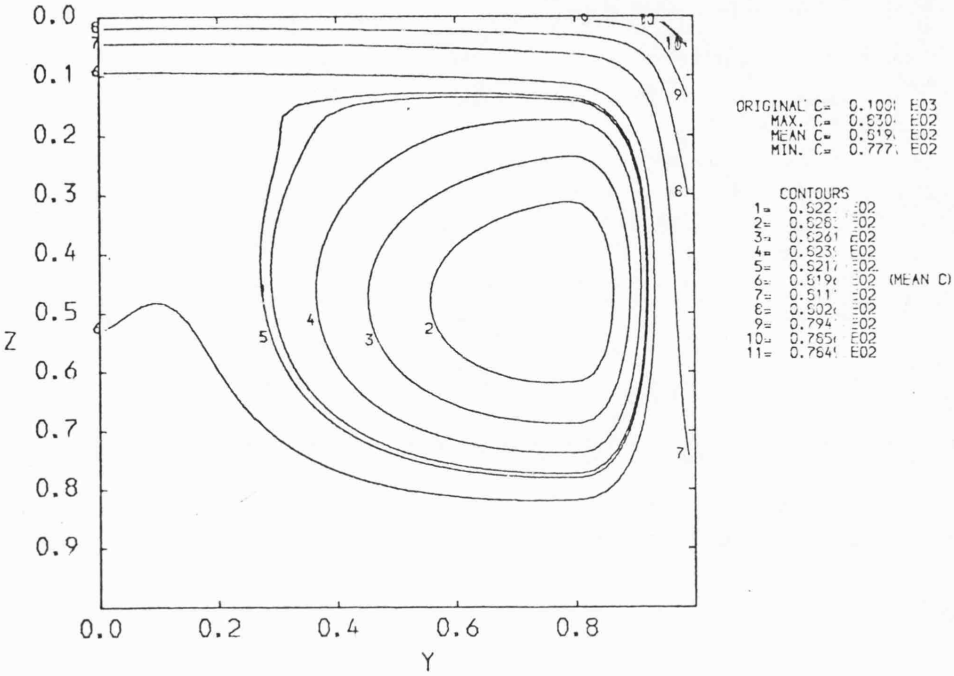

PLOT 7.2(h) LAMBDA= 2.00 T^{*}= 0.22000E05
WT= 0.100E-04

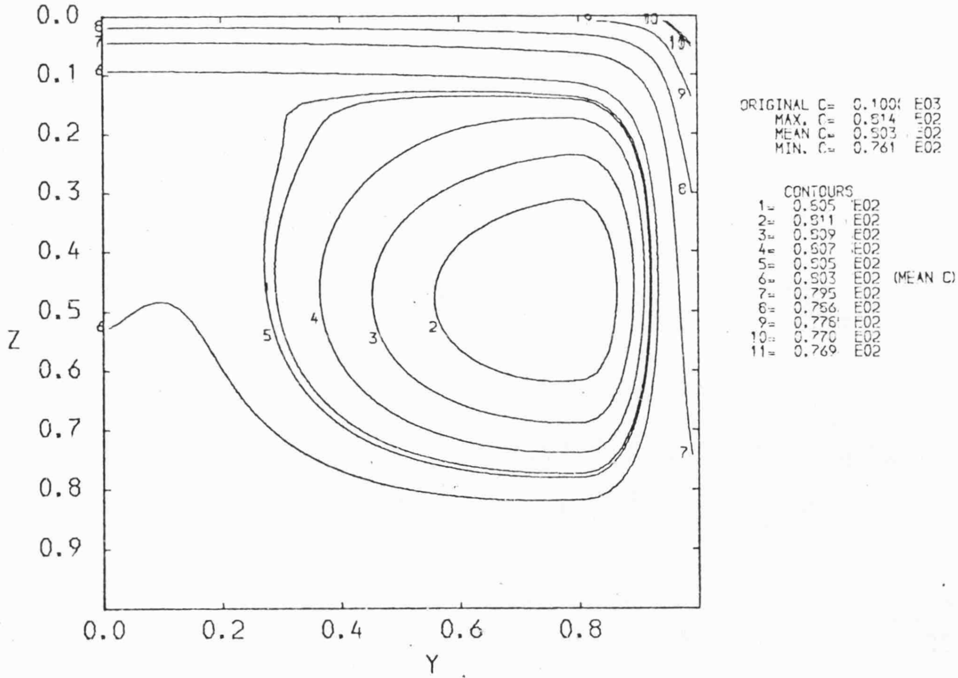

Fig. 7.3 Particle distribution in a Langmuir cell at various times t^*, for dimensionless sinking speed $W_T^* = 1x10^{-3}$ and cell spacing-to-depth ratio $\lambda_c^* = 0.5$.

PLOT 7.3(a) LAMBDA= 0.50 T*= 0.20000E03
WT= 0.100E-02

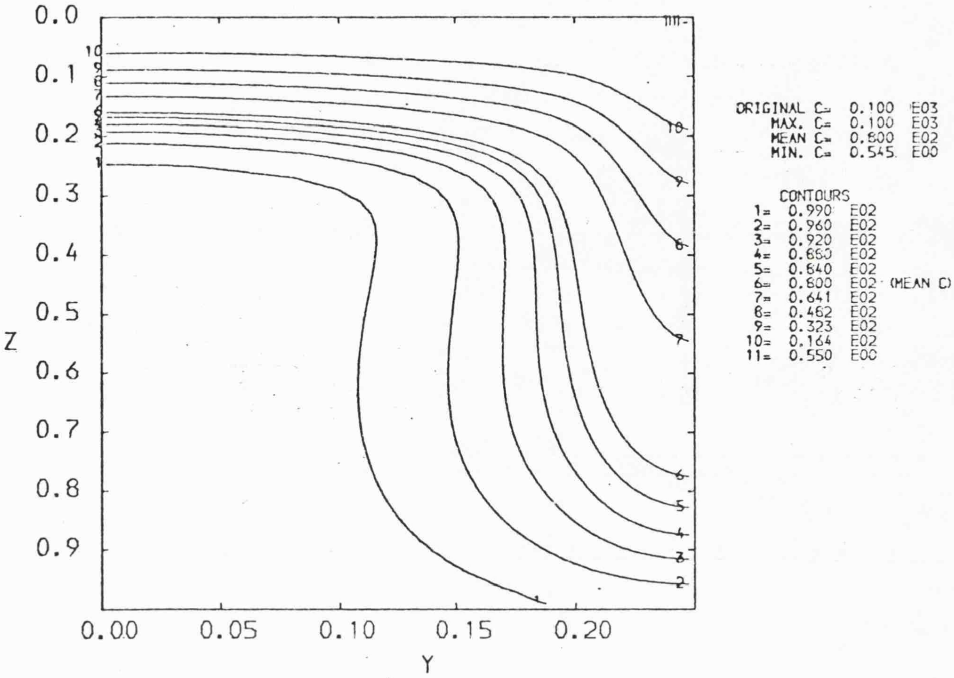

PLOT 7.3(b) LAMBDA= 0.50 T*= 0.40000E03
WT= 0.100E-02

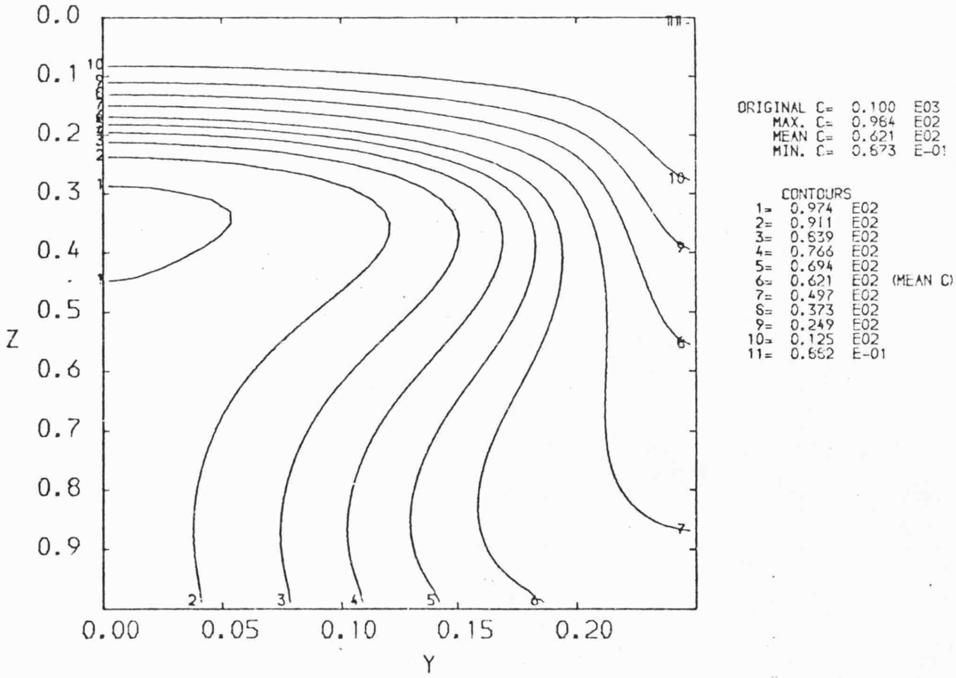

PLOT 7.3(c) LAMBDA= 0.50 T^*= 0.60000E03
WT= 0.100E-02

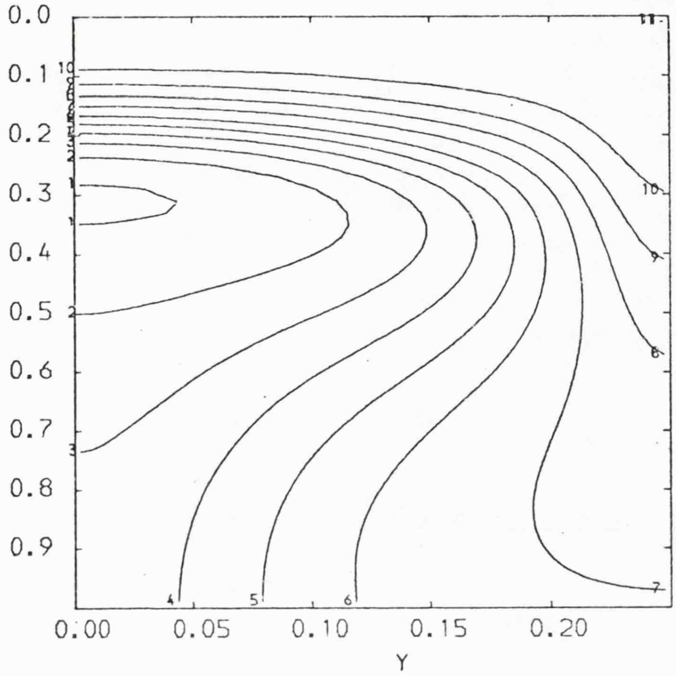

ORIGINAL C= 0.100 E03
MAX. C= 0.913 E02
MEAN C= 0.496 E02
MIN. C= 0.427 E-01

CONTOURS
1= 0.903 E02
2= 0.829 E02
3= 0.746 E02
4= 0.663 E02
5= 0.579 E02
6= 0.496 E02 (MEAN C)
7= 0.397 E02
8= 0.298 E02
9= 0.196 E02
10= 0.996 E01
11= 0.431 E-01

PLOT 7.3(d) LAMBDA= 0.50 T^*= 0.80000E03
WT= 0.100E-02

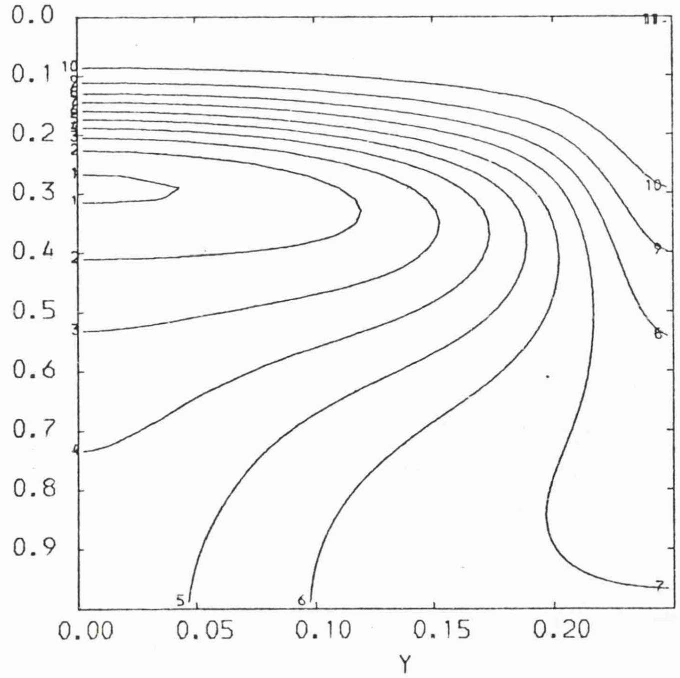

ORIGINAL C= 0.100 E03
MAX. C= 0.791 E02
MEAN C= 0.405 E02
MIN. C= 0.320 E-01

CONTOURS
1= 0.763 E02
2= 0.714 E02
3= 0.637 E02
4= 0.560 E02
5= 0.462 E02
6= 0.405 E02 (MEAN C)
7= 0.324 E02
8= 0.243 E02
9= 0.162 E02
10= 0.814 E01
11= 0.323 E-01

PLOT 7.3(e) LAMBDA= 0.50 T^*= 0.40000E04
WT= 0.100E-02

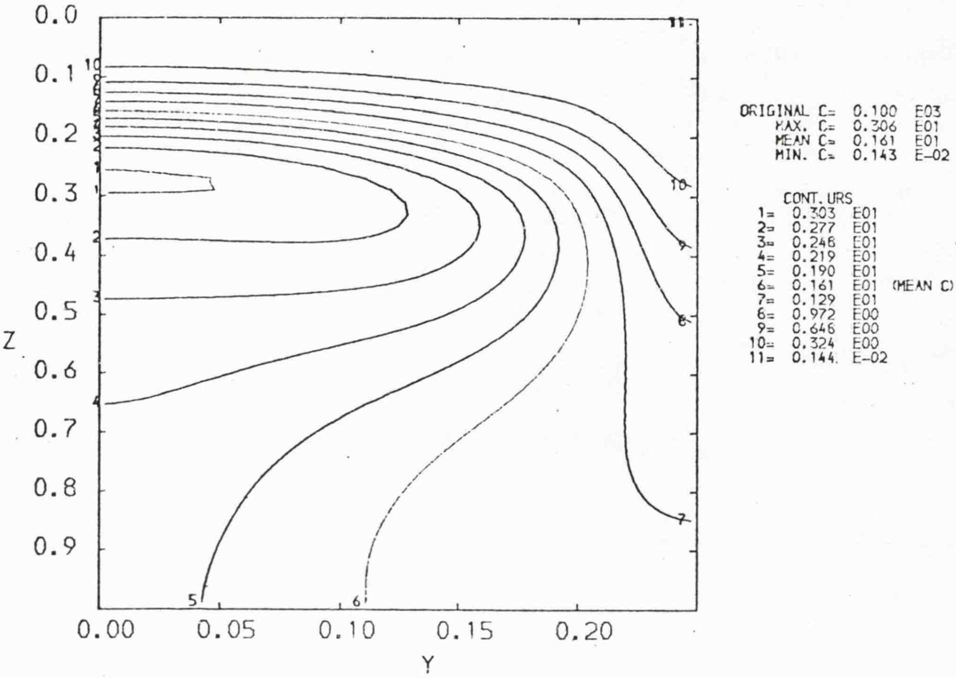

PLOT 7.3(f) LAMBDA= 0.50 T^*= 0.60000E04
WT= 0.100E-02

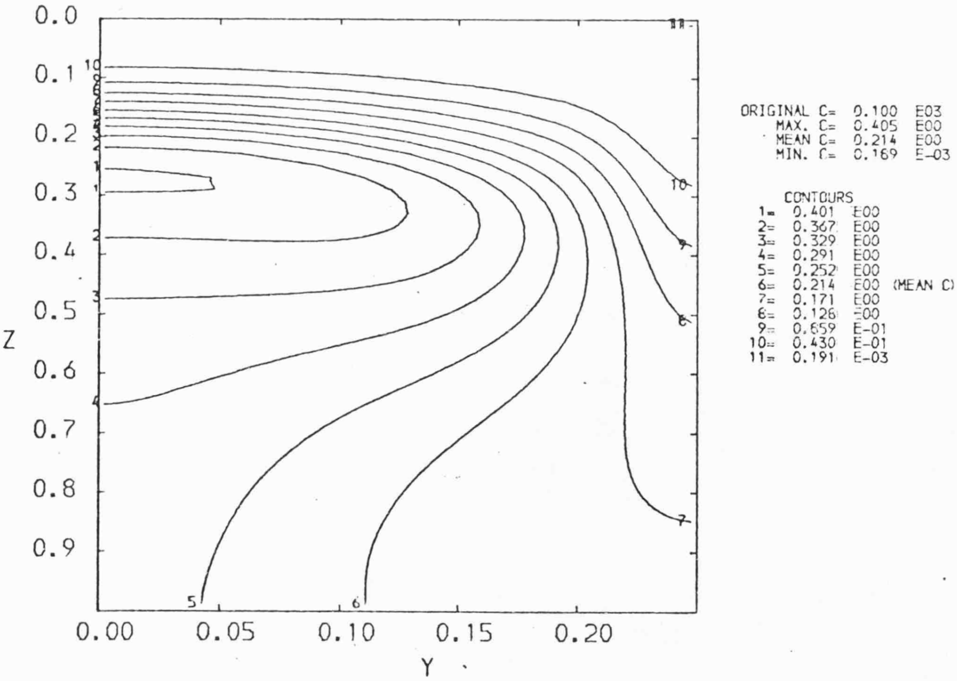

Fig. 7.4 Particle distribution in a Langmuir cell at various times t^*, for dimensionless sinking speed $W_T^* = 1 \times 10^{-5}$ and cell spacing-to-depth ratio $\lambda_c^* = 0.5$.

PLOT 7.4(a) LAMBDA= 0.50 T*= 0.20000E03
WT= 0.100E-04

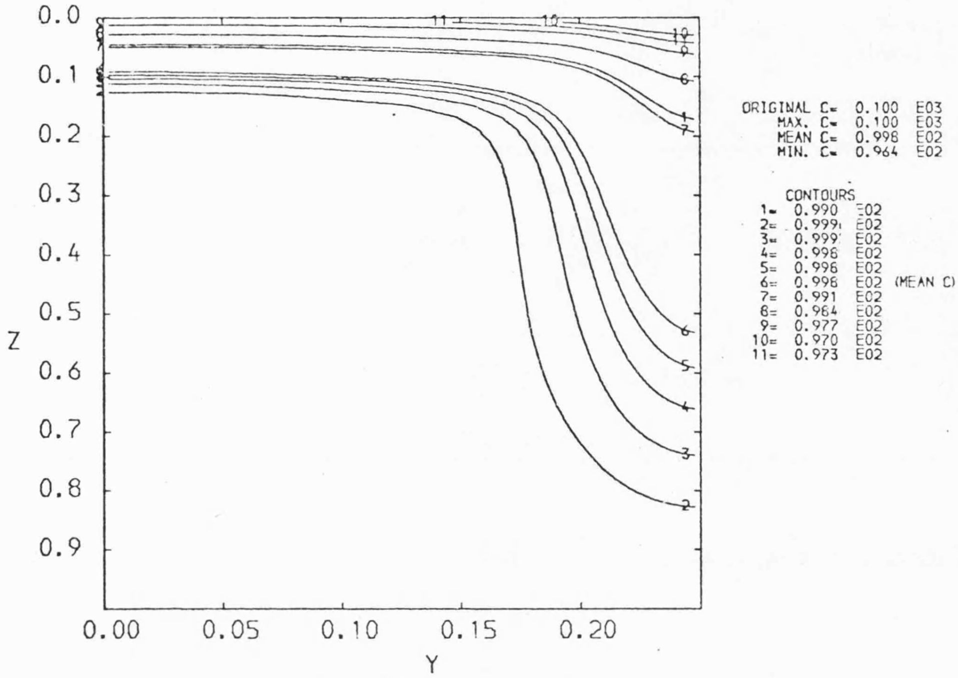

PLOT 7.4(b) LAMBDA= 0.50 T*= 0.40000E03
WT= 0.100E-04

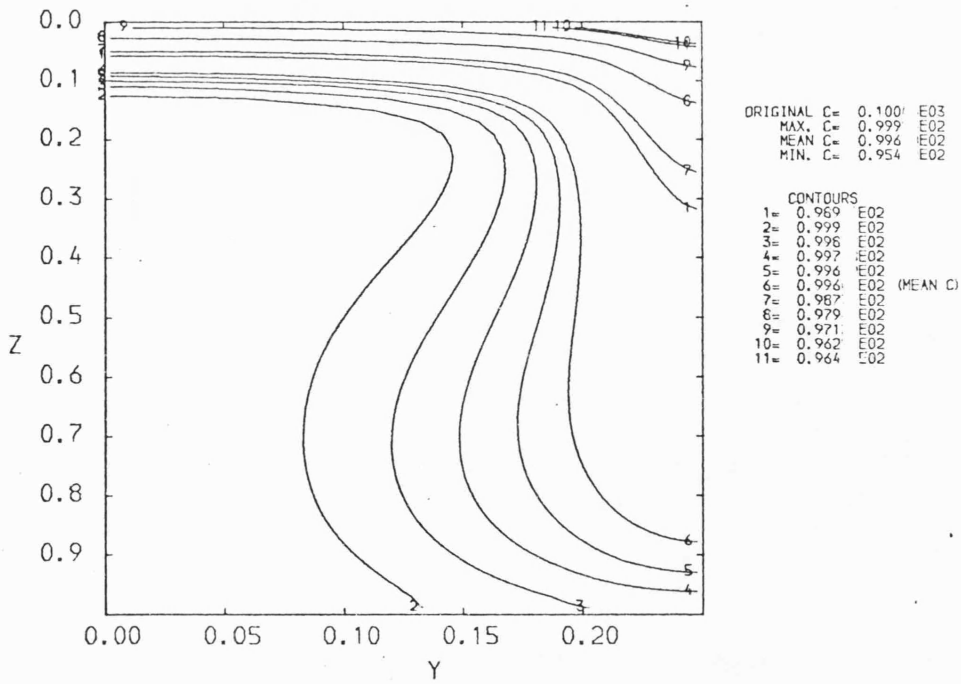

PLOT 7.4(c) LAMBDA= 0.50 T^*= 0.10000E04
WT= 0.100E-04

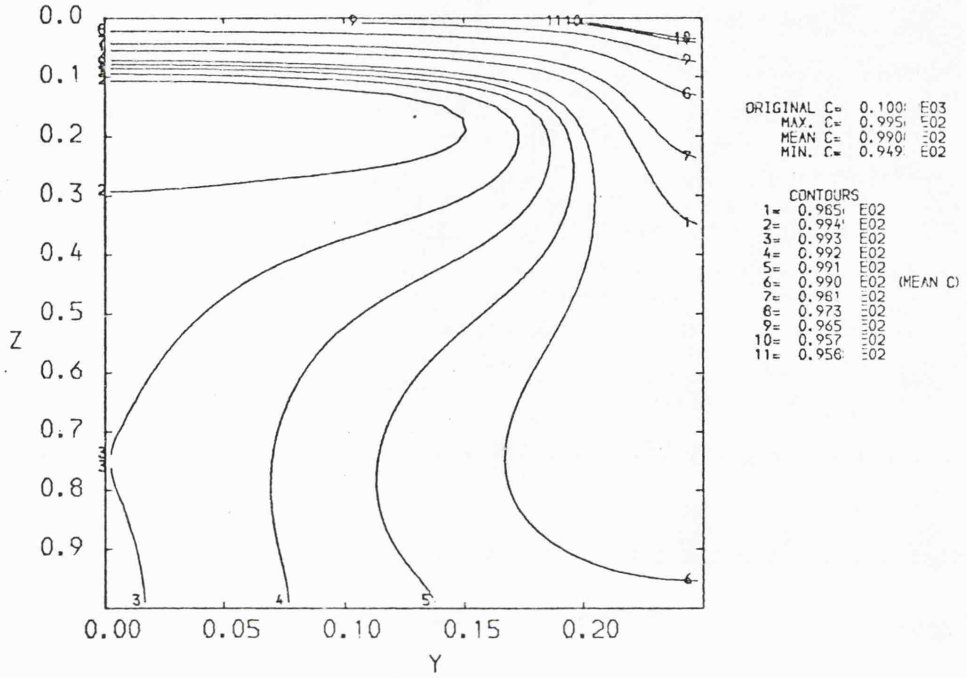

PLOT 7.4(d) LAMBDA= 0.50 T^*= 0.20000E04
WT= 0.100E-04

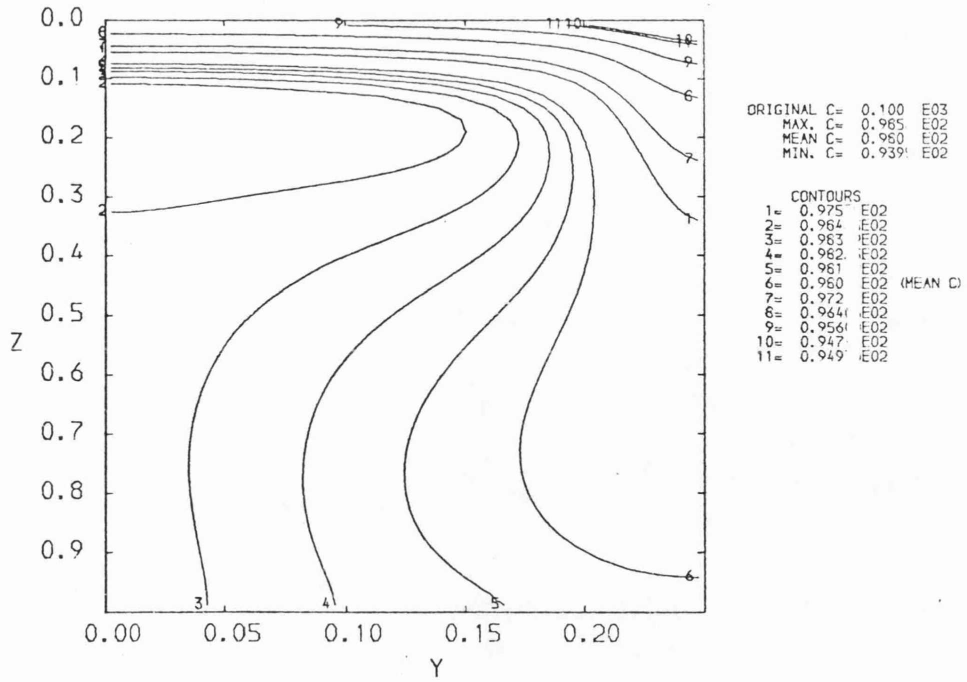

PLOT 7.4(e) LAMBDA= 0.50 T* = 0.20000E05
WT= 0.100E-04

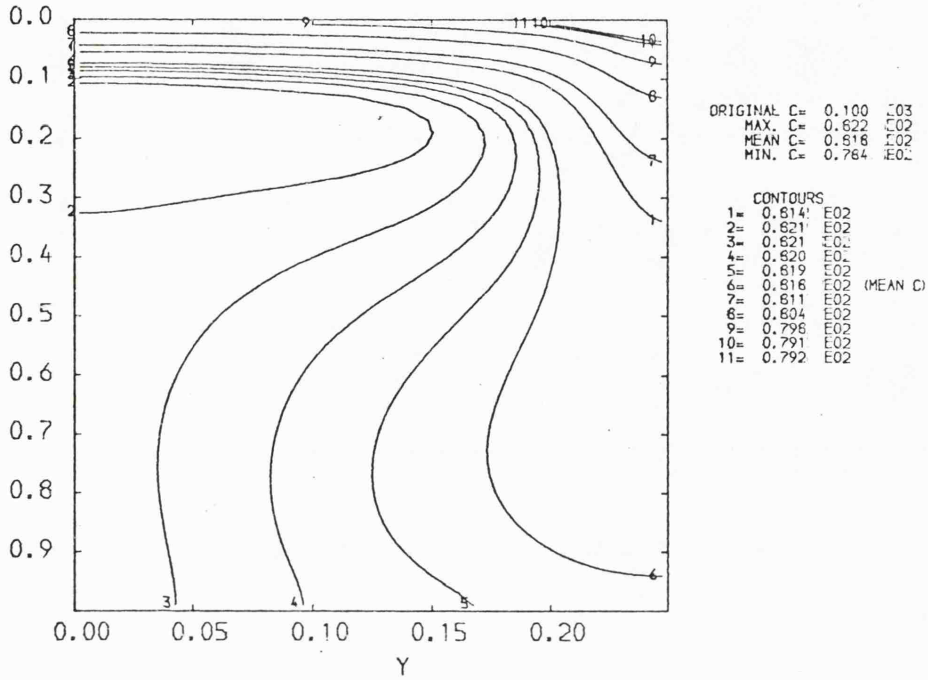

PLOT 7.4(f) LAMBDA= 0.50 T* = 0.22000E05
WT= 0.100E-04

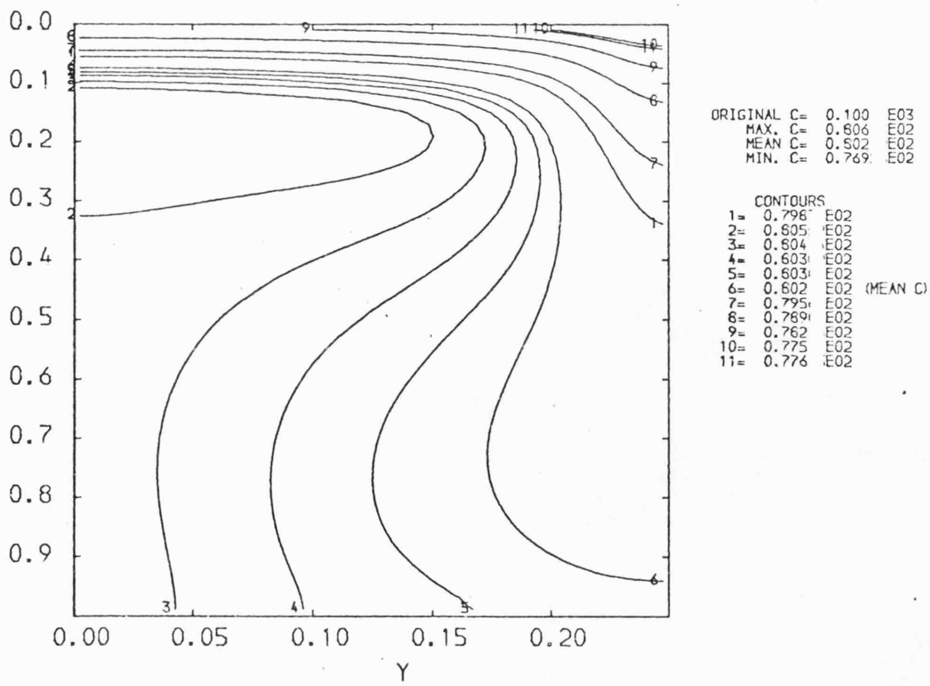

PLOT 7.4(g) LAMBDA= 0.50 T^{*}= 0.48000E05
WT= 0.100E-04

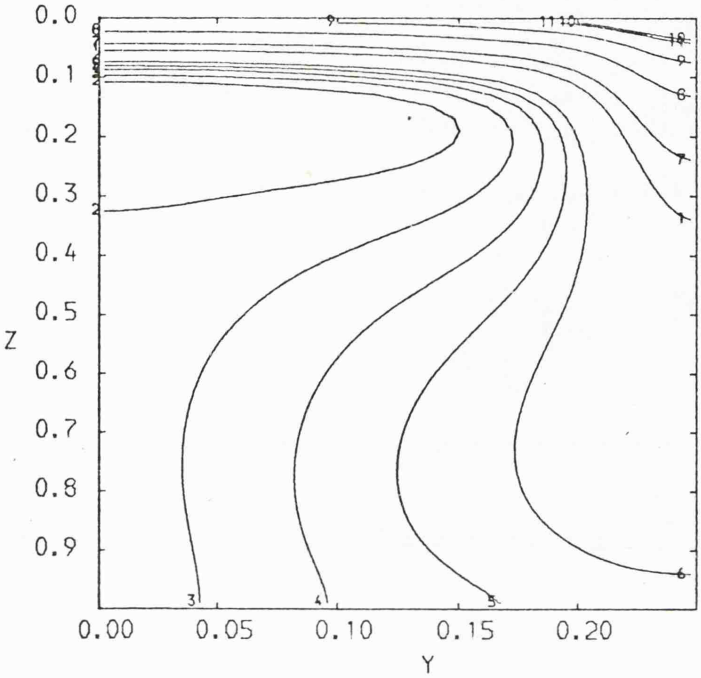

ORIGINAL C= 0.100 E03
MAX. C= 0.621 E02
MEAN C= 0.618 E02
MIN. C= 0.592 E02

CONTOURS
1= 0.615 E02
2= 0.620 E02
3= 0.620 E02
4= 0.619 E02
5= 0.616 E02
6= 0.616 E02 (MEAN C)
7= 0.613 E02
8= 0.608 E02
9= 0.603 E02
10= 0.597 E02
11= 0.598 E02

PLOT 7.4(h) LAMBDA= 0.50 T^{*}= 0.50000E05
WT= 0.100E-04

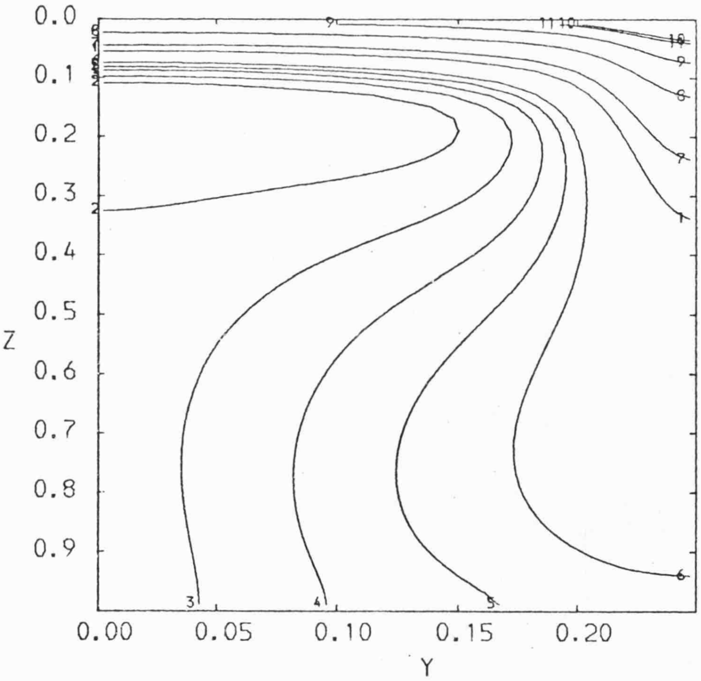

ORIGINAL C= 0.100 E03
MAX. C= 0.609 E02
MEAN C= 0.605 E02
MIN. C= 0.561 E02

CONTOURS
1= 0.603 E02
2= 0.605 E02
3= 0.607 E02
4= 0.607 E02
5= 0.606 E02
6= 0.605 E02 (MEAN C)
7= 0.600 E02
8= 0.596 E02
9= 0.591 E02
10= 0.586 E02
11= 0.586 E02

Fig. 7.5 Particle distribution in a Langmuir cell at various times t^*, for dimensionless sinking speed $W_T^* = -1\times10^{-3}$ and cell spacing-to-depth ratio $\lambda_c^* = 2.0$.

PLOT 7.5(a) LAMBDA= 2.00 T* = 0.20000E03
WT= -0.100E-02

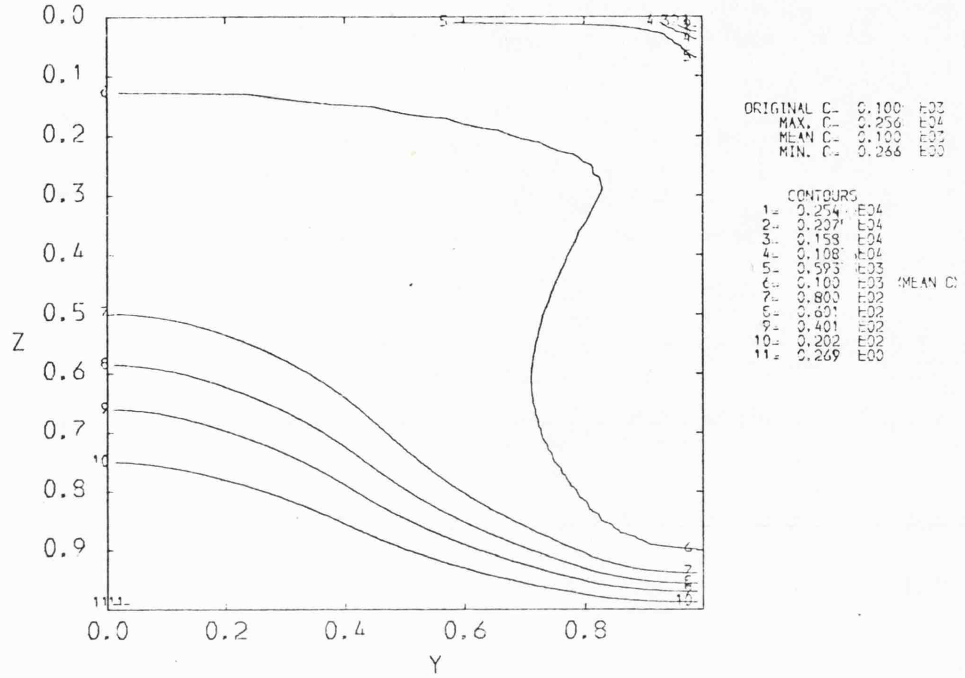

PLOT 7.5(b) LAMBDA= 2.00 T* = 0.40000E03
WT= -0.100E-02

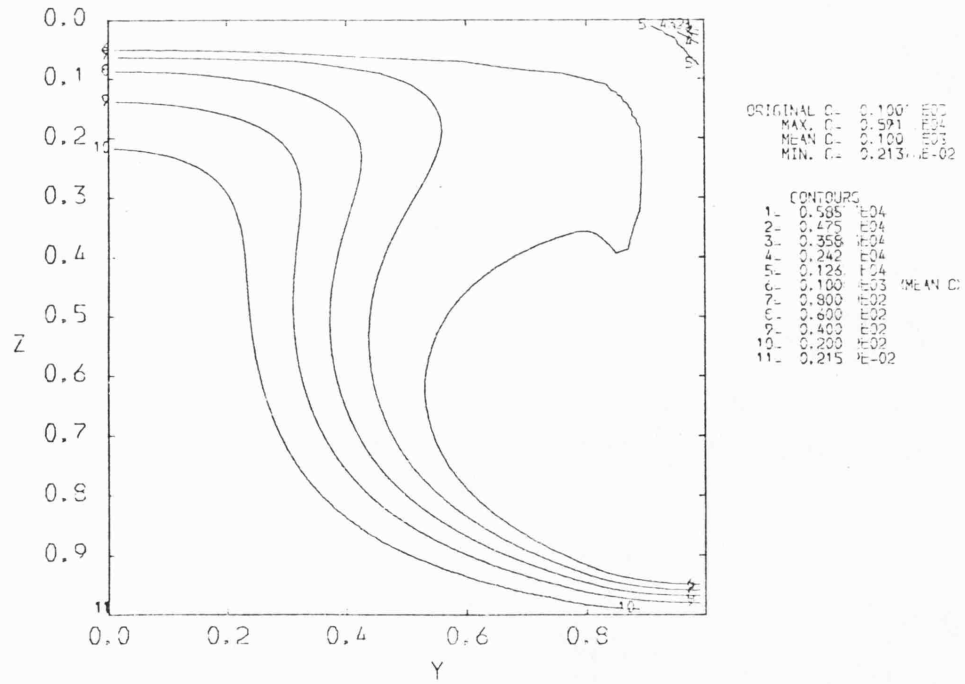

PLOT 7.5(c) LAMBDA= 2.00 T^*= 0.60000E03
WT= -0.100E-02

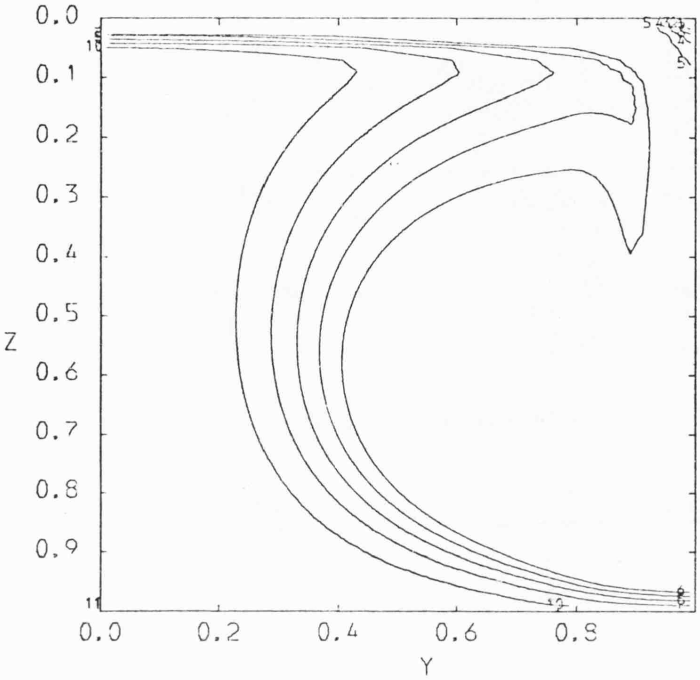

ORIGINAL C= 0.100 E03
MAX. C= 0.734 E04
MEAN C= 0.100 E03
MIN. C= 0.771 E-03

CONTOURS
1= 0.726 E04
2= 0.589 E04
3= 0.444 E04
4= 0.299 E04
5= 0.154 E04
6= 0.100 E03 (MEAN C)
7= 0.800 E02
8= 0.600 E02
9= 0.400 E02
10= 0.200 E02
11= 0.778 E-03

PLOT 7.5(d) LAMBDA= 2.00 T^*= 0.80000E03
WT= -0.100E-02

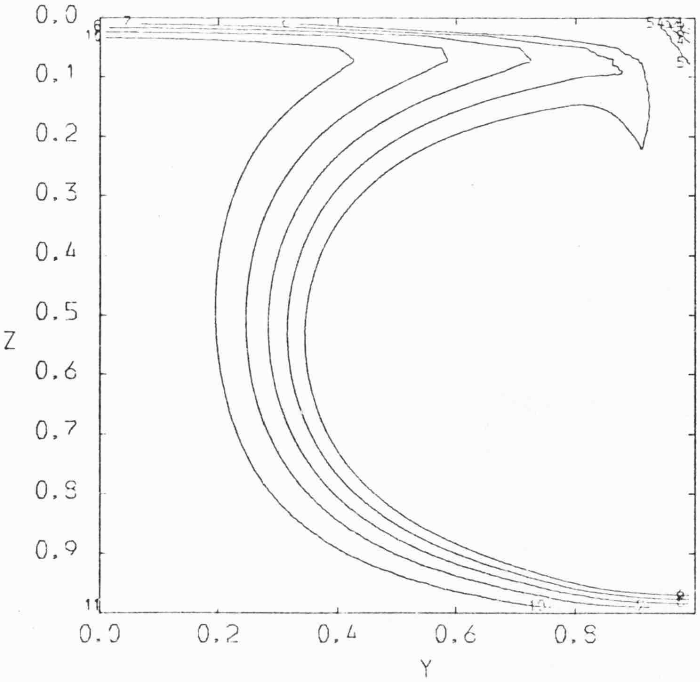

ORIGINAL C= 0.100 E03
MAX. C= 0.547 E04
MEAN C= 0.100 E03
MIN. C= 0.120 E-02

CONTOURS
1= 0.541 E04
2= 0.439 E04
3= 0.332 E04
4= 0.224 E04
5= 0.117 E04
6= 0.100 E03 (MEAN C)
7= 0.800 E02
8= 0.600 E02
9= 0.400 E02
10= 0.200 E02
11= 0.121 E-02

PLOT 7.5(e) LAMBDA= 2.00 T* = 0.10000E04
WT= -0 100E-02

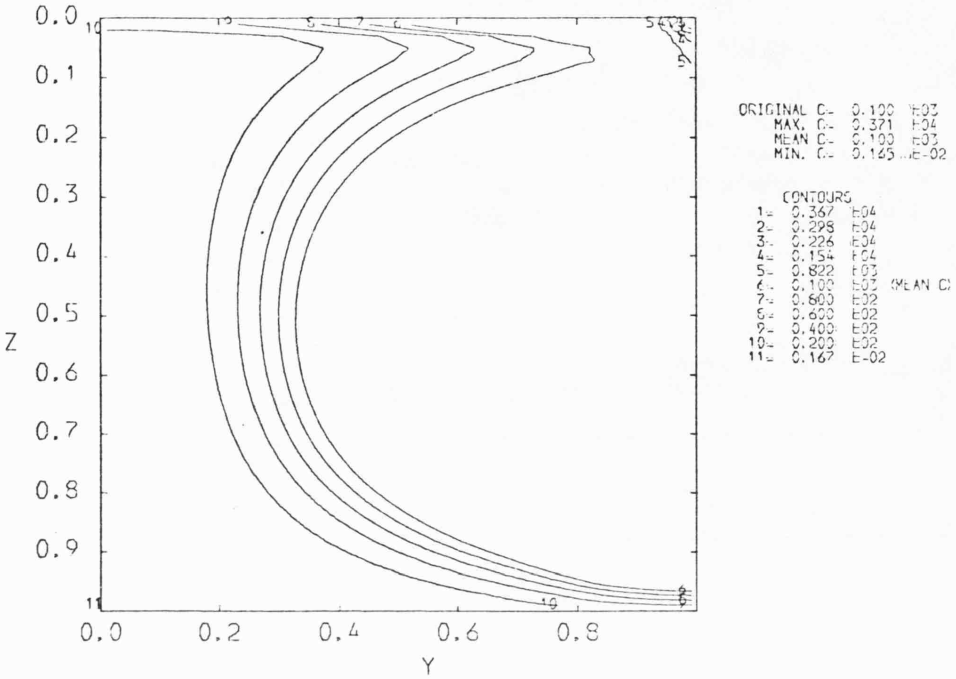

PLOT 7.5(f) LAMBDA= 2.00 T* = 0.20000E04
WT= -0.100E-02

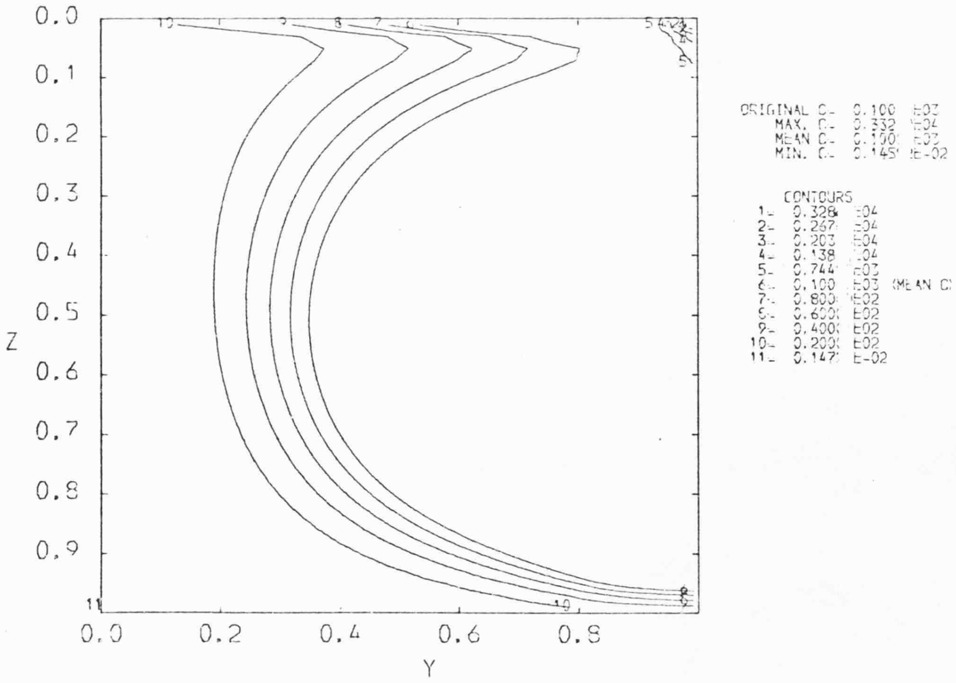

PLOT 7.5(g) LAMBDA= 2.00 T^*= 0.80000E04
WT= -0.100E-02

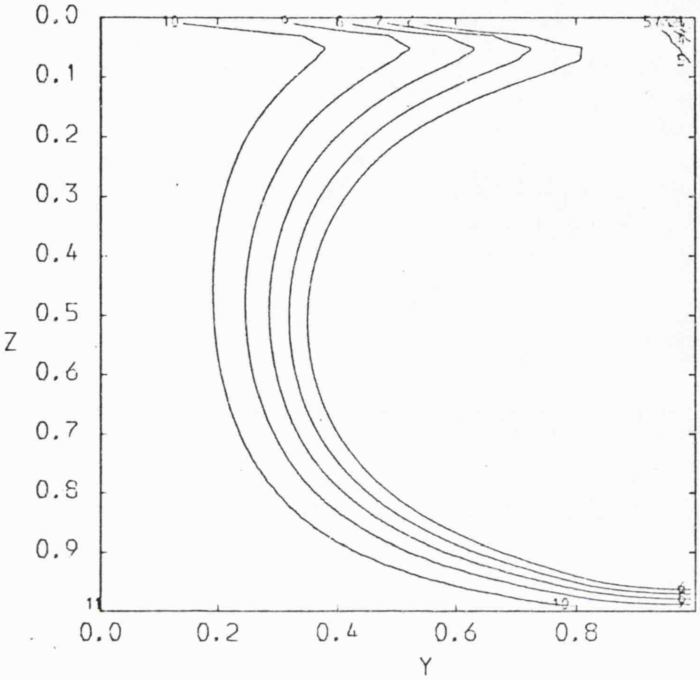

ORIGINAL C= 0.100 E03
MAX. C= 0.326 E04
MEAN C= 0.100 E03
MIN. C= 0.141 E-02

CONTOURS
1= 0.323 E04
2= 0.263 E04
3= 0.199 E04
4= 0.136 E04
5= 0.732 E03
6= 0.100 E03 (MEAN C)
7= 0.800 E02
8= 0.600 E02
9= 0.400 E02
10= 0.200 E02
11= 0.143 E-02

PLOT 7.5(h) LAMBDA= 2.00 T^*= 0.10000E05
WT= -0.100E-02

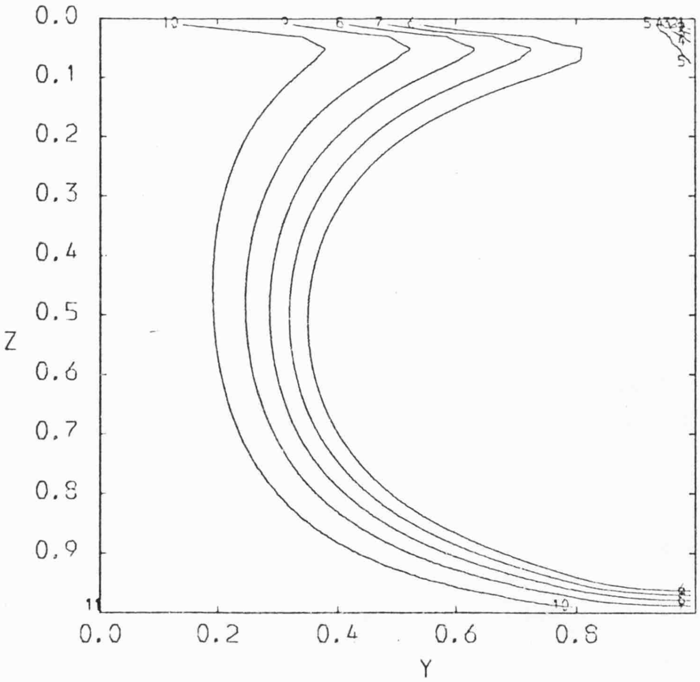

ORIGINAL C= 0.100 E03
MAX. C= 0.326 E04
MEAN C= 0.100 E03
MIN. C= 0.141 E-02

CONTOURS
1= 0.323 E04
2= 0.263 E04
3= 0.199 E04
4= 0.136 E04
5= 0.732 E03
6= 0.100 E03 (MEAN C)
7= 0.800 E02
8= 0.600 E02
9= 0.400 E02
10= 0.200 E02
11= 0.143 E-02

Fig. 7.6 Particle distribution in a Langmuir cell at various times t^*, for dimensionless sinking speed $W_T^* = -1\times10^{-5}$ and cell spacing-to-depth ratio $\lambda_c^* = 2.0$.

PLOT 7.6(a) LAMBDA= 2.00 T*= 0.20000E03
WT= -0.100E-04

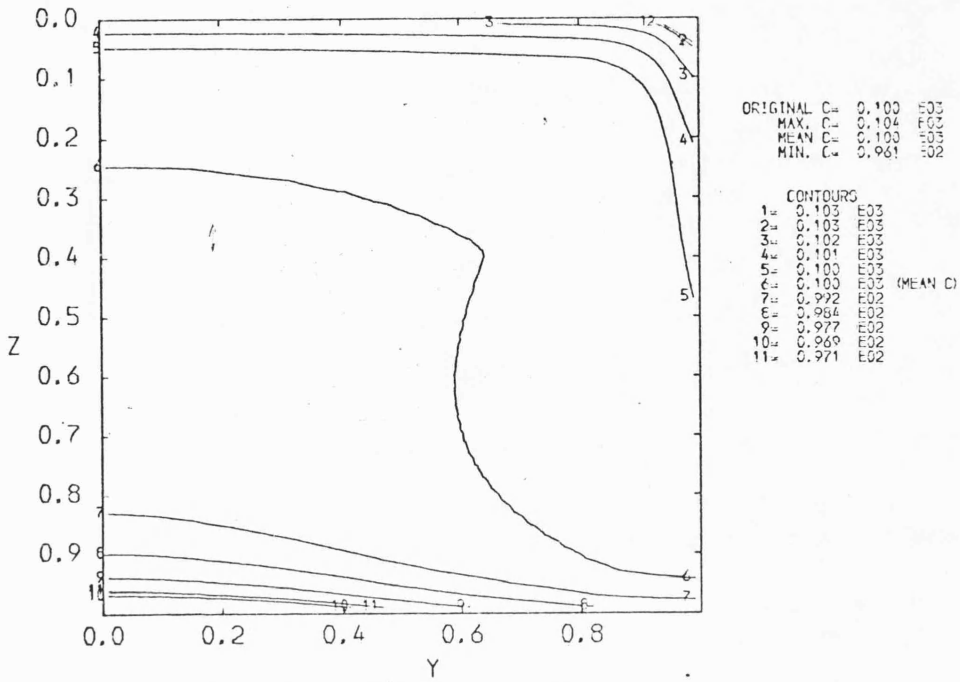

PLOT 7.6(b) LAMBDA= 2.00 T*= 0.40000E03
WT= -0.100E-04

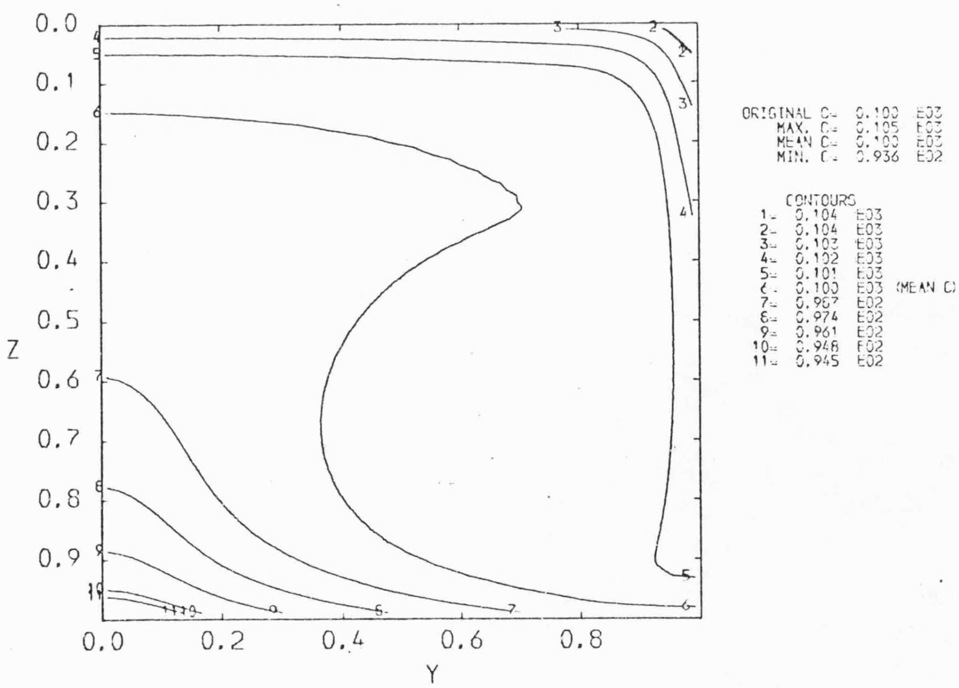

PLOT 7.6(c) LAMBDA= 2.00 T* = 0.10000E04
WT= -0.100E-04

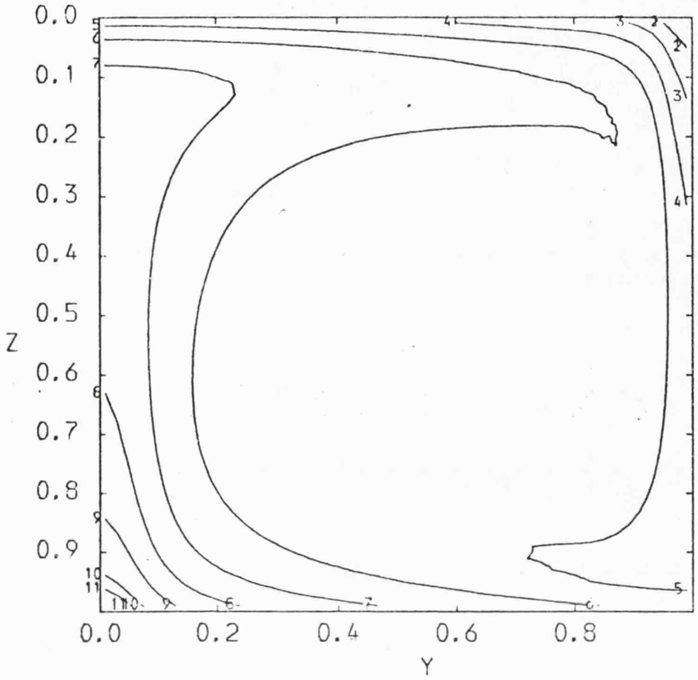

ORIGINAL C= 0.100 E03
MAX. C= 0.105 E03
MEAN C= 0.100 E03
MIN. C= 0.923 E02

CONTOURS
1= 0.104 E03
2= 0.104 E03
3= 0.103 E03
4= 0.102 E03
5= 0.101 E03
6= 0.100 E03 (MEAN C)
7= 0.984 E02
8= 0.969 E02
9= 0.954 E02
10= 0.935 E02
11= 0.932 E02

PLOT 7.6(d) LAMBDA= 2.00 T* = 0.20000E04
WT= -0.100E-04

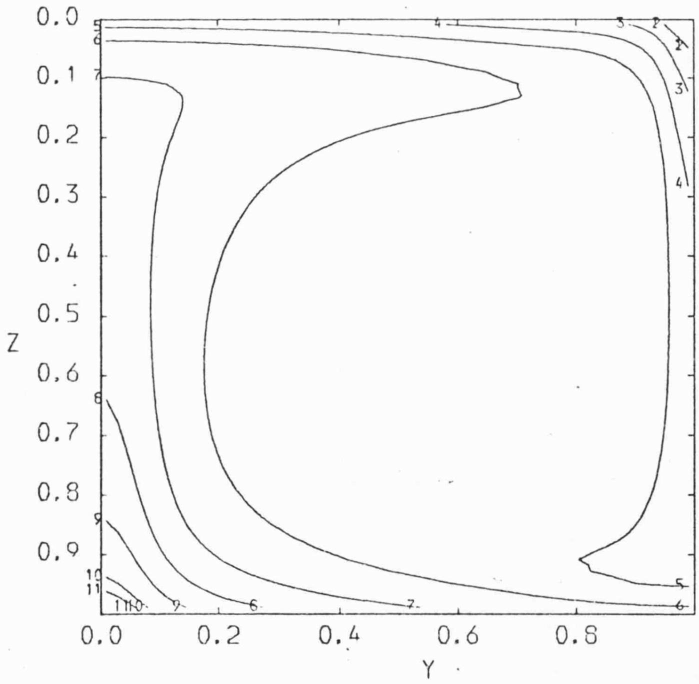

ORIGINAL C= 0.100 E03
MAX. C= 0.105 E03
MEAN C= 0.100 E03
MIN. C= 0.923 E02

CONTOURS
1= 0.104 E03
2= 0.104 E03
3= 0.103 E03
4= 0.102 E03
5= 0.101 E03
6= 0.100 E03 (MEAN C)
7= 0.984 E02
8= 0.969 E02
9= 0.953 E02
10= 0.938 E02
11= 0.932 E02

PLOT 7.6(e) LAMBDA= 2.00 T* = 0.40000E04
WT= -0.100E-04

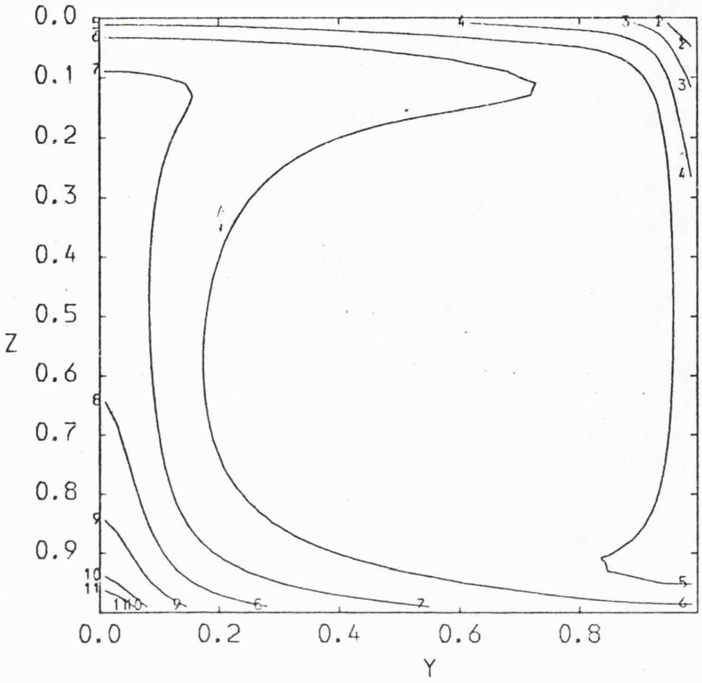

ORIGINAL C= 0.100 E03
MAX. C= 0.104 E03
MEAN C= 0.100 E03
MIN. C= 0.923 E02

CONTOURS
1= 0.103 E03
2= 0.103 E03
3= 0.102 E03
4= 0.101 E03
5= 0.100 E03
6= 0.100 E03 (MEAN C)
7= 0.984 E02
8= 0.969 E02
9= 0.954 E02
10= 0.938 E02
11= 0.932 E02

PLOT 7.6(f) LAMBDA= 2.00 T* = 0.60000E04
WT= -0.100E-04

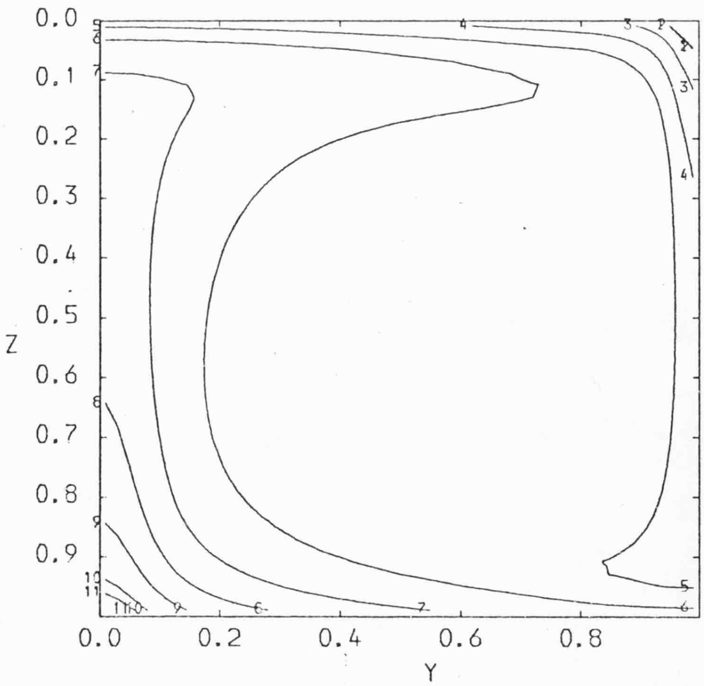

ORIGINAL C= 0.100 E03
MAX. C= 0.104 E03
MEAN C= 0.100 E03
MIN. C= 0.923 E02

CONTOURS
1= 0.103 E03
2= 0.103 E03
3= 0.102 E03
4= 0.101 E03
5= 0.100 E03
6= 0.100 E03 (MEAN C)
7= 0.984 E02
8= 0.969 E02
9= 0.954 E02
10= 0.938 E02
11= 0.932 E02

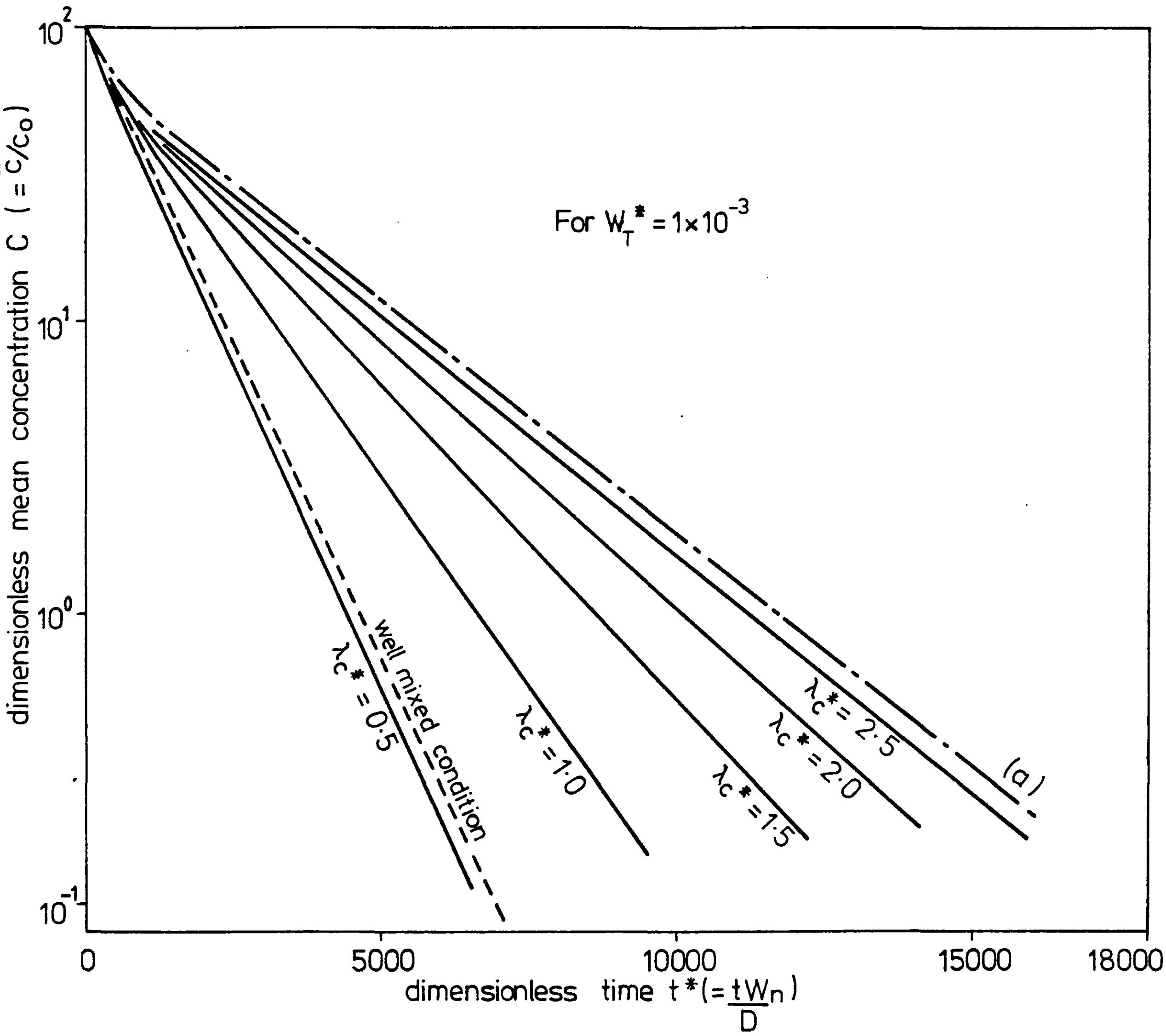

Fig. 7. 7. Effects of variation of cell size (λ_c^*) on the mean concentration of particles ($\bar{c}^*$) in a Langmuir cell at various time t^*. Curve (a) represents the situation where the maximum upwelling velocity is a half of the maximum downwelling velocity and $\lambda_c^* = 2{\cdot}0$

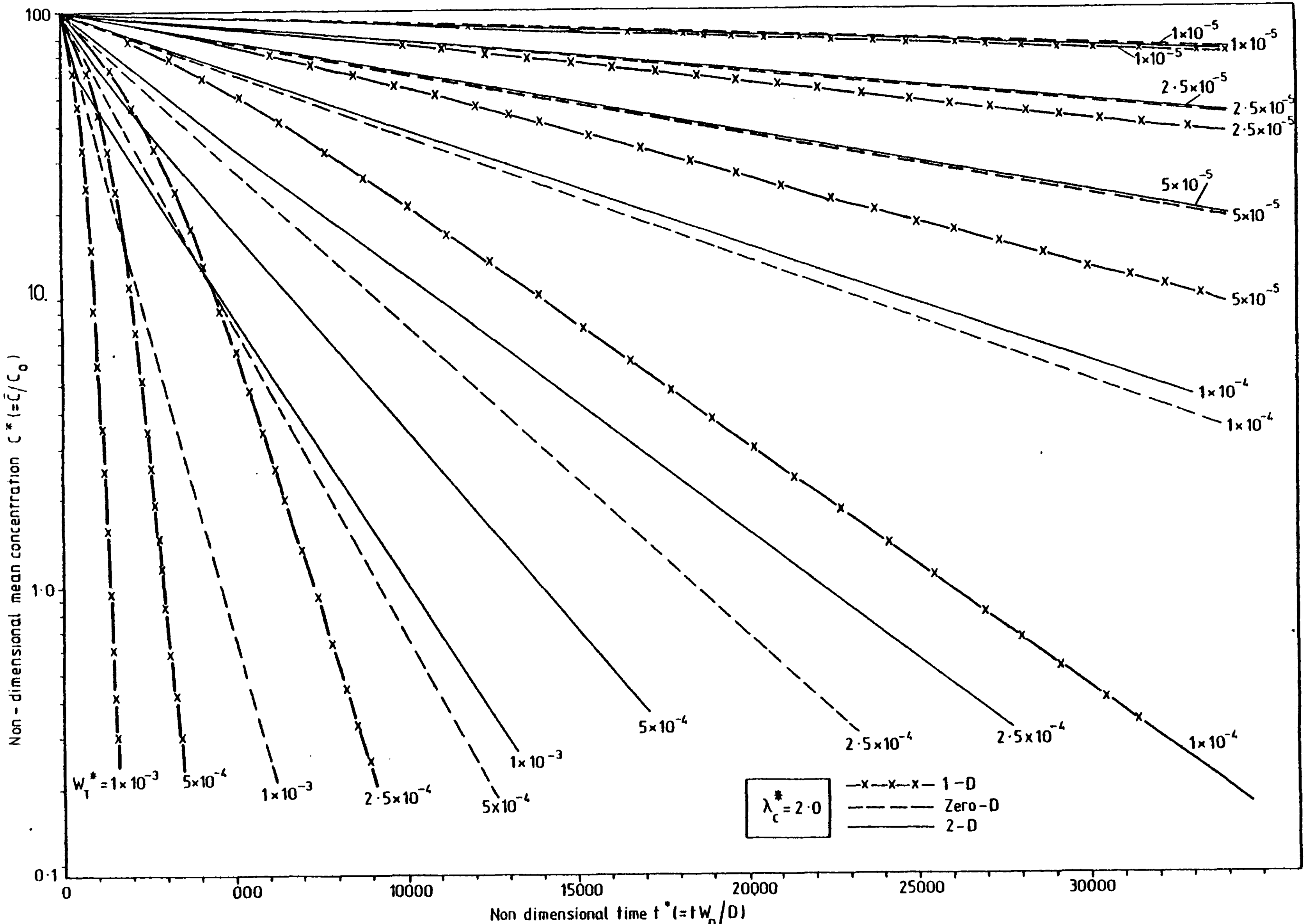

Fig. 7·8 Non-dimensional mean particle concentration as a function of non-dimensional time, for row-spacing-to-depth ratio $\lambda_c^* = 2{\cdot}0$ and various non-dimensional sinking speeds W_r^*, as predicted by 2-D model, 1-D model, and zero-dimensional model.

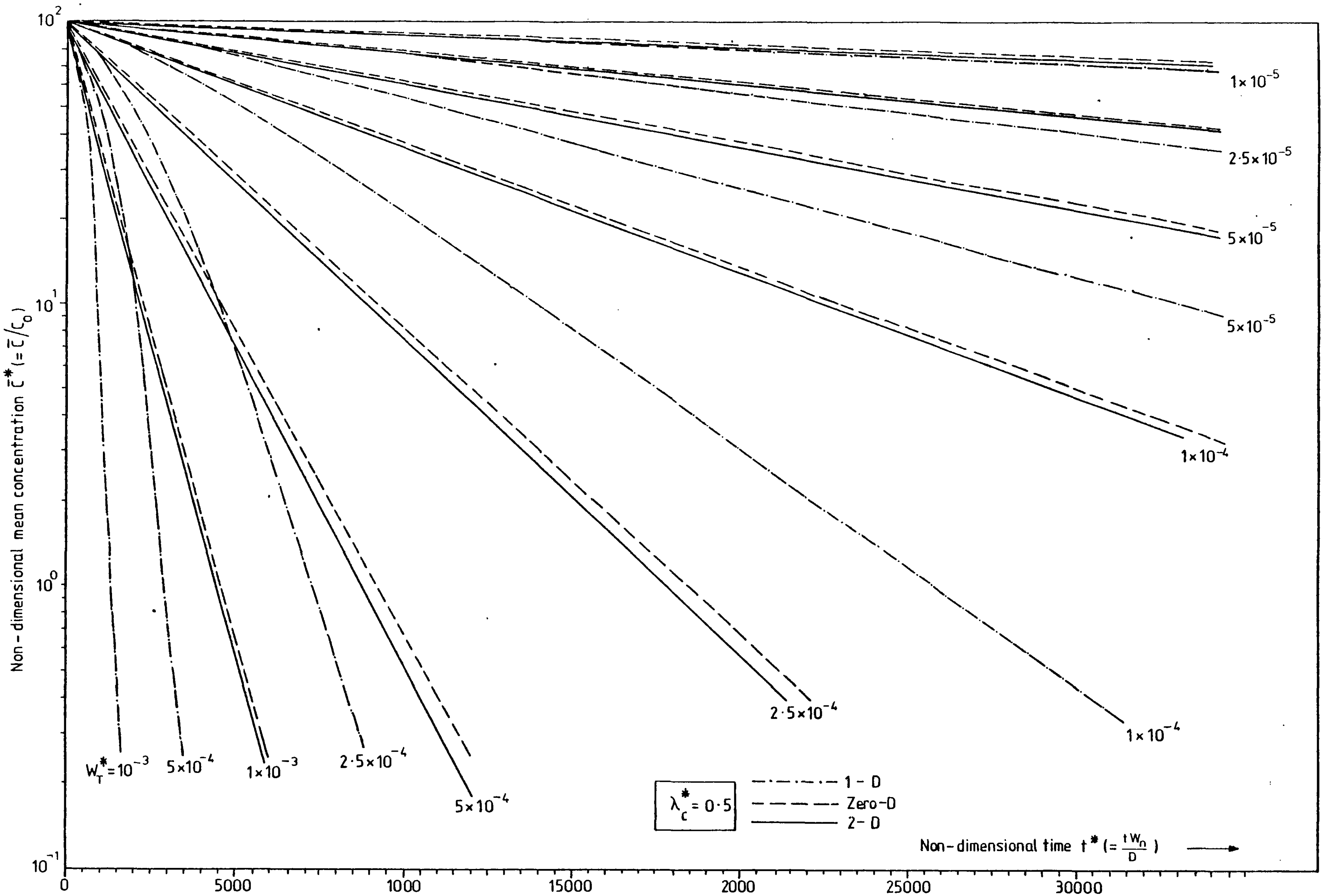

Fig. 7.9 Non-dimensional mean particle concentration as a function of non-dimensional time, for row spacing-to-depth ratio λ_c^* 0·5, and various non-dimensional sinking speeds W_T^*, as predicted by 2-D model, 1-D model, and zero-dimensional model.

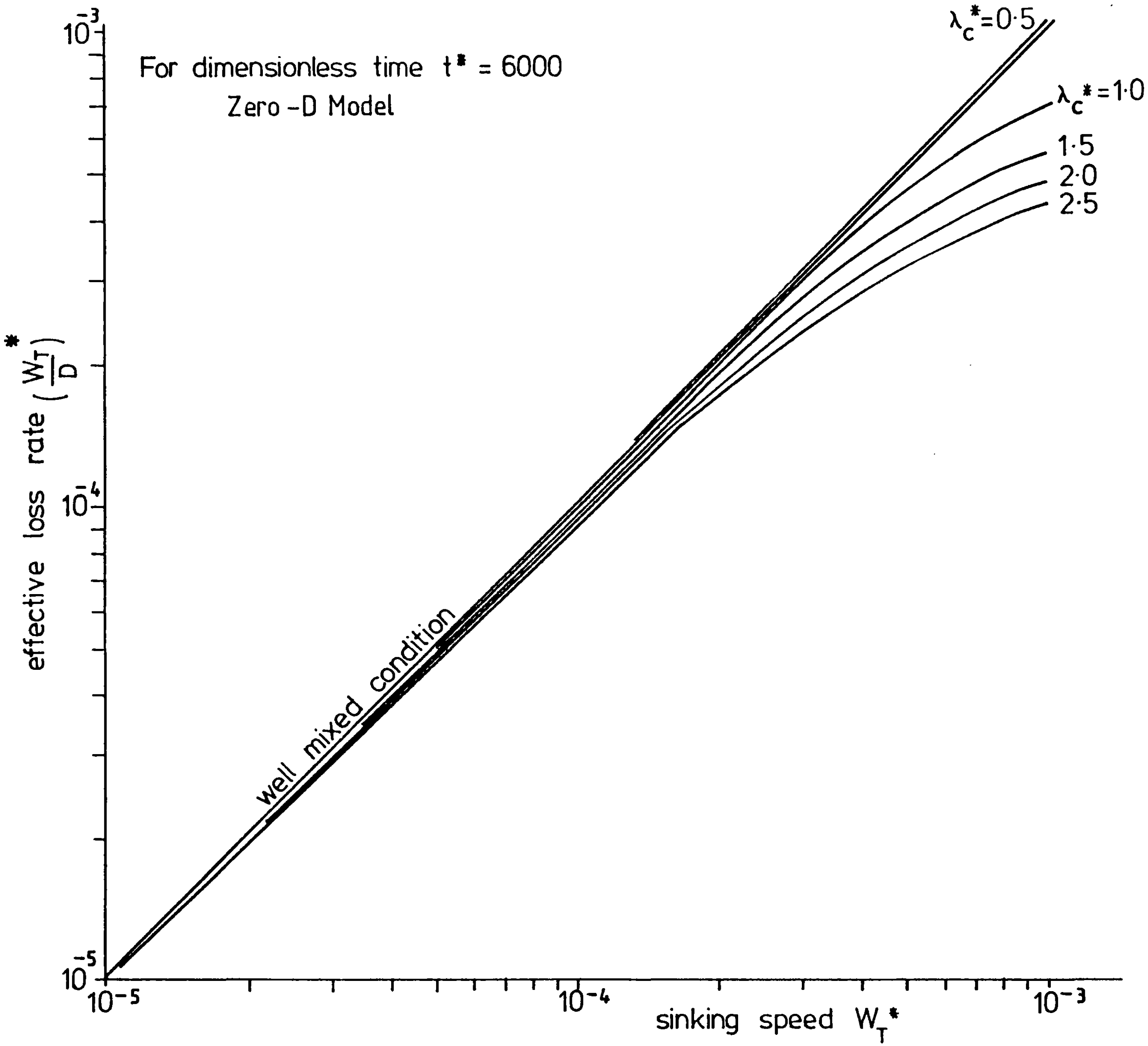

Fig. 7. 10. Plot of dimensionless effective loss rate against dimensionless sinking speeds, for various values of dimensionless cell size (λ_c^*) when dimensionless time (t^*) equals 6000

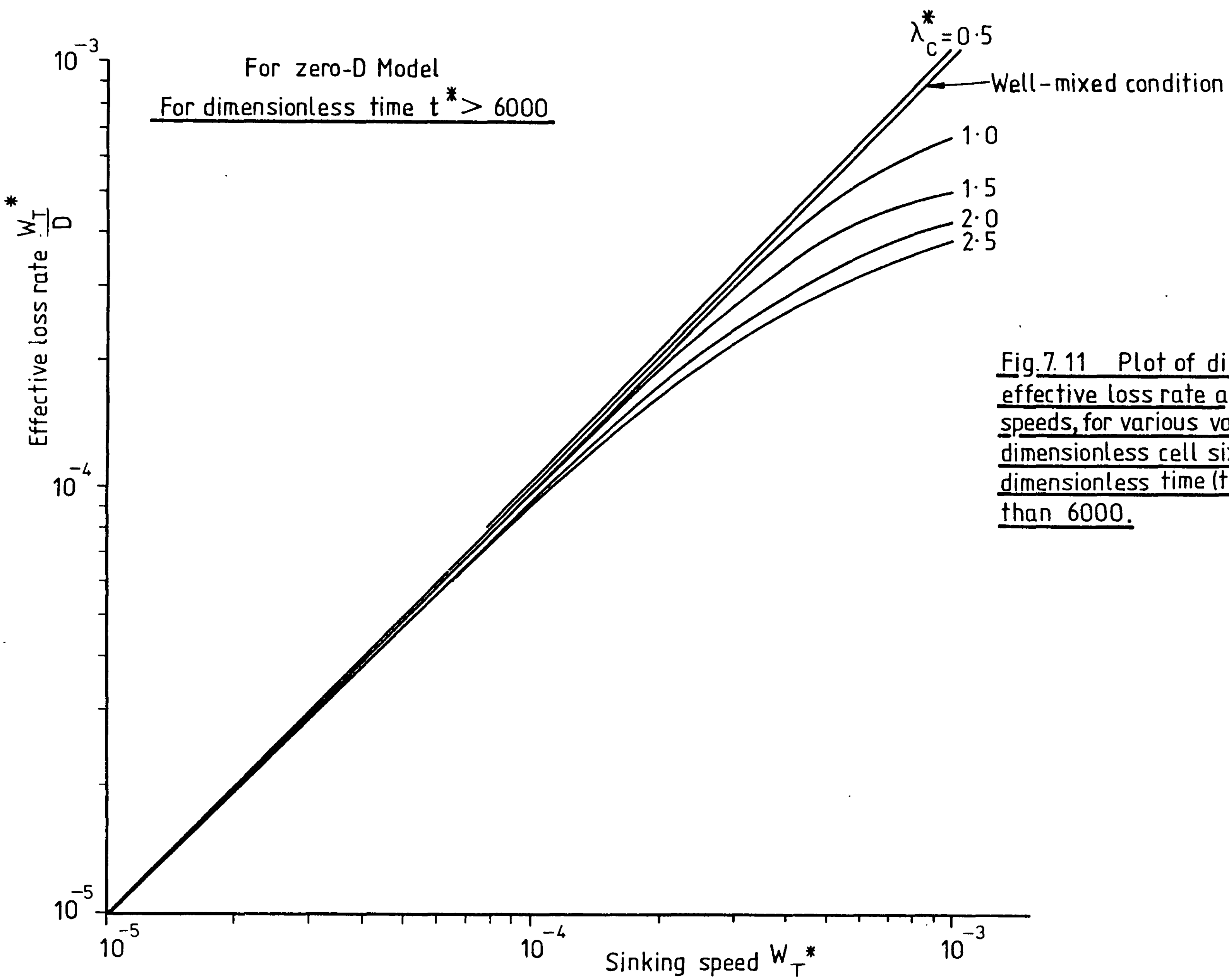

Fig. 7.11 Plot of dimensionless effective loss rate against sinking speeds, for various values of dimensionless cell size (λ_c^*), when dimensionless time (t^*) is greater than 6000.

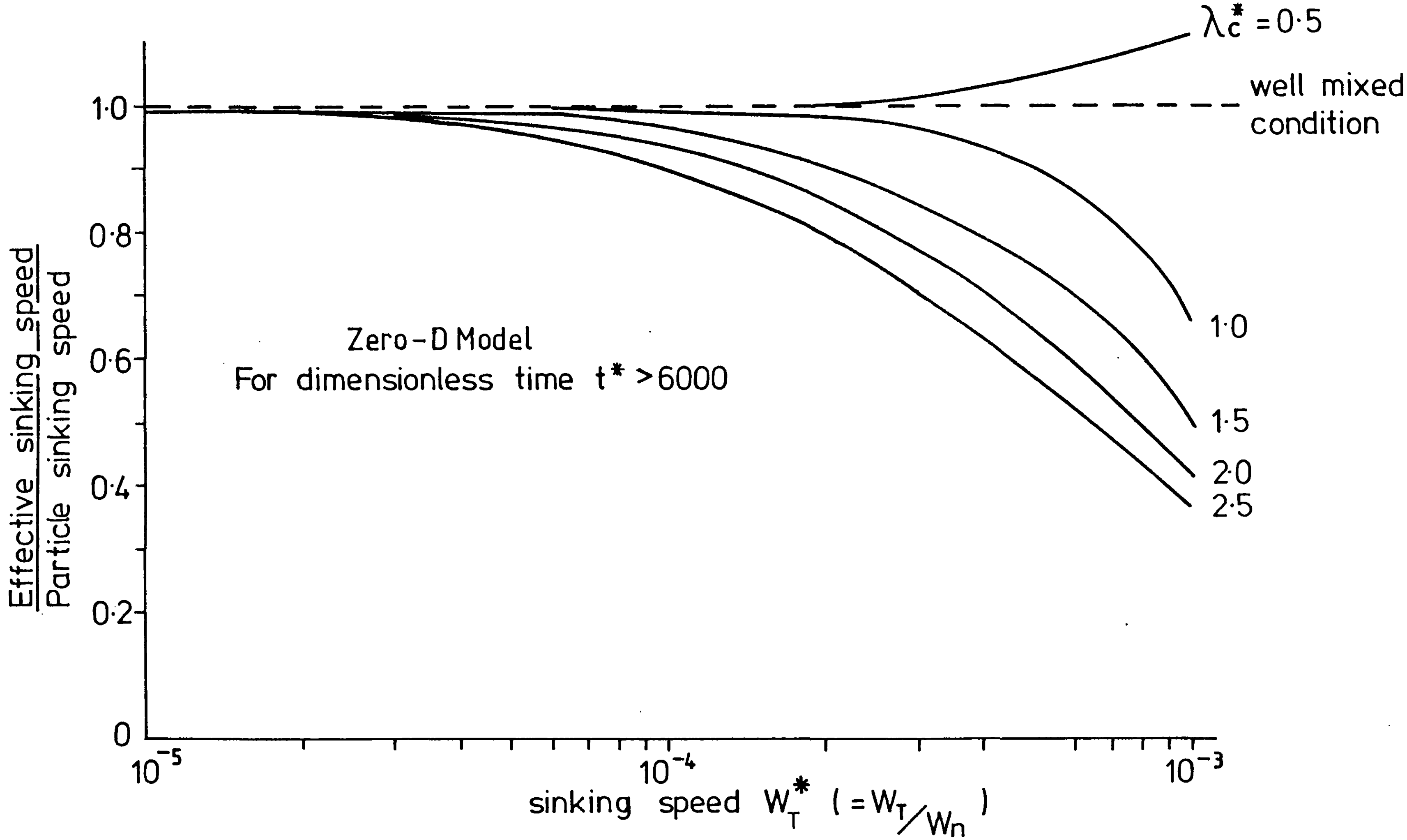

Fig. 7. 12. Plot of the ratio of effective speed to terminal sinking speed against non-dimensional particle sinking speed, for some values of dimensionless cell size (λ_c^*), when time t^* is greater than 6000

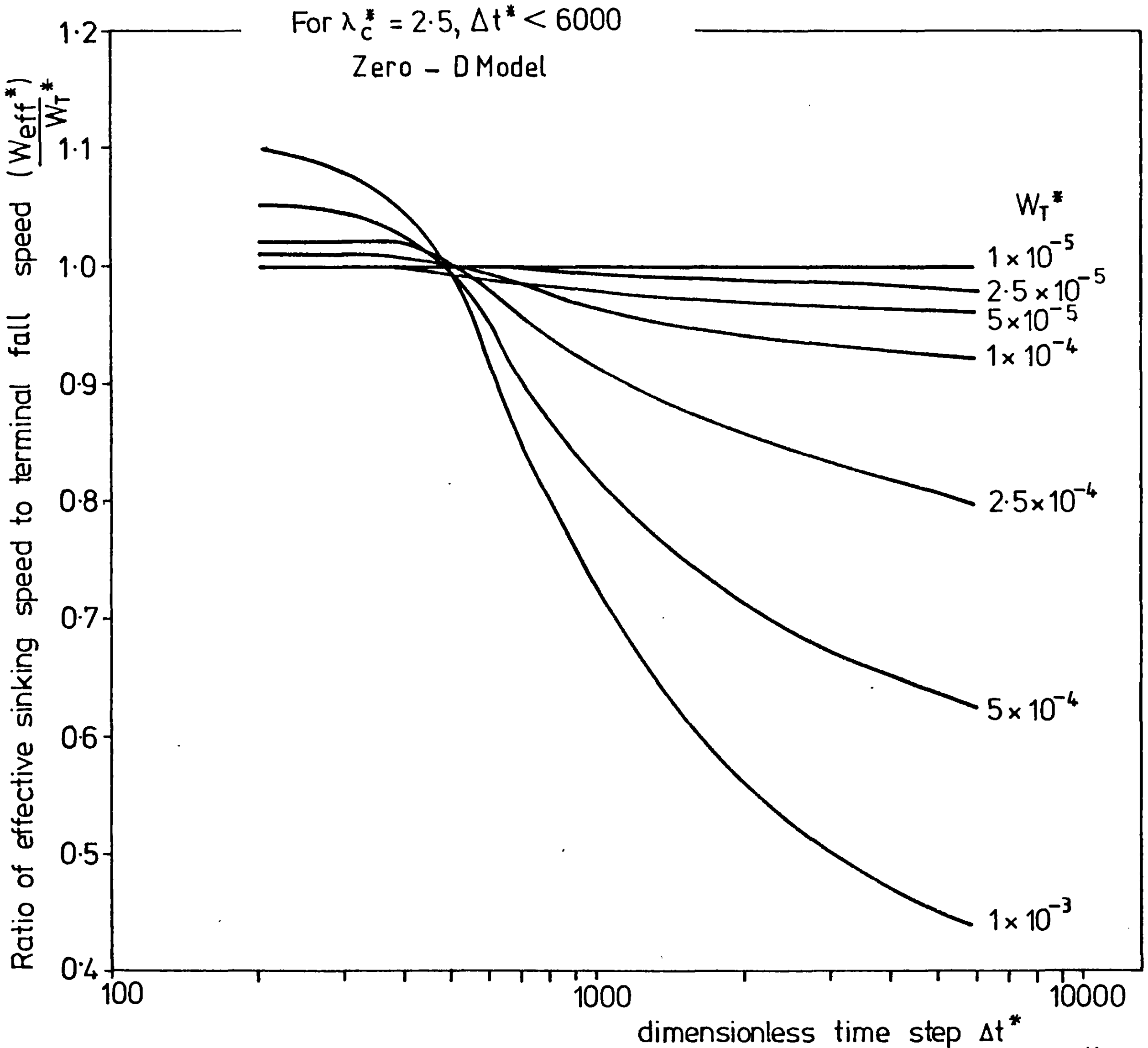

Fig. 7 12a. Variations of ratio of effective sinking speed to particle fall speed with time-step length and partical of speed, for row spacing-to-depth ratio $\lambda_c^* = 2{\cdot}5$ and the time step length less than 6000

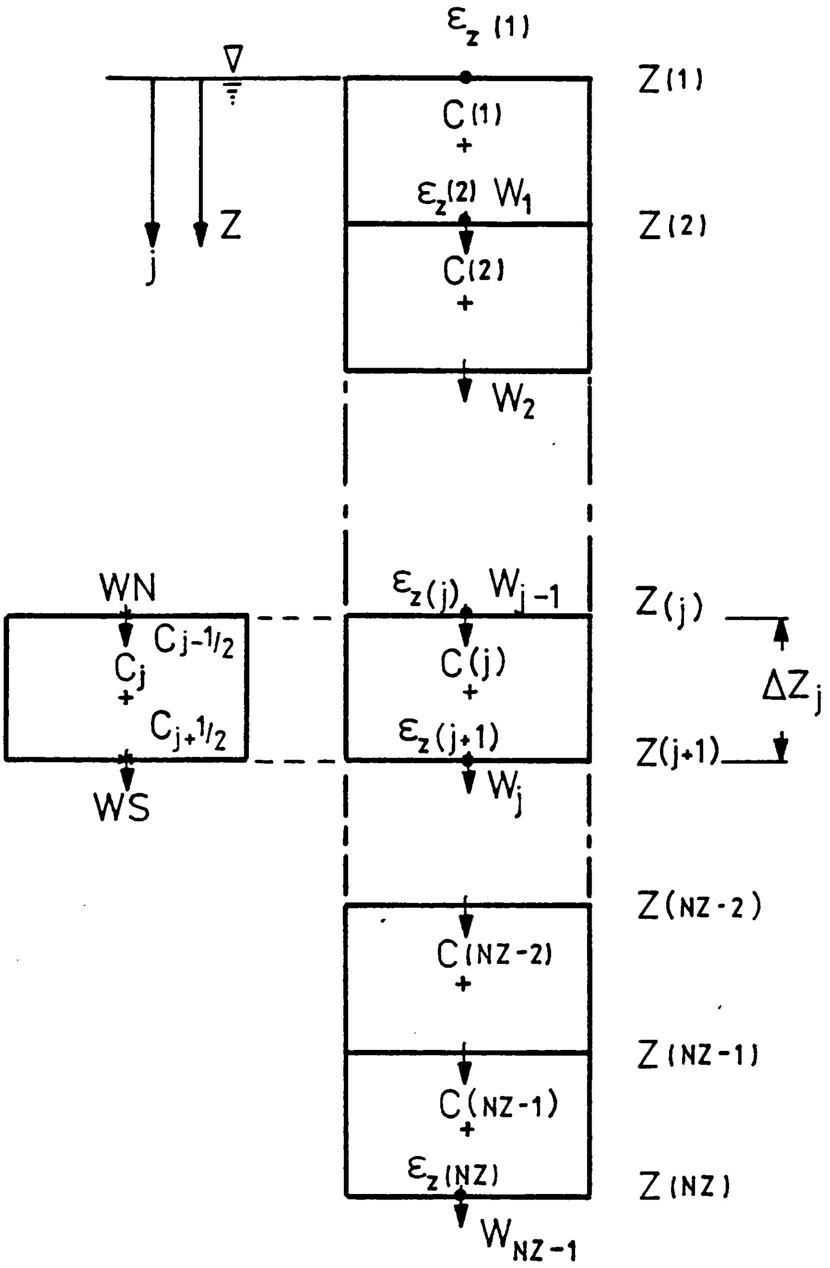

Fig 7. 13. Grid structure and variable locations in 1-D model

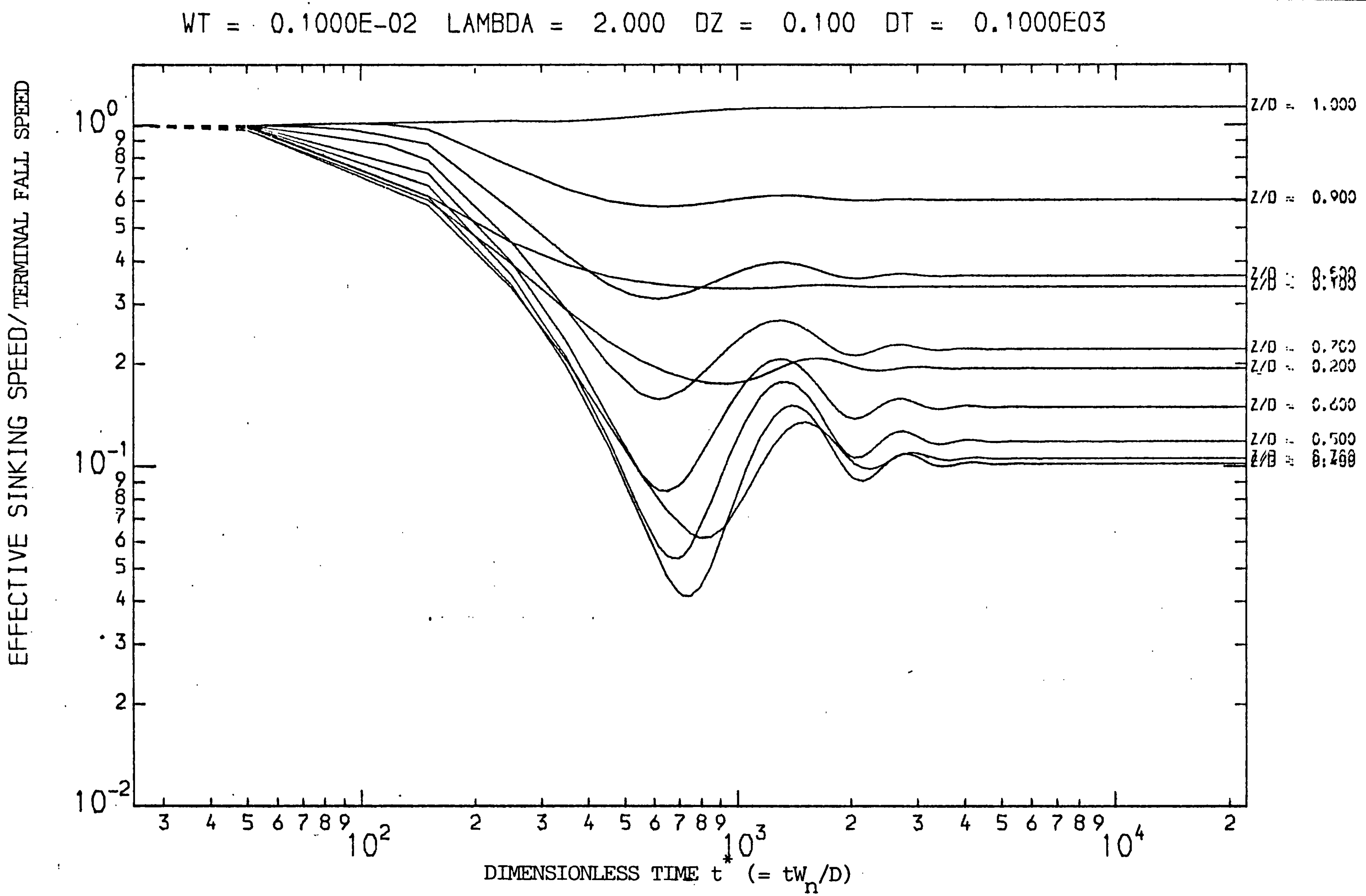

Fig. 7.14 Effective sinking speeds as functions of time t^* and depths z^* in the one-dimensional model, for $\lambda_c^* = 2.0$ and $W_T^* = 1\times10^{-3}$.

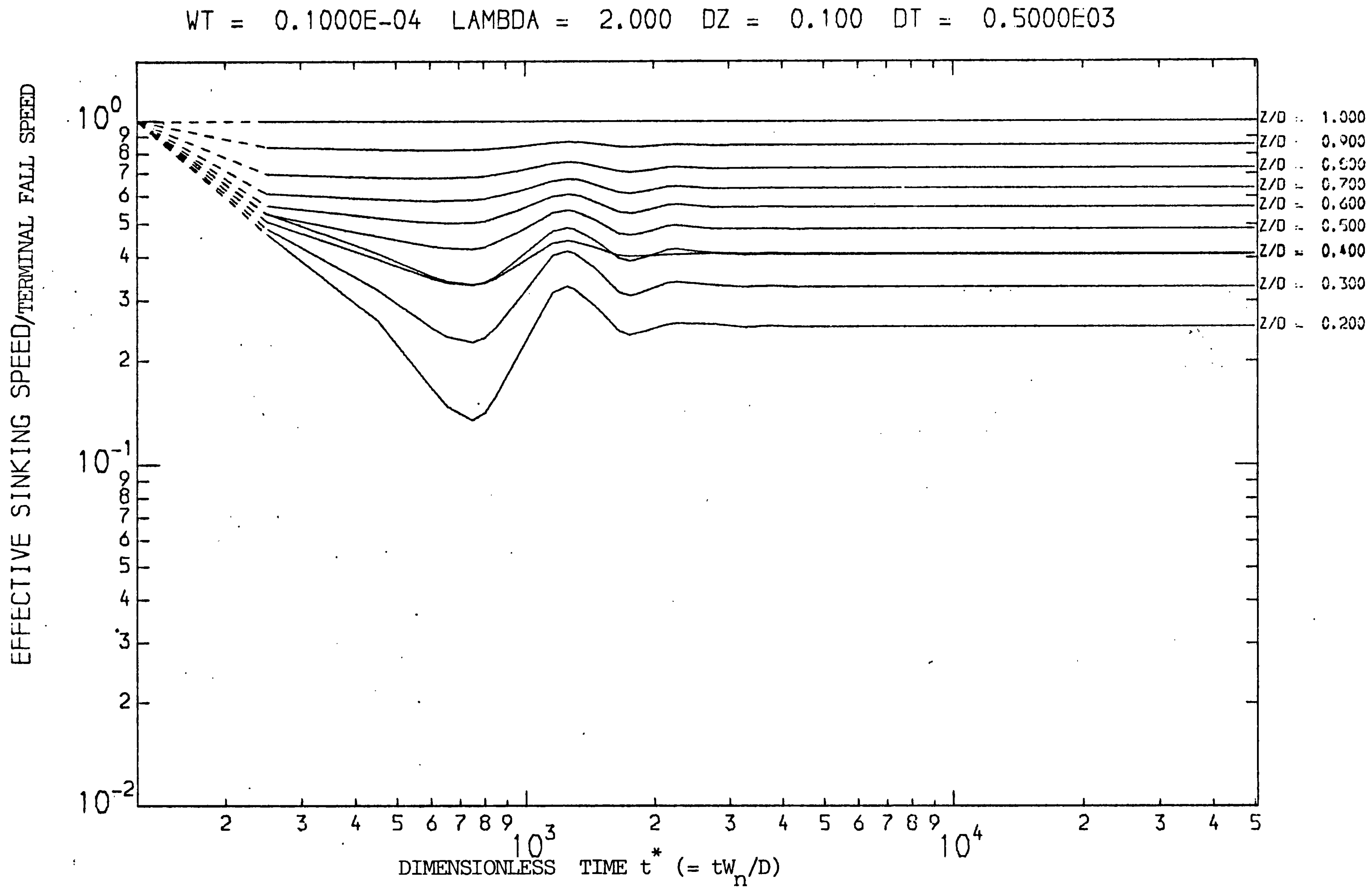

Fig. 7.15 Effective sinking speeds as functions of dimensionlees time t^* and dimensionless depth z^* in the one-dimensional model for $\lambda_c^* = 2.0$ and $W_T^*=1x10^{-5}$

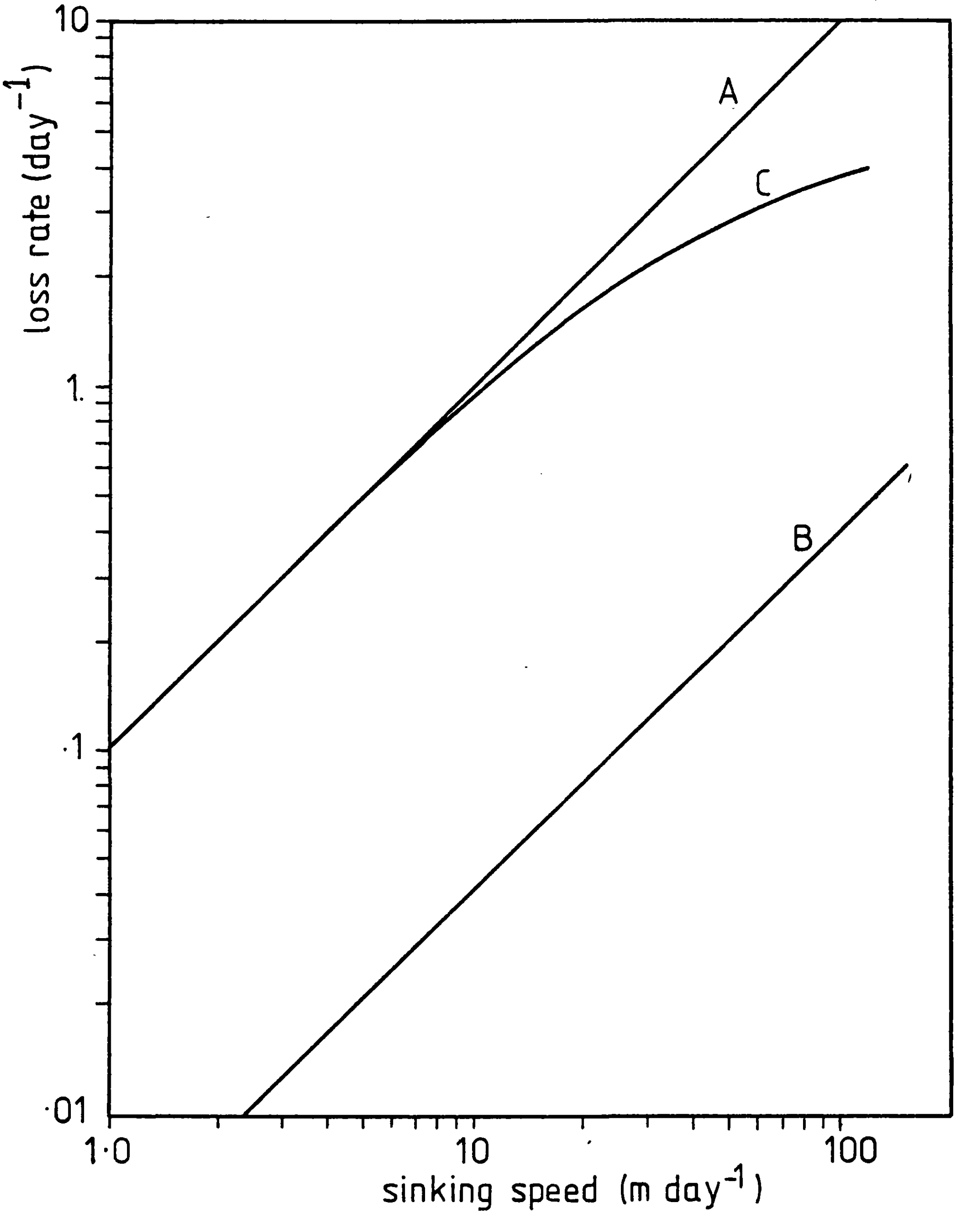

Fig. 7·16 Loss rates for particles of various sinking speeds, as predicted by algebraic relationship (loss rate = sinking speed/depth; curve A), Titman and Kilham's model (curve B), and present model (curve C) for $\lambda_c/D = 2{\cdot}0$, depth $D = 10$ m, wind speed $W_n = 1 \text{ms}^{-1}$.

SOME EFFECTS OF LANGMUIR CIRCULATION ON SUSPENDED PARTICLES IN LAKES AND RESERVOIRS

CHAPTER 8 PRELIMINARY LABORATORY EXPERIMENTS ON LANGMUIR CIRCULATIONS

Two preliminary laboratory experiments are described, the purposes of which are understanding basic mechanisms involved in Langmuir circulation phenomena. The first experiment was devised to investigate the dependence of the Langmuir circulation scale of motion on wind-wave parameters, in order to find some approximate criteria for estimating Langmuir cell size from environmental data. The second experiment is concerned with the effects of a circulating motion, analogous to that in a Langmuir cell, on the distribution and settling of suspended particles. Although natural conditions cannot be precisely modelled because of laboratory limitations and little appreciation of the relative significance of the similitude criteria, many fundamental features of the circulation and the general behaviour of suspended particles in the circulating motion are exhibited.

CHAPTER 8 PRELIMINARY LABORATORY EXPERIMENTS ON LANGMUIR CIRCULATION

8.1. A Wind-Wave Tank Experiment

Recent laboratory experiments on Langmuir circulation performed by Faller and Caponi (1978) have shown that the scale of the circulation can be related to the dominant wave length of the surface wind-generated waves. In order to corroborate their results and hence to test a relationship of the form

$$\frac{\lambda_c}{D} = \Phi\left(\frac{H_{1/3}}{D}\right) , \tag{8.1}$$

in which λ_c is the row spacing (twice the Langmuir cell width), D is the cell depth, and $H_{1/3}$ is the significant wave height, an essentially similar experiment in a wind-wave tank was conducted. This relationship (equation (8.1)) is considered to be more convenient than that of Faller and Caponi in that, it has been shown elsewhere (Chapter 4), the significant wave height $H_{1/3}$ is a function of wind speed and fetch length.

8.1.1. Experimental Apparatus and Procedure

Langmuir cells were generated in a wind-wave tank which had been modified from a wave channel of dimensions 10 m (length) x 0.9 m (width) x 0.30 m (height), by installing a wooden roof over the channel (see Fig.8.1). An air stream was drawn over the channel by an axial fan mounted at its end. The test section, located at the middle part of the channel, was covered by a removable perspex roof. The channel floor at the test section was painted white to provide a good contrast for photographs. During the experiment, water depth was varied between 3 to 5 cm with the roof fixed at 23 cm above the channel bed. A sloping beach was provided at the outlet end of the channel to minimise wave reflection. Although air speed was varied, it was not precisely measured in this experiment; only rough indications were obtained from a hand-held anemometer in the inlet section.

The average dominant wavelength λ_w of wind-generated waves was measured from photographs of the wave profiles visible through the glass side of the tank. Treating these photographs as representing a continuous record of a wave train for a given water depth and wind speed, the lengths of successive waves were obtained by measuring the distance between the wave crests by means of a linear scale located in the photograph. Approximately 10 to 20 waves were considered adequate for averaging since, from visual observation, wave lengths did not differ appreciably.

A conductivity probe, Fig.8.2, fitted near the side of the tank, was used to measure water surface displacement at the test section as a function of time, from which data on the significant wave height, $H_{1/3}$, were determined. The probe consists of two 1 mm diameter heating wires, separated by a distance of 2 mm , and stretched vertically, perpendicular to the water surface, between two fixed supports. Water between these two wires forms a conducting medium and the displacement of its surface alters the resistance between the wires. This resistance was measured by an a.c. excited bridge arrangement. The output signal representative of the wave pattern was traced by a pen chart recorder. No attempt was made to linearise the response. The probe was calibrated before each series of experiments.

Observations of the cell spacing λ_c were made by sprinkling potassium permanganate $(KMnO_4)$ dye crystals across the tank immediately before the commencement of the experiment. Once formed, the spacings of the cells that extend down the water depth were evident from the somewhat regular spacing of the longitudinal dye bands which formed across the tank. Figure 8.3 shows, in a schematic diagram, the position of these dye bands at the bottom of the tank in relation to the Langmuir cells. Photographs were taken at intervals of the dye pattern development for subsequent determination of average cell spacing. Figure 8.4 illustrates some examples of the dye bands as viewed from above the test section.

8.1.2. Determination of Average Cell Spacing

The experiment is similar to those conducted by Faller and Caponi (1977, 1978) who described the evolution of the dye bands. Current observations, which accord with their description, were as follows:

Soon after the arrivals of waves at the test section, intense downward motion becomes apparent in the dye pattern at the tank bed. This downward motion quickly aligns dye layers into regular bands and the width of the bands increases with time. The confluence of dye into bands indicates the presence of Langmuir circulation (see Fig.8.3). After about 2 to 3 minutes, the number of bands appears to be relatively constant though the position of the bands may change with time, which makes determination of their number difficult. The appropriate time interval was selected as the bands reached a somewhat steady state and the average cell spacing λ_c was determined at this time, taking two cells per wavelength, by

$$\lambda_c = 2\,W/N_c \quad , \tag{8.2}$$

in which W is the width of the tank; N_c is the number of cells inferred from the dye system, which is equal to $(n_b + n_c - 1)$; n_b is the number of dye bands, and n_c is the number of clear lanes across the width of the tank.

8.1.3. Determination of Wave Height, $H_{1/3}$

From the water displacements recorded on the pen chart recorder, a sample of 100 or more waves were used to determine the significant wave height $H_{1/3}$. For each wave length, the wave height was determined by subtracting the height of the intervening trough from the average height of successive wave crests, or in the case of successive troughs, it is found by subtracting the average height of the two bordering troughs from the height of the two intervening wave crest. A calibration curve was used to convert the heights of the crests and troughs into water depths. The significant wave height $H_{1/3}$ was then determined by averaging the largest one-third of the wave heights.

8.1.4. Results

A summary of results obtained is given in Table 8.1. The dimensionless cell spacings λ_c/D are shown as a function of dimensionless average dominant wave length λ_w/D in Fig.8.5, and are seen to confirm the results of Faller and Caponi. The experimental data λ_c/D are plotted against $H_{1/3}/D$ in Fig.8.6, together with some data from natural situations, in which a fully developed sea is assumed. From both sets of data, the trend of these data points indicates some correlation between Langmuir cell spacing (λ_c/D) and the significant wave height $(H_{1/3}/D)$ of wind waves, suggesting that they are essentially the same phenomena. A dash-line is tentatively drawn to show this trend. This curve is drawn towards the left of field data to account for the possibility of overestimating the significant wave height $H_{1/3}$.

8.2. A Particle Settling Experiment

The primary objects of this experiment are to illustrate the mechanism by which settling of particles is affected by Langmuir circulation and to obtain quantitative data.

8.2.1. Experimental System

The experiment was carried out in an open-top clear perspex tank of the outer dimensions 0.5 m (length) x 0.5 m (height) x 0.18 m (width), filled with tap water of the temperature about 20°C . The tank (illustrated in Fig.8.7) consists of two compartments separated by means of a withdrawable steel plate. The upper chamber represents the circulation cell of approximately square section (0.4 m x 0.38 m) with the width of 0.15 m , in which motion is induced by two belt systems situated in the chamber and driven at variable speeds from outside by two electric motors. Only parts of the belts are exposed to water. The right belt is driven faster than the left one which runs at a fixed slow speed. The lower compartment represents the quiescent region below the Langmuir circulation cell and contains three particle collection boxes. Above and inside these boxes, horizontal motions are eliminated by honeycomb sections.

8.2.2. Flow Measurements

Flow measurements and quantitative data on the speed and direction of the circulation were obtained by stroboscopic photography*. Expandable translucent polystyrene particles, of the diameter between 420 to 500 μm, were used as tracers. These particles have a specific gravity between 1.03 and 1.05. They were immersed in water at 95°C for 5 seconds and then cooled quickly to below 60°C. This resulted in a white appearance with the specific gravity reduced to about 1.0. A 1 kW (14" trough) light source was enclosed in a box with a double slit arrangement to give a light beam some 12 mm wide over the central length of the chamber. A strip mirror was installed below the honeycomb to augment illumination in the lower part of the chamber. The camera used is the Hasselblad 500 ELM (80 mm lens) with Kodak Tri-X 120 films. The reflected light entering the camera was mechanically interrupted by a 400 mm diameter aluminium disc having 6 equally spaced slots cut from its edge; the solid portions between the slots being of the same length as the slots. This disc was mounted on the spindle of a variable speed electric motor. For a certain predetermined exposure time, dependent on the speed of the circulation system, a series of dashes on the photographic plate was thus produced, from which flow measurements and velocities could be deduced. Some photographs of the flow patterns obtained by this technique are shown in Fig.8.8.

8.2.3. Velocity Measurements

From a series of dashed streaks on the photographs, which were traced over a known interruption frequency, the magnitudes of the velocity vectors, and hence horizontal and vertical components of velocity, were determined. This was done by comparing the length between the centres

* (Naib, 1966)

of adjacent dashes with a linear scale included in the photograph. By repeating measurements on several photographs taken under identical conditions, mean values are obtained by an averaging procedure. Since these velocities are obtained at random points over the flow, an interpolation procedure can be used to estimate the velocities at regular grid points for easy presentation and averaging. In these experiments, the distances between the distances between centres of selected dashes covering most parts of the photograph were derived on a digitisation table, relative to the known dimensions of the reference axes in the picture, which were the left and lower boundaries of the illuminated plane. A computer program, written to compute the length of any line from a pair of digitised coordinates, gave local orientations and velocity vectors. Finally, the program interpolated these velocities at regular grid points and plotted the vectors. Four different circulation patterns were produced by varying the belt speeds, and shown in Figs. 8.9 to 8.12.

8.2.4. Particle Sinking Loss Measurements

From the measurements of sinking loss of particles at the end of an elapsed time, the mean rate of sinking of the particles in the circulation cell can be determined. Untreated polystyrene particles, having a specific gravity between 1.03 and 1.05, diameter between 420 and 500 μm, and an average terminal fall speed in still tapwater (18°C to 20°C) of 0.5 cm/s, were used. At the beginning of the experiment, 5.0 grams of the particles were introduced in a circulation of known profile, the water being stirred gently to obtain as uniform a concentration as possible, with the plate separating the upper and lower chambers closed. At time zero, the plate was pulled out and the particles began to settle. When a very small amount of particles remained in the circulation (some 9 to 10 minutes), the separation plate was closed. Water and particles in the upper chamber were drained off and no attempt was made to recover them. The particles in the collecting boxes were dried and weighed. During the circulation, it was generally observed that a small number of particles escaped through the gaps at the belt openings and were lost from the system.

8.2.5 Results

From the photographs of the flow patterns and velocity vectors shown in Figs. 8.9 to 8.12, it is seen that intense water motion in the downward direction was induced by the belt in the form of a narrow jet, accelerating along the solid boundary and deflecting at the bottom right hand corner into the main flow. In general, circulating flows were created though they are not symmetrical. It is impossible to control the shape of the circulation. Secondary flow was observed near the left boundary, giving rise to some mixing there. The centre of circulation is, in all cases, at about the cell centre.

Using nigrosine dye as an indicator it was apparent that the flow in the laboratory apparatus is laminar but unsteady, the latter arising from both belt movement and the oscillation of the water surface. In effect, this introduces some degree of mixing in the circulation but at a lower level than a turbulent mixing action. The jet on the right side of the figures and the flow close to the lower boundary cause some transfer of particles by entrainment out of the central core. Particles were seen to be circulated around the cell by the motion imposed by the rotating belts. The unsteadiness of the flow results in particles coming into contact with the right side of the cell, being entrained into the downward jet, subsequently moving to the lower boundary and sinking.

Similar settling could well occur with turbulent diffusion processes but with a greater particle transfer to the outer zone resulting from the strong turbulent mixing.

At the end of an elapsed time of approximately 9.50 minutes a small quantity of particles were observed to be left in suspension. The losses by sinking were measured and these are summarised together with other circulation variables in Table 8.2. The distribution of these sinking losses across the cell width are shown in Fig.8.13, and are generally the same in all four cases. These curves show there is an increase in sinking towards the upwelling zone. The measurements indicate that the total sinking losses also are approximately the same in these four cases, being about 4.0 grams out of the initial particle mass of 5.0 grams. This equality of the total sinking losses and essentially similar distribution of sinking losses across the cell width suggest that the increase in belt speed has had little effect on the degree of mixing and particle transfer. Such a consequence is anticipated from the flow conditions obtained. Since the flow is laminar, increasing unsteadiness, brought about by higher belt speeds, does not have a significant effect on particle transfer.

If the experimental results are compared with calculations made when turbulent diffusivity is present and which result in complete mixing,the latter condition leads to only 2.52×10^{-3} grams of particles remaining in circulation after 9.5 minutes, that is practically all particles settle out. The comparison suggests that circulation currents do affect the particle settling rate. If the laboratory experiment and this calculation are considered to represent lower and upper bounds to the particle sinking problem, in a practical situation the amount of particles remaining in suspension will lie between these two extreme cases, sinking losses depending on the intensity of turbulence present. For the laboratory experiment, the ratio of the effective sinking speed to particle fall speed is estimated to be 0.2 . Using the computer prediction model described in Chapter 6 to be representative of settling in a Langmuir cell, then, for the conditions of cell spacing-to-depth ratio $(\lambda_c/D) = 2.0$ and (range of) particle fall speed to maximum upwelling speed ratios used in the experiment, the computer model predicts the ratio of effective sinking speed to fall speed to lie between 0.4 and 1.0 , these values being higher than that determined experimentally under unsteady laminar flow conditions. It is thus apparent that Langmuir circulation does reduce the particle sinking loss, the degree of such reduction apparently decreasing as turbulence intensity increases. With high turbulent intensity, the fully mixed situation is approached.

An indication of particle aggregation in the circulation region may be obtained by photographing particles in the model cell at an instant of time after the circulation has commenced. By dividing the cell region into several equal grid volumes, the number of particles in each indicates the relative particle concentration distribution over the cell. An example is shown in Fig.8.14 at time 3.0 minutes after zero for the experimental condition number 3 . Particle aggregation is present, and the concentration contours generally resemble those obtained by the computer model described in Chapter 6, i.e. a high concentration core is present in the upwelling zone and small particle concentrations may be seen under the convergence region and in the downwelling zone.

8.3. Significance of Experiments

8.3.1. The Wind-Wave Tank Experiment

Natural conditions cannot be modelled in this experiment because of laboratory limitations and the difficulty of appreciating the relative significance of similitude criteria. These demand that both geometric and dynamic similarity are attained.

Since Langmuir circulation is generated by interactions of wind and waves and is affected by a number of environmental factors, the characteristic length λ of the circulation is anticipated to be a function of the variables listed below.

shape,
depth of water, D
wave height, H
local velocity of wind, W_n
local velocity of water, W_a
gravitational acceleration, g
water density, ρ
local air density variation, $\Delta\rho_a$
water viscosity, μ
air viscosity, μ_a
surface tension force in water, σ
thermal conductivity of water, k
specific heat of water, c
local temperature of water, T_w .

Thus

$$f(\lambda, \text{shape}, D, H, W_n, W_a, g, \rho, \Delta\rho_a, \mu, \mu_a, \sigma, k, c, T_w) = 0. \quad (8.3)$$

Dimensional analysis of these variables yields 11 dimensionless groups, i.e. $\frac{\lambda}{D}$; shape ; $W_n \frac{\rho_a H}{\mu_a}$ - (Reynolds number of wind) ;

$W_w \frac{\rho D}{\mu}$ - (Reynolds number of water) ; $\frac{W_w^2}{gH}$ - (Froude number) ; $\Delta\rho_a/\rho$;
$\frac{\rho W_w^2 H}{\sigma}$ - (Weber number) ; $\frac{\mu c}{k}$ - (Prandtl number) ; $\frac{W_w^2}{cT_w}$ - (Ekert number) ;

ρ/ρ_a ; μ/μ_a .

In any experiment it is impossible to satisfy all these conditions simultaneously. A number of gross assumptions must be made.

(i) Effects of Reynolds number are neglected, assuming that the characteristics examined do not vary appreciably with Reynolds number. This is a necessary assumption if Froude number dependency dominates the problem for Froude number and Reynolds number cannot be satisfied simultaneously. However, if Langmuir circulation is turbulence-driven, it is, at least, necessary for the test to be conducted at such a Reynolds number that the water flow under experimental conditions is turbulent. This places a restriction on the size of acceptable test apparatus.

(ii) Weber number effects are neglected, assuming that the tests are not going to be conducted at such a small scale that surface tension forces become significant.

(iii) Ekert number effects are neglected, assuming in the first instance that the Langmuir circulation phenomenon is not significantly temperature driven.

(iv) The air-water interface is modelled with a laboratory air-water interface so that ρ/ρ_a and μ/μ_a are the same for the model and the full scale.

(v) The Prandtl number conditions is assumed to be satisfied.

Under these restricted conditions,

$$\frac{\lambda}{D} = f\left(\text{shape}, \frac{H}{D}, \frac{W_w^2}{gH}, \frac{\Delta\rho_a}{\rho}\right) . \tag{8.4}$$

Since the water velocity can be related to the wind speed, and if geometric similarity is achieved, the wave height is a function of wind speed, thus ignoring the effect of $\Delta\rho_a/\rho$, equation (8.4) can be reduced to

$$\frac{\lambda}{D} = f\left(\frac{W_n^2}{gH} \text{ or } \frac{W_n^2}{gD} \; ; \; \text{shape}\right) , \tag{8.5}$$

where D is the water depth which influences Langmuir circulation, being the total water depth if the lake is shallow or the thermocline depth if the lake is deep. Shape in the above equation implies correct geometrical scaling of the surrounds. It is anticipated that the modelled waves will be distorted to some minimal extent, but the gross features of the circulation phenomenon are produced.

Equation (8.5) has been used in Chapter 4 to correlate oceanic data on the size of Langmuir cells with wind speeds, assuming open sea situations in which shape is not an important parameter. The correlating curve (see Fig.4.4) suggests a form

$$\frac{\lambda_c}{D} = f\left(\frac{W_n^2}{gD}\right) \tag{8.6}$$

where λ_c is the row spacing and D is the thermocline depth.

Natural conditions which resemble those in the laboratory are those in shallow lakes and mud flats, where regular Langmuir circulation has often been observed to extend down to the bed. Because of depth limitation in the laboratory apparatus and the necessity to raise the wind speed high enough (usually greater than 3 m/s) to produce gravity waves, the range of Froude number in the prototype cannot be reproduced in the model apparatus. Taking typical values of wind speed in lakes to be 10 m/s and water depth (or thermocline depth) of 10 m, then the Froude number for this condition is about 1.0. Using laboratory wind speed ≐ 3 m/s and water depth of 6 cm, the Froude number achieved is about 15.0. Because of this lack of similitude, laboratory results must be viewed with caution.

Following Faller and Caponi's (1977, 1978) presentation, the present experimental data have been plotted in Fig. 8.15 according to the equation

$$\frac{\lambda_c}{D} = f\left(\frac{H_{1/3}}{D}\right) , \tag{8.1}$$

in which Froude number effects have been ignored. The plotted points show a correlating trend, suggesting that the results may not be particularly sensitive to changes in the Froude number. It could be that the effects of wind speed have been largely absorbed by the surface wave height, and the Langmuir circulation scale is more dependent on the available energy stored in the waves. Published data, predominantly those of Faller and Woodcock (1964), have been superimposed in Fig. 8.15 assuming fully-developed oceans in which the significant wave height can be estimated from wind speed. Although there is some scattering of data, an apparent trend can be observed, implying that the relationship suggested by equation (8.1) is applicable.

These field data fall on the lower end of the plot, having small values of $H_{1/3}/D$, and the data were obtained under different values of Froude number from those in the laboratory. From the plotted points, it is apparent that these two sets of points follow a similar correlating curve or at least are close members of a family of curves, suggesting that they are subjected to essentially the same phenomena. A smooth curve has been tentatively drawn slightly to the left of the oceanic data to account for an overestimate of the significant wave height $H_{1/3}$, through both sets of data, to indicate the correlating trend. It may be argued that since there is a difference in the lower boundary of Langmuir cells (the thermocline for the oceanic cases, whereas this boundary is rigid in the laboratory), a single curve should not be drawn through both sets of data. If this were the case, the erodible boundary curve should lie somewhat below the laboratory points, indicating a slightly smaller cell width because some energy has been spent in eroding the thermocline. However there is not enough overlap of data to indicate where such a curve should lie. Also the oceanic data are too scattered to position this curve accurately. More data in the intermediate values are required to justify this argument. For the present, the experimental data may well represent an extreme case of the Langmuir cell extending to the bottom and the oceanic data represent an extreme condition of deep Langmuir cells with erodible boundaries. An empirical prediction such as this is required so that an estimate may be made of Langmuir circulation effects on sinking loss of particles (Chapter 7), which is dependent upon the cell spacing-to-depth ratio λ_c/D .

More accurate and extensive measurements on Langmuir circulation in laboratory and natural conditions are certainly required if a significant overlap of data is to be obtained, and to further substantiate the correlation equation (8.1), in which it is assumed that Froude number effects have little influence compared with the $H_{1/3}/D$ ratio. In the field investigation, additional measurements of the surface wave variables, including wind speeds, wind direction and fetch lengths are needed. The effects of difference in the lower boundary could well be investigated in the laboratory by using erodible fluid boundaries, through the use of two immiscible fluids (a diagrammatic sketch of such an arrangement is illustrated in Fig.8.16). This would provide data on an extreme condition for the Langmuir cell with an erodible lower boundary, through which an improved empirical curve could well be drawn. In future laboratory experiments, efforts should be made to minimise the surface tension effects by generating waves with large enough heights, say, greater than 20 mm. In the present experiment, the generated waves could have been influenced, to some extent, by surface tension forces because of the smallness of their heights.

8.3.2. The Particle Settling Experiment

Just as in the wind-tank experiment, complete dynamic similarity of the circulation flow and of the particle motion cannot be achieved in the laboratory apparatus described above. The similarity in the distribution of particles in a circulation cell and the sinking loss from it demands that similarity is achieved in modelling both the circulation flow and the particle motion.

8.3.2.1. The Circulating Flow

Similarity in both the mean flow and the turbulent eddies is necessary if advective and turbulent (diffusive) transport of particles in the cell is to reproduce the natural situation. Because of Reynolds number limitations the turbulent condition cannot be achieved in the present apparatus. Treating the water motion induced by the belt to be analogous to that over a flat plate of characteristic length D which travels in still water of kinematic viscosity ν at a uniform speed U, the critical Reynolds number required for transition to turbulence is about 2×10^6 (Francis, 1975). The maximum value presently obtained is about 1.2×10^5, resulting in an unsteady laminar flow in the cell. Because of this limitation, the results obtained are not quantitatively significant but give a pictorial representation of the circulating flow in a cell and the behaviour of particle settling through it. Qualitatively, the model has demonstrated the circulation effects in causing reduction in sinking losses.

It is apparent that the most important criterion of similarity for the circulating flow is the Reynolds number. To achieve a sufficiently high Reynolds number, a larger model and probably a faster belt speed would be required. Assuming the critical Reynolds number, based on the downwelling velocity at the belt and the depth of water, to be 2×10^6, the depth of water (i.e. the size of the tank), D, may be related to the downwelling velocity, U, by $D(m) \geq 2/U(m/s)$. For instance, if the tank size is 2 m x 2 m, then the belt must induce a water speed of at least 1 m/s.

Although turbulent circulating flow in the laboratory apparatus can be produced by increasing the tank size and perhaps running at higher belt speed, the resulting circulation may not be strictly similar to that within Langmuir cells for at least two reasons:-

(a) Generating Mechanisms. Because of differences in the generating mechanism, i.e. mechanically generated in the laboratory apparatus while the real Langmuir circulation is caused by a highly complex interaction of surface wave and wind effects, it is unlikely the flow pattern and the velocity profile will be reproduced exactly. There is little data available about the circulation shape and velocity profile within the cell. Thus it is probable that only the gross features of the circulation will have been adequately reproduced.

(b) Turbulent Intensity. The flow in the epilimnion of a lake can become turbulent at a Reynolds number which is much less than the criterion $R_c = 2 \times 10^6$ based on the moving flat plate (in the vertical direction) analogy. For example, taking the downwelling speed in a lake under, say, 4.0 m/s wind to be 0.04 m/s and the mixed layer depth of 5.0 m, the Reynolds number for this condition is 2×10^5. There are reasons to believe that the flow in the mixed layer is turbulent under this condition (Hutchinson, 1957; Mortimer, 1974; Smith, 1975). However, it must be appreciated that the natural phenomenon is much more complex than the laboratory situation and the model of a boundary layer generated on a moving surface is unlikely to be directly applicable to full scale. In the full scale situation the flow is strongly three-dimensional in character and the transition and may well be affected by dimensions in the plane normal to the Langmuir cells.

Having established turbulent flow in a laboratory model of a Langmuir cell, the model would serve a valuable rôle in quantitatively assessing the effect of such a cell on particle distribution and sinking rates. Under laboratory conditions, experiments of this sort are much more readily performed than in the natural environment.

8.3.2.2. Particle Motion

Similarity of concentration distribution of suspended particles will result if the bulk transport of these particles in similar flow systems are in similitude. This requires, in addition, the satisfaction of non-dimensional numbers governing the motion of discrete particles within a turbulently flowing fluid. Exact similarity of both the flow patterns and the resulting particle transport cannot be achieved in the current experiment because all the requisite similitude criteria have not been satisfied.

In a turbulent flow system, particle distribution and hence sinking loss will significantly depend upon the following variables:-

$$\mu \ , \ \rho \ , \ d \ , \ V_f \ , \ L \ , \ g(\rho_s - \rho) \ , \ \rho_s$$

in which μ = the fluid dynamic viscosity ; ρ = the fluid density ; d = the particle diameter (size); V_f = the characteristic fluid velocity ; L = the characteristic length for a fluid ; ρ_s = the particle (grain) mass density ; $g(\rho_s - \rho)$ = the specific weight of particle in fluid. Dimensional analysis of the above variables yields the following dimensionless products, which represent a possible form of similitude criteria:-

$$\frac{V_f d}{\nu} \ , \ \frac{V_f}{[g(s - 1)d]^{\frac{1}{2}}} \ , \ \frac{L}{d} \ , \ s$$

in which, $s = \rho_s/\rho$ = the density ratio; and $\nu = \mu/\rho$ the fluid kinematic viscosity. Study of these parameters indicates that the dynamical reproduction of particle transport using the same prototype fluid in a small scale model is not possible, hence a number of gross approximations have to be made.

(i) The effects of changes in the Reynolds number $(V_f d/\nu)$ is not significant if the Reynolds number is sufficiently high for turbulent flow to be established (Yalin, 1971).

(ii) The effect of the density ratio $s(= \rho_s/\rho)$, apart from its inclusion in the specific weight in the term $V_f/[g(s - 1)d]^{\frac{1}{2}}$ (or alternatively in the terminal settling velocity), will be neglected. Yalin (1971) argues that this approximation is plausible if the properties to be simulated are related to the totality of the moving grains (i.e. to the transport of granular materials en masse), not to the motion of the individual grain. Adequate prediction of the sediment transport rates in open channels shown by many sediment transport models which neglect the ratio s, provides some evidence that the influence of s on the transport rate is minimal.

(iii) The ratio L/d cannot be satisfied identically in a small scale model. This ratio must be neglected and its significant is conjectural.

Hence the only remaining criterion to be satisfied is that the effective Froude number ,

$$\frac{V_f}{[g(s-1)d]^{\frac{1}{2}}}$$

should be the same for the model as for the prototype. An alternative form of the Froude number has been used by Rouse (1940) by replacing $[g(s-1)d]^{\frac{1}{2}}$ by W_T, the terminal fall velocity of particles, and the similarity criterion becomes

$$\frac{V_f}{W_T} .$$

This form of the similarity criterion, in which the particles are characterised by W_T, has been used in section 8.2.5 to compare qualitatively the sinking loss rates from the present experiment with the computer predictions.

8.3.3. General Conclusions

It is concluded that laboratory experiments do have a potential rôle to play in studying certain aspects of Langmuir circulation phenomenon and its effects, such as the dependence of the geometry of the circulation cells on the wind/wave parameters, and the distribution and settling characteristics of particles in the turbulent circulating flow analogous to a Langmuir cell. The wind/wave tank experiment illustrates the mechanism by which the circulations are developed and the particle settling experiment, by isolating the circulating phenomenon, is capable of being conducted under the necessary similitude conditions. The difficulties experienced with the present laboratory equipment, which are common to all types of experimentation on scale models, arise from the inability to satisfy all the similitude requirements because of the laboratory limitations. However, by keeping only those similarity criteria that are significant, adequate similarity may be claimed for practical purposes, as shown by the wind/wave tank experiment. Although the results of the present experiments are necessarily illustrative, several methods of measurements have been established, which could well be used in future investigations. Reduction of the similitude criteria in section 8.3.2.2 of this study must be regarded as conjectural, requiring further experimentation and field data for verification.

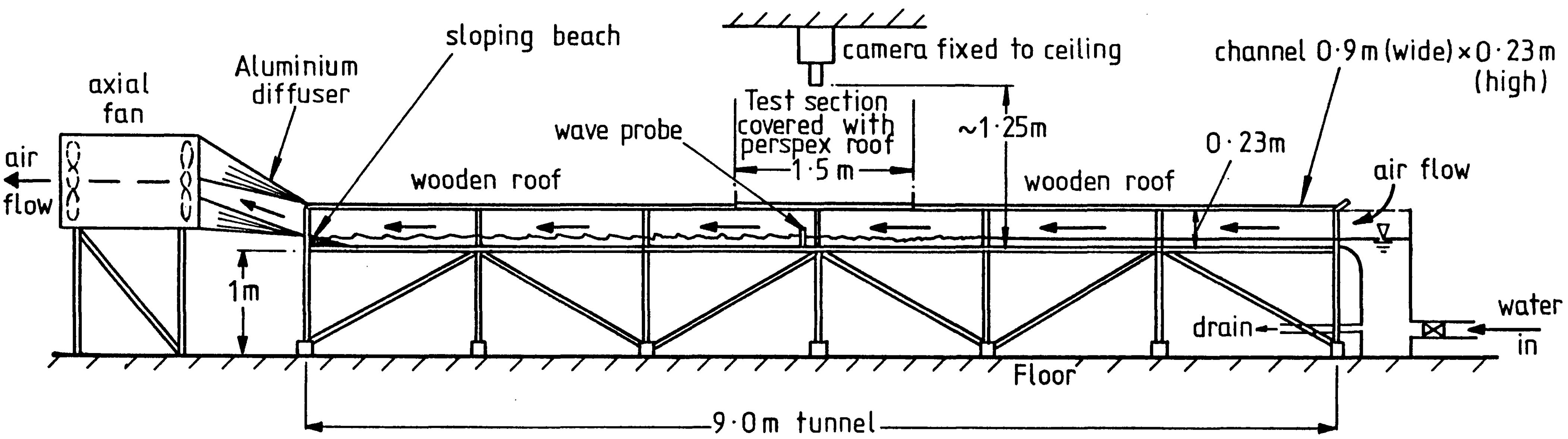

Fig 8·1 Schematic diagram showing a wind-wave tank arrangement used in the present experiment.

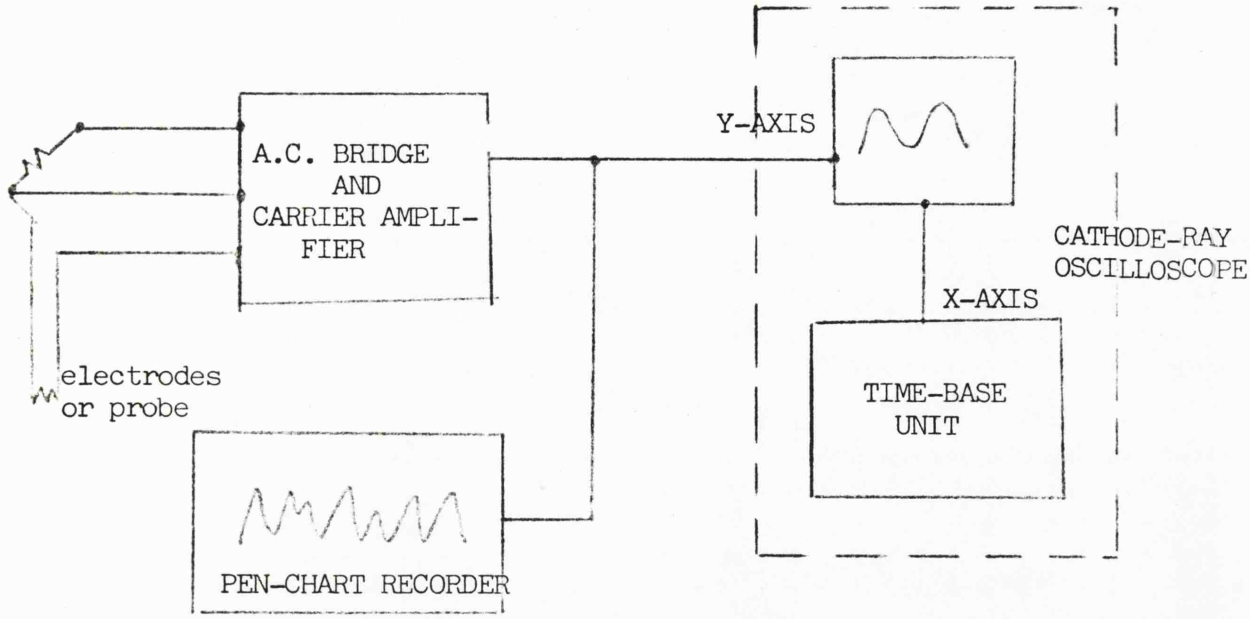

(a) Schematic diagram of the conductivity probe unit

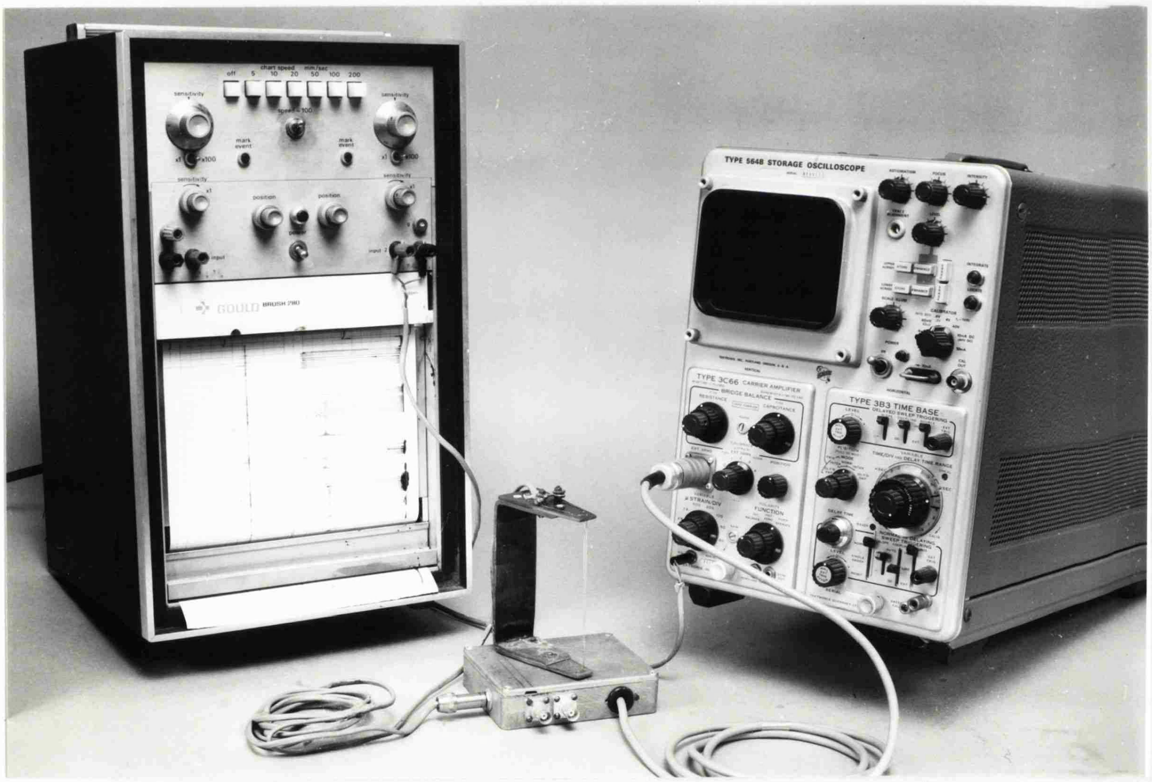

(b) Photograph showing the conductivity probe and recording devices used in the wind-wave tank experiment

Fig. 8.2 Illustrations of the conductivity probe arrangement for measuring wave heights

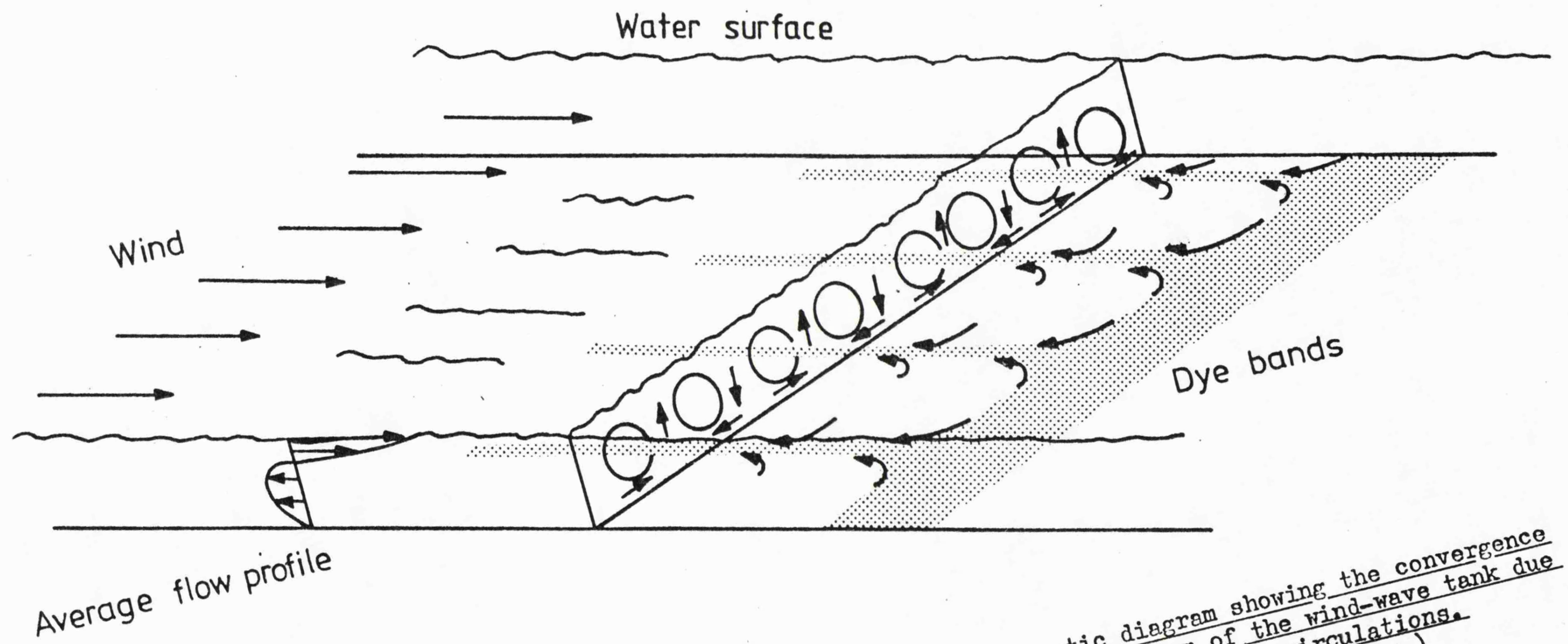

Fig. 8·3 A schematic diagram showing the convergence of dye at the bottom of the wind-wave tank due to the action of Langmuir circulations. (After Faller and Caponi, 1977)

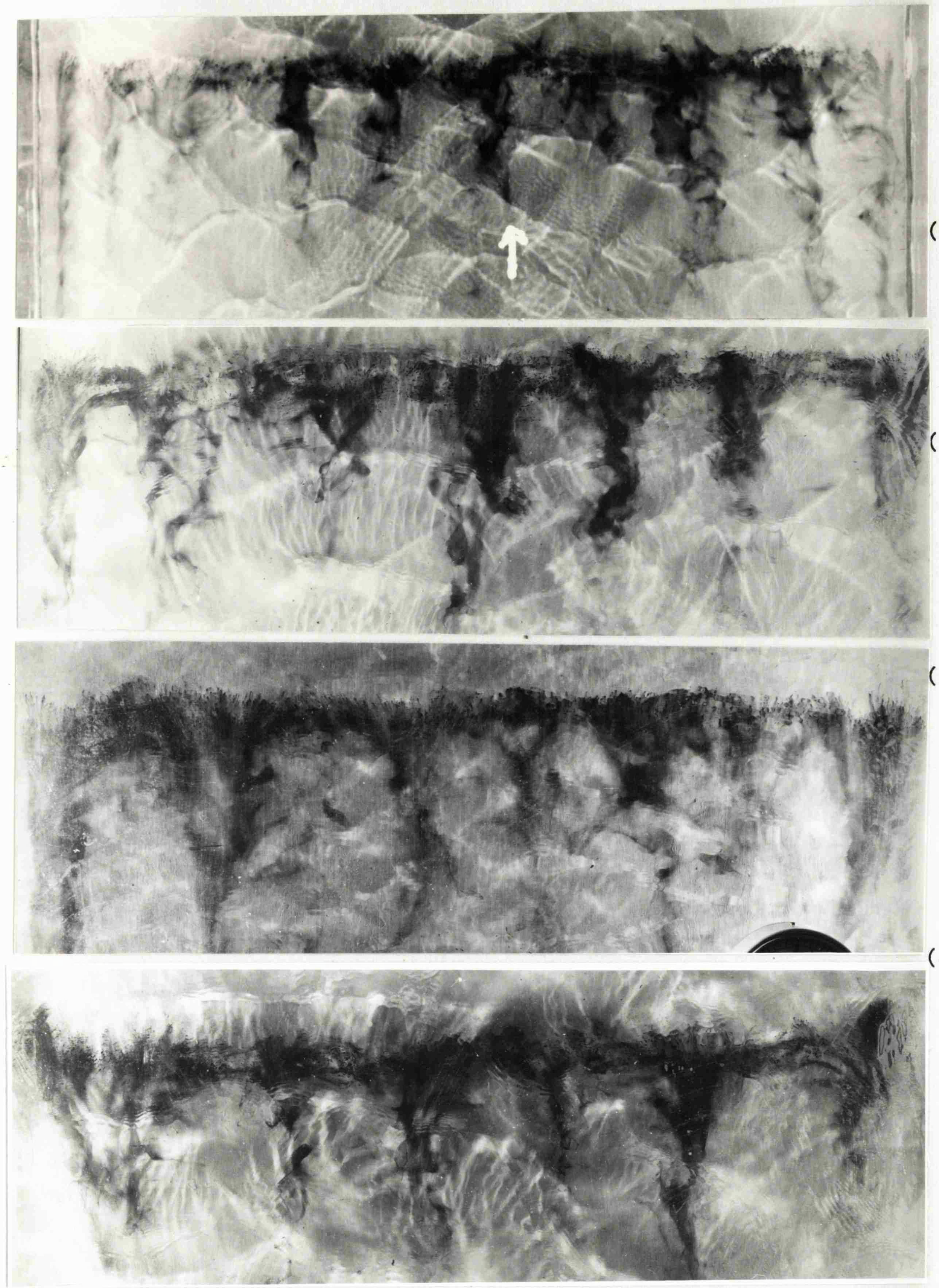

(a)

(b)

(c)

(d)

Fig. 8.4 Photographs showing dye bands in the wind-wave tank for various conditions as viewed from above the test-section. (a) Run No. 5; (b) Run No. 7; (c) Run No. 8; (d) Run No. 10. (see Table 8.1 for details)

Table 8.1 Summary of Results in Wind-Wave Tank (Width W = 0.91 m) Experiment

RUN NUMBER =	4a	5	6	7	8	9	10	11	12	13
Wind setting	4	3	2	3	2	3	4	5	6	7
Number of dye bands (n_b)	7,8	10	10	7	7	7,6	6	6	4,5	5,4
Number of clear lanes (n_c)	8,9	11	11	8	8	8,7	7	7	5,6	6,5
Number of cells ($N_c=n_b+n_c-1$)	14,16	20	20	14	14	14,12	12	12	8,10	10,8
Mean cell spacing $\lambda_c = 2W/N_c$ cm	12.25	9.14	9.14	13.06	13.06	14.15	15.24	15.24	20.58	20.58
Significant wave height ($H_{1/3}$) cm	0.95	0.68	0.46	0.85	0.36	0.91	1.21	1.37	1.51	1.54
Average wave length (λ_w) cm	-	-	5.37	8.80	5.87	10.52	11.38	13.63	17.4	17.0
Depth of water (D) cm	3	3	4	4	5	5	5	5	5	5
λ_c/D	4.08	3.05	2.29	3.27	2.61	2.83	3.05	3.05	4.115	4.115
λ_w/D	-	-	1.34	2.2	1.17	2.10	2.28	2.73	3.48	3.40
$H_{1/3}/D$	0.317	0.227	0.115	0.213	0.072	0.182	0.242	0.274	0.302	0.308

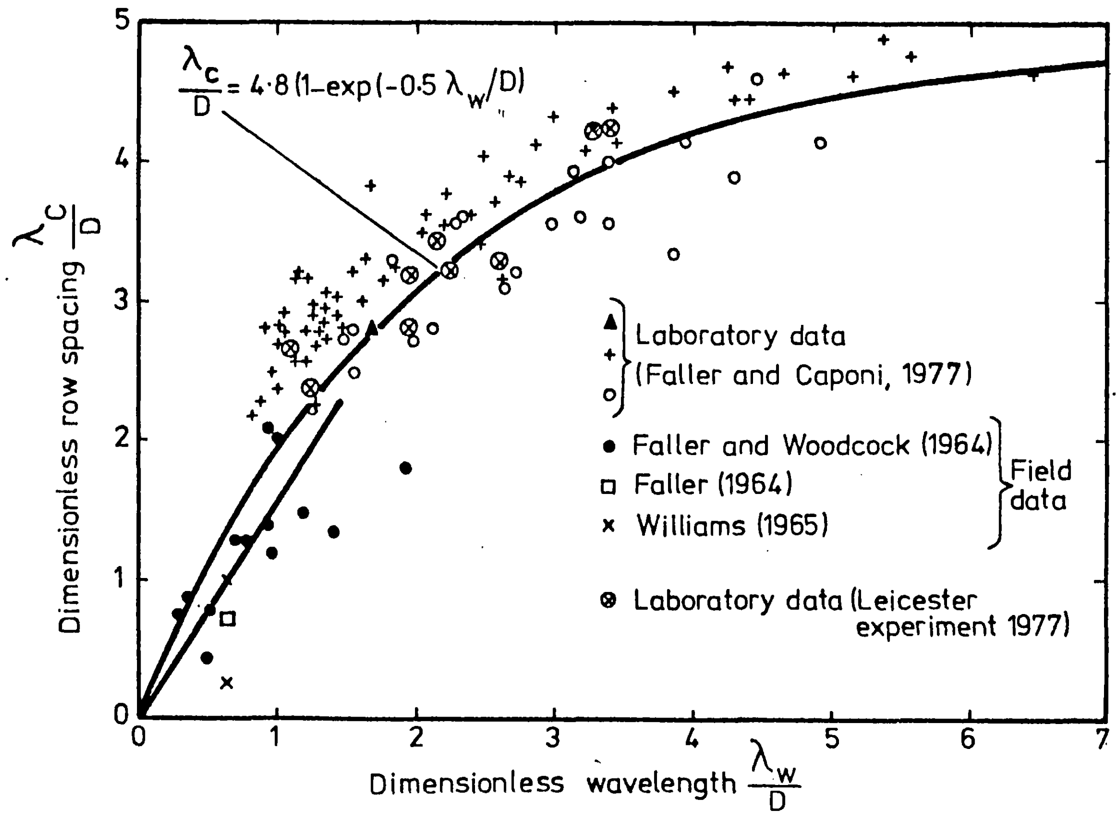

Fig. 8·5 Correlation between row spacings and dominant wave lengths.

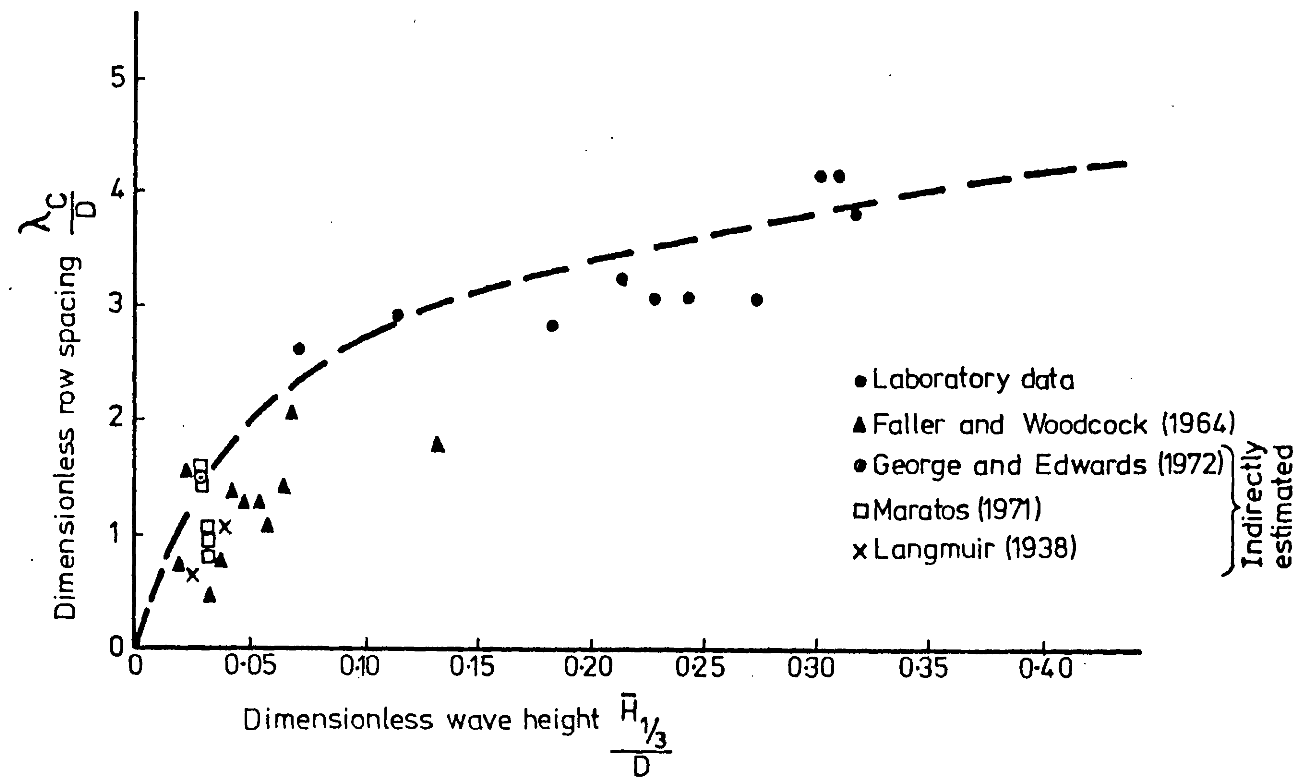

Fig 8·6 Correlations between row spacing and significant wave heights.

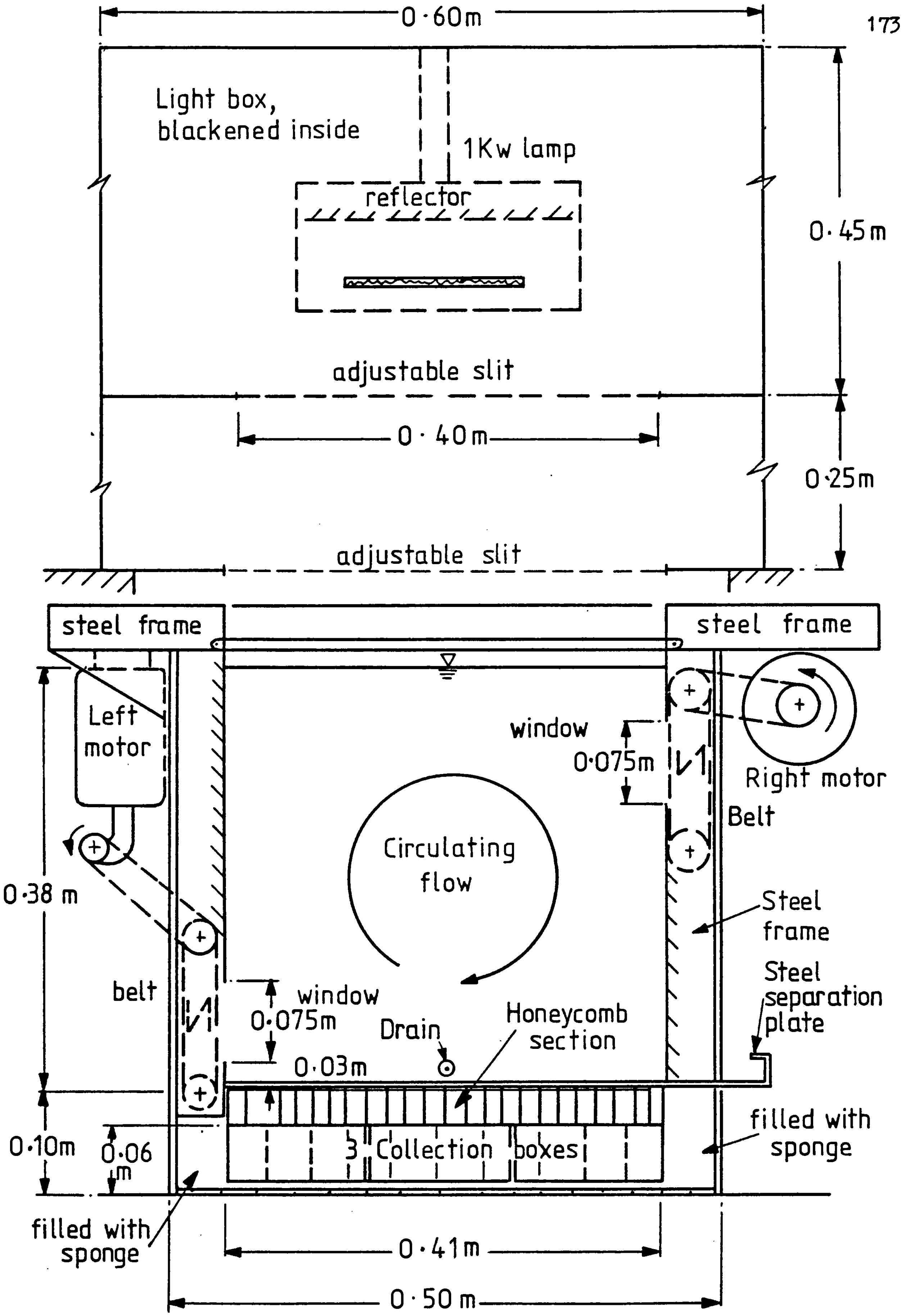

Fig. 8·7 (a) Schematic diagram of the basic apparatus for studying particle settling in circulating flows.

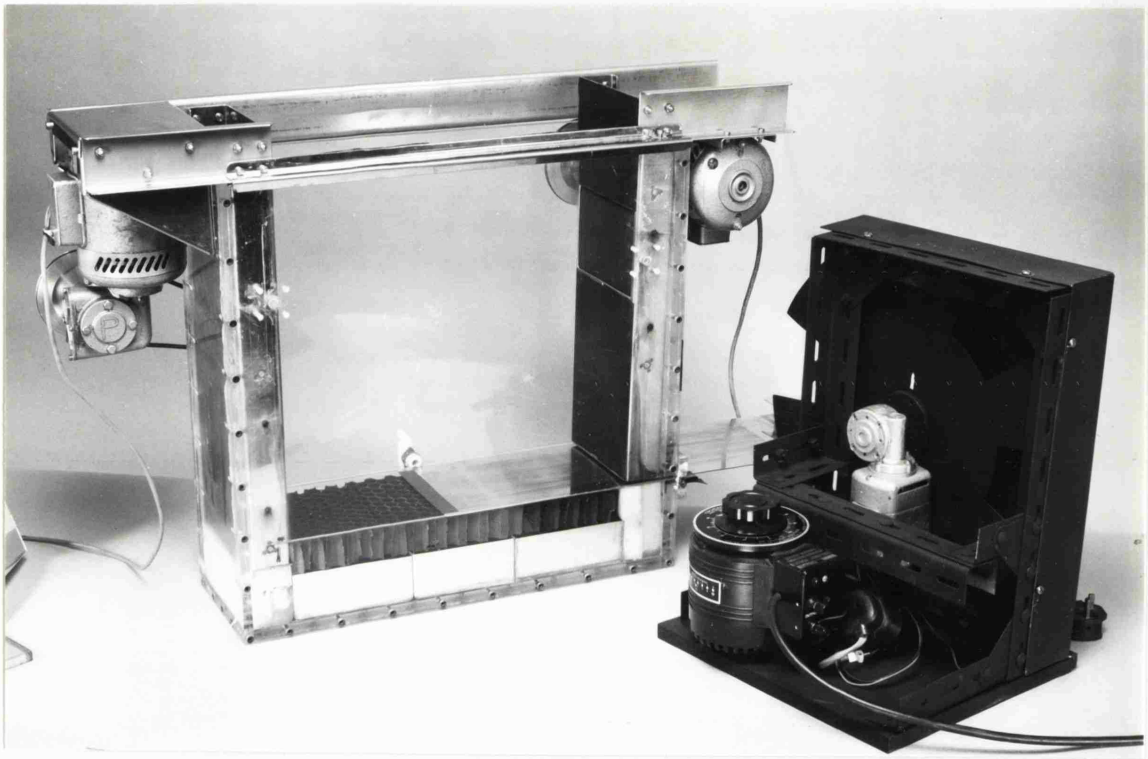

Fig. 8.7(b) Photograph of the particle settling tank and the light strobing device.

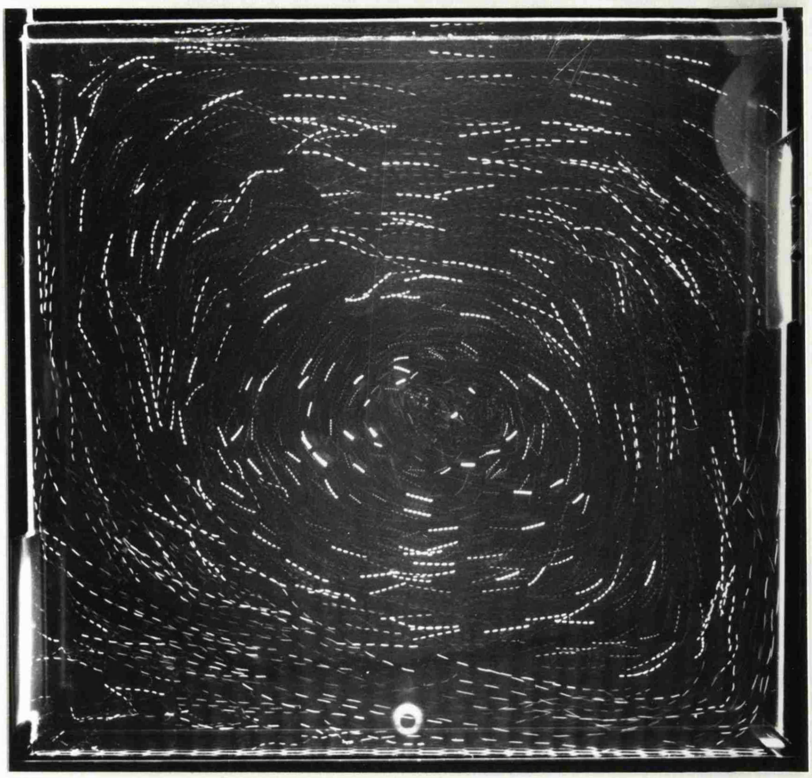

(a)

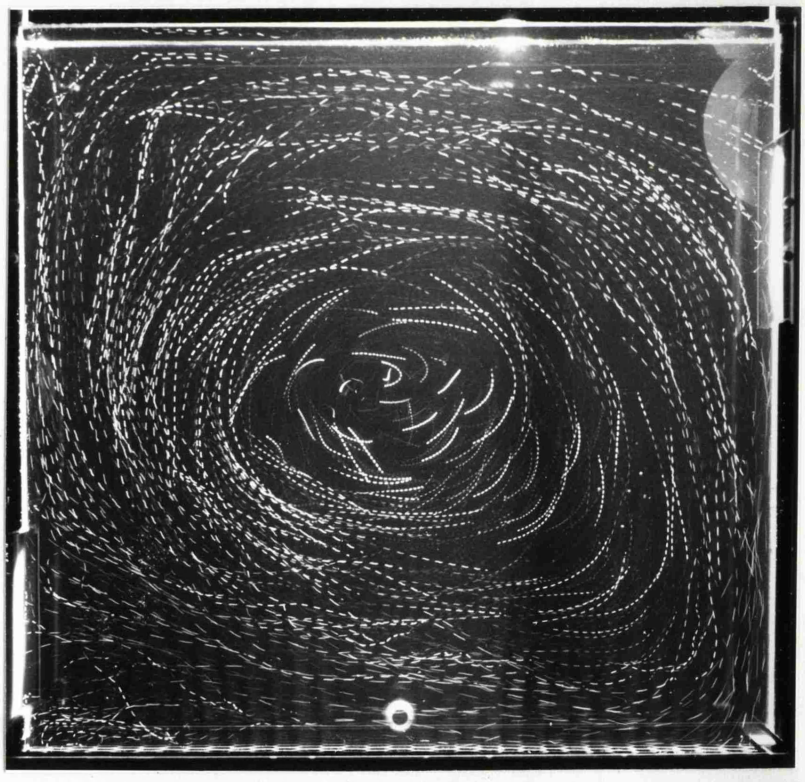

(b)

Fig. 8.8 Examples of photographs of the flow patterns obtained by stroboscopic photography. (a) the exposure time is short; (b) exposure time is long.

(a)

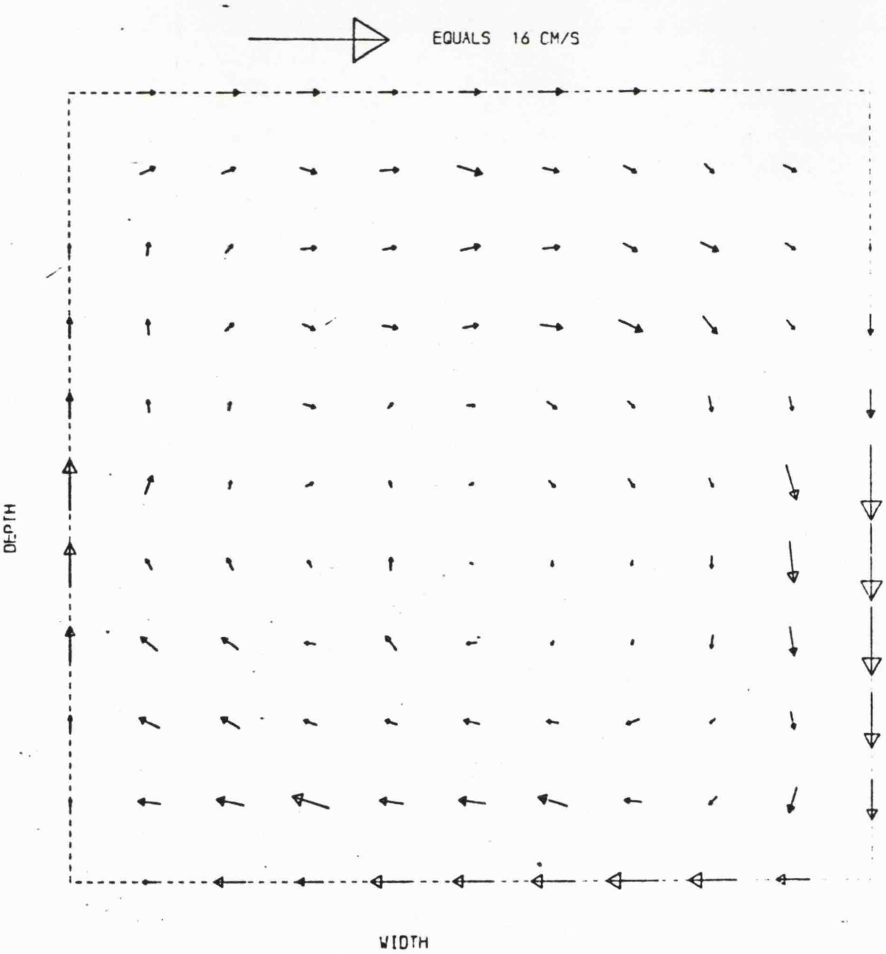

(b)

Fig. 8.9 Circulation flow pattern for experimental condition number 1; (a) the photgraph of flow pattern; (b) velocity vectors deduced from photograph in (a)

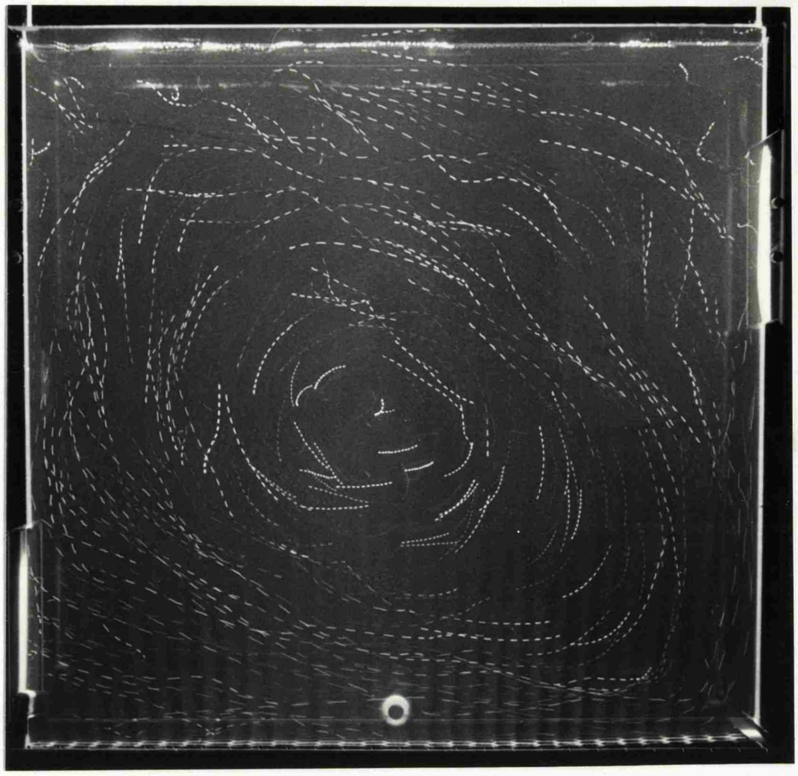

(a)

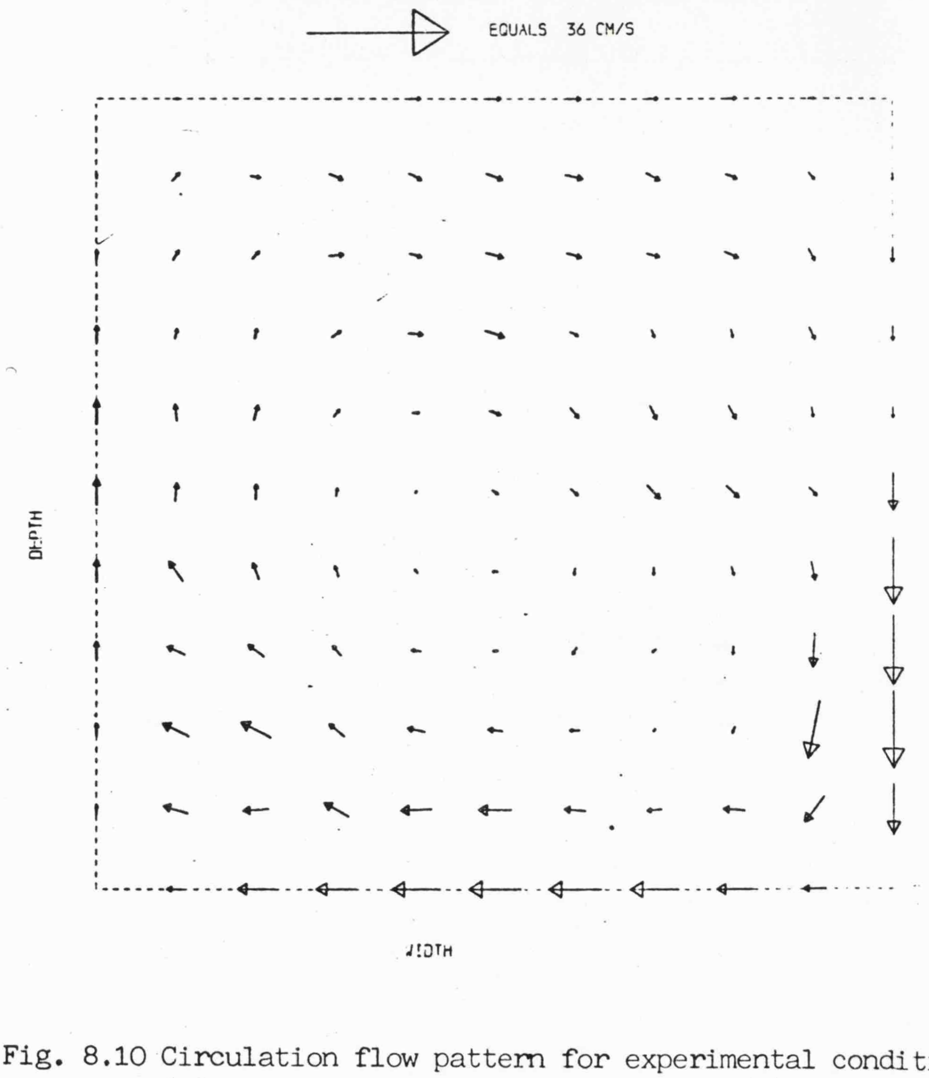

(b)

Fig. 8.10 Circulation flow pattern for experimental condition number 2.
(a) the photograph of flow pattern; (b) velocity vectors deduced from photograph in (a)

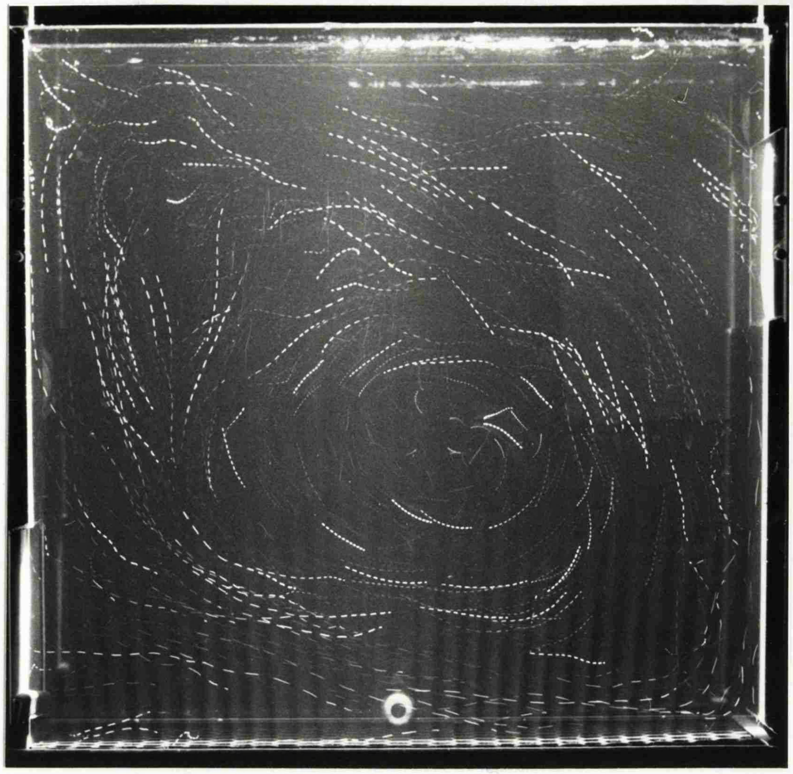

(a)

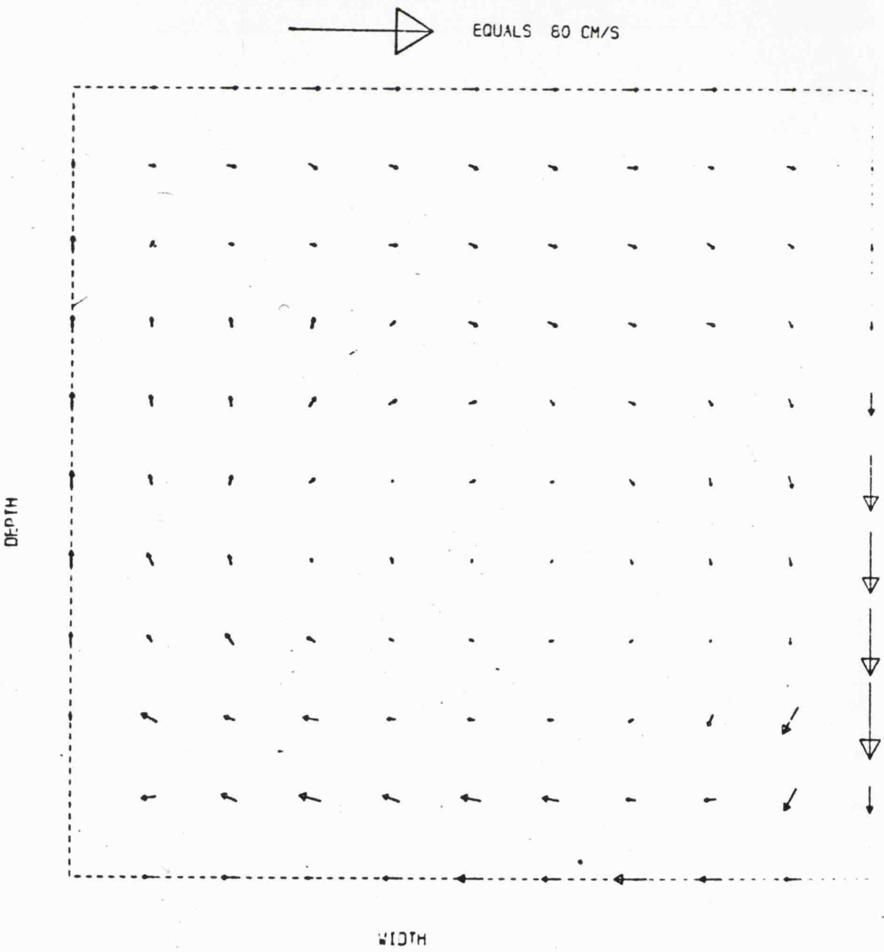

(b)

Fig. 8.11 Circulation flow pattern for experimental condition number 3. (a) the photograph of flow pattern; (b) velocity vectors deduced from photograph in (a)

(a)

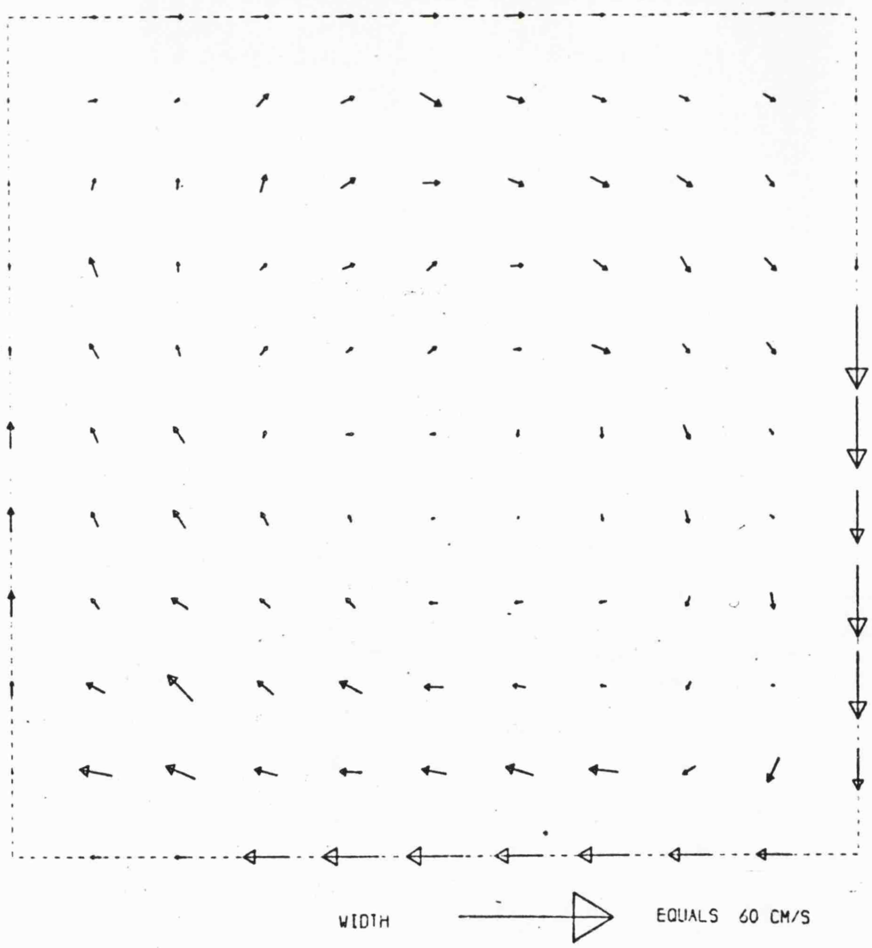

(b)

Fig. 8.12 Circulation flow pattern for experimental condition number 4. (a) the photograph of flow pattern; (b) velocity vectors deduced from photograph in (a)

Table 8.2

Summary of Results of Particle Settling Experiment

Experimental condition No.	1	2	3	4
Belt speed (Variac setting) Right Left	 105 102	 115 105	 120 105	 125 104
Av. max. upwelling velocity (W_u) cm/s	4.0	7.0	8.3	13.0
Av. max. downwelling velocity (W_d) cm/s	11.5	16.7	40.0	32.0
Flow pattern and velocity	Fig.8.9	Fig.8.10	Fig.8.11	Fig.8.12
Particles: diameter μm ≈ fall speed (W_T) cm/s	500 0.5	500 0.5	500 0.5	500 0.5
Centre of rotation: x^* y^*	0.55 0.45	0.55 0.45	0.55 0.45	0.55 0.55
W_u/W_d	0.34	0.42	0.21	0.40
W_T/W_u	0.12	0.07	0.06	0.04
Original mass of particle at t = o) (grams)	5.0	5.0	5.0	5.0
Total sinking loss at t = 9.5 min. (grams)	3.993	3.971	3.971	4.111

Note Dimensions of experimental cell:

0.38 m (height) x 0.41 m (length) x 0.15 m (width)

$$\frac{\lambda_c}{D} \simeq 2.0 .$$

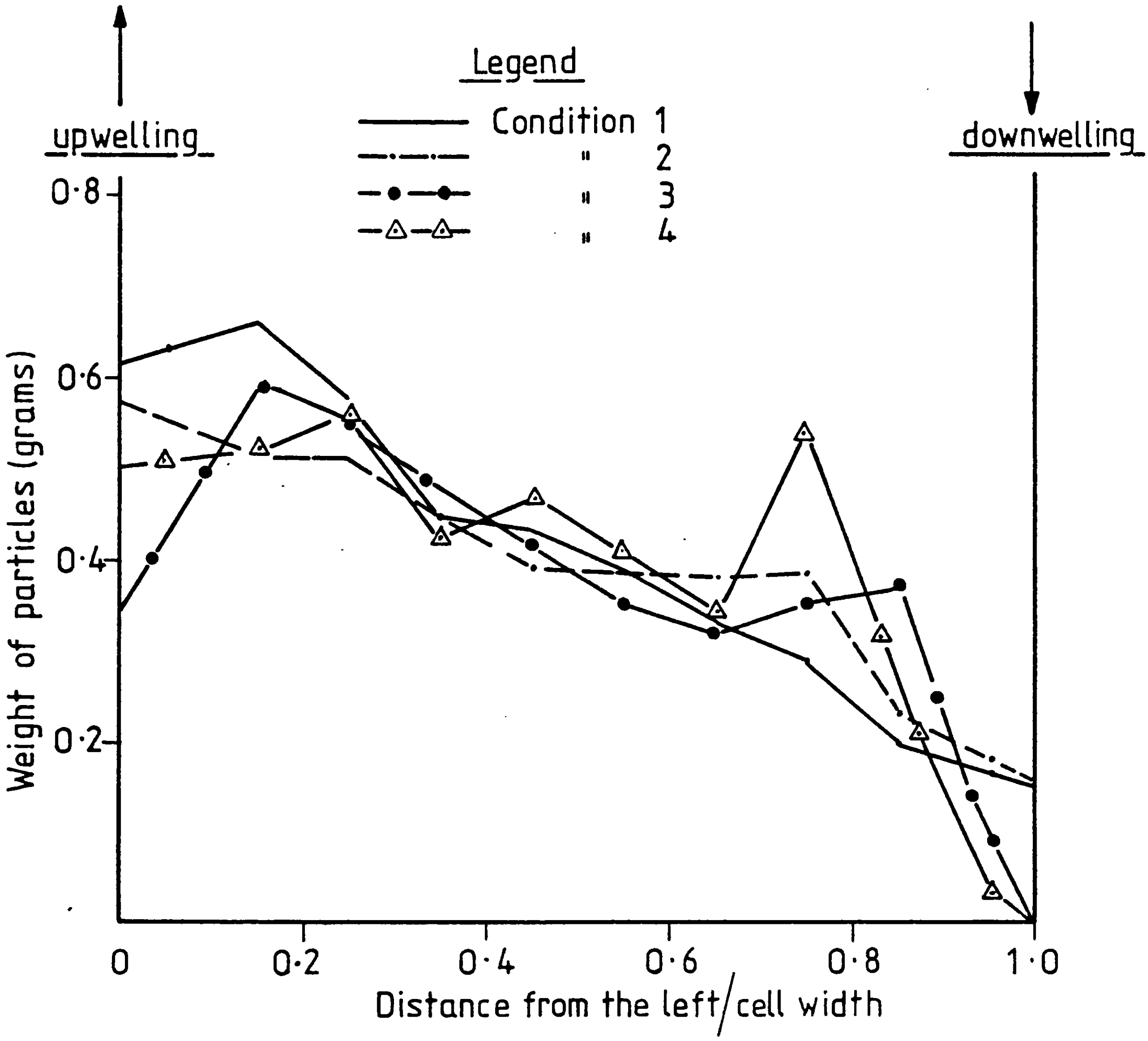

Fig. 8·13 Distribution of particle sinking losses across the cell width in various experimental conditions at time 9·50min from beginning, original weight = 5·0 grams.

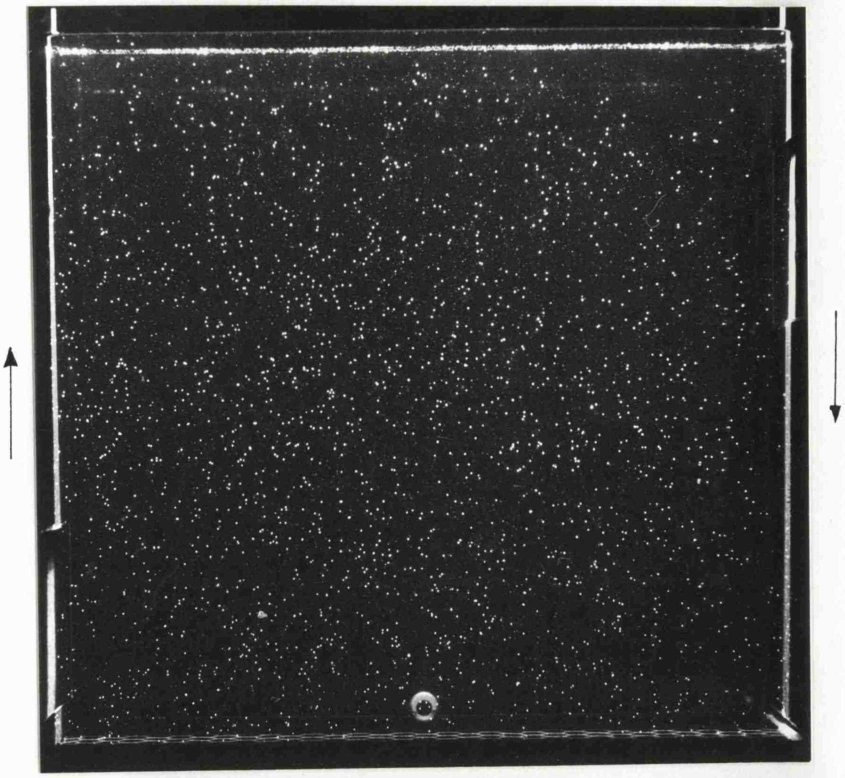

(a)

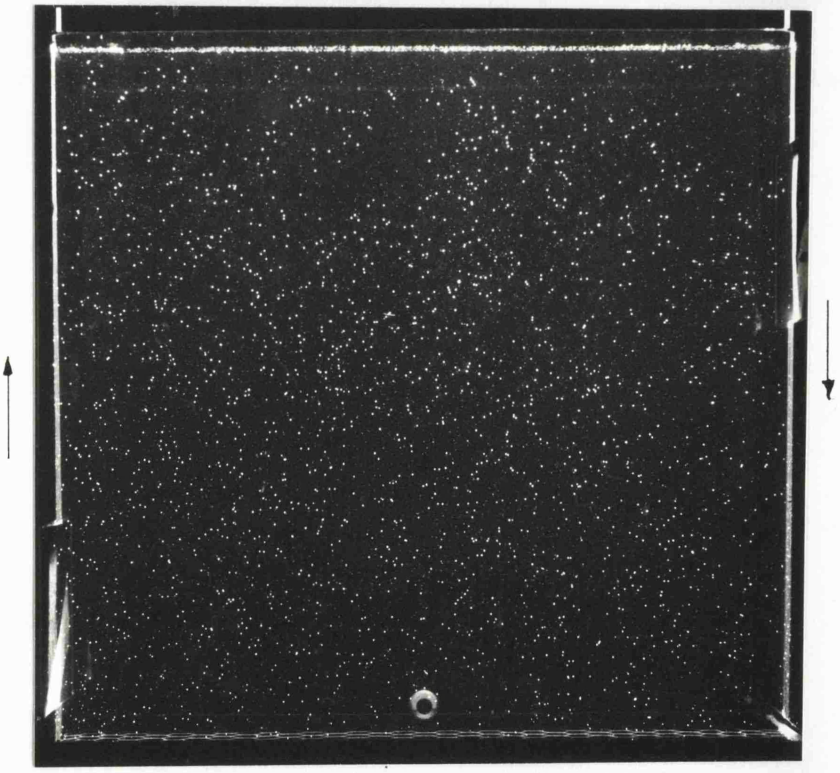

(b)

Fig. 8.14 An example of the relative distribution of particles in the particle settling tank deduced from photographs for experimental condition No. 3. (a) and (b) are photographs taken at about 3.0 minutes after the start of the experiment, at 4 seconds apart; (c) the average particle counts for 10x10 uniform grid after being corrected for unequal light beam width; and (d) the contour of relative particle distribution obtained from (c), units on the contours are arbitrary.

PARTICLE DISTRIBUTION

Values averaged from particle counts in **Photograph Numbers** J6(1)-8 and J6(1)-7 , and being corrected for unequal widths of illumination between top and bottom of the tank.

	i = 1	2	3	4	5	6	7	8	9	10
j = 1	9.5	14.5	9.0	13.5	7.5	12.0	8.5	5.5	2.5	1.0
2	22.0	15.0	19.3	13.2	8.9	13.2	19.3	15.0	12.2	6.1
3	14.1	15.0	18.5	15.4	18.0	19.4	13.6	11.9	11.0	7.5
4	20.7	19.5	20.0	21.2	23.2	20.3	14.5	14.1	11.6	13.7
5	24.2	19.5	23.0	29.0	23.0	23.0	17.9	18.7	13.2	8.6
6	24.4	18.1	20.8	20.7	13.7	14.1	19.6	18.5	15.2	11.1
7	18.1	16.3	18.1	19.2	16.3	16.0	15.3	17.4	16.3	7.4
8	13.4	17.1	17.7	16.4	20.4	17.1	16.4	16.4	17.7	9.4
9	14.4	12.2	18.8	15.4	12.8	18.2	13.1	14.1	13.4	10.2
10	16.7	15.5	15.5	16.7	11.2	12.7	13.3	12.4	11.8	7.1

8.14(c)

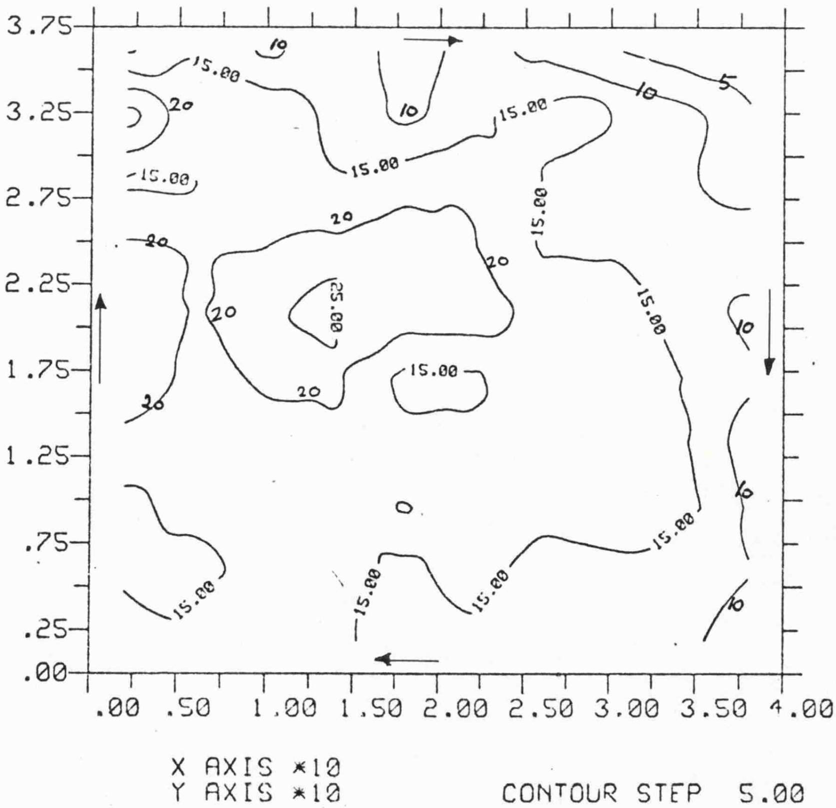

8.14(d)

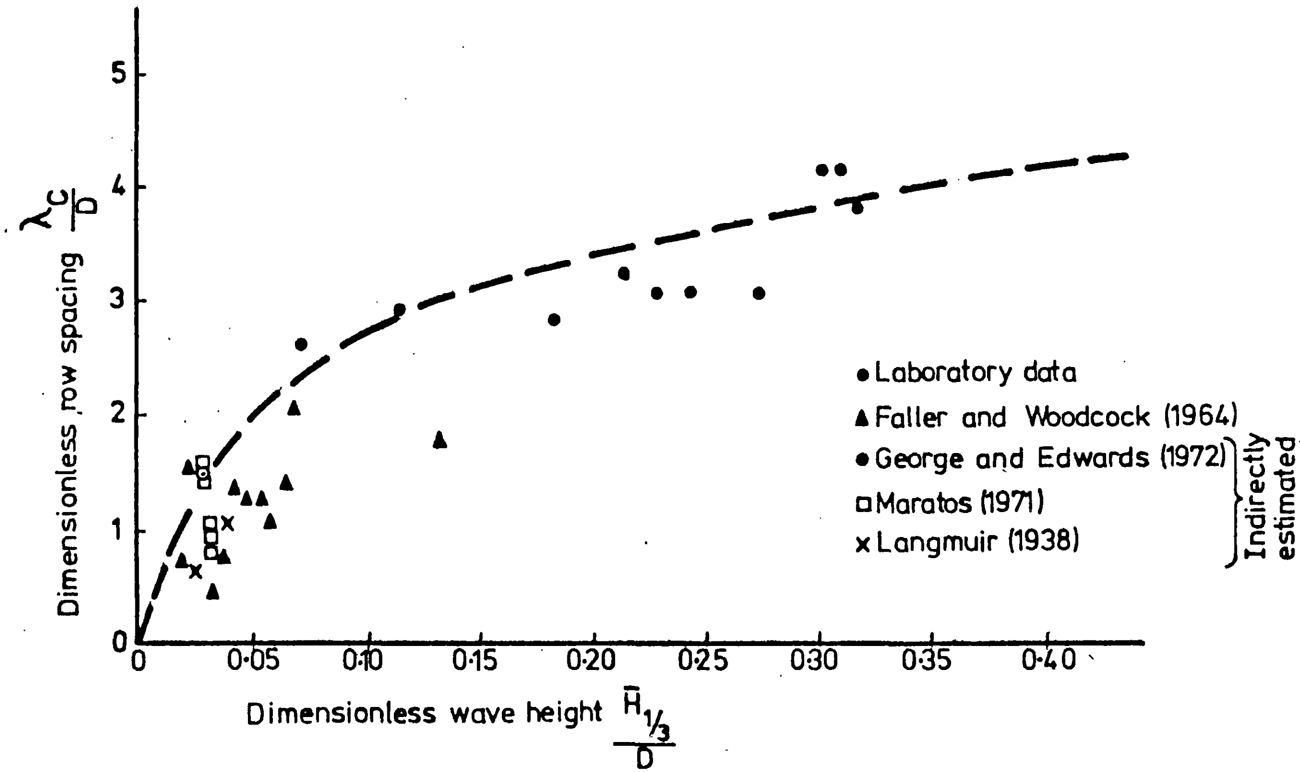

Fig 8·15 Correlations between row spacing and significant wave heights.

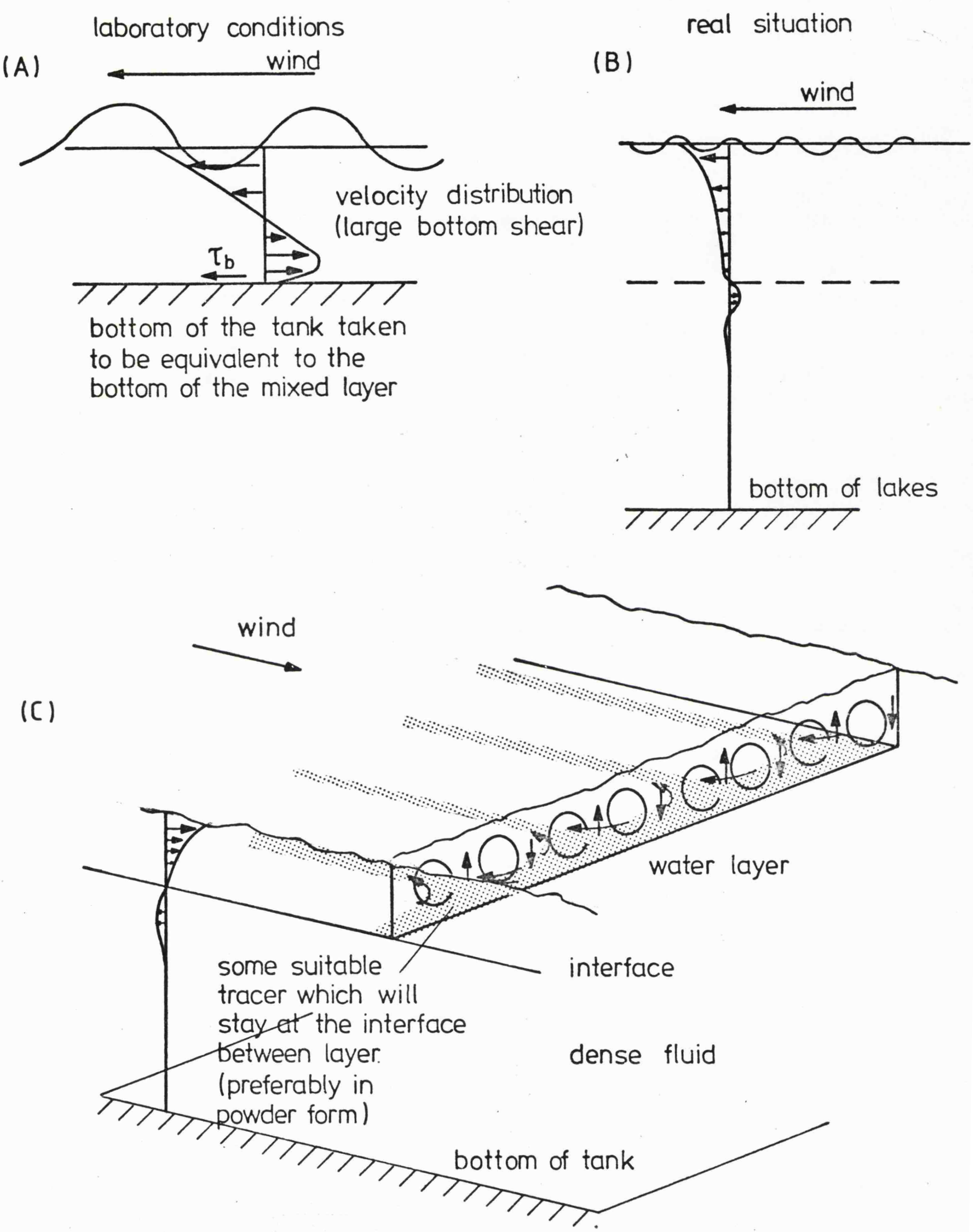

Fig. 8.16 (a) and (b) Waves and vertical velocity profiles in a wind wave tank and in a lake. (c) Schematic diagram of a recommended wind-wave tank, using two layers of fluids of different densities with tracer or dye introduced at at the interface to represent closer to real situations.

SOME EFFECTS OF LANGMUIR CIRCULATION ON SUSPENDED PARTICLES IN LAKES AND RESERVOIRS

CHAPTER 9 RELEVANCE OF LANGMUIR CIRCULATION TO WATER QUALITY PROBLEMS

The relevance of the basic findings of the present study to water quality problems, especially in the modelling of algal population in the mixed layer of lakes and reservoirs, is discussed. Suggestions for further work are outlined.

CHAPTER 9 RELEVANCE OF LANGMUIR CIRCULATION TO WATER QUALITY PROBLEMS

9.1. Water Quality Models

Accurate prediction of changes of algal population and suspended matter in the mixed layer is important in the management of water quality in lakes and reservoirs. Two types of mathematical model have been commonly used for quantitative predictions. These are the one-dimensional model in which the variations of the quantity in the vertical direction are described, and the zero-dimensional well-mixed compartment model, in which the constituents in the epilimnion are regarded as being uniformly distributed at all times. In these models the changes in suspended matter are considered to result from sinking and turbulence, and, if the constituent is algae, the changes due to biological processes such as photosynthesis, respiration, etc., are also included. The effect of large-scale water currents, such as the Langmuir circulation, which could carry suspended particles throughout the mixed layer depth in a circulating motion and thus alter the net settling of particles from a given location, are not accounted for in these models. Baca et al. (1974) have shown that their one-dimensional water quality model is particularly sensitive to the value of sinking speed of algae. Thus there is a need to specify more accurately the settling rates of algae in the mixed layer if reliable and realistic predictions of the algal population are to be obtained. In view of the manner in which Langmuir circulation readily forms in lakes when the wind speed exceeds 3 m/s , a common occurrence, the significance, or otherwise, of the effect of this circulation on the settling rates of algae and other suspended particles are required to be ascertained quantitatively. This constitutes the principal aim of the present study.

9.2. Significance of Langmuir Circulation to the Settling of Algae and other Particles

9.2.1. Summary of Relevant Results

Langmuir circulation has been shown (Chapter 7) to affect particle distribution within it and the extent of the effect is dependent upon the dimensionless sinking (fall) speed of the particle W_T^* , cell spacing-to-depth ratio λ_c^* , and dimensionless time t^* . As a rough rule, it has been found that for the dimensionless sinking speed $W_T^* \lesssim 1 \times 10^{-5}$, i.e. particles with small settling velocity in a strong circulating current, Langmuir circulation produces essentially uniform particle distribution over the cell, regardless of the cell size (λ_c^*) and time (t^*) . For $W_T^* > 1 \times 10^{-5}$ up to 1×10^{-3} (the maximum value used), a varying degree of particle aggregation occurs in the Langmuir cell, depending on the dimensionless cell size λ_c^* and dimensionless time t^* . Comparisons between the predictions by the two-dimensional (Langmuir cell) model, the one-dimensional model, and the zero-dimensional model, of the total quantity of particles remaining in the mixed layer at the end of various times (see section 7.4), show clearly that the one-dimensional model always gives an underestimation while the zero-dimensional model only underestimates the particle quantity when W_T^* is greater than 1×10^{-5} . This indicates that, when Langmuir circulation is present, the settling speeds in the one-dimensional model and the zero-dimensional model (when $W_T^* > 1 \times 10^{-5}$) must be smaller than the conventionally used values.

In order to avoid gross error in the prediction of the suspended particles in the mixed layer, effective sinking speeds must be used, which are defined as the net sinking speeds in the conventional models which give equivalent particle distribution profiles and sinking losses as those in the Langmuir cell (see section 7.5). Based on the numerically simulated data of the particle distribution in the Langmuir cell, the variations of the effective sinking speeds with dimensionless cell size λ_c^*, dimensionless sinking speed W_T^*, and dimensionless time t^* are illustrated for the zero-dimensional model in Figs. 7.10, 7.11, 7.12, and 7.12a. A percentage reduction in the sinking speed as large as 63% is obtained for $\lambda_c^* = 2.5$ and $W_T^* = 1 \times 10^{-3}$, whereas for $W_T^* = 1 \times 10^{-4}$, the reduction falls to about 10% (c.f. Fig.7.12).

The effective sinking speeds for the one-dimensional model are illustrated as functions of dimensionless time t^* and dimensionless depth z^* for the cases of $\lambda_c^* = 2.0$ and $W_T^* = 1 \times 10^{-3}$ and 1×10^{-5}, respectively, in Figs. 7.14 and 7.15. In these cases, the variations of the effective sinking speeds are complicated especially during the early transient period ($t^* \leq 6000$), making them cumbersome to apply in practice. To simplify the picture, these effective speeds are averaged throughout the simulation period and presented as a function of W_T^* for the case of $\lambda_c^* = 2.0$ in Fig.9.1. In general, the effective sinking speed decreases with depth to a short distance below the water surface and then increases with depth to the still water value at the lower boundary of the mixed layer. Since essentially uniform distribution results when $W_T^* \leq 1 \times 10^{-5}$, in this case the effective sinking speed (W_{eff}) may be equally well defined by the linear increase from zero at the lake surface to the terminal fall speed (W_T) at the lower boundary, i.e.

$$W_{eff}(z) = \left(\frac{z}{D}\right) \cdot W_T \qquad (9.1)$$

in which z = depth from the lake surface; D = depth of the mixed layer.

9.2.2. Langmuir Circulation Effect on Algal Particles

The above discussion applies in general for suspended particles with varying sinking speeds approximately in the range of 1 m/day to 200 m/day under the wind speed of 3 m/s to about 10 m/s , which should cover most conditions in lakes, the heavy sinking speeds belonging to the coarse sediment particles. Before discussing the implication of Langmuir circulation effect on algal particles, it should be noted that there are basically two types of simulation models concerning the prediction of algal population dynamics and patterns of productivity. The first type of model, exemplified by those of Chen and Orlob (1972), Male (1973), and Tang (1975), treats the phytoplankton as a single unit, without regard to differences among species. The other type of model, e.g. Rutherford (1976a), attempts to simulate the seasonal periodicity in individual species in relation to the succession of algal species and the magnitude of algal bloom. In this type, several species of algae are considered and each is characterised with species-specific sinking speeds and other biological parameters.

Values of sinking rates of some freshwater phytoplankton have been published in the literature (Hutchinson, 1967; Titman and Kilham, 1976; Lund, 1959). From these published data, a range of values may be established in which for healthy cells of the phytoplankton, the sinking rates lie between 2.1 to 0.0 m/day , and for senescent cells, between 7.0 to 0.0 m/day . It is also noted from several simulation models of the first type that the maximum value of the sinking rate used is about 1.0 m/day . Based on these values and the minimal wind speed of 3 m/s , the maximum value of the non-dimensional sinking speed for the growing cells would be 8.7×10^{-6} and, for the senescent cells is 2.7×10^{-5} . Therefore it can be concluded that for most phytoplankton in freshwater the value of W_T^* is far less than 1×10^{-5} under the wind speed which can create Langmuir circulation. In such cases, Langmuir circulation is strong, creating essentially uniform distribution of particles throughout the cell regardless of the value of Langmuir cell size (λ_c^*). There is therefore no need to correct the sinking loss term in the zero-dimensional model. However, in the one-dimensional model, effective sinking speeds must be used to give uniform distribution and these speeds may be estimated from equation (9.1).

For the water quality models which simulate several algal species, some of the algal species may have higher sinking rates, for instance the diatoms, whose sinking speeds may be as high as 18.0 m/day for the growing cells, and higher for the senescent cells. Using these sinking speeds and a wind of 3 m/s, W_T^* is about 7.0×10^{-5}, when some aggregation of particles occurs in the Langmuir cell and, hence, correction to the sinking loss terms in both models will need to be made. Reduction to the sinking loss as high as 6% can occur in the zero-dimensional model, while in the one-dimensional model, further reduction in the effective sinking speeds is evident from Fig.9.1. Even a small percentage of particles, retained in the mixed layer, may be significant to the total population since the retained algae will be continually swept in and out of the euphotic zone, where growth by photosynthesis is active, giving rise to some significant increase in population over long time durations.

9.2.3. Effect on Other Particulate Matter

Apart from algal particles, other particulate matter and organisms, such as the sediment particles, zooplankton, detritus or dead cells, are similarly affected by Langmuir circulation. Because the dead cells will settle slower there will be a greater opportunity for them to be decomposed by bacteria thereby releasing their nutrient contents to the epilimnion and stimulating further growth potential to the algae. The reduction in the net settling of sediment particles not only affects turbidity in water, which is related to growth of algae, but may have relevance to the sedimentation process in the lake or reservoir as well. Retained sediment caused by the Langmuir circulation will be carried further by the surface current and deposit over larger distance downwind from the point of entry. However, the distribution of zooplankton is expected to be different from that of the inert particles because of their ability to swim and orientate themselves according to light intensity and Langmuir circulation currents, hence the effective sinking speed concept is not applicable to these organisms.

9.3. Model Limitations

The foregoing discussions are based on the computed particle distribution in a Langmuir cell obtained from a two-dimensional advection-diffusion equation, in which suspended particles are treated as being passive contaminants to turbulent flow. In the present study Langmuir circulation is assumed to occur in stratified lakes. In shallow lakes where the cells extend to the bed, no re-suspension of particles back into the main flow has been assumed to occur (i.e. no scouring). The most severe limitation to the model is the necessarily empirical nature of the circulation flow field. However, at the present state of knowledge, in which no well-proven theoretical model exists, it represents the best available information. The structure of the model is basically sound, being based on the two-dimensional advection-diffusion mass transport equation, but it relies on the appropriate description of advective flow field and turbulent diffusion parameters. The subprocess models, e.g. the Langmuir circulating flow, turbulent diffusion, and particle sinking, have been separately considered and selected on their merit in their individual processes. Once inter-related, the combined model has been shown to provide some quantitative assessment and insight into the effect of the circulating flow in the Langmuir cells on the distribution and settling of suspended particles, especially the algal particles, the most important constituent affecting lake and reservoir water quality. Although field and experimental data are unavailable for verification, this analytical study demonstrates that Langmuir circulation effects on the settling characteristics of suspended particles and algae, which have been ignored by most modellers, demand a more careful evaluation before accurate prediction can be anticipated from the conventional water quality models.

9.4. Suggestions for Further Work

1. Verification of the model predictions of particle distribution is clearly required. This entails simultaneous measurement of the concentration of some labelled particles of known sinking speed, at sufficient points in a Langmuir cell after it has been formed for some time in a lake. Wind speeds must be recorded as well as the size of the Langmuir cell (i.e. the width and depth). A number of these measurements at successive time intervals would be required. At the present stage of experimental technique this would be a sophisticated and demanding study.

2. The importance of Langmuir circulation in causing algal aggregation can also be investigated quantitatively by making surface fluorescence profiles perpendicularly and in parallel to the wind direction at a time when the Langmuir circulation has been clearly observed. Such a measurement cannot differentiate between algal species.

3. The model prediction depends on the reliability of the input. Attempts should be made to obtain more detailed information on both the velocity field and the turbulent diffusion field associated with Langmuir circulation. This requires both the development of a technique and suitable instrumentation, such as remotely-controlled hot-film anemometer. Having established the velocity field, the method of interpretation of results in terms of turbulent diffusion coefficients is of real significance.

4. In view of extreme difficulties in making field measurements to assess the effect of Langmuir circulation on the distribution and settling of particles, laboratory experiments conducted in a circulating flow tank provide an alternative way of gaining useful information. In terms of the ability to regulate the parameters associated with the particles and the circulating flow, such experiments are much more readily performed in the laboratory than in the natural environment. In order to produce turbulent flow, it would be necessary to increase the tank size, say, to about 3.0 m depth and the belt speed to about 1 m/s .

5. More accurate and extensive measurements on the scale of motion of Langmuir circulation in both laboratory and natural environment are certainly required in order to further substantiate the empirical relationship between the cell spacing-to-depth ratio (λ_c/D) and the dimensionless significant wave height $(H_{1/3}/D)$, given in Fig.8.6.

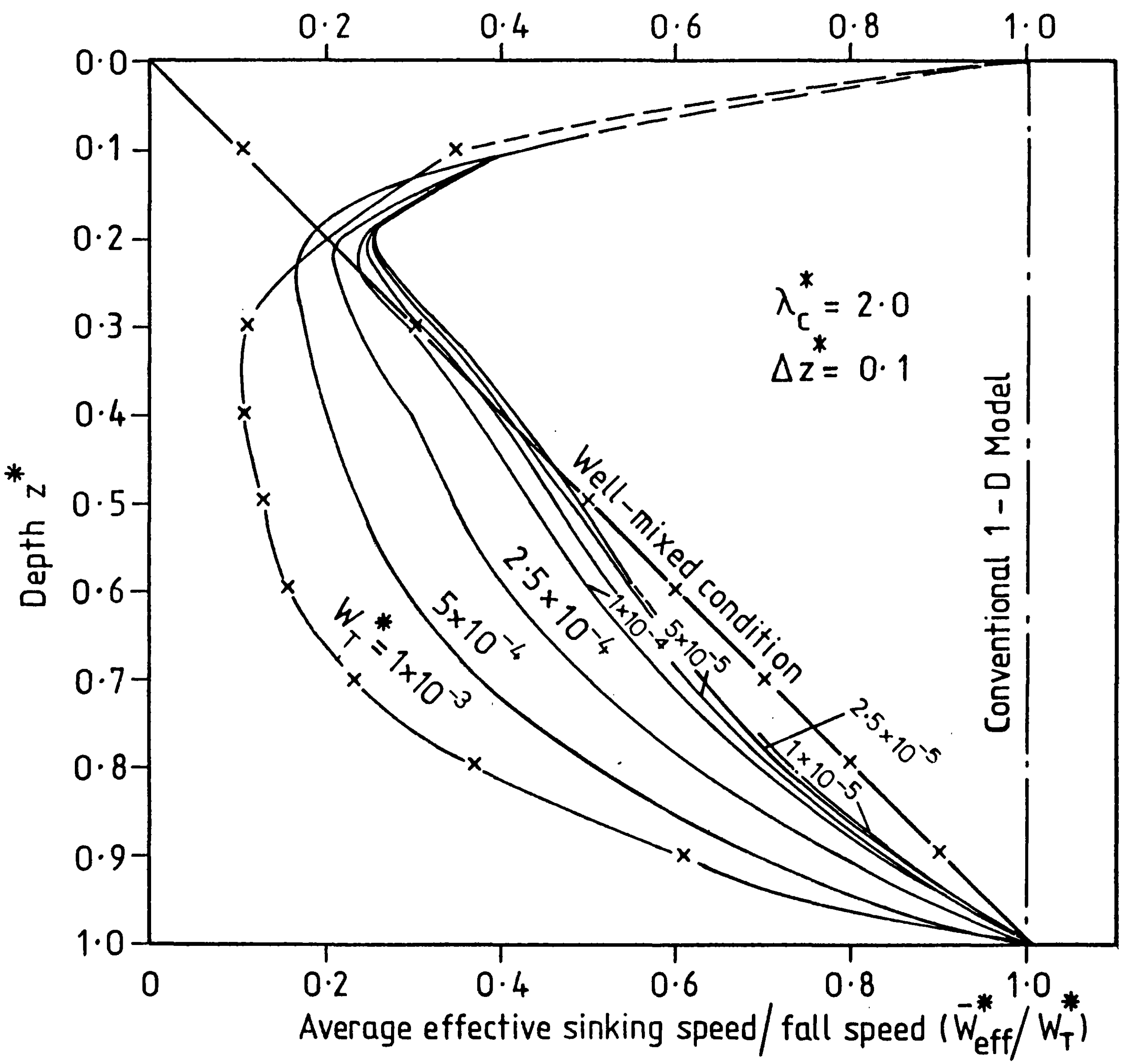

Fig. 9·1 Variations of average effective sinking speeds in the 1 – D model, where row spacing/depth (λ^*_c) = 2·0 and depth interval ΔZ^* = 0·1 for different values of sinking speeds.

CONCLUSIONS

1. Langmuir circulation affects particle distribution and hence sinking loss from the mixed layer, the extent of this effect depending primarily upon the dimensionless sinking speed W_T^* and the ratio of cell spacing-to-depth λ_c^*. (Sections 7.2 to 7.5)

2. When the dimensionless time is about $t^* = 6000$, an equilibrium exists between the relative distribution of particles in a Langmuir cell, in which there is a balance between the sinking loss and the advective and turbulent tranfers of particles. (Section 7.2)

3. When the dimensionless sinking speed W_T^* is less than or equal $1\text{x}10^{-5}$, the effect of the circulating flow and turbulence being large compared with the settling velocity, the particle distribution is essentially uniform throughout the Langmuir cell and is independent of the dimensionless cell size λ_c^* and dimensionless time t^*. When $W_T^* > 1\text{x}10^{-5}$ aggregation of particles results, with particles being concentrated in the central and upwelling regions. This effect becomes more pronounced as W_T^* and λ_c^* increase but approches the uniformly distributed condition as the dimensionless cell size λ_c^* and/or the dimensionless sinking speed W_T^* decrease. (Section 7.2)

4. Comparisons of suspended particle prediction by the conventional one-dimensional model and the zero-dimensional model on the one hand with the two-dimensional model on the other show that the one-dimensional model consistently predicts larger sinking losses for all values of W_T^* and λ_c^* while the zero-dimensional model gives larger sinking losses when W_T^* is greater than $1\text{x}10^{-5}$. If $W_T^* \leq 1\text{x}10^{-5}$, the prediction by the zero-dimensional model is identical to that of the two-dimensional model. The settling speeds used in both the one-dimensional model and the zero-dimensional model (when $W_T^* > 1\text{x}10^{-5}$) must be reduced in order to produce

the distribution profile and sinking losses observed when Langmuir circulation is present. (Section 7.4)

5. The effect of Langmuir circulation on particle suspension may be incorporated into the conventional models by utilising the effective sinking speed in place of the terminal fall speed. Generally, the effective sinking speed is a function of W_T^*, λ_c^* , and t^*, and for the one-dimensional model, it is also a function of z^* . (Section 7.5)

6. In the zero-dimensional model, when the dimensionlesss particle sinking speed W_T^* is $\lessdot$ 1x10^{-5} the effective speed equal to the terminal fall speed of the particle. But when W_T^* is > 1x10^{-5} the effective is smaller than the terminal fall speed, specific values for a large cell spacing-to-depth ratio λ_c^* = 2.5 being some 90% of the terminal fall speed when W_T^* = 1x10^{-4} and some 37% when W_T^* is as large as 1x10^{-3}. (Section 7.5.1)

7. In the one-dimensional model, the effective sinking speed concept must be applied regardless of particle sinking speed. Its value is generally smaller near the lake surface, gradually increasing to the terminal fall velocity at the lower boundary of the mixed layer. For W_T^* $\lessdot$ 1x10^{-5} where uniform distribution of particle occurs, the effective sinking speed may be taken as increasing linearly from zero at the lake surface to the terminal fall speed at the lower boundary of the mixed layer. (Section 9.2.1)

8. Considering the range of sinking speeds for various freshwater algal cells, it is found that for phytoplankton W_T^* is (with some exceptions) less than 1x10^{-5}under nornal wind conditions in lakes and reservoirs, thus uniform distribution results in the Langmuir cell. No correction to the sinking speed is needed in the zero-dimensional model, but in the one-dimensional model a linear increase of effective sinking speed with depth

must be incorporated. (Sections 7.5.2 and 9.2.2)

9. The sinking speed of the diatom cells, which are much heavier than the phytoplankton, are reduced by as much as 6% as a consequence of the Langmuir circulation. Though small, this could cause a significant population increase. (Section 9.2.2)

10. The gross features of Langmuir circulation can be modelled in the laboratory provided that adequate similitude criteria are observed. In the wind-wave tank, laboratory results and few published field data suggest that the Langmuir cell (dimensionless) scale of motion (λ_c/D) is related to the (dimensionless) significant wave height ($H_{1/3}/D$) , and the effect of Froude number on the phenomenon is minimal. In the particle-settling tank, it would appear that significant results could be obtained if flow Reynolds number and particle Froude number similitude are observed. (Sections 8.3.1 and 8.3.2)

APPENDIX I

COMPUTER PROGRAM LISTING

The computer program for the computation of the particle distribution and settling in a Langmuir cell is included. Although the program has been written specifically for a 51 x 51 uniform grid system, the extension to include other numbers of grid points, non-uniform grid spacings, or variable diffusion coefficients is straightforward. The inputs to the program are:-

1. Number of mesh points in y- and z- directions (NY, and NZ) ;
2. Langmuir cell spacing-to-depth ratio (LAMBDA) ;
3. Dimensionless sinking speed of particles (WT) ;
4. Time interval to write vertical profile of particle (TSTEP) ;
5. Time step to be used in the integration by the ADI-CDS finite difference method (DT) ;
6. Maximum number of time step for the run (DNT) .

The graphical subroutine library GHOST, which is a common subroutine library available at many computer installations, is used throughout for graphical outputs.

A condensed flow diagram illustrating the major operations of the program is given.

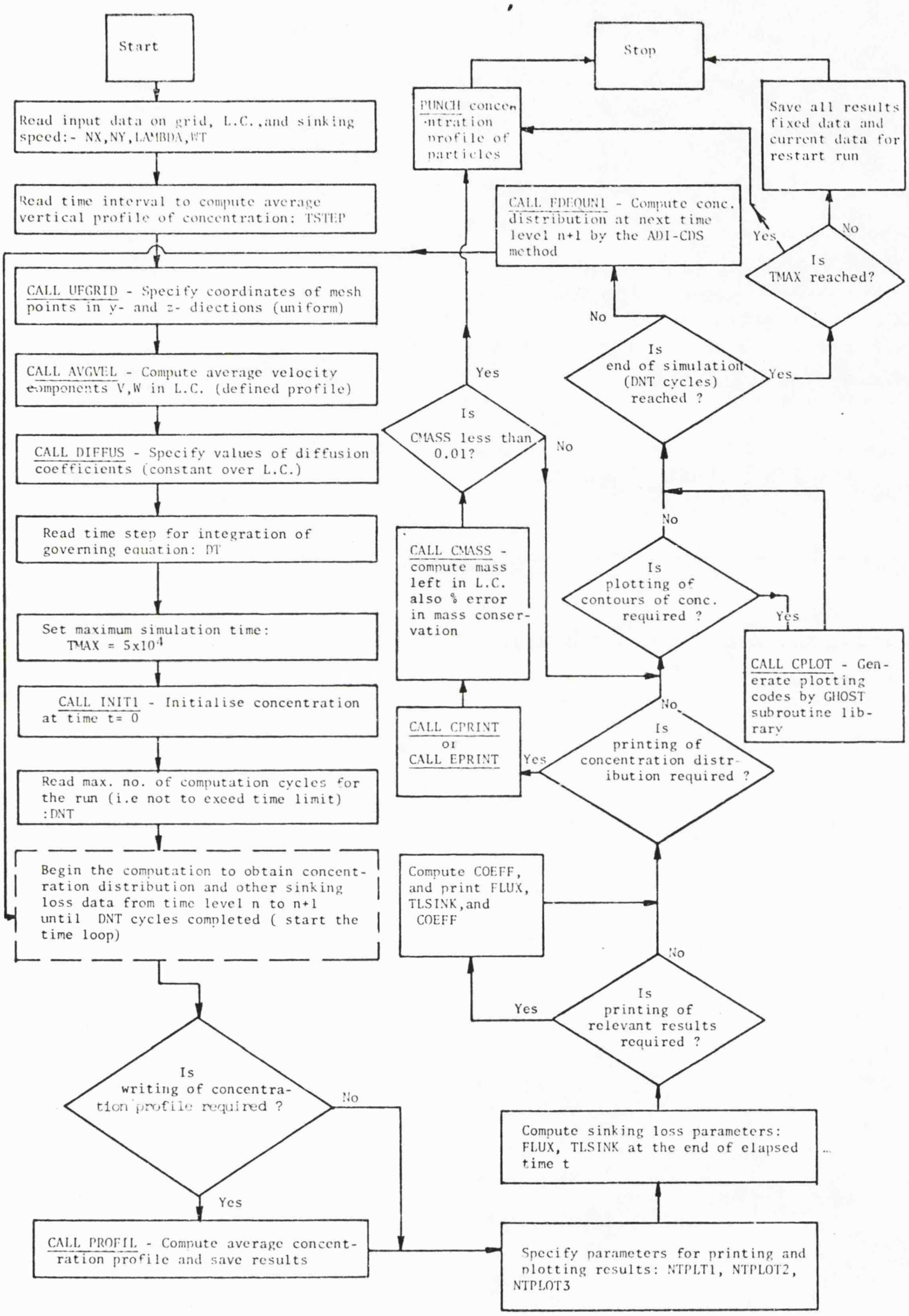

MAJOR STEPS IN THE COMPUTATIONS (IN THE MAIN PROGRAM)

```
      PROGRAM MAIN(INPUT,OUTPUT,TAPE3,TAPE4,TAPE10,TAPE11,TAPE1=INPUT,
     *TAPE2=OUTPUT)
      REAL LAMBDA
      INTEGER DNT
      DIMENSION V(50,50),W(50,50),C(50,50),CSTAR(50,50)
      DIMENSION F(51),Y(51),Z(51)
      COMMON V,W,C,CSTAR
      COMMON/PARA/F,Y,Z,NY,NZ,WT
      COMMON/CONST/ WO,PI,LAMBDA
C
C
C     PROGRAM I
C
C     PROGRAM TO CALCULATE TIME DISTRIBUTION OF PARTICLE
C     CONCENTRATION WITHIN A LANGMUIR CIRCULATION AND PARTICLE
C     SINKING LOSS FROM IT FOR A GIVEN PARTICLE SINKING SPEED
C     (WT), LANGMUIR CIRCULATION SIZE (LAMBDA), AND GRID
C     DISCRETISATION (NY,NZ)
C
C
C     WRITE A DATA AT THE BEGINNING OF FILES TO START THE FILES
C
      ITEST=100
      WRITE(2,1979) ITEST
 1979 FORMAT(1H1/1X,I5)
      WRITE(3) ITEST
      WRITE(4) ITEST
      WRITE(10) ITEST
      WRITE(11,900) ITEST
  900 FORMAT(1X,I5)
C
C     SWITCH ON PLOTTER AND SPECIFY MAXIMUM NUMBER OF FRAMES
C
      CALL PAPER(1)
      CALL GPSTOP(18)
C
C     READ GRIDS, SIZE OF LANGMUIR CELL, SINKING SPEED
C
      READ(1,1000) NY,NZ,LAMBDA,WT
 1000 FORMAT(2I3,F5.3,E10.4)
      WRITE(2,1100) NY,NZ,LAMBDA,WT
 1100 FORMAT(1H1/1H0,55X,15HDATA AND RESULTS/56X,16(1H*)/1H0,1X,3HNY=,
     *I3,3X,3HNZ=,I3,3X,21HWIDTH-TO-DEPTH RATIO=,F5.3,3X,14HSINKING SPEE
     *D=,E10.4)
C
C     READ TIME INTERVAL TO WRITE CONCENTRATION PROFILE ON FILE 11
C
      READ(1,1200) TSTEP
 1200 FORMAT(E11.4)
      WRITE(2,1300) TSTEP
 1300 FORMAT(1H0,7HTSTEP =,E11.4)
C
C     DEFINE CONSTANTS
C
      PI=4.0*ATAN(1.0)
      WO=0.85E-2
C
C     SPECIFY COORDINATES OF GRIDS
C
      CALL UFGRID
C
C     COMPUTE AVERAGE VELOCITIES V AND W
C
      CALL AVGVEL
C
C     PRINT THE COMPUTED VELOCITIES
C
      II=(NY-1)/10
      JJ=II
      NNY=NY-1
      NNZ=NZ-1
      WRITE(2,2000)
 2000 FORMAT(1H0,20X,25HHORIZONTAL AVG FLOWS (V'S),/21X,26(1H*)//)
      NNY2=NY-2
      DO 10 J=1,NNZ,JJ
   10 WRITE(2,2001) J,(V(I,J),I=1,NNY2,II),V(NNY2,J)
 2001 FORMAT(3X,2HJ=,I3,3X,11(1PE11.3))
      WRITE(2,2002) (I,I=1,NNY2,II),NNY2
 2002 FORMAT(//11X,11(3X,2HI=,I3,3X))
      WRITE(2,2003)
 2003 FORMAT(1H0,20X,24HVERTICAL AVG FLOWS (W'S),/21X,24(1H*)//)


      DO 20 J=1,NNZ,JJ
   20 WRITE(2,2001) J,(W(I,J),I=1,NNY,II),W(NNY,J)
      WRITE(2,2002) (I,I=1,NNY,II),NNY
C
C     SPECIFY VALUES OF DIFFUSION COEFFICIENTS
C
      CALL DIFFUS
C
C     READ LENGTH OF TIME STEP
C
      READ(1,2004) DT
 2004 FORMAT(E10.4)
      TMAX=5.0E+4
      DTMIN=DT
      DELT=DT/2.
      NTMAX=TMAX/DT+1
      WRITE(2,5000) DTMIN,TMAX,NTMAX,DT
 5000 FORMAT(//1X,6HDTMIN=,E11.4,3X,5HTMAX=,E11.4,3X,6HNTMAX=,I6,3X,
     *3HDT=,E11.4//)
C
C     WRITE FIXED DATA IN FILE 3
C
      WRITE(3) WT,LAMBDA,NY,NZ,DT,NTMAX
      WRITE(3) (Y(I),I=1,NY)
      WRITE(3) (Z(J),J=1,NZ)
      WRITE(3) (F(J),J=1,NZ)
      WRITE(3) ((V(I,J),I=1,NNY2),J=1,NNZ)
      WRITE(3) ((W(I,J),I=1,NNY),J=1,NNZ)
C
C     WRITE INITIAL DATA ON FILE 11
C
      WRITE(11,1400) WT,LAMBDA,TSTEP
 1400 FORMAT(1X,E11.4,1X,F6.3,1X,E11.4)
```

```
C
C     INITIALISE CONCENTRATION AT T= 0
C
      CALL INIT1
C
C     COMPUTE INITIAL MASS IN L.C.
C
      CALL MASS(CMASS)
      CMASS0=CMASS
      WRITE(3) CMASS0
      WRITE(2,6500) CMASS0
6500  FORMAT(1H0,35HORIGINAL MASS OF PARTICLES IN L.C. =,1PE11.3)
C
C     INITIALISE TOTAL MASS OF PARTICLE IN L.C. AT T= 0
C
      TLSINK=0.0
C
C     READ MAXIMUM NUMBER OF COMPUTATION CYCLES FOR THIS RUN
C
      READ(1,4004) DNT
4004  FORMAT(I6)
      WRITE(2,4005) DNT
4005  FORMAT(/1X,6H DNT =,I6/1H1)
C
C     INITIALISE COUNTING INDICES FOR RESULTS TO BE WRITTEN ON
C     FILES 4 AND 11, AND NUMBERING OF CONTOUR PLOTS
C
      ICOUNT=0
      NUMBER=1
      KCOUNT=1
C
C     COMPUTE PARTICLE FLUX, TOTAL SINKING LOSS, AND CORRECTION
C     COEFFICIENTS
C
      WRITE(2,4000)
4000  FORMAT(1X,12HTIME STEP(N),4X,9HTIME   (T),4X,21HMASS FLUX OF PARTIC
     *LE,3X,22HTOTAL MASS OF PARTICLE,4X,10HCORRECTION)
      WRITE(2,4001)
4001  FORMAT(1X,12(1H*),4X,9(1H*),6X,16HOUT OF L.C. / WT,6X,22HSINKING O
     *UT OF L.C./WT,3X,11HCOEFFICIENT/30X,21(1H*),3X,22(1H*),3X,11(1H*))
      WRITE(2,4003)
4003  FORMAT(1H0)
      NT1=1
      NT2=NT1+DNT
      IF(NT2.GE.NTMAX) NT2=NTMAX
C
C     SAVE COMPUTED RESULTS IN FILE 4
C


      WRITE(4) WT,LAMBDA,NY,NZ
C
C     COMPUTE INITIAL FLUX OF PARTICLE OUT OF L.C.
C
      FLUX=0.0
      IF(WT.LE.0.0) GOTO 78
      DO 77 I=1,NNY
      DYIJ=Y(I+1)-Y(I)
      DFLUX=C(I,NNZ)*DYIJ
   77 FLUX=FLUX+DFLUX
C
C     COMPUTE PARTICLE CONCENTRATION DISTRIBUTION
C
   78 DO 51 N=NT1,NT2
      NNN=N-1
      T=NNN*DT
C
C     TEST IF WRITING OF VERTICAL CONCENTRATION PROFILE REQUIRED
C
      ITIME=INT(T)
      ITSTEP=INT(TSTEP)
      IF(MOD(ITIME,ITSTEP).EQ.0) CALL PROFIL(T,NUMBER)
C
C     DEFINE INCREMENTS TO PRINT RESULTS
C
      IF(T.LE.1.0E+3) NPLOT1=10
      IF(T.LE.1.0E+3) NPLOT2=25
      IF(T.LE.1.0E+3) NPLOT3=50
      IF(T.GT.1.0E+3) NPLOT3=500
      IF(T.GT.1.0E+3.AND.T.LE.1.0E+4) NPLOT1=100
      IF(T.GT.1.0E+3.AND.T.LE.1.0E+4) NPLOT2=250
      IF(T.GT.1.0E+4) NPLOT1=500
      IF(T.GT.1.0E+4) NPLOT2=1250
C
C     BOOK-KEEPING TOTAL MASS OF PARTICLES SINKING OUT OF
C     L.C. AT END OF ELAPSED TIME T
C
      IF(N.EQ.NT1) GOTO 52
      DLOSS1=DLOSS2
      DLOSS2=FLUX
      TLSINK=TLSINK+0.5*DT*(DLOSS1+DLOSS2)
      GOTO 53
   52 DLOSS2=FLUX
C
C     TEST IF PRINTING OF RESULTS TO BE DONE
C
   53 IF(MOD(NNN,NPLOT1).NE.0) GOTO 54
      IF(N.EQ.1) CCOEF=1.0
      IF(N.NE.1) CCOEF=TLSINK/(CMASS0*T)
      WRITE(2,4002) N,T,FLUX,TLSINK,CCOEF
4002  FORMAT(4X,I6,6X,F11.4,10X,F7.2,15X,E11.4,12X,F7.3)
      WRITE(4) T,FLUX,CCOEF
      ICOUNT=ICOUNT+1
C
C     TEST IF PRINTING OF CONCENTRATION TO BE DONE
C
   54 IF(MOD(NNN,NPLOT2).NE.0) GOTO 70
      IF(WT.GT.0.) CALL CPRINT(N,T)
      IF(WT.LE.0) CALL FPRINT(N,T)
```

```
C
C      COMPUTE PARTICLE MASS CONSERVATION ERROR AT THE SAME TIME
C  -   TO PRINT CONCENTRATION DISTRIBUTION
C
       CALL MASS(CMASS)
       CERROR=(CMASS0-CMASS-TLSINK*WT)*100.0/CMASS0
       WRITE(2,4100) CMASS,CERROR
 4100  FORMAT(1H0,25X,33HPARTICLE MASS REMAINING IN L.C. =,F10.4,/21X,
      *39HERROR IN MASS CONSERVATION (PARTICLE) =,F10.4,2X,1H%,/)
C
C      TEST IF NO PARTICLES LEFT IN LANGMUIR CIRCULATION
C
       IF(CMASS.LT.0.01) GOTO 55
C
C      TEST IF PLOTTING OF CONCENTRATION DISTRIBUTION REQUIRED
C
   70  CONTINUE
       IF(MOD(NNN,NPLOT3).NE.0.OR.NNN.EQ.0) GOTO 71
       CALL CPLOT(T,KCOUNT)
       KCOUNT=KCOUNT+1
   71  CONTINUE
C


C      TEST IF END OF SIMULATION REACHED
C
       IF(N.EQ.NT2) GOTO 55
C
C      COMPUTE CONCENTRATION DISTRIBUTION
C
       CALL FDEQN1(DELT,FLUX)
   50  CONTINUE
   55  CONTINUE
C
       WRITE(2,6000) TCOUNT
 6000  FORMAT(1H1,56HNO. OF RESULTS BEING SAVED IN FILE TOBRES FROM THIS
      *RUN=,I6)
       IF(N.EQ.NTMAX) GOTO 62
C
       WRITE(10) WT,LAMBDA,NY,NZ
       WRITE(10) N,T,FLUX,TLSINK,CCOEF
       WRITE(10) KCOUNT
       WRITE(10) ((C(I,J),I=1,NNY),J=1,NNZ)
C
       WRITE(2,5700) N
 5700  FORMAT(1H1,5(1H*),63HCOMPUTATIONS INCOMPLETE, PROGRAM SAVES THE FO
      *LLOWING DATA AT N=,I6,5(1H*))
       WRITE(2,5800) N,T,FLUX,TLSINK,CCOEF
 5800  FORMAT(1H0,2HN=,I6,3X,2HT=,E11.4,3X,5HFLUX=,E11.4,3X,7HTLSINK=,
      *E11.4,3X,6HCCOEF=,F5.2)
       WRITE(2,5805) KCOUNT
 5805  FORMAT(1H0,1X,8HKCOUNT =,I6)
       IF(WT.GT.0.) CALL CPRINT(N,T)
       IF(WT.LE.0.) CALL EPRINT(N,T)
       GOTO 56
   62  WRITE(2,5600)
 5600  FORMAT(1H0,5(1H*),20HSIMULATION COMPLETED,5(1H*))
   56  CONTINUE
       CALL GREND
       STOP
       END

       SUBROUTINE AVGVEL
       REAL LAMBDA
       DIMENSION V(49,50),W(50,50),C(50,50),CSTAR(50,50)
       DIMENSION F(51),Y(51),Z(51)
       COMMON V,W,C,CSTAR
       COMMON/PARA/F,Y,Z,NY,NZ,WT
       COMMON/CONST/ W0,PI,LAMBDA
C-----------------------------------------------------------------------
C
C    SUBROUTINE TO COMPUTE AVERAGE HORIZONTAL VELOCITIES, V(I,J)'S,WHICH
C    WHICH ARE DEFINED ON THE R.H. FACES OF CONTROL VOLUME ELEMENTS,AND
C    AVERAGE VERTICAL VELOCITIES,W(I,J)'S, DEFINED AT THE BOTTOM FACES OF
C    THE ELEMENTS,OF SOLID  PARTICLES HAVING SINKING SPEED WT. THESE
C    VALUES ARE THEN STORED IN 2-D ARRAYS V AND W.
C
C-----------------------------------------------------------------------
C
C    START TO COMPUTE V'S ROW BY ROW FROM J=1 TO J=NZ-1
C
       DIVIDE=0.4*LAMBDA
       FACTOR=0.2*W0*LAMBDA/PI
       AA=1.25*PI/LAMBDA
       BB=5.0*PI/LAMBDA
       NNY1=NY-1
       NNY2=NY-2
       NNZ=NZ-1
       DO 1 J=1,NNZ
       Z1=Z(J+1)
       Z2=Z(J)
       DZIJ=Z1-Z2
       A=SIN(PI*Z1)-SIN(PI*Z2)
       DO 1 I=1,NNY2
       Y1=Y(I+1)
C
C    TEST IF Y IS IN THE REGION OF UPWELLING OR DOWNWELLING
C
       IF(Y1.LE.DIVIDE) B=SIN(AA*Y1)
       IF(Y1.GT.DIVIDE) B=SIN(2.5*PI-BB*Y1)
    1  V(I,J)=FACTOR*B*A/DZIJ
C
C    COMPUTE W'S COLUMN BY COLUMN FROM I=1 TO I=NY-1
C
       DO 2 I=1,NNY1
       Y1=Y(I+1)
       Y2=Y(I)
       DYIJ=Y1-Y2
       IF(Y1.LE.DIVIDE) A=SIN(AA*Y1)-SIN(AA*Y2)
       IF(Y2.GE.DIVIDE) A=SIN(2.5*PI-BB*Y1)-SIN(2.5*PI-BB*Y2)
       IF(Y1.GT.DIVIDE.AND.Y2.LT.DIVIDE) A=SIN(2.5*PI-BB*Y1)
      *-SIN(AA*Y2)
       DO 2 J=1,NNZ
       Z1=Z(J+1)
       B=SIN(PI*Z1)
    2  W(I,J)=-(FACTOR*B*A/DYIJ)+WT
       RETURN
       END
```

```
      SUBROUTINE DIFFUS
      DIMENSION F(51),Y(51),Z(51)
      COMMON/PARA/F,Y,Z,NY,NZ,NT
C-----------------------------------------------------------------------
C
C  TO COMPUTE THE VALUES OF VERTICAL COEFFICIENTS OF DIFFUSION BY A
C  SIMPLE EMPIRICAL RELATIONSHIP:-    ,
C
C          F=2.0E-5*WIND SPEED*DEPTH OF THE THERMOCLINE
C
C  THE COEFFICIENTS ARE ASSUMED TO BE CONSTANT IN THE MIXED LAYER.
C
C-----------------------------------------------------------------------
      DO 1 J=1,NZ
      F(J)=2.0E-5
    1 CONTINUE
      WRITE(2,100)
  100 FORMAT(1H0,22HDIFFUSION COEFFICIENTS/1X,22(1H*))
      WRITE(2,200) ((J,F(J)),J=1,NZ)
  200 FORMAT(3X,2HJ=,I6,5X,F11.4)
      RETURN
      END
```

```
      SUBROUTINE INIT1
      DIMENSION V(49,50),W(50,50),C(50,50),CSTAR(50,50)
      DIMENSION F(51),Y(51),Z(51)
      COMMON V,W,C,CSTAR
      COMMON/PARA/F,Y,Z,NY,NZ,NT
C-----------------------------------------------------------------------
C
C  TO INITIALISE CONCENTRATIONS AT ALL GRID POINTS TO A CONSTANT VALUE
C  OF 100.0
C
C
C-----------------------------------------------------------------------
      NNY=NY-1
      NNZ=NZ-1
      DO 1 J=1,NNZ
      DO 1 I=1,NNY
    1 C(I,J)=100.0
      RETURN
      END
```

```
      SUBROUTINE FDEQN1(DT,FLUX)
      DIMENSION V(49,50),W(50,50),C(50,50),CSTAR(50,50)
      DIMENSION E(51),Y(51),Z(51)
      DIMENSION B(51),G(51)
      COMMON V,W,C,CSTAR
      COMMON/PARA/E,Y,Z,NY,NZ,WT
C
C
C     SUBROUTINE TO COMPUTE CONCENTRATION DISTRIBUTION OF PARTICLES
C     IN L.C. AT TIME T+DT GIVEN INITIAL CONCENTRATION AT TIME T BY
C     ADI METHOD USING THOMAS ALGORITHM TO SOLVE TRIDUAGONAL SYSTEM OF
C     EQUATIONS
C
C
      NY1=NY-1
      NZ1=NZ-1
C
C     ROW CALCULATIONS (Y - SWEEP)
C
C     COMPUTE COEFFICIENTS AA,BB,CC,DD AND THEN B(I), G(I)
C
      DO 10 J=1,NZ1
      DZIJ=Z(J+1)-Z(J)
      F2=DT/DZIJ
      DO 20 I=1,NY1
      DYIJ=Y(I+1)-Y(I)
      EY=.5*(E(J+1)+E(J))
      F1=DT/DYIJ
      IF(I.EQ.1) GOTO 11
      IF(I.EQ.NY1) GOTO 12
      VE=V(I,J)
      VW=V(I-1,J)
      SE=(Y(I+1)-Y(I))/(Y(I+2)-Y(I))
      SW=(Y(I)-Y(I-1))/(Y(I+1)-Y(I-1))
      DYE=.5*(Y(I+2)-Y(I))
      DYW=.5*(Y(I+1)-Y(I-1))
      AA=F1*(-VW*(1.-SW)-EY/DYW)
      BB=1.+F1*(VE*(1.-SE)-VW*SW+EY/DYE+EY/DYW)
      BB=BB-AA*B(I-1)
      CC=F1*(VE*SE-EY/DYE)
      B(I)=CC/BB
      GOTO 13
   11 VE=V(I,J)
      SE=(Y(I+1)-Y(I))/(Y(I+2)-Y(I))
      DYE=.5*(Y(I+2)-Y(I))
      AA=0.
      BB=1.+F1*(VE*(1.-SE)+EY/DYE)
      CC=F1*(VE*SE-EY/DYE)
      B(I)=CC/BB
      GOTO 13
   12 VW=V(I-1,J)
      SW=(Y(I)-Y(I-1))/(Y(I+1)-Y(I-1))
      DYW=.5*(Y(I+1)-Y(I-1))
      AA=F1*(-VW*(1.-SW)-EY/DYW)
      BB=1.+F1*(-VW*SW+EY/DYW)
      BB=BB-AA*B(I-1)
      CC=0.
      B(I)=CC/BB
   13 IF(J.EQ.1) GOTO 14
      IF(J.EQ.NZ1) GOTO 15
      WS=W(I,J)
      WN=W(I,J-1)
      EZS=E(J+1)
      EZN=E(J)
      SS=(Z(J+1)-Z(J))/(Z(J+2)-Z(J))
      SN=(Z(J)-Z(J-1))/(Z(J+1)-Z(J-1))
      DZS=.5*(Z(J+2)-Z(J))
      DZN=.5*(Z(J+1)-Z(J-1))
      EE=C(I,J-1)*F2*(WN*(1.-SN)+EZN/DZN)
      FF=C(I,J)*(1.+F2*(-WS*(1.-SS)+WN*SN-EZS/DZS-EZN/DZN))
      GG=C(I,J+1)*F2*(-WS*SS+EZS/DZS)
      DD=EE+FF+GG
      GOTO 16
   14 WS=W(I,J)
      SS=(Z(J+1)-Z(J))/(Z(J+2)-Z(J))
      EZS=E(J+1)
      DZS=.5*(Z(J+2)-Z(J))
      EE=0.
      FF=C(I,J)*(1.+F2*(-WS*(1.-SS)-EZS/DZS))
      GG=C(I,J+1)*F2*(-WS*SS+EZS/DZS)
      DD=EE+FF+GG


      GOTO 16
   15 WN=W(I,J-1)
      WS=W(I,J)
      IF(WT.LE.0.0) WS=0.
      EZN=E(J)
      DZN=.5*(Z(J+1)-Z(J-1))
      SN=(Z(J)-Z(J-1))/(Z(J+1)-Z(J-1))
      SNZ=-.5*DZIJ/DZN
      EE=C(I,J-1)*F2*(-WS*SNZ+WN*(1.-SN)+EZN/DZN)
      FF=C(I,J)*(1.+F2*(-WS*(1.-SNZ)+WN*SN-EZN/DZN))
      GG=0.
      DD=EE+FF+GG
   16 IF(I.EQ.1) G(I)=DD/BB
      IF(I.GT.1) G(I)=(DD-AA*G(I-1))/BB
   20 CONTINUE
C
C     PREDICT CONCENTRATION AT HALF TIME STEP BY BACK SUBSTITUTION
C
      CSTAR(NY1,J)=G(NY1)
      NY2=NY-2
      DO 30 K=1,NY2
      I=NY1-K
   30 CSTAR(I,J)=G(I)-B(I)*CSTAR(I+1,J)
   10 CONTINUE
```

```
C
C     COLUMN CALCULATIONS (Z - SWEEP)
C
C     COMPUTE COEFFICIENTS AA,BB,CC,DD, AND THEN B(J), G(J)
C
      DO 50 I=1,NY1
      DYIJ=Y(I+1)-Y(I)
      F1=DT/DYIJ
      DO 60 J=1,NZ1
      DZIJ=Z(J+1)-Z(J)
      EY=.5*(E(J+1)+E(J))
      F2=DT/DZIJ
      IF(J.EQ.1) GOTO 61
      IF(J.EQ.NZ1) GOTO 62
      WN=W(I,J-1)
      WS=W(I,J)
      EZS=E(J+1)
      EZN=E(J)
      DZS=.5*(Z(J+2)-Z(J))
      DZN=.5*(Z(J+1)-Z(J-1))
      SS=(Z(J+1)-Z(J))/(Z(J+2)-Z(J))
      SN=(Z(J)-Z(J-1))/(Z(J+1)-Z(J-1))
      AA=F2*(-WN*(1.-SN)-EZN/DZN)
      BB=1.+F2*(WS*(1.-SS)-WN*SN+EZS/DZS+EZN/DZN)
      CC=F2*(WS*SS-EZS/DZS)
      BB=BB-AA*B(J-1)
      B(J)=CC/BB
      GOTO 63
 61   WS=W(I,J)
      EZS=E(J+1)
      DZS=.5*(Z(J+2)-Z(J))
      SS=(Z(J+1)-Z(J))/(Z(J+2)-Z(J))
      AA=0.
      BB=1.+F2*(WS*(1.-SS)+EZS/DZS)
      CC=F2*(WS*SS-EZS/DZS)
      B(J)=CC/BB
      GOTO 63
 62   WN=W(I,J-1)
      WS=W(I,J)
      IF(WT.LE.0.0) WS=0.
      EZN=E(J)
      DZN=.5*(Z(J+1)-Z(J-1))
      SN=(Z(J)-Z(J-1))/(Z(J+1)-Z(J-1))
      SNZ=-.5*DZIJ/DZN
      AA=F2*(WS*SNZ-WN*(1.-SN)-EZN/DZN)
      BB=1.+F2*(WS*(1.-SNZ)-WN*SN+EZN/DZN)
      BB=BB-AA*B(J-1)
      CC=0.
      B(J)=CC/BB
 63   IF(I.EQ.1) GOTO 64
      IF(I.EQ.NY1) GOTO 65
      VE=V(I,J)
      VW=V(I-1,J)
      DYE=.5*(Y(I+2)-Y(I))
      DYW=.5*(Y(I+1)-Y(I-1))
      SE=(Y(I+1)-Y(I))/(Y(I+2)-Y(I))
      SW=(Y(I)-Y(I-1))/(Y(I+1)-Y(I-1))

      EE=CSTAR(I-1,J)*F1*(VW*(1.-SW)+EY/DYW)
      FF=CSTAR(I,J)*(1.+F1*(-VE*(1.-SE)+VW*SW-EY/DYE-EY/DYW))
      GG=CSTAR(I+1,J)*F1*(-VE*SE+EY/DYE)
      DD=EE+FF+GG
      GOTO 66
 64   VE=V(I,J)
      DYE=.5*(Y(I+2)-Y(I))
      SE=(Y(I+1)-Y(I))/(Y(I+2)-Y(I))
      EE=0.
      FF=CSTAR(I,J)*(1.+F1*(-VE*(1.-SE)-EY/DYE))
      GG=CSTAR(I+1,J)*F1*(-VE*SE+EY/DYE)
      DD=EE+FF+GG
      GOTO 66
 65   VW=V(I-1,J)
      DYW=.5*(Y(I+1)-Y(I-1))
      SW=(Y(I)-Y(I-1))/(Y(I+1)-Y(I-1))
      EE=CSTAR(I-1,J)*F1*(VW*(1.-SW)+EY/DYW)
      FF=CSTAR(I,J)*(1.+F1*(VW*SW-EY/DYW))
      GG=0.
      DD=EE+FF+GG
 66   IF(J.EQ.1) G(J)=DD/BB
      IF(J.GT.1) G(J)=(DD-AA*G(J-1))/BB
 60   CONTINUE
C
C     ESTIMATE CONCENTRATION AT END OF TIME STEP BY BACK SUBSTITUTION
C
      C(I,NZ1)=G(NZ1)
      NZ2=NZ-2
      DO 70 K=1,NZ2
      J=NZ1-K
 70   C(I,J)=G(J)-B(J)*C(I,J+1)
 50   CONTINUE
C
C     COMPUTE FLUX OUT OF L.C. AT THE END OF TIME INCREMENT.  PUT FLUX=
C     ZERO FOR BUOYANT PARTICLES.  FLUX GENERALLY GIVEN BY CS*WS
C
C     ESTIMATE CS BY LINEAR EXTRAPOLATION FROM VALUES OF C AT TWO
C     ADJACENT NODE POINTS INSIDE L.C.
C
      J=NZ1
      DZIJ=Z(J+1)-Z(J)
      DZN=.5*(Z(J+1)-Z(J-1))
      SNZ=-.5*DZIJ/DZN
      FLUX=0.
      IF(WT.LE.0.0) GOTO 80
      DO 85 I=1,NY1
      DYIJ=Y(I+1)-Y(I)
      CS=(1.-SNZ)*C(I,J)+SNZ*C(I,J-1)
      DFLUX=CS*DYIJ
 85   FLUX=FLUX+DFLUX
 80   RETURN
      END
```

```
      SUBROUTINE EPRINT(N,T)
      DIMENSION V(49,50),W(50,50),C(50,50),CSTAR(50,50)
      DIMENSION E(51),Y(51),Z(51)
      COMMON V,W,C,CSTAR
      COMMON/PARA/E,Y,Z,NY,NZ,WT
C
C     TO PRINT CONCENTRATION AT SELECTED GRID POINTS IN
C     E-FORMAT
C
C
      WRITE(2,1050) T,N
1050  FORMAT(1H0,30X,53HTHE DISTRIBUTION OF PARTICLE CONCENTRATION AT TI
     *ME T=,1PE11.4,3H(N=,I6,1H),//)
      II=(NY-1)/10
      IF(NZ.LE.51) JJ=1
      IF(NZ.GT.51.AND.NZ.LE.101) JJ=2
      NNY=NY-1
      NNZ=NZ-1
      DO 1 J=1,NNZ,JJ
      WRITE(2,1051) J,(C(I,J),I=1,NNY,II),C(NNY,J)
    1 CONTINUE
      WRITE(2,1052) (I,I=1,NNY,II),NNY
1051  FORMAT(3X,2HJ=,I3,3X,11(1PE11.3))
1052  FORMAT(//11X,11(3X,2HI=,I3,3X))
      RETURN
      END



      SUBROUTINE MASS(CMASS)
      DIMENSION V(49,50),W(50,50),C(50,50),CSTAR(50,50)
      DIMENSION E(51),Y(51),Z(51)
      COMMON V,W,C,CSTAR
      COMMON/PARA/E,Y,Z,NY,NZ,WT
C
C     SUBROUTINE TO COMPUTE TOTAL MASS OF PARTICLE
C     REMAINING IN L.C. AT TIME T.  IT ASSUMES THAT
C     CONCENTRATION FOR EACH CONTROL VOLUME IS GIVEN
C     BY THE VALUE AT THE CENTRE OF THE VOLUME
C
      CMASS=0.0
C
C     SUM UP MASS OF PARTICLE ROW BY ROW OVER
C     THE LANGMUIR CIRCULATION CELL
C
      NNZ=NZ-1
      NNY=NY-1
      DO 1 J=1,NNZ
      DZIJ=Z(J+1)-Z(J)
      DO 2 I=1,NNY
      DYIJ=Y(I+1)-Y(I)
      DCMASS=C(I,J)*DYIJ*DZIJ
      CMASS=CMASS+DCMASS
    2 CONTINUE
    1 CONTINUE
      RETURN
      END



      SUBROUTINE CPRINT(N,T)
      DIMENSION V(49,50),W(50,50),C(50,50),CSTAR(50,50)
      DIMENSION E(51),Y(51),Z(51)
      COMMON V,W,C,CSTAR
      COMMON/PARA/E,Y,Z,NY,NZ,WT
C
C     SUBROUTINE TO PRINT PARTICLE CONCENTRATION DISTRIBUTION
C     AT GRID POINTS IN F-FORMAT
C
      WRITE(2,1050) T,N
1050  FORMAT(1H0,30X,53HTHE DISTRIBUTION OF PARTICLE CONCENTRATION AT TI
     *ME T=,1PE11.4,3H(N=,I6,1H),//)
      RNY=NY/21
      JNY=INT(RNY)
      IF(RNY-JNY.LT.1.) JNY=JNY+1
      IF(RNY.LT.1.) JNY=1
      IF(NZ.LE.51) JNZ=1
      IF(NZ.GT.51.AND.NZ.LE.101) JNZ=2
      NNY=NY-1
      NNZ=NZ-1
      DO 1 J=1,NNZ,JNZ
      WRITE(2,1051) J,(C(I,J),I=1,NNY,JNY),C(NNY,J)
    1 CONTINUE
      WRITE(2,1052) (I,I=1,NNY,JNY),NNY
1051  FORMAT(1H0,1X,2HJ=,I2,21(F6.1))
1052  FORMAT(1H0,4H  I=,4X,20(I2,4X),I2)
      RETURN
      END
```

```
      SUBROUTINE UFGRID
      REAL LAMBDA
      DIMENSION F(51),Y(51),Z(51)
      COMMON/PARA/F,Y,Z,NY,NZ,WT
      COMMON/CONST/ WO,PI,LAMBDA
C
C     SUBROUTINE TO GENERATE UNIFORM GRIDS
C
      DELY=.5*LAMBDA/(NY-1)
      DELZ=1./(NZ-1)
      DO 1 I=1,NY
    1 Y(I)=(I-1)*DELY
      DO 2 J=1,NZ
    2 Z(J)=(J-1)*DELZ
      WRITE(2,1005)
 1005 FORMAT(1H0/1X,4HY(I)/1X,4H****/1H0)
      WRITE(2,1020) ((I,Y(I)),I=1,NY)
 1020 FORMAT(1X,3HI =,I3,3X,F5.3)
      WRITE(2,1015)
 1015 FORMAT(1H0/1X,4HZ(J)/1X,4H****/1H0)
      WRITE(2,1030) ((J,Z(J)),J=1,NZ)
 1030 FORMAT(1X,3HJ =,I3,3X,F5.3)
      RETURN
      END




      SUBROUTINE AVGELO
      REAL LAMBDA
      DIMENSION V(49,50),W(50,50),C(50,50),CSTAR(50,50)
      DIMENSION F(51),Y(51),Z(51)
      COMMON/V,W,C,CSTAR
      COMMON/PARA/F,Y,Z,NY,NZ,WT
      COMMON/CONST/ WO,PI,LAMBDA
C
C     SUBROUTINE TO COMPUTE AVERAGE HORIZONTAL AND VERTICAL
C     VELOCITIES OF PARTICLE WITH SINKING SPEED WT.
C     IN THIS ROUTINE UPWELLING VELOCITY EQUALS A HALF OF
C     DOWNWELLING VELOCITY.
C
C     COMPUTE HORIZONTAL VELOCITIES (V) ROW BY ROW
C
      DIVIDE=LAMBDA/3.0
      FACTOR=WO*LAMBDA/(3.0*PI)
      Q=2.0*PI/LAMBDA
      P=Q/2.0
      NY1=NY-1
      NY2=NY-2
      NZ1=NZ-1
      DO 10 J=1,NZ1
      Z2=Z(J+1)
      Z1=Z(J)
      DZIJ=Z2-Z1
      CC=SIN(PI*Z2)-SIN(PI*Z1)
C
      DO 20 I=1,NY2
      Y2=Y(I+1)
C
C     TEST IF Y IN REGION OF UPWELLING OR DOWNWELLING
C
      IF(Y2.LE.DIVIDE) BB=SIN(P*Y2)
      IF(Y2.GT.DIVIDE) BB=SIN(1.5*PI-Q*Y2)
      V(I,J)=FACTOR*BB*CC/DZIJ
   20 CONTINUE
   10 CONTINUE
C
C     COMPUTE VERTICAL VELOCITIES (W) COLUMN BY COLUMN
C
      DO 30 I=1,NY1
      Y2=Y(I+1)
      Y1=Y(I)
      DYIJ=Y2-Y1
      IF(Y2.LE.DIVIDE) CC=SIN(P*Y2)-SIN(P*Y1)
      IF(Y1.GE.DIVIDE) CC=SIN(1.5*PI-Q*Y2)-SIN(1.5*PI-Q*Y1)
      IF(Y1.LT.DIVIDE.AND.Y2.GT.DIVIDE) CC=SIN(1.5*PI-Q*Y2)
     *-SIN(P*Y1)
      DO 40 J=1,NZ1
      Z2=Z(J+1)
      BB=SIN(PI*Z2)
      W(I,J)=-(FACTOR*BB*CC/DYIJ)+WT
   40 CONTINUE
   30 CONTINUE
      RETURN
      END
```

```
      SUBROUTINE PROFIL(T,NUMBER)
      DIMENSION CSUM(10)
      DIMENSION V(49,50),W(50,50),C(50,50),CSTAR(50,50)
      DIMENSION F(51),Y(51),Z(51)
      COMMON V,W,C,CSTAR
      COMMON/PARA/ F,Y,Z,NY,NZ,WT
C
C     SUBROUTINE TO COMPUTE AVERAGE CONCENTRATION PROFILE AT
C     TIME T, USING UNIFORM VERTICAL GRID DZ=1/10
C
      NNY=NY-1
      WRITE(2,1100) T,NUMBER
1100  FORMAT(1H0,29HMEAN CONCENTRATION V.S. DEPTH,1X,3HT =,F11.4,
     *1X,7HNUMBER=,I6/1X,29(1H*)/2X,1HK,3X,4HC(K)//)
C
C     INITIALISE DATA
C
      M1=1
      M2=5
      K=1
C
   10 CONTINUE
      SUM=0.0
      DO 100 J=M1,M2
      DO 100 I=1,NNY
      SUM=SUM+C(I,J)
  100 CONTINUE
      CSUM(K)=SUM/(5*50)
      WRITE(2,1200) K,CSUM(K)
1200  FORMAT(1X,I2,1X,F11.4)
      M1=M1+5
      M2=M2+5
      K=K+1
      IF(M1.LT.51) GOTO 10
C
C     WRITE DATA ON FILE 11
C
      WRITE(11,1300) NUMBER,T
1300  FORMAT(1X,I6,1X,F11.4)
      WRITE(11,1400) (CSUM(K),K=1,10)
1400  FORMAT(5(1X,F14.7))
      NUMBER=NUMBER+1
      RETURN
      END
```

```
      SUBROUTINE CPLOT(T,KCOUNT)
      REAL LAMBDA
      DIMENSION V(49,50),W(50,50),C(50,50),CSTAR(50,50)
      DIMENSION E(51),Y(51),Z(51)
      DIMENSION A(50,50),HT(11)
      COMMON V,W,C,CSTAR
      COMMON/PARA/E,Y,Z,NY,NZ,WT
      COMMON/CONST/WO,PI,LAMBDA
      EQUIVALENCE (A,CSTAR)
C
C     SUBROUTINE TO PLOT PARTICLE DISTRIBUTIONS IN A L.C.
C     AT A SELECTED TIME, USING "GHOST LIBRARY".
C
      NNY=NY-1
      NNZ=NZ-1
C
C     COMPUTE SUM OF PARTICLE MASS LEFT IN LANGMUIR CELL
C
      CMASS=0.0
      DO 10 J=1,NNZ
      DZIJ=Z(J+1)-Z(J)
      DO 20 I=1,NNY
      DYIJ=Y(I+1)-Y(I)
      DCMASS=C(I,J)*DYIJ*DZIJ
      CMASS=CMASS+DCMASS
   20 CONTINUE
   10 CONTINUE
      DO 100 J=1,NNZ
      K=51-J
      DO 100 I=1,NNY
      A(I,K)=C(I,J)
  100 CONTINUE
      CMAX=0.0
      CMIN=1.0E+5
      DO 1 J=1,NNZ
      DO 1 I=1,NNY
      IF(CMAX.LT.A(I,J)) CMAX=A(I,J)
      IF(CMIN.GT.A(I,J)) CMIN=A(I,J)
    1 CONTINUE
      CMAX1=0.99*CMAX
      CMIN1=1.01*CMIN
      CMEAN=CMASS/(0.5*LAMBDA)
      DIFF1=(CMAX-CMEAN)/5.
      DIFF2=(CMEAN-CMIN)/5.
      HT(1)=CMAX
      DO 2 K=2,5
      HT(K)=HT(K-1)-DIFF1
    2 CONTINUE
      HT(1)=CMAX1
      HT(6)=CMEAN
      DO 3 K=7,10
      HT(K)=HT(K-1)-DIFF2
    3 CONTINUE
      HT(11)=CMIN1
C
C     EXPRESS CONTOUR HEIGHT AS RATIO OF MEAN HEIGHT
C
      DO 333 K=1,11
      HT(K)=HT(K)/CMEAN
  333 CONTINUE
      DO 444 J=1,NNZ
      DO 444 I=1,NNY
      A(I,J)=A(I,J)/CMEAN
  444 CONTINUE
C
      XMAX=0.5*LAMBDA
      XMIN=0.0
      DDX=XMAX/5.
      DDXX=0.5*XMAX/NNY
      XMAX1=XMAX-DDXX
      XMIN1=XMIN+DDXX
C
C     USE GHOST PLOTTING ROUTINES TO PLOT GRAPHS
C
      CALL BLKPEN
      IF(MOD(KCOUNT,2).NE.0) GOTO 78
      IF(MOD(KCOUNT,2).EQ.0) GOTO 79
   78 CONTINUE
      CALL PSPACE(0.325,0.675,0.55,0.90)
      CALL CSPACE(0.25,0.75,0.5,0.95)
      GOTO 80


   79 CONTINUE
      CALL PSPACE(0.325,0.675,0.1,0.45)
      CALL CSPACE(0.25,0.75,0.0,0.5)
   80 CONTINUE
      CALL CTRMAG(8)
      CALL PLACE(1,1)
      CALL TYPECS(5HPLOT ,5)
      CALL TYPENI(KCOUNT)
      CALL CTRMAG(10)
      CALL PLACE(17,1)
      CALL TYPECS(8HLAMBDA= ,8)
      CALL TYPENF(LAMBDA,2)
      CALL TYPECS(5H  T= ,5)
      CALL TYPENF(T,5)
      CALL PLACE(13,2)
      CALL TYPECS(4HWT= ,4)
      CALL TYPENF(WT,3)
      CALL MAP(XMIN,XMAX,1.0,0.0)
      CALL WINDOW(XMIN,XMAX,1.0,0.0)
      CALL BORDER
      CALL SCALST(DDX,0.1)
      POINTZ=-0.15*XMAX
      POINTY=0.55*XMAX
      CALL PLOTCS(POINTZ,0.55,1HZ,1)
      CALL PLOTCS(POINTY,1.1,1HY,1)
      CALL WINDOW(XMIN1,XMAX1,0.99,0.01)
      CALL REDPEN
```

```
      CALL CONTRA(A,1,50,50,1,50,50,HT,1,11)
      CALL CTRMAG(5)
      IF(MOD(KCOUNT,2).NE.0) CALL CSPACE(0.7,1.0,0.5,0.85)
      IF(MOD(KCOUNT,2).EQ.0) CALL CSPACE(0.7,1.0,0.0,0.4)
      CALL PLACE(1,1)
      CALL TYPECS(12HORIGINAL C= ,12)
      CALL TYPENF(100.0,5)
      CALL PLACE(5,2)
      CALL TYPECS(8HMAX. C= ,8)
      CALL TYPENF(CMAX,5)
      CALL PLACE(5,3)
      CALL TYPECS(8HMEAN C= ,8)
      CALL TYPENF(CMEAN,5)
      CALL PLACE(5,4)
      CALL TYPECS(8HMIN. C= ,8)
      CALL TYPENF(CMIN,5)
      CALL PLACE(6,7)
      CALL TYPECS(8HCONTOURS,8)
      DO 66 K=1,11
      JK=K
      CALL CRLNFD
      IF(JK.LT.10) CALL SPACE(1)
      CALL TYPENI(JK)
      CALL TYPECS(2H= ,2)
      CALL TYPENF(HT(K),5)
      IF(JK.NE.6) GOTO 66
      CALL SPACE(1)
      CALL TYPECS(8H(MEAN C),8)
66    CONTINUE
      IF(MOD(KCOUNT,2).EQ.0) CALL FRAME
      RETURN
      END
```

REFERENCES

ASSAF, G., GERRARD, R., & GORDON, A.L. 1971. Some mechanisms of oceanic mixing revealed in aerial photographs. J.Geophys.Res. 76: 6550 - 6572.

BACA, R.G., LORENZEN, M.W., MUDD, R.D., & KIMMEL, L.V. 1974. A generalised water quality model for eutrophic lakes and reservoirs. U.S. Environmental Protection Agency, Washington D.C.

BENGSTON, L. 1973. Conclusions about turbulent exchange coefficients from model studies. Hydrology of Lakes: IAHS Publ. No.109, pp. 306-312.

BOWDEN, K.F. 1970. Turbulence II. Ann. Rev. Oceanogr. Mar. Biol. 8: 11 - 32.

BRETSCHNEIDER, C.L. 1966. Wave generation by wind, deep and shallow water. p.133-196. In A.T. Ippen (ed.) Estuary and Coastline Hydrodynamics. McGraw-Hill.

BRUSH, L.M., HO, W.H., & SINGAMSETTI, S.R. 1962. A study of sediment in suspension. Intern. Assoc. Sci. Hydr., Commiss. Land Erosion (Bari). Pub. No. 59, pp. 293-310.

CHEN, C.W., & ORLOB, G.T. 1972. Ecologic simulation for aquatic environments. Water Resour. Eng. Walnut Creek, Calif. 156p.

CRAIK, A.D.D. 1970. A wave-interaction model for the generation of windrows. J. Fluid. Mech. 41: 801 - 821.

CRAIK, A.D.D. 1977. The generation of Langmuir circulations by an instability mechanism. J. Fluid Mech. 81: 209 - 223.

CRAIK, A.D.D., & LEIBOVICH, S. 1976. A rational model of Langmuir Circulations. J. Fluid Mech. 73: 401 - 426.

FALLER, A.J. 1964. The angle of windrows in the ocean. Tellus. 16: 363 - 370.

FALLER, A.J. & WOODCOCK, A.H. 1964. The spacing of windrows of Sargassam in the ocean. J. Mar. Res. 22: 22 - 29.

FALLER, A.J. 1969. The generation of Langmuir circulations by the eddy pressure of surface waves. Limmol Oceanogr. 14: 504 - 513.

FALLER, A.J. 1971. Oceanic Turbulence and the Langmuir Circulation. Ann. Rev. Ecol. Syst. 2: 201 - 236.

FALLER, A.J., & CAPONI, E.A. 1977. A laboratory study of wind-driven Langmuir circulations. Tech. Note No. BN - 861. Univ. of Maryland. College Park. 68p.

FALLER, A.J. 1978. Experiments with controlled Langmuir circulations. Science 201: 618 - 620.

FALLER, A.J. & CAPONI, E.A. 1978. Laboratory studies of wind-driven Langmuir circulations. J. Geophys. Res. 83: 3617 - 3633.

FASHAM, M.J.R. 1978. Oceanogr. and Marine Biol. Ann. Rev. 16: 43 - 79.

GAMELSRØD, T. 1975. Instability of Couete flow in a rotating fluid and origin of Langmuir circulations. J. Geophys. Res. 80: 5069 - 5079.

GARRET, C.J.R. 1976. Generation of Langmuir circulations by surface waves - a feedback mechanism. J. Mar. Res. 34: 117 - 130.

GEORGE, D.G., & EDWARDS, R.W. 1976. The effect of wind on the distribution of chlorophyll A & crustacean plankton in a shallow eutrophic reservoir. J. Appl. Ecol. 13 (3): 667 - 690.

GORDON, A.L. 1970. Vertical momentum flux accomplished by Langmuir Circulations. J. Geophys. Res. 75: 4177 - 4179.

HARRIS, G.P. & LOTT, J.N.A. 1973. Observation of Langmuir Circulation in Lake Ontario. Linnol. Oceanogr. 18: 584 - 589.

HUTCHINSON, G.E. 1957. A treatise on Limnology, Vol.1, John Wiley & Sons, Inc., New York.

HUTCHINSON, G.E. 1967. A treatise on limnology, Vol.II. Introduction to Lake Biology and the limno-plantation. J. Wiley, New York.

ICHIYE, T. 1967. Upper ocean boundary layer flow determined by dye diffusion. Phys. of Fluids, Suppl. 5270 - 5277.

JOBSON, H.E. & SAYRE, W.W. 1970. Vertical transfer in open channel flow. J. Hyd. Div., ASCE, 96: 703 - 724.

KATZ, B., GERRARD, R., & COSTIN. M. 1965. Response of dye tracers to sea surface conditions. J. Geophys. Res. 70: 5505 - 5513.

KRAUS, E.B. 1967. Organised convection in the ocean surface layer resulting from slicks and wave radiation stress. Phys. of Fluids. Suppl. 5294 - 5297.

KUETTNER, J.P. 1971. Cloud bands in the earth's atmosphere. Tellus. XXIII: 404 - 425.

LANGMUIR, I. 1938. Surface motion of water induced by winds. Science 87: 119 - 123.

LEIBOVICH, S. 1977a. On the evolutions of the system of wind drift currents and Langmuir circulations in the ocean. Part 1 Theory and Average Current. J. Fluid Mech. 79: 715 - 743.

LEIBOVICH, S. 1977b. Convective instability of stably stratified water in the ocean. J. Fluid Mech. 82: 561 - 581.

LEIBOVICH, S., & RADHAKRISHNAN, K. 1977. On the evolution of the system of wind drift currents and Langmuir circulations in the ocean, Part 2 Structures of the Langmuir vertices. J. Fluid Mech. 80: 481 - 507.

LEIBOVICH, S., & ULRICH, D. 1972. A note on the growth of small scale Langmuir circulations. J. Geophys. Res. 77: 1683 - 1688.

LUND, J.W.G. 1959. Buoyancy in relation to ecology of the freshwater phytoplankton. Br. Phycol. Bull. 1: 1 - 17.

MALE, L.M. 1973. A temporal-spatial model for studying nutrient cycling dynamics of a phytoplankton production system. Part 1 - development of model. Center Quant. Sci. Forestry, Fish., Wildl. Univ. Wash. Quant. Sci. Pap. 35. 29p.

MARATOS, A. 1971. A study of the nearshore surface characteristics of windrows and Langmuir circulations in Monterey Bay. M.Sc. thesis, U.S.Naval Postgraduate School, Monterey.

MOBLEY, C.D. & FALLER, A.J. 1977. A numerical model of wind and wave generated Langmuir circulations. IPST. Tech. Note BN 857. University of Maryland, College Park.

MORTIMER, C.H. 1974. Lake hydrodynamics. Mitt. int. Verein. theo. angew. Limnol. 20: 124 - 197.

MYER, G.E. 1968. A field investigation of Langmuir circulations. Proc. 12th Conf. on Great Lakes Res., Ann Arbor Michigan. pp.625-663.

MYER, G.E. 1971. Structure and Mechanics of Langmuir circulations in a small inland lake. Ph.D. dissertation. State Univ. New York, Albany.

MURRAY, S.P. 1970. Settling velocities and vertical diffusion of particles in turbulent water. J. Geophys. Res. 75: 1647 - 1654.

MURTHY, C.R. 1976. Horizontal diffusion characteristics in Lake Ontario. J. Phys. Oceanogr. 6: 76 - 84.

NEUMANN, G. & PIERSON, W.J. 1966. Principles of physical oceanography. Prentice-Hall, 545 pp.

OWEN, R.W. Jr. 1966. Small-scale, horizontal vortices in the surface layer of the sea. J.Mar.Res. 24: 56 - 65.

PEACEMAN, D.W., & RACHFORD, H.H. 1955. The numerical solution of parabolic and elliptic differential equations. J. Soc. Ind. App. Math. 3: 28 - 41.

PEACEMAN, D.W. 1977. Numerical solution of first-order hyperbolic problems in one dependent variable. In "Fundamentals of Numerical Reservoir Simulations", Elsevier, p. 65 - 82.

POLLARD, R.T. 1976. (The early draft of POLLARD (1977))

POLLARD, R.T. 1977. In "A Voyage of Discovery" edited by M.V.Angel, supplement to Deep Sea Research, 24: 235 - 251.

ROACHE, P.J . 1972. Computational fluid dynamics. Hermosa publishers, Albuquerque, N.M. 434 pp.

ROUSE, H. 1938. Experiments on the mechanics of sediment suspension. Proc. 5th Interm. Congr. Appl. Mech. Cambridge, Mass.

ROUSE, H. 1940. Criteria for similarity in transport of sediment. Proc. Hydaulic Conf., Bull. 20, Univ. of Iowa Studies in Engineering, pp. 33 - 49.

RUTHERFORD, J.C. 1976. A review of mathematical modelling techniques for water quality in impoundments. Water Research Centre, Medmenham, Bucks. Report No. ILR 577, 38p.

RUTHERFORD, J.C. 1976a. Modelling of water quality in impoundments - Brief description of a model for Farmoor Reservoir. Paper No. ILR 597. Water Research Centre, Medmenham, Bucks.

SCOTT, J.T., MYER, G.E., STEWART, R. & WALTHER, E.G. 1969. On the mechanisms of Langmuir circulation and their rôle in epilimnion mixing. Limnol. Oceanogr. 14: 498 - 503.

SAYRE, W.W. 1968. Dispersion of mass in open-channel flow: Hydraulic Papers. Colo. State Univ., No.3, 73p.

SMAYDA, T.J. 1970. The suspension and sinking of phytoplankton in the sea. Oceanogr. Mar. Biol. Ann. Rev. 8: 358 - 414.

SMITH, I.R. 1975. Turbulence in lakes and rivers. Freshwater Biological Association. Sci. Pub. No.29, 79p.

STEWART, R. & SCHMITT, R.K. 1968. Wave interaction and Langmuir circulations. Proc. of 11th Conf. on Great Lakes Res.

STOMMEL, H. 1949. Trajectories of small bodies sinking slowly through convection cells. J. Mar. Res. 8: 24 - 29.

SUTCLIFFE, W.H., BAYLOR, E.R. & MENZEL, D.W. 1963. Sea surface chemistry and Langmuir circulations. Deep-Sea Res. 10: 233 - 243.

SUTCLIFFE, W.H., SHELDON, R.W., PRAKASH, A., & GORDON, E.C. Jr. 1971. Relations between wind speed, Langmuir circulation, and particle concentration in the ocean. Deep-Sea Res. 18: 639 - 644.

TANG, C. H-W. 1975. A multi-parametric lake model. Ph.D. thesis, University of Washington. 135 p.

TITMAN, D., & KILHAM, P. 1976. Sinking in freshwater. Phytoplankton: some ecological implications of cell nutrient status and physical mixing processes. Limnol. Oceanogr. 21: 409 - 417.

von ROSENBERG, D.U. 1969. Method for Numerical Solution of Partial Differential Equations. American Elsevier Publishing Co. Inc., New York.

WALTHER, E.G. 1967. Wind streaks, M.Sc. thesis, State University of New York at Albany.

WELLANDER, P. 1963. On the generation of wind streaks on the sea surface by action of surface film. Tellus XV: 67 - 71.

WIEGEL, R.L. 1964. Oceanographical Engineering, Prentice-Hall, Inc., Engelwood Cliffs, N.J.

WOODCOCK, A.H. 1944. A theory of surface water motion deduced from wind-induced motion of the Physalia. J. Mars. Res. 5: 196 - 205.

WOODCOCK, A.H. 1950. Subsurface pelagic sargassum. J. Mar. Res. 9: 77 - 92.

WU, J. 1973. Prediction of near-surface drift currents from wind velocity. Proc. ASCE. Hyd. Div. HY9. 1291 - 1302.

YALIN, M.S. 1971. Theory of hydraulic models. Macmillan.

ADDITIONAL REFERENCES

FRANCIS, J.R.D. 1975. Fluid Mechanics for engineering students. (4th ed.). Arnolds. 370p.

GEORGE, D.G., & EDWARDS, R.W. 1973. Daphnia distribution within Langmuir circulations. Limnol. Oceanogr. 18: 798 - 800.

STOMMEL, H. 1951. Streaks on natural water surfaces. Weather. 6: 72 - 74.

NAIB, S.K.A. 1966. Photographic method for measuring velocity profiles in a liquid jet. The Engineer. June 24. p.961 - 963.

OGATA, A. & BANKS, R. 1961. A solution of the differential equation of longitudinal dispersion in porous media. Prof. Paper No. 411-A. U.S. Geological Survey, Washington, D.C.